Thyroid Ultrasound

From Simple to Complex

Alexander N. Sencha
Yury N. Patrunov
Editors

Springer

Thyroid Ultrasound

Alexander N. Sencha • Yury N. Patrunov
Editors

Thyroid Ultrasound

From Simple to Complex

Springer

Editors
Alexander N. Sencha
Obstetrics, Gynecology and Perinatology
Ministry of Health
Moscow
Russia

Yury N. Patrunov
Department of Ultrasound Diagnostics
Yaroslavl Railway Clinic
Yaroslavl
Russia

ISBN 978-3-030-14450-0 ISBN 978-3-030-14451-7 (eBook)
https://doi.org/10.1007/978-3-030-14451-7

This Springer imprint is published by the registered company Springer Nature Switzerland AG
The registered company address is: Gewerbestrasse 11, 6330 Cham, Switzerland

Preface

The book is based on our own research and experience in the application of modern multiparametric ultrasound for the diagnosis of thyroid disease. Special attention is paid to the technologies of modern ultrasound beginning with conventional gray-scale examination and Doppler imaging ending with elastography and contrast-enhanced technique. Complex analysis of the diagnostic value of basic and innovative technologies is provided. Ultrasound-guided fine needle puncture biopsy is also reviewed in detail.

Special focus is put on the practical aspects of echography. The characteristic features of the normal thyroid gland are highlighted. Diffuse changes and thyroid lesions are discussed in depth. Close attention is paid to their early detection with special accent to differential diagnosis of thyroid tumors. TIRADS classification as a practical approach to the stratification of the risk of thyroid malignancies is provided. The authors summarized their own experience in utilization of qualitative parameters of compression elastography and quantitative data of shear-wave elastography, and analyzed the possibilities, diagnostic significance, advantages and disadvantages of these methods in diagnosis of thyroid lesions. The role of contrast-enhanced ultrasound in differential diagnosis of thyroid neoplasms is comprehensively discussed based on clarification of tumoral neoangiogenesis. The place of various ultrasound options in algorithms and programs of diagnostic search and differentiation is disputed.

The material is well structured and presented in the form of reference information. It is succinct and comprehensive. The monograph pushes you to think, compare, and analyze. It aims to assist specialists of ultrasound diagnostics, radiologists, endocrinologists, oncologists, surgeons, and general practitioners to systematize their knowledge on the ultrasound diagnosis of thyroid diseases, the principles and techniques of multiparametric ultrasound imaging, contrast ultrasound, and ultrasound guided biopsy. The monograph will be of interest to the wide range of specialists from the beginners in ultrasound diagnostics, students, and residents to experienced radiologists and experts of postgraduate education.

The edition is well illustrated with a large number of echograms, schemes, figures, and tables.

Moscow, Russia — Alexander N. Sencha
Yaroslavl, Russia — Yury N. Patrunov

Contents

Introduction

The diagnostic capabilities for the diseases of the thyroid gland are constantly being improved due to the development of knowledge and technology. Over the past 20–30 years, ultrasound imaging became the leading modality in the early and differential diagnosis of thyroid abnormalities. Improvement of diagnostic equipment with the emergence of new technologies and modalities makes the work of the ultrasound diagnostician more automated and standardized, effective, and less subjective. However, the obtained results still largely depend on the timeliness and correct choice of effective imaging techniques, and a comprehensive analysis of their data. Adequate diagnostic tactics determine the volume and the cost for the following treatment. Rational sequence of manipulations is important: from simple and low-cost to more complex and less accessible, from non-invasive to minimally invasive, from outpatient to inpatient, from organ-preserving to radical.

In order to manage the diseases properly, it is not enough just to apply the ultrasound probe, but is important to understand the things you see, analyze, and make prognosis. The technology of automatic analysis is still imperfect and requires further technical and intellectual improvement. The physician needs fundamental and systemic knowledge of the indications and limitations of the ultrasound method, as well as the specific features of the thyroid gland and neck tissues in normal and diseased condition. Knowledge and experience with strict following the methodology of the examination are more important than ever. It determines the vector and the accuracy of the diagnostic search resulting in the correct and timely conclusion.

To make a "conventional" thyroid ultrasound is not a big issue today. It is much more important (and therefore more difficult) to perform the studies at such an expertly high level with constant and reproducible quality, which would be fully trusted by other colleagues, clinicians, and patients. It is even more difficult to work in continuous cooperation with colleagues-clinicians to follow-up the patients under the therapy to assess the tiny ultrasound changes. Many expectations are related to the improvement and standardization of ultrasound conclusions in connection with the implementation of TIRADS system. It facilitates the stratification of the risk of thyroid malignancies and determination of further management. In such a case, standards and algorithms that are clear for any doctor are of high importance.

The authors of this monograph attempted to summarize and analyze all issues and perspectives of ultrasound diagnostics of various thyroid diseases based on

literature and personal experience. They analyze the results of more than 100,000 exams of the thyroid gland with utilization of the whole spectrum of multiparametric ultrasound, more than 5000 ultrasound-guided biopsies, and more than 1200 contrast-enhanced ultrasound studies conducted in 2000–2018. This extensive experience permitted to form well-grounded opinion about the possibilities of ultrasound imaging at the current level of medicine.

Undoubtedly, all problems of ultrasound diagnostics of thyroid diseases have not been solved yet. As always, the reader is left with the opportunity for analysis, reflection, comments, further scientific search, and practical verification. We hope for favorable reader's comments and suggestions, which will be gratefully accepted and taken into consideration in further practical work and scientific research.

Dear friends and colleagues, we wish you further professional achievements! Knowledge is power. Be strong!

Abbreviations

3D	Three-dimensional image reconstruction
3DPD	Three-dimensional power Doppler imaging (3D-reconstruction of the image in the vascular mode)
4D	Real-time three-dimensional imaging
AIT	Autoimmune thyroiditis
AITD	Autoimmune thyroid disease
AJCC	American Joint Committee on Cancer
AT	Acute thyroiditis
ATA	American Thyroid Association
BI-RADS	Breast imaging reporting and data system
BSA	Body surface area
BSRTC	Bethesda system for reporting thyroid cytopathology
CCA	Common carotid artery
CDI	Color Doppler imaging
CEUS	Contrast-enhanced ultrasound
CPD	Color pixel density
CT	Computed tomography
EDV	End diastolic velocity
FNA	Fine needle aspiration
FNAB	Fine needle aspiration biopsy
hCG	Human chorionic gonadotropin
HPT	Hyperparathyroidism
IJV	Internal jugular vein
ITA	Inferior thyroid artery
IVF	In vitro fertilization
LN	Lymph node(s)
MEN	Multiple endocrine neoplasia
MRI	Magnetic resonance imaging
PDI	Power Doppler imaging
PET	Positron emission tomography
PI	Pulsatility index
PSV	Peak systolic velocity
PTH	Parathyroid hormone
PW	Pulsed-wave Doppler

RI	Resistive index
SAT	Subacute thyroiditis
SPECT	Single photon emission computed tomography
STA	Superior thyroid artery
SWE	Shear wave elastography (elastometry)
TIRADS	Thyroid imaging reporting and data system
TSH	Thyroid stimulating hormone
US	Ultrasound (echography)
USE	Ultrasound elastography

1 Current State of the Problem of Thyroid Diseases: Principles and Technology of Thyroid Ultrasound

Alexander N. Sencha, Yury N. Patrunov, Stanislav V. Pavlovich, Liubov A. Timofeyeva, Munir G. Tukhbatullin, and Antonina A. Smetnik

Iodine deficiency in endemic regions and high incidence of thyroid disorders remain important social and medical problems. Prevention and treatment of thyroid diseases are important priority projects of national healthcare systems in many countries of the world. The diseases of the thyroid gland rank second among all endocrine pathology in terms of prevalence. They are registered in 8–20% of the adult population of the world. According to the WHO reports, more than 200 million people suffer from this pathology. The number exceeds 50% in endemic regions [1–6].

A. N. Sencha (✉)
Department of Visual and Functional Diagnostics, National Research Center for Obstetrics, Gynecology and Perinatology, Ministry of Healthcare of the Russian Federation, Moscow, Russia

Y. N. Patrunov
Department of Ultrasound Diagnostics, Center for Radiological Diagnostics of Non-State Healthcare Institution Yaroslavl Railway Clinic of JSC "Russian Railways", Yaroslavl, Russia

S. V. Pavlovich
Academic Council of National Research Center for Obstetrics, Gynecology and Perinatology, Ministry of Healthcare of the Russian Federation, Moscow, Russia

L. A. Timofeyeva
Department for Internal Diseases Propaedeutic, Course of Diagnostic Radiology of Medical Faculty of Federal State Budget Educational Institution of Higher Education "I. N. Ulianov Chuvash State University", Cheboksary, Russia

M. G. Tukhbatullin
Department of Ultrasound Diagnostics, Kazan State Medical Academy – Branch Campus of the Federal State Budget Educational Institution of Further Professional Education, "Russian Medical Academy of Continuing Professional Education" of the Ministry of Healthcare of the Russian Federation, Kazan, Russia

A. A. Smetnik
Department of Gynecological Endocrinology, National Medical Research Centre for Obstetrics, Gynecology and Perinatology, Ministry of Healthcare of the Russian Federation, Moscow, Russia

A. N. Sencha, Y. N. Patrunov (eds.), *Thyroid Ultrasound*,
https://doi.org/10.1007/978-3-030-14451-7_1

Thyroid cancer accounts for 1–3% of all malignant tumors. Recent studies demonstrate the increase in the incidence of thyroid diseases inclusive with malignant neoplasms in virtually all countries [5, 7–12]. For example, in the USA, the incidence of thyroid cancer in 1973–2009 increased 3.6 times, from 3.5 to 12.5 cases per 100,000 population [13–15]. The incidence of thyroid malignancies grows mainly due to differentiated thyroid cancer.

Mortality of patients with malignant thyroid tumors exhibits a persistent tendency to decrease. For example, in Russia the number of deaths within a year from the date of diagnosis of malignant thyroid neoplasm in 2007–2017 decreased from 5.9% to 3.5% [16]. It may be the consequence of both achievements in early diagnosis of thyroid cancer associated with widespread introduction of ultrasound imaging and new approaches to treatment and follow-up.

Oncological awareness is an important component of professional activities of any diagnostician. Undoubtedly, this applies to the diagnosis of thyroid lesions. According to Davydov [1], the risk of malignancy in diffuse toxic goiter is 2.5–8.4%, in nodular goiter 4.6–31.4%, in autoimmune thyroid disease (AITD) 1.2–8.2% (nodular type of AIT – 4.7–29.5%), and in thyroid adenoma 5.0–24.4%.

The principle tasks of thyroid ultrasound (US) are to detect the thyroid gland; to characterize its relationship with the other neck tissues; to assess the size and volume, margins, and echostructure; to characterize the pathology; to define the condition of the surrounding organs and lymph nodes; to determine the further diagnostic tactics; and to suggest the type of further treatment and follow-up.

The following methods are utilized in the diagnosis of thyroid diseases:

1. Preoperative
   a. Primary:
      - Palpation of the thyroid gland and the lymph nodes of the neck
      - Thyroid US
      - Determination of thyroid hormones and TSH in blood
   b. Additional:
      - US-guided fine-needle aspiration biopsy (FNAB) with cytology
      - Determination of antithyroid antibodies
      - Thyroid radionuclide scan
      - X-ray of the mediastinum with contrasted esophagus
      - Computed tomography (CT)
      - Magnetic resonance imaging (MRI)
      - Molecular-genetic typing of a tumor
      - Other
2. Intraoperative
   a. Intraoperative thyroid US
   b. Urgent histological investigation in cases of suspected thyroid malignancy
3. Postoperative
   a. Basic
      - Histological examination of the excised thyroid tissue
   b. Additional
      - Immunohistochemical examination of the tumor (detection of tumor markers)

Radiological methods, such as US, thyroid radionuclide scan, CT, MRI, and general radiography, are especially valuable for diagnosing thyroid diseases. Modern examination of the thyroid gland involves application of various methods in an optimal combination and sequence to reveal morphological and functional changes. To date, none of the diagnostic methods can claim absolute certainty and infallibility. When choosing diagnostic methods, it is necessary to take into account its advantages and disadvantages, such as radiation exposure (for radionuclide scan, X-ray, and CT), limited information (for palpation), long duration of the study, availability (MRI, PET/CT), etc. With different thyroid diseases, the diagnostic value of the methods is not the same. It often depends on concomitant diseases, previous treatment, patient's age, individual features of thyroid location, and some other factors.

One promising method is molecular-genetic typing of the tumor before surgery to determine the biological potential and detect patients with increased oncologic risk. Clinical guidelines for molecular diagnostics of thyroid FNA of the European and American thyroid associations indicate the importance and perspectives of the molecular-genetic panel in the diagnosis of thyroid cancer, the differentiation of thyroid lesions BSRTC categories 3 and 4. In particular the definition of the mutation markers BRAF V600E, RAS/MAPK, RET/PTC, EIF1AX, and AKT1 and their combined use in the diagnostic panels ThyroSeg v2, Afirma, TheGenX, Thyra MIR, and others is sown valuable [11].

Thyroid ultrasound is readily available, noninvasive, and highly informative. Thus, US is the leading imaging modality. Its safety and comparatively low cost are additional factors in favor of the wide use of sonography for diagnosing thyroid diseases. Since the first report of the application of US for diagnostic purposes was published, no scientifically proven adverse effect resulting from the medical use of US has been reported. It is possible that harmful effects may be identified in the future. However, the evidence available indicates that the benefits of US to patients are much greater than the risks, if any exist. Diagnostic doses of ultrasound do not accumulate, and the US examinations are short enough not to cause any significant biological effect. Hence, US can be performed several times without any limitations on the time interval between sessions. This enables the pathology to be assessed dynamically.

Modern US scanners are sensitive enough to differentiate fluid and solid thyroid lesions of 1 mm in size. Sonography can be effective in the detection of retrosternal goiter when it is in the upper mediastinum. However, localization of the goiter below the tracheal bifurcation limits the possibilities of US. One disadvantage of thyroid US is its high dependence on the level of training, experience, and skills. The variability in the results obtained when different US specialists examine the same patient is 10–30%. The diagnostic value and reproducibility of the method depend significantly on the quality of the equipment.

The sensitivity of the echography in the diagnosis of thyroid cancer is 69–100%, specificity 55–98%, and diagnostic accuracy 54–99% [3, 4, 7, 17, 18]. Color Doppler imaging (CDI), power Doppler imaging (PDI), 3D image reconstruction, multiplanar scan, ultrasound elastography (USE), contrast-enhanced ultrasound (CEUS), and other modern options increase the value of conventional ultrasound.

The incidence of metastatic deposits in regional lymph nodes in differentiated thyroid cancer reaches 50–60% [13, 19, 20]. The diagnostic value of US in the detection of thyroid cancer metastases in neck lymph nodes is also high. The sensitivity is 76–100%, specificity 72–91%, and diagnostic accuracy 82–94% [13, 19, 21].

The logistics of diagnostic care with implementation of ultrasound imaging, the routing of patients with various pathology of the thyroid gland, the sequence of diagnostic procedures, and the choice of treatment and further tactics are illustrated with the following chart flow (Fig. 1.1).

One main task of thyroid US is to analyze the nature of changes in the thyroid parenchyma with stratification of the risk of thyroid cancer and the necessity of FNAB.

Combination of several diagnostic modalities is most effective and permits the character and the severity of the pathology to be assessed. Modern complex diagnostics do not assume the use of all possible methods. It is necessary to find a rational range and sequence of diagnostic techniques to obtain the maximum information in each case.

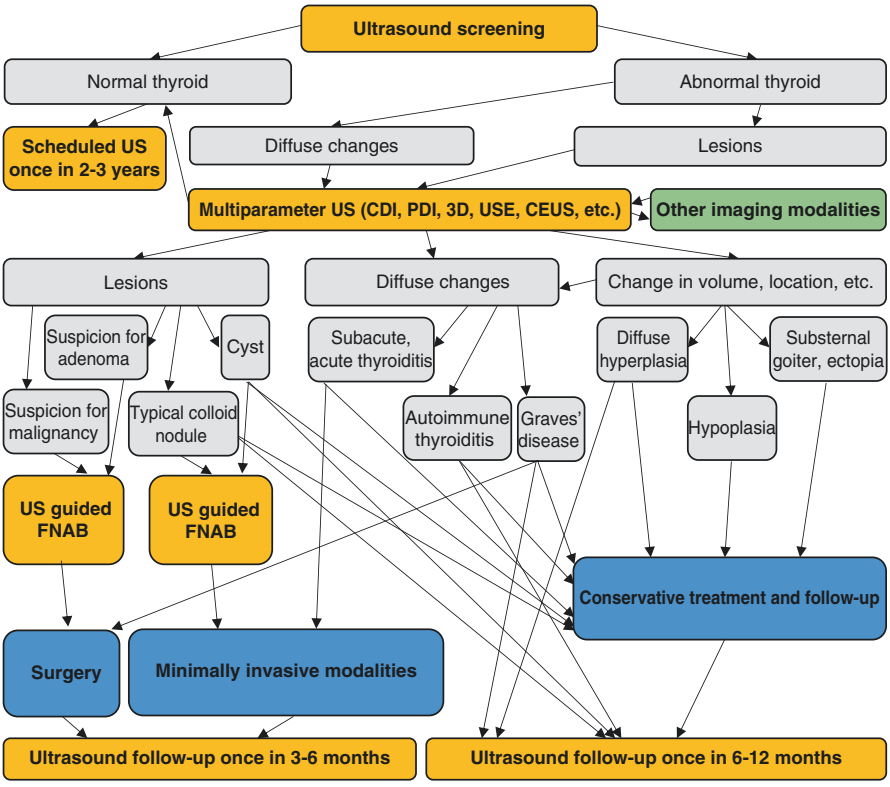

Fig. 1.1 The position of multiparametric ultrasound in the diagnostic flow in patients with thyroid diseases

1.1 Principles and Indications for Thyroid Ultrasound

Ultrasound (US) examination is a noninvasive study of the human body with scanning devices using ultrasound waves. It is based on differences between the abilities of different tissues to reflect US waves (cyclic sound pressure of an elastic medium with a frequency greater than 20,000 Hz).

The first US examination of small parts was reported by Howry et al [22]. in 1955. Thyroid sonography (A- and B-scan) was first introduced in 1966–1967 [23]. The first reports on the possibilities of differentiation of thyroid structures with ultrasound were published in 1971 [24]. It has been widely practiced since the 1970s and is now one of the most popular radiological methods for diagnosing thyroid diseases. Modern US scanners permit real-time imaging of organs with constant monitoring of their motion.

Thyroid US has the following advantages:

- It is relatively simple, rapid to perform, and inexpensive.
- It is painless and noninvasive.
- There is no need for any special preparation of the patient before the examination.
- There are no contraindications.
- It is harmless and safe for the patient and staff. US can be used repeatedly in children, pregnant and nursing women, as well as seriously ill patients with severe concomitant pathology.
- Patients can be examined regardless of their medications, including thyroid blocking agents.
- It is a high-resolution technique.
- The differential diagnosis is based on sonographic options, such as Doppler modalities, 3D image reconstruction, ultrasound elastography, and others.
- It is possible to additionally use ultrasound contrast agents to study blood supply.
- It supports documentation of video data and static images, as well as easy transmission via modern communication channels with virtual consultations.
- It provides easy guidance for minimally invasive modalities.

A patient is indicated for thyroid US in the following cases:

- Complaints that are often a consequence of thyroid pathology: dyspnea, cough, irritability, palpitation, precordial discomfort
- Palpated masses in the anterior neck
- Thyroid pathology detected by other methods
- Cardiovascular pathology, predominantly heart rhythm abnormalities
- Persistent diseases of ENT organs (such as larynx, pharynx, trachea), dysphonia, or aphonia
- Dysphagia
- Monitoring of the efficacy of treatment of thyroid diseases
- Postoperative follow-up

Sonography can be utilized as a screening method for thyroid diseases. It permits early detection of patients who are at an increased risk of developing a thyroid disease. Screening is an effective initial stage of evaluation within a target population. It helps to pinpoint a possible thyroid abnormality at an early stage and includes the elements of differential diagnosis that result in subsequent thorough examination and timely treatment in appropriate cases.

The advantages of US as a screening method are patient safety, reproducibility, reduced dependence on the quality of the equipment and operator skill, speed, availability, and low cost. The disadvantage of US screening is its comparatively low diagnostic accuracy. A negative screening study does not guarantee the absence of the disease, and sometimes a positive study does not necessarily prove that a thyroid pathology is present. In practice, one example of screening is thyroid US performed by a general practitioner with a simple (e.g., only grayscale) scanner. The exam aims to divide patients into two generalized categories: those whose thyroids are grossly normal and those with suspicious abnormalities in their thyroids (see Fig. 1.1).

Patients with thyroid abnormalities are subject to further qualified in-depth multiparametric US. The latter assumes the detection and differential diagnosis of diffuse changes and focal lesions, which is necessary to determine further tactics.

However, it is necessary to understand and not to confuse screening and in-depth comprehensive diagnostics. These concepts never replace each other. High availability of US in recent years due to the development of a wide network of private commercial diagnostic centers significantly improves screening but very seldom improves the final differential diagnostics. It is not an issue to undergo routine US in everyday life, but it is important to have final US performed by highly qualified specialist on expert scanner to get an accurate and reproducible conclusion.

1.2 Technique of Thyroid Ultrasound

1.2.1 General Assessment of the Thyroid Gland

Special preparation of the patient for thyroid US is not required. The patient is advised to remove cloves and jewelry from the neck. The positioned is supine with a pillow under the shoulders to maintain neck extension (Fig. 1.2). Seriously ill

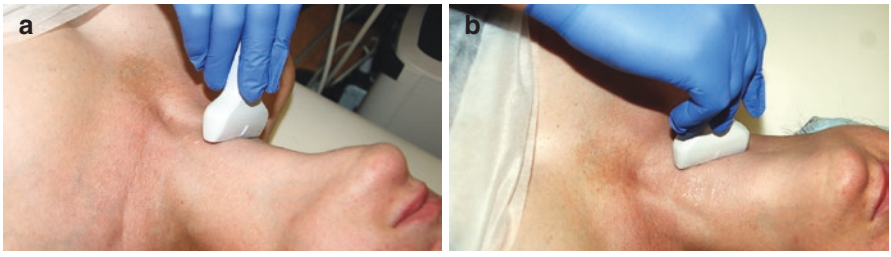

Fig. 1.2 Ultrasound examination of the thyroid gland. The position of the ultrasound probe. (**a**) Transverse thyroid scan. (**b**) Longitudinal thyroid scan

patients can be seated upright in a hard-backed chair with their back and shoulders straight, neck mildly hyperextended, and head turned slightly away from side of interest.

A linear probe with a frequency of 5–18 MHz (usually 7.5–12 MHz) is necessary for thyroid US. A 3.5–5 MHz convex probe is sometimes more suitable for measurements of large thyroids. A sector probe with a frequency of 2.5–5 MHz may be required for the substernal thyroid.

An outline of an US examination is provided below:

1. The thyroid as a whole
   - Location (typical, dystopia, ectopia)
   - Dimensions and volume (also in comparison with the norm)
   - Margins (regular/irregular, accurate/indistinct)
   - Shape (typical; congenital anomalies: lobed constitution, aplasia, hypoplasia; goiter)
   - Echodensity (normal, increase, decrease)
   - Echostructure (homogeneous, heterogeneous)
   - Elasticity
   - Blood vessels of the thyroid parenchyma (intensity, symmetry)
2. Thyroid abnormalities
   - Character of changes (diffuse, focal, mixed)
   - Location (in lobes and segments)
   - Number of lesions
   - Margins of lesions (regular/irregular, accurate/indistinct)
   - Lesions size (in three mutually perpendicular planes)
   - Echodensity, echostructure of lesions
   - Elasticity of lesions
   - Vascularity of lesions
3. Mutual relations of the thyroid with the surrounding structures
4. The status of regional lymph nodes

Sufficient amount of ultrasound gel is applied to the neck to provide good contact of the US probe with the skin. The probe is positioned on the front surface of the neck, moved from the breastbone to the hyoid bone, and backward. The probe should produce minimal pressure in order to avoid both shape distortion of the thyroid anatomy and dislocation of the adjacent structures. The location of the thyroid gland is defined followed with measurements of the dimensions and volume calculation. Several scanning planes should be considered: transverse, longitudinal, and oblique for the right and the left lobes (Fig. 1.3).

Thyroid size assessment is based on the linear dimensions and the volumes of the lobes. It is important to measure the linear dimensions only in the transverse or longitudinal scans of the thyroid lobes that show the maximum value (Fig. 1.4). When choosing the cross section, it is necessary to follow the anatomical transverse plane and position the probe perpendicular to the skin with no angle. The longitudinal lobe dimension (the length) is the largest size of the lobe. It is actually obtained in the plane that deviates from the anatomical longitudinal plane of

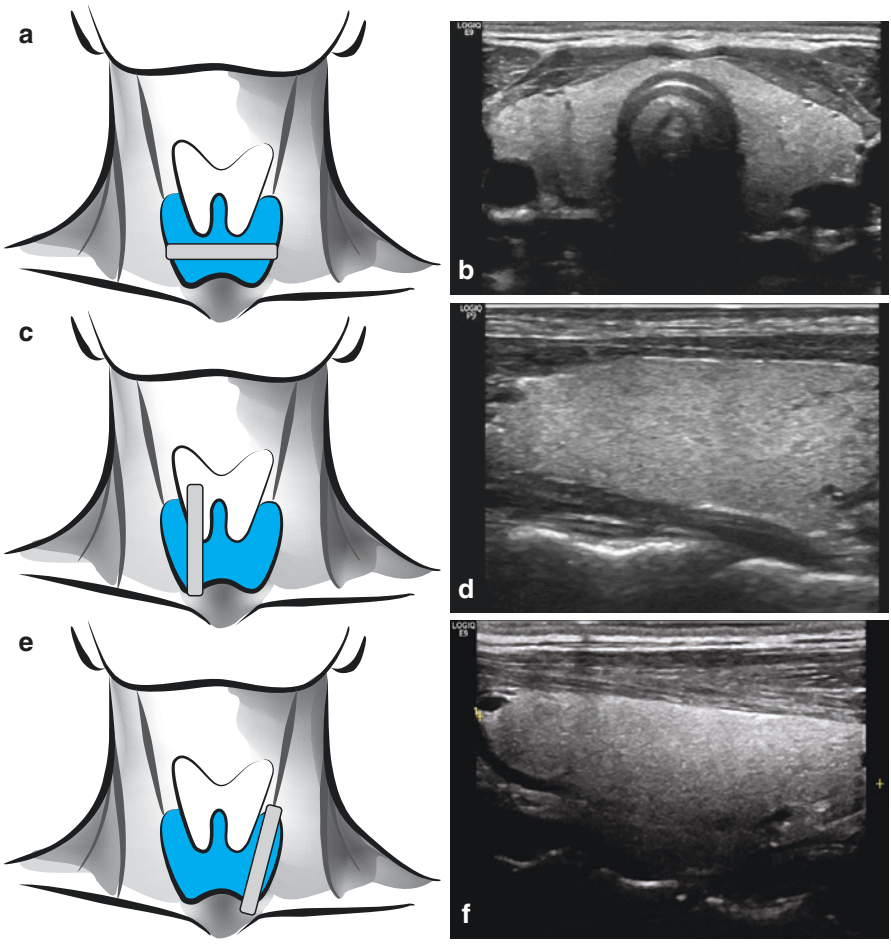

Fig. 1.3 Ultrasound examination of the thyroid gland. Basic scanning planes. (**a**) Transverse scan, scheme. (**b**) Transverse scan, grayscale US image. (**c**) Longitudinal scan, scheme. (**d**) Longitudinal scan, grayscale US image. (**e**) Oblique scan, scheme. (**f**) Oblique scan, grayscale US image

the neck. The optimal position of the probe is close to parallel with the inner edge of the sternomastoid muscle. Big thyroids cause difficulties in assessing the lengths of thyroid lobes. This is a consequence of them being much longer than the length of the US probe, meaning that the whole lobe cannot be viewed in one scanning range. The following techniques can be employed to solve this problem:

- Combining two scanning ranges (Figs. 1.4i, j and 4.2a)
- Use a "virtual convex" or trapezoid mode (Figs. 1.4h and 4.2b)
- Utilizing a convex probe (Fig. 4.2c)
- Panoramic scan (Fig. 4.2d)

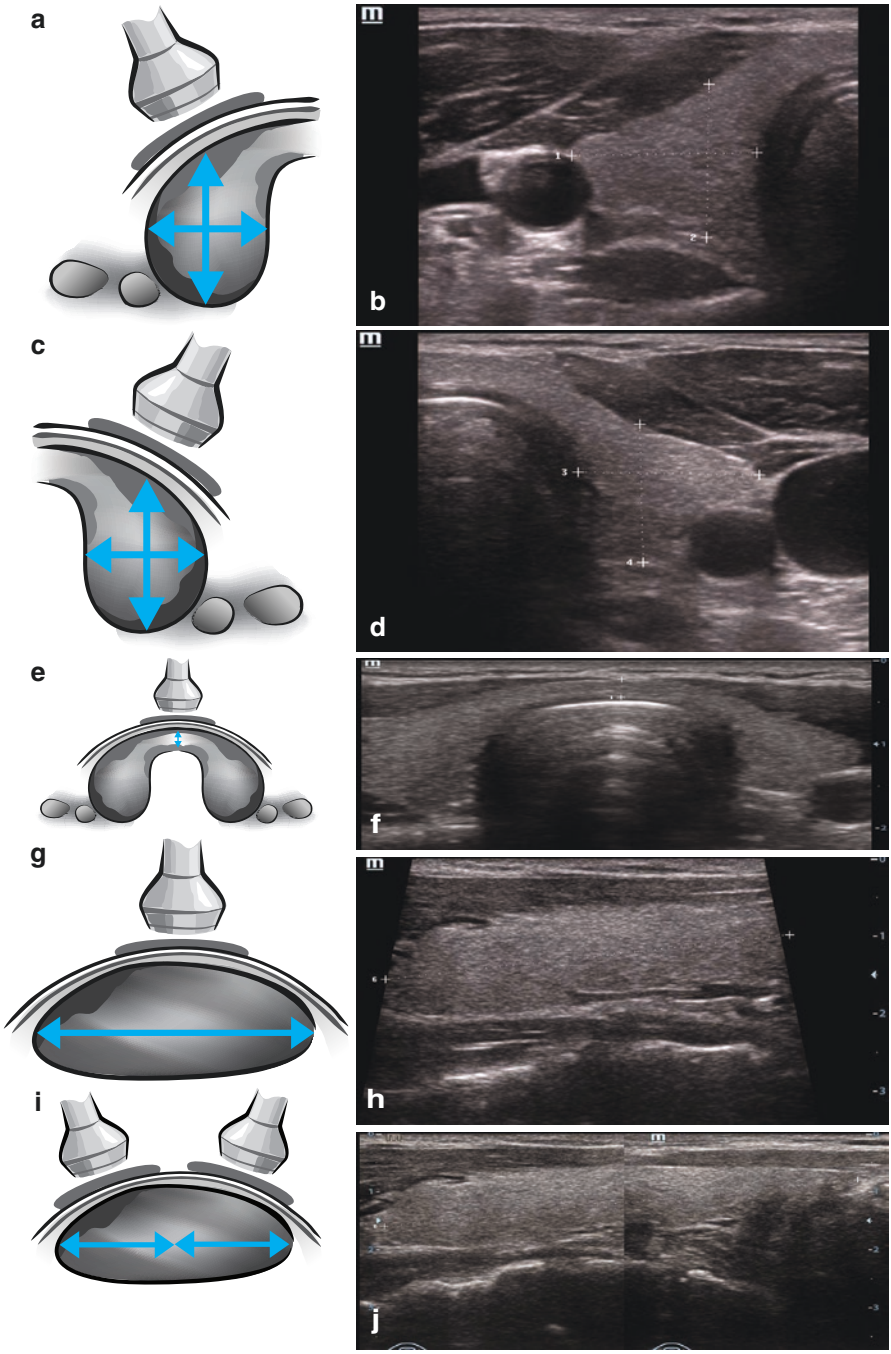

Fig. 1.4 Thyroid US. Measurements of the depth and the width of the right lobe, (**a**) scheme, (**b**) grayscale US image. Measurements of the depth and the width of the left lobe, (**c**) scheme, (**d**) grayscale US image. Measurements of the thickness of the isthmus, (**e**) scheme, (**f**) grayscale US image. Measurements of the length of the lobe, (**g**) scheme, (**h**) grayscale trapezoid US image, (**i**) combination of two scanning ranges, scheme, (**j**) combination of two scanning ranges, grayscale US image

Longitudinal and transverse scans are performed allowing the measurements of the depth (d), the width (w), and the length (l) of each lobe. The volume of the lobe is calculated by the formula: V (ml) = 0.479 × d × w × l (cm). The number 0.479 (0.524) in the formula is the correction factor for determining the volume of structures of the ellipsoid shape. The thyroid volume is the sum of the volumes of both lobes. The volume of the isthmus (thickness less than 10 mm) is not included.

The normal US dimensions of an adult thyroid can vary. A thyroid lobe is about 13–18 mm wide, 16–18 mm deep, and 45–60 mm long, while the isthmus is 2–6 mm deep. Usually, there is no significant difference in US dimensions between the right and left thyroid lobes. Separately defined linear parameters are of no value. It is important to note that only the total volume of the glandular tissue characterizes the size of the organ.

The volume of a normal thyroid in both adults and children is still the source of debate. The World Health Organization suggests a normal volume in men of 7.7–25 cm^3 and in women of 4.4–18 cm^3 [25]. The sonographically calculated thyroid volume in adults can be compared with recommended standards that depend on age, height, weight, and body surface area.

The optimal volume of the thyroid gland and criteria for its enlargement are currently being studied. No unified classification of thyroid enlargement based on sonographic data is being utilized yet. The classifications available are not accepted by the professional societies for general use. They anchor the US data to the degree of enlargement of the thyroid gland based on imperfect palpation and visual assessment (e.g., the 1994 WHO scale).

At the same time, only one aspect is important in most cases: whether the patient's thyroid volume differs from the norm. Many authors suggest that presenting the degree of deviation as a percentage may be of benefit for the dynamic assessment of changes in thyroid volume during treatment.

1.2.2 Retrosternal Goiter

The quality of US image is sometimes not as good as expected. It is often a consequence of individual neck features inclusive of retrosternal thyroid location. The goiter is termed substernal when it is fully or partially located below the suprasternal fossa. Thus, part of the thyroid gland is localized in the thorax, mainly in the anterior mediastinum, or rarely in the upper posterior mediastinum. Several terms are used to describe a substernal goiter, such as a "retrosternal," "intrathoracic," "cervico-mediastinal," or "mediastinal" goiter. These all mean that more than 80% of the gland lies within the thorax. This thyroid site is often observed in elderly people. The main causes of the "descending" of the gland into the mediastinum are a wide superior thoracic aperture, especially in brachymorphic patients, increased weight of the organ due to the growth of the goiter, the sucking action of the thorax, and force from muscles on the anterior surface of the neck. The development of an intrathoracic goiter from an aberrant (ectopic) thyroid is possible.

According to different authors, the frequency of substernal goiter in different countries ranges from 1% to 31% of the number of patients operated on for thyroid pathology [26, 27]. Substernal goiter is classified into the following five degrees:

1. The goiter tends to descend under the breast bone.
2. The largest part of the gland is dislocated below the suprasternal fossa, but swallowing brings it back to the neck.
3. The organ cannot be brought back to the neck completely with swallowing.
4. Only the upper poles of the thyroid lobes may be defined.
5. Complete intrathoracic location.

Intrathoracic goiter accounts for 8–10% of all mediastinal lesions and about 5% of all cases of goiter [28]. According to Pinsky et al. [29], thyroid cancer is detected more often in cases with substernal goiter than in cases with typical thyroid location.

The assessment of a "substernal location" is subjective to a certain degree due to the different positions of patients (upright or supine) and different degrees of patient head flexion during the examination. This naturally affects the thyroid site and appears clinically significant in cases of thyroid enlargement.

Substernal goiter shows symptoms related to the compression of the organs of the mediastinum, such as breathing difficulties in up to 39–65%, swallowing problems in up to 16% of cases, phonation disturbances, feelings of a lump in the throat, superior vena cava syndrome, and related complications [26, 30, 31]. In 30–50% of cases, substernal goiter progresses asymptomatically and is discovered during medical examinations for other reasons.

US, although successfully utilized to diagnose thyroid pathology at its typical site, exhibits significant limitations when applied to a substernal goiter. These result from the inability to achieve detailed visualization of the compartments of the gland that are located deeply in the mediastinum. Nevertheless, sonography may be effective in depicting a partially substernal goiter localized in the upper mediastinum.

The sonographer faces several difficulties when utilizing high-frequency linear probes of 7.5–15 MHz to examine a substernal thyroid. First, acoustic access to the substernal part of the gland is technically complex. A "short neck" prevents inclination of the probe, thus limiting the effective scanning range. To improve the situation, the patient is asked to throw their head back and turn it to the opposite side. This significantly extends the area available for manipulating the probe and elevates the deeper part of the thyroid lobe. It increases the efficacy of scanning and enables the larger part of the thyroid to be examined. However, if the retrosternal part of the gland has significant volume, the operator must use lower-frequency probes. Thus, a second problem inevitably arises: a decrease in the quality of the image, which does not allow the echostructure to be assessed with the desired precision. In such cases it is often impossible to differentiate the lesions with the grayscale scan or with Doppler mapping options (due to motion artifacts). Nevertheless, US supplies required information on thyroid size. Abnormal thyroid tissue can be identified well enough with low-frequency probes against the fat and mediastinal organs.

Sonography with microconvex or sector probes in the suprasternal fossa and intercostal parasternal access near to adjacent pulmonary tissue is useful. It is often possible to measure the anteroposterior and craniocaudal dimensions of the thyroid. The transverse dimension is often measured inaccurately because of wide acoustic shadowing posterior to the breast bone.

There are individual publications about the use of US to examine the intrathoracic component of a thyroid mass. They report that US permits the visualization of the mediastinum and the intrathoracic component of the thyroid, the definition of its location (anterior, posterior mediastinum, or mixed location), and the differentiation of an intrathoracic goiter from tumors with other origins and metastases in lymph nodes. Kazakevich [32] recommends US under the following circumstances:

- Suspicion for intrathoracic expansion of a tumor according to clinical examination or chest X-ray
- Dilation of the mediastinum of unknown genesis or suspicion of dilation of the mediastinum according to X-ray
- Detection of the substernal component of a tumor during standard thyroid US
- Widespread metastatic affection of cervical lymph nodes
- Malignant tumor in the inferior segments of the thyroid
- As a follow-up method after surgery for a tumor in the inferior compartment of the thyroid gland, the intrathoracic component of thyroid neoplasm, or widespread metastases in cervical or mediastinal lymph nodes

US of the mediastinum is performed with 3–5 MHz convex probes with a small scanning radius through the suprasternal, supraclavicular, and parasternal areas at the level of the first four intercostal spaces. Computed tomography is more often the method of choice for exactly assessing the structure of the mediastinum and for differential diagnosis between substernal goiter, lymphomas, and other masses of the thorax. The sensitivity of CT for mediastinal neoplasms is about 98.8%, with a diagnostic accuracy of 92.7% [33].

Chest radiography including X-ray of the mediastinum with contrasted esophagus and radionuclide scan are often mandatory. MRI, PET (more often in carcinomas), and SPECT also supply additional data in cases of substernal goiter.

Fine-needle aspiration biopsy is readily available and is of high diagnostic value. Nevertheless, it is not recommended by most authors due to the high risk of complications relating to damage to the large vascular structures and organs of the thorax. Substernal goiter is usually represented by a large mass. Therefore, the material obtained for biopsy cannot supply complete information on all areas of the lesion so that malignancy can be ruled out. According to Ignjatovic [34], complete correct diagnosis appears impossible to achieve in 20% of cases.

Modern multiparametric thyroid US is based on the following technologies:

1. Grayscale and its derivatives (tissue harmonics, etc.)
2. Noninvasive assessment of vascularity (color and power Doppler imaging, spectral pulsed-wave Doppler, B-flow, Microflow, etc.)

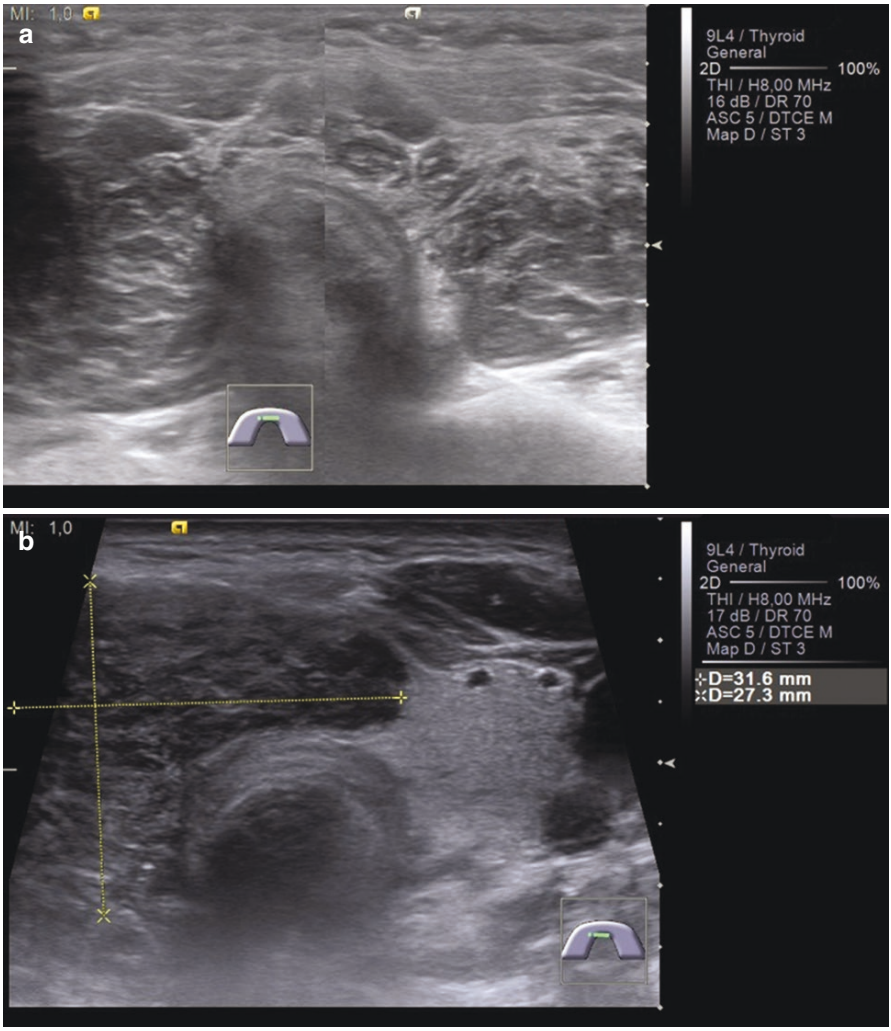

Fig. 1.5 Similar changes in the thyroid gland with US. Gray scale mode. (**a**) Diffuse changes in autoimmune thyroid disease. (**b**) Lesion of the right thyroid lobe

3. Assessment of tissue elasticity (ultrasound compression and shear wave elastography)
4. Contrast-enhanced ultrasound (invasive assessment of vascularity)
5. Postprocessing and reconstruction (3D/4D, panoramic scan, multislice view, adaptive coloring, etc.)

Grayscale (B-mode, 2D mode) is a well-known basic type of scanning that provides a real-time section image of the thyroid in typically 256 shades of gray (Fig. 1.5). It implicates 70–75% of all ultrasound data. For example, it allows direct characterization of the following aspects:

- Anatomical features of the thyroid gland (location, shape, symmetry of lobes, etc.)
- Thyroid size and volume
- Condition of the parenchyma (echodencity, homogeneity)
- Nature of the changes (diffuse, focal)
- Severity of disorders (number and size of lesions, etc.)
- Condition of the surrounding organs (e.g., invasion of the tumor)
- Neck lymph nodes

The gray scale mode is the means for thyroid detection. It permits precise determination of the location of the thyroid gland, the area of dystopia, aberrant lobes, and the variants of its shape.

The echodencity and echostructure of the normal thyroid gland are identical to the same of the submandibular salivary gland. The changes in the parenchyma may exhibit diffuse (all aspects of the thyroid gland are abnormal) or focal (limited area of abnormality) character.

Grayscale description along with the assessment of the echodensity of the whole thyroid gland implicates specification of the echodensity of the lesions. The latter is usually compared with that of the unchanged thyroid parenchyma. The following terms are utilized:

- Isoechoic—average echodensity—equal in echodensity to unchanged thyroid parenchyma
- Hypoechoic—decreased echodencity
- Hyperechoic—increased echodencity
- Mixed—with regions of different above-listed types of echodencity

The term echostructure supposes the description of the degree of heterogeneity. All changes within the thyroid gland may be ranged from homogeneous to heterogeneous according to their grayscale image.

Grayscale image may be substituted by a different color to follow the subjective perception of the examiner. The option is named adaptive coloring and represents 2D image in shades of some other color map (Fig. 1.6). Color inversion of the image is possible. This simple software option is often present in US scanners. Some researchers report that it helps to detect isoechoic thyroid lesions and define nodule contours and posterior acoustic phenomena, especially in small lesions.

The harmonic imaging (tissue harmonic imaging) is an algorithm that allocates the harmonic component of fluctuations after the base US impulse has passed though the tissues. It is incorporated as an option in grayscale scanners with standard probes and is commonly switched on by default in modern scanners. Tissue harmonic imaging emphasizes lesion margins, echostructure, fluid collections, and calcifications. It permits better detection of the US signs of thyroid cancer. According to Belashkin et al. [35], it improves the visualization quality and specifies features of colloid nodules in 80% of cases.

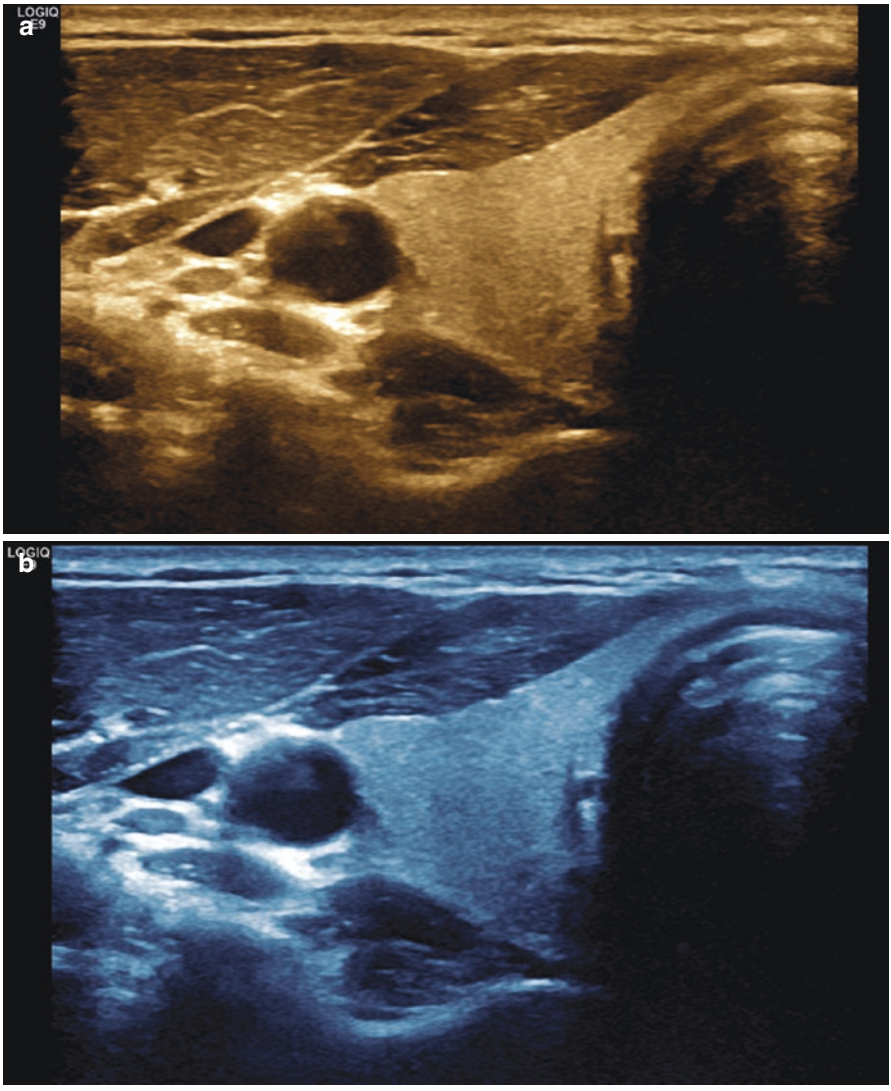

Fig. 1.6 (**a**, **b**) Thyroid US image. Adaptive color mode

Noninvasive assessment of vascularity traditionally bases on Doppler techniques.

Color Doppler imaging (CDI) is an US technology for visualizing vascular structures. It registers the blood flow velocity and uses color encoding to superimpose this velocity onto the grayscale image (Fig. 1.7).

Blood flow in thyroid parenchyma is an important ultrasound criterion of thyroid disorders. Its increase is typical for Grave's disease. Different changes in diffuse and local thyroid vascularity often accompany autoimmune thyroid disease. Significant decrease in vascular supply is always registered in focuses of subacute thyroiditis.

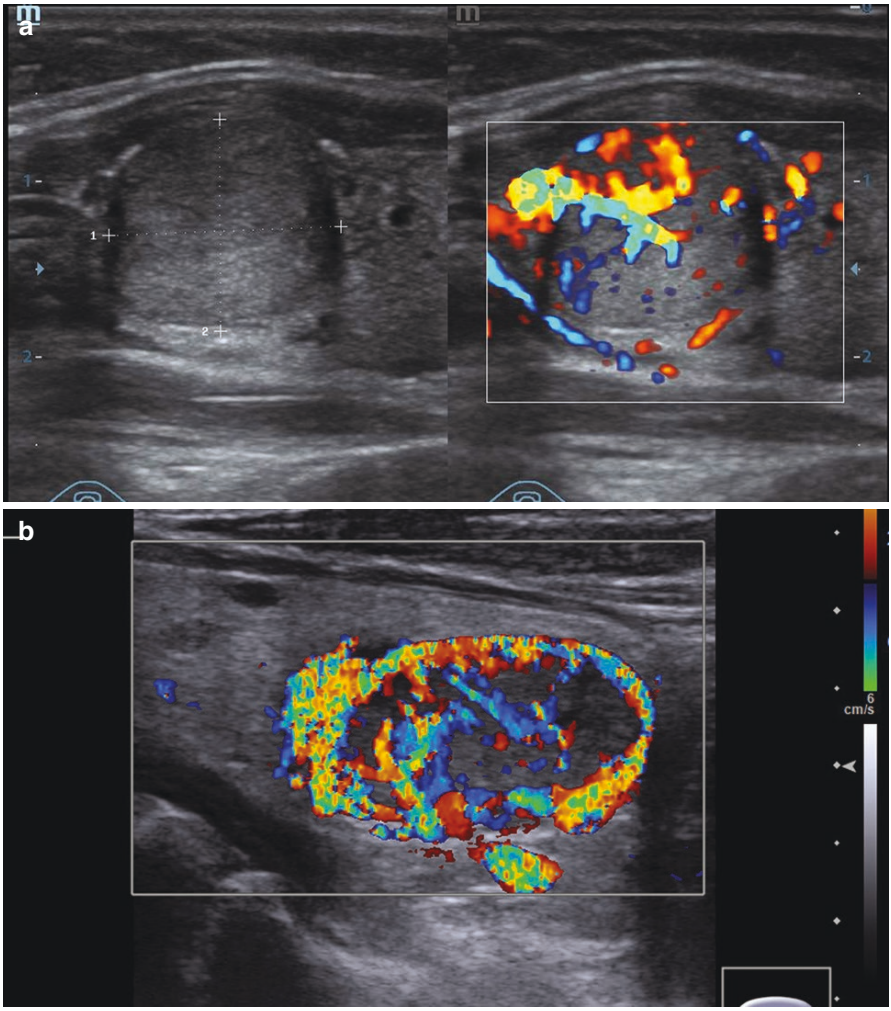

Fig. 1.7 (**a**, **b**) Thyroid US image. CDI mode

The vascularity of the parenchyma of the thyroid is usually characterized by the following criteria:

- Vascular pattern intensity
- Symmetry (between the lobes and the segments)
- Regularity of vascular structures within the thyroid parenchyma
- Deformations of the architectonics

CDI is quite subjective in assessment of the condition of the parenchymal blood flow. It much depends on the settings and the class of the scanner. Nevertheless, some attempts to make it more objective have been taken. The intensity of

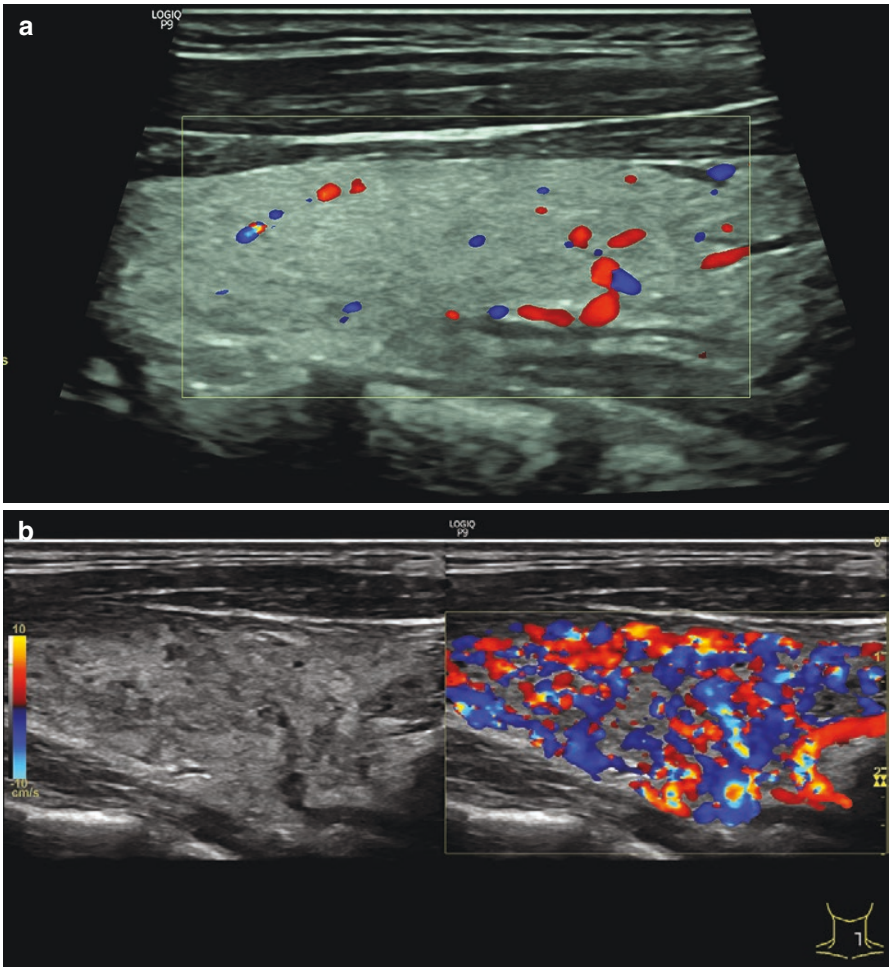

Fig. 1.8 CDI. Measurement of the average color pixels density index for the analysis of parenchymal blood flow. (**a**) CPD—5 to 10%. (**b**) CPD—80 to 90%

vascularity in diffuse thyroid diseases is sometimes characterized by the number and the density of color pixels within the parenchyma using the following methods:

1. The average color pixel density (CPD index) is numerically expressed as the ratio of the area covered by color pixels to the total area of the image (in parts or percent). The CPD index is considered normal in the range between 3% and 15% (Fig. 1.8).
2. Scoring the average number of color-coded images of vessels in area units (e.g., 1 cm^2). The proposed reference range for vessel density is between 0.4 and 2.5 vessels per 1 cm^2 of normal thyroid tissue.

3. Counting the total number of vessels within the longitudinal scan of the thyroid lobe. Only color spots from separate vessels are taken into account. The reference range for a normal thyroid is between five and ten visible vessels within the lobe scan.

In our opinion, CPD is more appropriate for general use. Being yet subjective, it is fast and effective in quantitative analysis of parenchymal blood flow. It is especially efficient in follow-up patients by the same examiner on the same US scanner. It requires identical settings of the scanner and examination in the same location of the thyroid gland. With certain experience and utilization of patient's images database, it is easily reproducible.

Assessment of the vascularity of the lesion is reported to facilitate their differentiation. It implicates the terms of vascular pattern and flow intensity. Thyroid lesions may exhibit the following types of vascular pattern (Fig. 1.9):

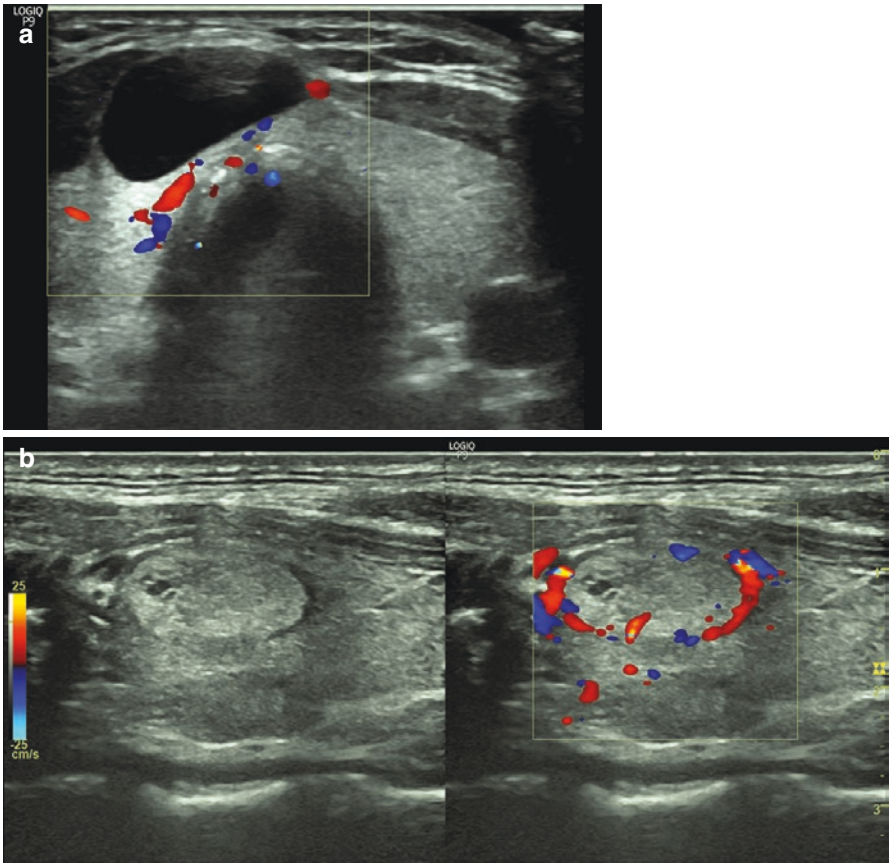

Fig. 1.9 Thyroid nodules. CDI mode. Different patterns of vascularization. (**a**) Avascular pattern. (**b**) Peripheral vascularization. (**c**) Central vascularization. (**d**) Hypervascular nodule with mixed vascularization

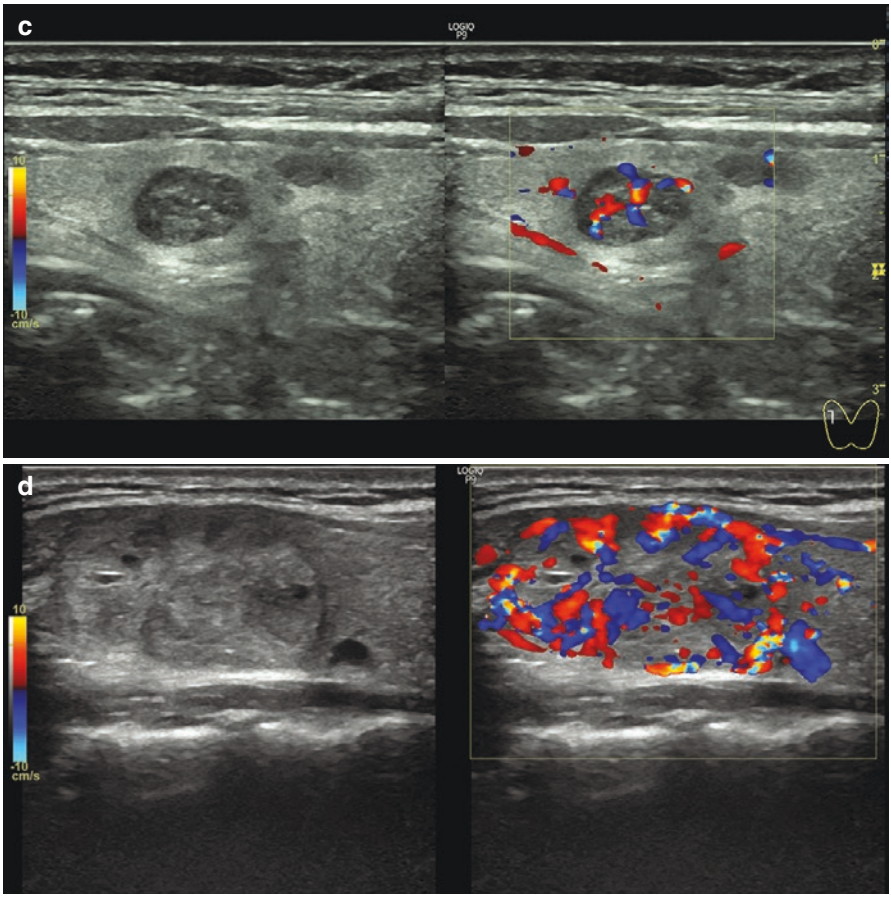

Fig. 1.9 (continued)

1. Avascular. No blood flow is detected within the lesion
2. Peripheral (perinodular). Blood flow is mainly registered at the periphery of the lesion, often in the shape of a rim.
3. Central (intranodular). Single or multiple vessels are detected within the thyroid lesion without any peripheral rim-like flow.
4. Mixed. Vascularization in both peripheral and central aspects of the lesion.

In addition to vascular pattern, the intensity of vascularity is assessed based on comparison with the surrounding thyroid parenchyma. It is usually characterized with the following terms:

1. Hypervascular lesions show increased blood flow, which often can be registered as a peripheral rim and multiple arterial and venous vessels within the lesion, representing a “color crown” sign.

2. Nodules with a medium degree of vascularization have the same intensity of blood flow as the thyroid parenchyma.
3. Hypovascular nodules demonstrate poor vascularization as compared with the surrounding parenchyma.
4. Avascular nodules have no inner color spots and no peripheral rim.

Some types of vascularization are characteristic for selected lesions. For example, cysts are avascular. The hypervascular mixed type of blood flow is suspicious for follicular lesion. However, there is no consent about the value of CDI for differential diagnosis of thyroid cancer yet. Khadra et al. [36] published the meta-analysis of 89 publications and 14 prospective studies inclusive of 4154 thyroid nodules. They reported that utilization of vascular flow on CDI may not accurately predict malignancy in thyroid nodules.

CDI has some disadvantages, such as distortions of the Doppler spectrum (aliasing artifact), baseline noise, and dependence on the angle of the US beam.

Power Doppler imaging (PDI) is 3–5 times more sensitive than the CDI. It demonstrates a decreased dependence on the angle between the US beam and the blood flow and has a lower noise-to-signal ratio. It permits images of smaller vessels with sharper contours to be obtained (Fig. 1.10).

The technologies based on non-Doppler imaging of blood flow facilitate assessment of microvascularity (Fig. 1.11). The presentation of these techniques is similar to the image of contrast-enhanced ultrasound. It gives valuable information about the distribution of small vessels (architectonics) but lacks time-related data (assessment of wash-in and washout phases of blood flow is impossible).

In pulsed-wave (PW) Doppler, a curve resulting from the Doppler shift is produced via computer processing. This permits the analysis of the velocity and spectral parameters of the blood flow as well as the calculation of some indices (Fig. 1.12).

PW Doppler is valuable for diagnosis and follow-up the patient thyroid disorders, accompanied with thyrotoxicosis. In untreated Grave's disease, thyroidal artery flow velocity and PSV are significantly increased [37]. The PSV can differentiate between thyrotoxicosis owing to Grave's disease from subacute thyroiditis or amiodarone-induced thyrotoxicosis type 2, where the blood flow is reduced.

Joish et al. [38] suggest the following normal values in the superior thyroid artery (STA) in euthyroid patients: the average peak systolic velocity (PSV) is 16.94 ± 5.3 cm/s; the resistance index (RI) is 0.5 ± 0.1; and the pulsatility index (PI) is 0.93 ± 0.31.

PW Doppler can confirm difference in blood flow within the nodule as compared to that in the surrounding parenchyma. Blood flow within the nodule is defined by both its morphological structure and its size and may vary substantially, which complicates the interpretation. However, the data about the value of PW Doppler in differentiation between benign and malignant lesions is still disputable. Some researchers demonstrate that malignant nodules have RI (over 0.73) and PI (over 1.3) higher as compared with benign nodules [39].

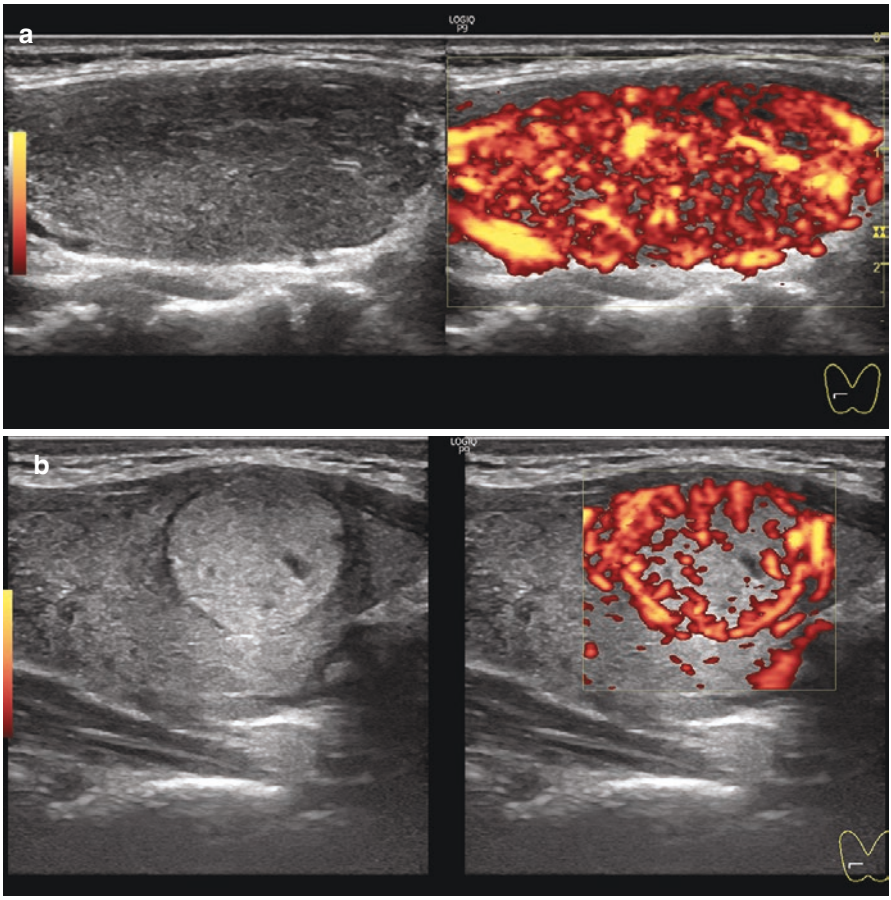

Fig. 1.10 (**a**, **b**) Thyroid US image. Power Doppler imaging

Our own research revealed no regularity in blood flow parameters. PW Doppler data in thyroid nodules show a wide dispersion and do not carry significant additional information. This precludes PW Doppler from being used for the differential diagnosis of thyroid nodules, although it may be used as an accessory feature.

Ultrasound elastography (USE) is an imaging technique based on the difference in the elastic properties (stiffness) of normal and diseased tissues. USE is a machine analog of palpation. Structures that are hard with palpation exhibit hard features with elastography. Hence, it permits to detect hard tumors on soft background. Many authors report that it helps to diagnose and differentiate cancer at early stage and to specify its invasion [40–46].

It is available as an option for modern US scanners. The manufacturers of ultrasound equipment often use various methods of elastography with their own trademarks, for example, Natural Touch (Mindray), eSie Touch (Siemens), ElastoScan

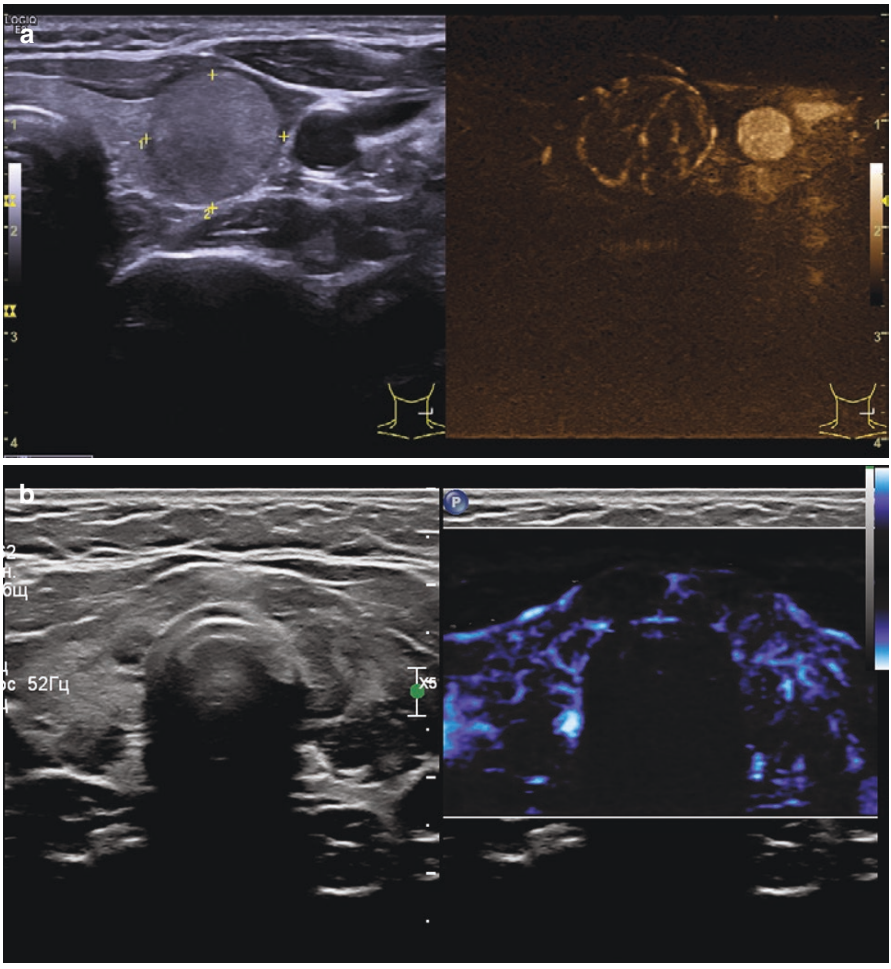

Fig. 1.11 Thyroid US image. Examples of non-Doppler imaging of blood flow. (**a**) B-flow. (**b**) Microflow

(Samsung Medison), Real-Time Tissue Elastography HI-RTE (Hitachi), ElastoQ (Toshiba), and just elastography (GE, Philips) and many others.

Ophir et al. [43] was the first to introduce elastography for diagnostics in the early 1990s of the twentieth century. Ultrasound elastography techniques can be divided into two major groups, as follows:

- Strain imaging
- Shear wave imaging

Traditionally, the principle method of strain imaging is compression elastography. The technology determines tissue deformation with strain under compression

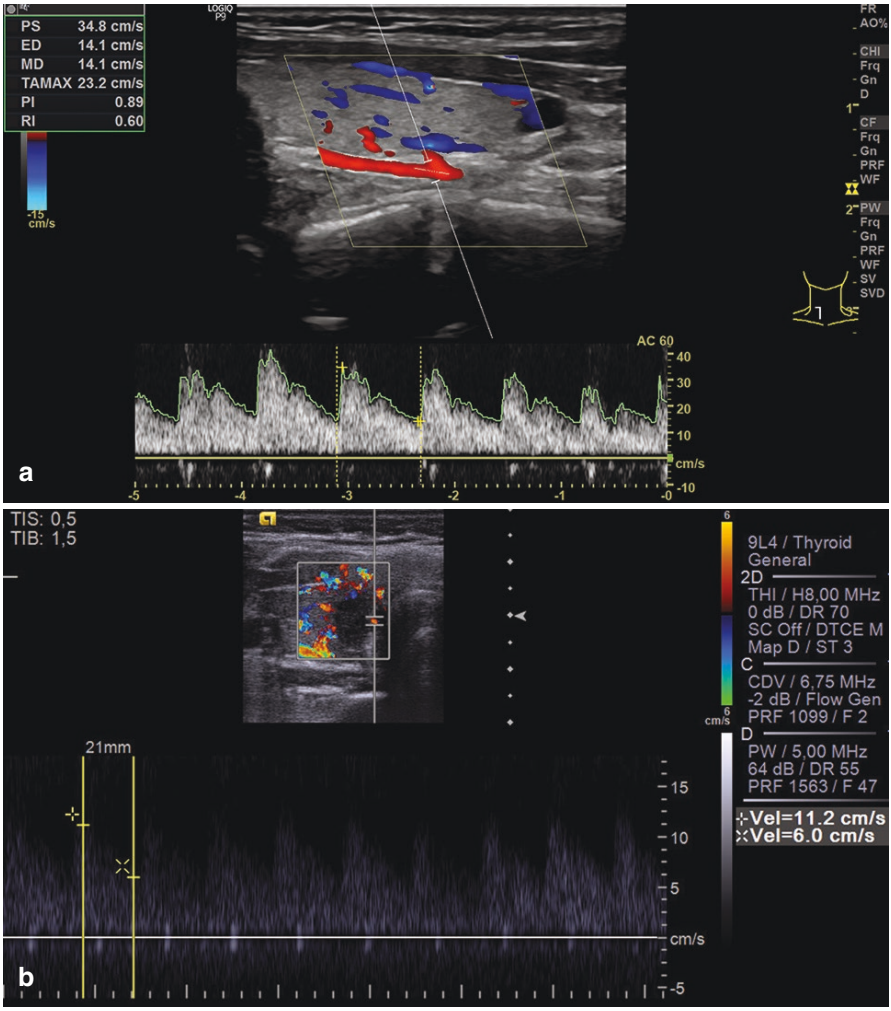

Fig. 1.12 (**a**, **b**) Thyroid US image. Pulsed-wave Doppler mode

and can compute relative stiffness (elasticity coefficient). Compression can be applied artificially from the outside, for example, by the hand of the examiner or special vibrator. Alternatively, pulsation of the walls of the major vessels and heart can be used as strain factors. The difference in tissue elasticity results in the difference in strain.

When carrying out compression USE, the ultrasound probe is positioned perpendicular to the skin over the thyroid gland and the lesion. Additional external pressure with the probe is rhythmically applied one to two times per second to the entire surface with displacement of 1–5 mm. Total compression usually lasts for 2–5 s until several static images with minor noise and artifacts are displayed. To improve

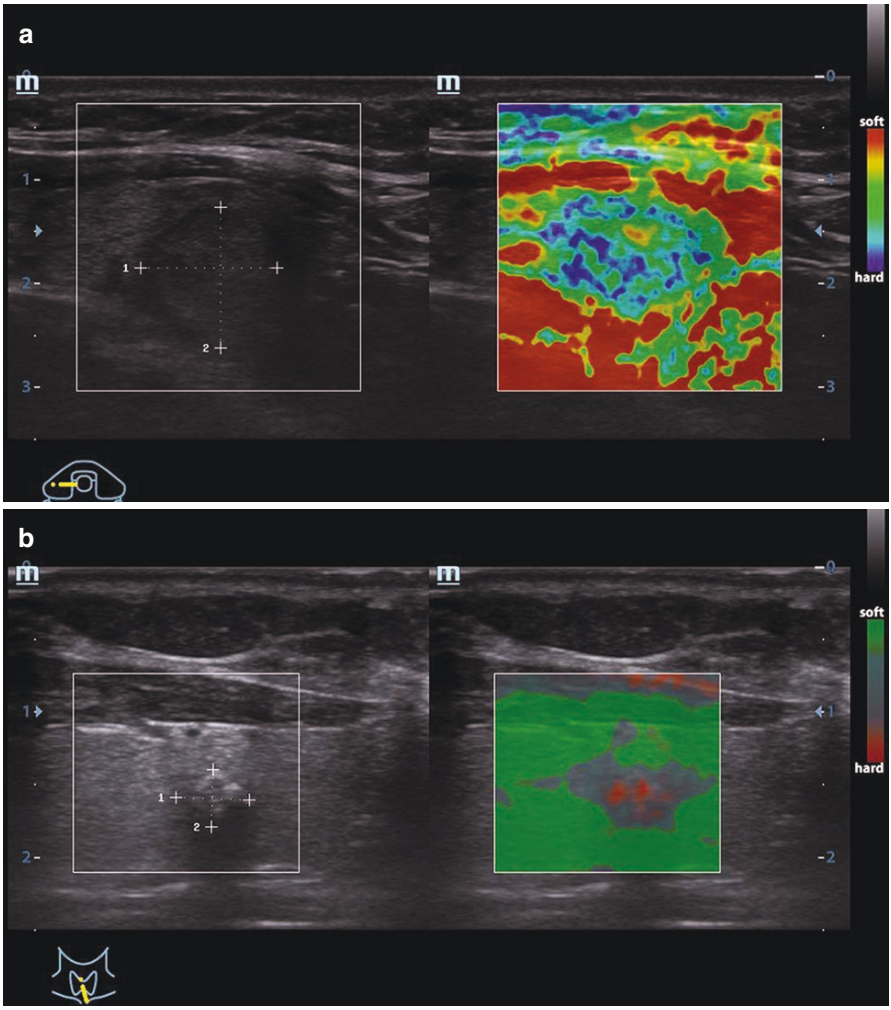

Fig. 1.13 (**a**, **b**) Thyroid US image. USE. Different color of the nodules reflects different stiffness

interobserver reliability and effectively control the degree of compression, the scanner displays a special reference icon (in the shape of a circle, spring, scale, index, etc.). As a result, a color "compressive" image superimposed over greyscale image is displayed on the screen. Certain color map is used to code tissue stiffness (Fig. 1.13). Hard structures are usually colored with dark or blue. Soft areas are usually marked with light or red. Intermediate colors are applied, respectively. Scanners usually offer several color maps, such as "blue-green-red," shades of gray, or customized maps with shades of red or other colors. Abnormal tissues often have their own strain characteristics. Hard lesions are suspicious for malignancy.

The following elastographic features of thyroid lesions are necessary to assess [44]:

- Presence and intensity of the color pattern in the structure of the lesion
- Type of color (hard, soft, mixed)
- Homogeneous/heterogeneous
- Size of colored area in comparison with the size of grayscale size of the lesion
- Differentiation of colored zone from the surrounding tissues

Itoh et al. [47], Rago et al. [48], and Zubarev et al. [46] specify a five-point scale of elasticity score with USE. A score of 1 corresponded to even elasticity of the entire lesion (i.e., the entire lesion was evenly shaded in green). A score of 2 indicated elasticity in large part of the nodule, with some areas of no strain (i.e., the hypoechoic lesion had a mosaic pattern of green and blue). A score of 3 indicated elasticity only at the peripheral part of the lesion (i.e., the peripheral part of lesion was green, and the central part was blue). A score of 4 indicated no elasticity in the entire hypoechoic lesion (i.e., the entire lesion was blue, but its surrounding area was not included). A score of 5 indicated no elasticity in the entire lesion and in the surrounding area (i.e., both the entire hypoechoic lesion and its surrounding area were blue). The higher score corresponded to the increased risk of malignancy

Compression USE is relatively simple to perform, but it is not easily reproducible. Uniform compression of the whole thyroid gland is impossible due to short probe aperture. Neck structure, especially the trachea, prevents from compression of both lobes together. Compression of individual parts (one lobe or isthmus) that contain lesions is much easier and efficient. Park et al. [49] demonstrated very high interobserver variability with free hand compression USE.

The data on the diagnostic value of USE in thyroid lesions are contradictory. The sensitivity ranges from 73% to 100% with specificity of 60–95% [12, 44, 50–53]. USE permits assessment of only the lesions that were detected with conventional ultrasound. It cannot be used as a screening method. USE supplies additional data that is sometimes crucial for the indication of FNAB. Garra (2011) reported that biopsy could be avoided in approximately 15% of lesions that would ordinarily be biopsied without increasing the rate of missed cancers. According to Sencha et al. [55], USE decreases the number of FNAB by 6.9%, thereby reducing the risk of complications and the level of patient's stress associated with invasive procedure.

Quantitative (digital) data are more objective for assessment of tissue elasticity. These methods utilize shear wave technology and are often named elastometry. As opposed to manual compression elastography, they induce tissue strain with a standardized machine-generated impulse. It could be a mechanical impulse for transient elastography (which is generally used for liver stiffness assessment) or ultrasound impulse of high energy. They are significantly less operator-dependent.

The technology of share-wave elastography is based on the fact that the shear wave velocity depends on tissue strain. The harder the tissue (which is common for malignant tumors), the higher the shear wave velocity. Measurement of shear

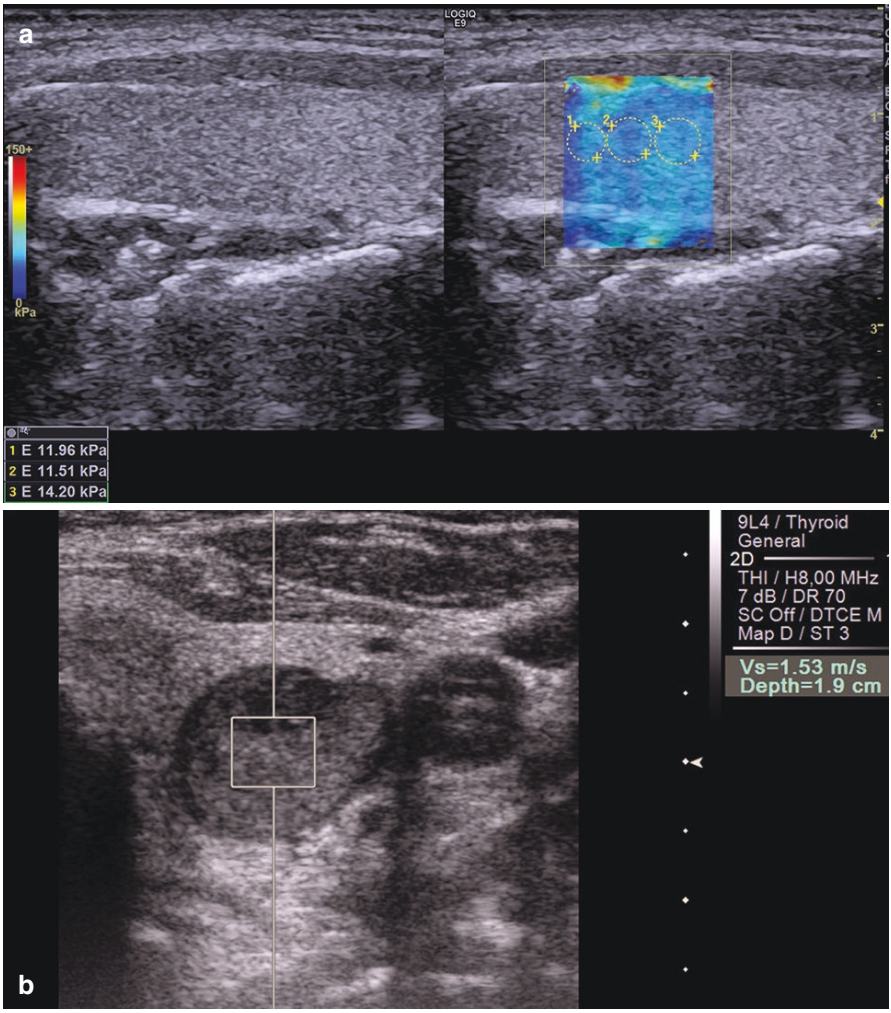

Fig. 1.14 Elastometry. Echograms. (**a**) Shear wave elastography of the thyroid gland. Measuring the Young's modulus in the thyroid parenchyma. (**b**) Virtual Touch Tissue Quantification. Measurement of shear wave velocity in a thyroid lesion

wave velocity permits assessment of tissue rigidity. Higher velocity corresponds to harder tissue.

There are the following true quantitative indicators of rigidity/elasticity of tissues (Fig. 1.14):

- Young's modulus (measured in kPa)
- Shear wave velocity (m/s)

There are also several indexes that are based on two above-listed indicators. However, some elasticity indices, such as strain ratio, are semiquantitative since

they are calculated on the basis of qualitative data. Heterogeneous soft tissues can have complex pattern of shear wave propagation due to reflections from the boundaries of structures with different acoustic impedance resulting in data distortion.

Shear wave elastometry has different trade names in US scanners of different manufacturers, such as VTTQ (Virtual Touch Tissue Quantification), Siemens; Natural Touch, Mindray; TE (Transient Elastography), Echosens; ElastQ and ElastPQ, Philips; SWE (Shear Wave Elastography), SuperSonic Imagine; etc. The technology of shear wave elastography was first implemented in FibroScan system for liver examination. Several studies on assessment of the thyroid gland with shear wave elastography were conducted [42, 56–62]. Shear wave elastography provides

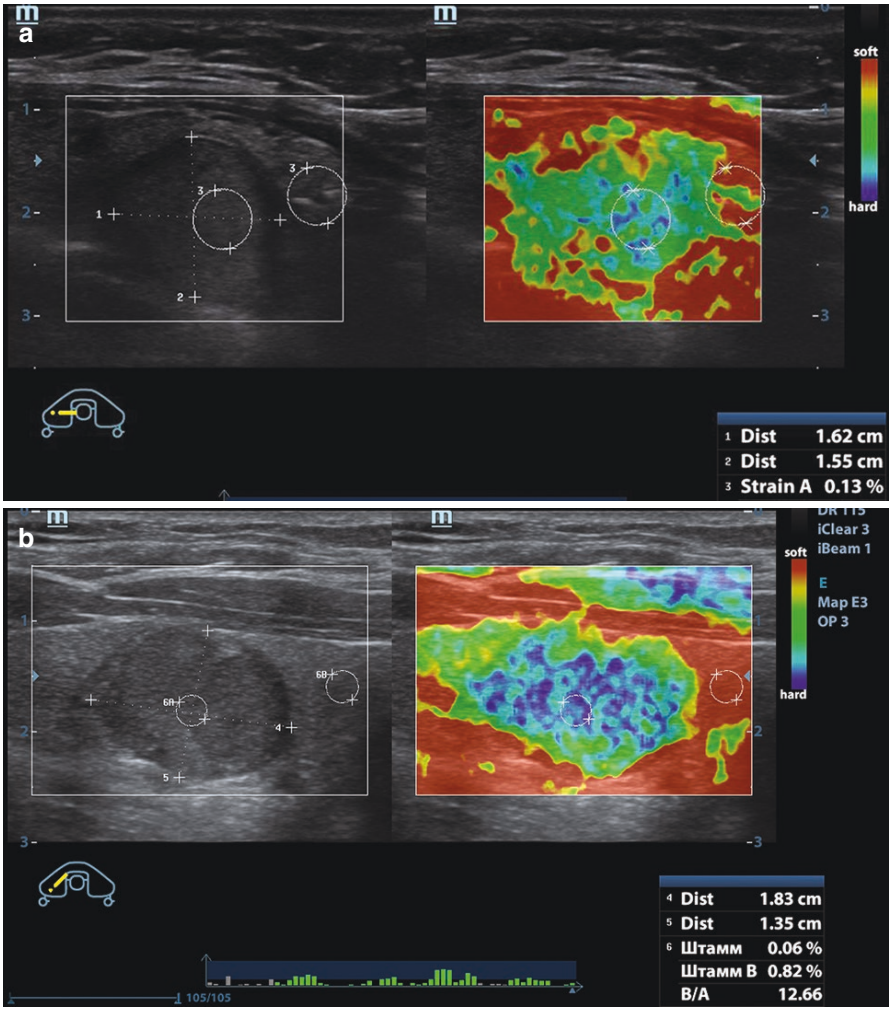

Fig. 1.15 (**a**, **b**) Measurement of the strain ratio. Echograms

more reliable data as compared with compression USE. It is less dependent on operator's experience and exhibits smaller interobserver variability [42, 63].

Definition of Young's modulus facilitates ultrasound differentiation of thyroid cancer [40]. The technique of the study is easy and fast to perform.

Stiffness (Young's modulus) of thyroid lesions over 50 kPa is usually suspicious for malignancy. According to Sebag et al. [61], Magri et al. [64], Ivanishina [40], and Mitkov et al. [18], the Young's modulus (stiffness) exhibits the following values: in AITD 5–69 kPa, in benign thyroid lesions 30–50 kPa, and in malignant tumors 15–150 kPa. The sensitivity of shear wave elastography in differential diagnosis of thyroid cancer is 85–100% with specificity of 78–94% [40, 42, 44, 58, 61].

The elasticity of thyroid lesion is usually compared with surrounding normal thyroid tissue or other structures and is presented with strain ratio index. Strain ratio, which is calculated as the ratio of Young's modulus (or shear swave velocity) in the lesion and the reference tissue, is a real quantitative parameter. In some cases, the scanner has the software to make similar calculation based on compression USE without measurement of specific digital values for every target area. In spite of the numerical expression, it is semiquantitative in these cases (Fig. 1.15). Malignant thyroid lesions in our own study demonstrated the average strain ratio of 3.4 ± 0.84.

According to Sencha et al. [44] and Ivanishina [40], the sensitivity of shear wave elastography in the diagnosis of thyroid cancer is 78–86% with specificity of 82–90%.

USE is a relatively new modality. Prospects for its practical use are not quite clear yet. Nevertheless, it supplies important additional data for assessment the character of tissue changes and is expected to facilitate detection of early cancer and differential diagnosis of thyroid lesions [40–42, 45, 50, 55].

Contrast-enhanced ultrasound (CEUS) is the technology that uses intravenously administered contrast agents for the assessment of vascularity. Its sensitivity is higher than the sensitivity of CDI and PDI [65–70].

The first reports on the use of contrast agents for diagnostic ultrasound were published in 1969 [71]. The first contrast-enhanced ultrasound studies of the thyroid gland with attempts to differentiate carcinomas, benign nodules, and follicular adenomas utilized Levovist® contrast medium [72]. The second-generation contrast agent SonoVue® (Lumason® for USA) (Bracco Swiss SA, Switzerland) is one popular ultrasound contrast medium approved for the use in many countries including Europe (EMA) and USA (FDA). It is proven safe and well tolerated.

CEUS in diagnosis of thyroid diseases is briefly discussed in available literature. Data on its diagnostic value is controversial. Recent studies demonstrated statistically significant differences in qualitative and quantitative characteristics of contrast enhancement of benign and malignant thyroid lesions [65, 68, 70, 73, 74].

The technique of CEUS is identical for different organs and is well described for liver study. Contrast agent is a suspension of sulfur hexafluoride microbubbles surrounded by a phospholipid shell. Since microbubbles are very fragile and easily destroyed with conventional US, CEUS requires special "contrast" option of ultrasound scanner that works with low mechanical index. The medium is administered as an intravenous bolus injection (Fig. 1.16a). It quickly arrives to the thyroid gland with intensive contrasting and rapidly washes out. In the "contrast" mode, the screens are usually divided into two parts

that show real-time grayscale image and contrast image (sepia colored). Video (cineloop) recording and time registration should start simultaneously with introduction of contrast agent and last not less than 180 s. It permits the analysis of the cine in all phases (arterial, venous, and delayed) after the end of the procedure.

SonoVue® is an intravascular contrast agent and circulates only within vessel lumen. It permits precise assessment of thyroid vascularity. Thyroid CEUS is characterized with some important qualitative criteria, such as intensity of blood supply, distribution of vessels, and dynamics of wash-in and washout. High vascularity of the thyroid parenchyma with dense rate of microvessels results in its strong overall

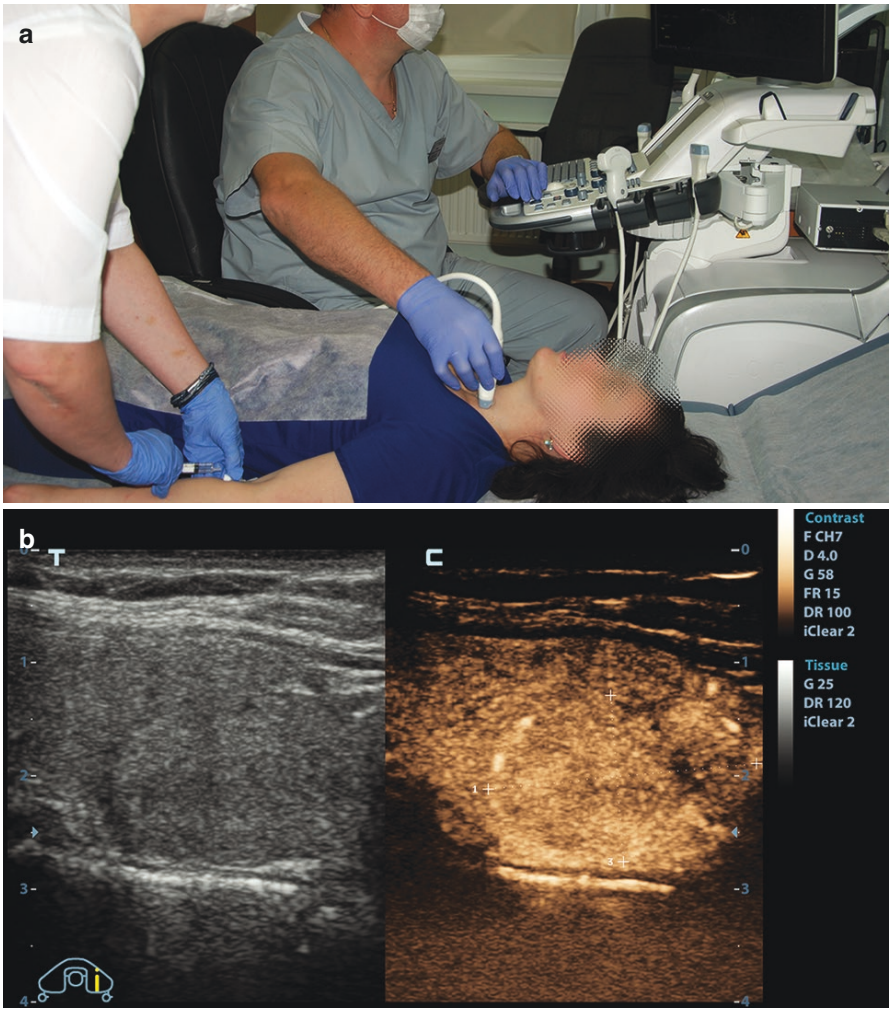

Fig. 1.16 Thyroid CEUS with 2.4 ml of SonoVue®. (**a**) Photo of the position of the patient and medical staff. (**b**) Arterial phase of contrast enhancement of a thyroid lesion. Sonogram. (**c**) Time-intensity curve of contrast enhancement. (**d**) Numerical data on contrast enhancement dynamics

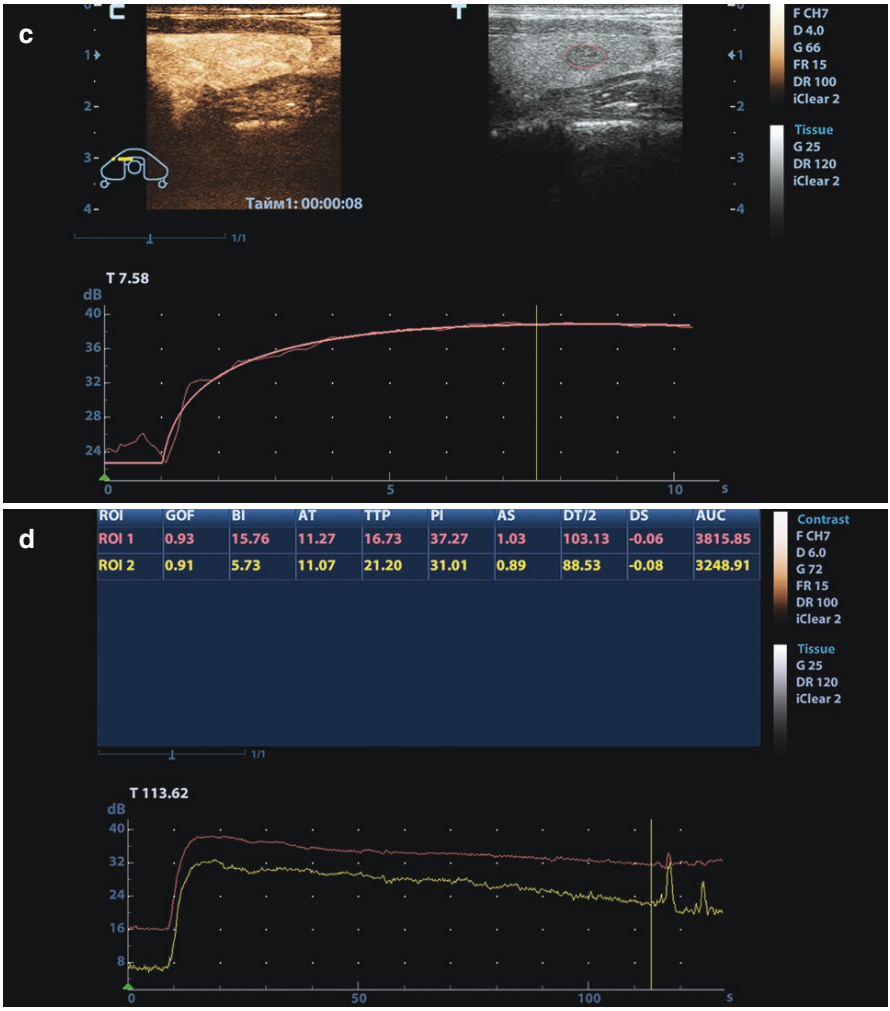

Fig. 1.16 (continued)

contrast enhancement. Diffuse and focal abnormalities affect vascularity and exhibit characteristic features with CEUS (Fig. 1.16b–d).

Thyroid lesions demonstrate various contrast patterns that contribute to the differential diagnosis. The below-listed principle features of accumulation and distribution of the contrast agent allow to identify the types of thyroid lesions [67, 75]:

1. Presence and intensity of contrast enhancement as compared with normal thyroid parenchyma:
   - No enhancement
   - Hypoenhancement

- Isoenhancement
- Hyperenhancement

2. Regularity of accumulation and distribution of contrast agent within the structure of the lesion:
   - Homogeneous enhancement
   - Heterogeneous enhancement
3. Clarity of margins with contrast enhancement:
   - Clear distinct margins
   - Rough indistinct margins
4. Velocity of contrast accumulation (wash-in) in comparison with normal thyroid parenchyma
   - Fast accumulation
   - Accumulation equal to normal parenchyma
   - Slow accumulation
5. Velocity of washout in comparison with normal thyroid parenchyma:
   - Fast washout
   - Washout equal to normal parenchyma
   - Slow washout

Benign thyroid nodules exhibit different contrast enhancement, but peripheral ring-shaped pattern is highly specific (sensitivity 83%, specificity 94%, positive predictive value 94%, negative predictive value 84%, overall accuracy 89%) [68]. Hypoenhancement is often registered in papillary thyroid cancer [65]. Heterogeneous contrast enhancement is a characteristic for malignant masses (sensitivity 98%, specificity 86%, positive predictive value 93%, negative predictive value 95%, overall accuracy 94%) [70].

Quantitative assessment of contrast enhancement is a more objective tool to obtain more reliable and reproducible data. It bases on the analysis of time-intensity curve in individual predefined areas and is a derivative of perfusion. The analysis with appropriate software covers the cine segment from the beginning of contrast agent injection to complete washout and can be displayed as time-intensity curve, table with numerical data, color map, etc. (Fig. 1.16c, d).

The following quantitative indexes are often calculated:

- Time to peak (TTP, s)—the time from the beginning of contrast medium injection to the maximum contrast enhancement
- Peak intensity (PI, Db)—maximum intensity of contrast enhancement within the marked area of interest
- Descend time to one-half (DT/2, s)—the time of washout from the maximum contrast enhancement to half the maximum value

There are several other quantitative indexes of CEUS. Contrast enhancement depends on individual physiological features of the patient. CEUS procedure is operator-dependent in many aspects. Hence, quantitative indicators of contrast enhancement are often presented in the form of indices obtained from the ratio of

values from ROI of normal surrounding thyroid parenchyma and ROI of the lesion to make evaluation even more objective. According to Turtulici et al. [76], mean values of peak index (peak thyroid/peak nodule) and TTP index (TTP thyroid/TTP nodule) were 1.78 ± 0.60 (range 1.13–2.61) and 0.56 ± 0.35 (range 0.22–1.16) for malignant nodules and 1.09 ± 0.52 (range 0.43–2.93) and 0.99 ± 0.13 (range 0.70–1.23) for benign ones, respectively. Setting a threshold at 0.60 for TTP index, the sensitivity was 66%, specificity was 100%, accuracy was 94%, and positive predictive value was 100%. CEUS also shows good correlation with cytological and histological features of such lesions.

According to Jiang et al. [77] and Sencha et al. [74], CEUS with quantitative analysis increases in the diagnostic value in differentiation of thyroid nodules with calcifications (sensitivity 90%, specificity 92%, positive predictive value 88%, negative predictive value 93%, accuracy 91%) compared with standard ultrasound (sensitivity 50%, specificity 77%, positive predictive value 59%, negative predictive value 69%, accuracy 66%). CEUS is a promising method of differential diagnosis of benign and malignant thyroid masses and may be a useful addition to FNAB [74, 78, 79].

CEUS has the following advantages over conventional US:

- High-quality imaging of vessels independently of insonation angle and blood velocity
- Qualitative and quantitative assessment of microcirculation, specification of tumoral neoangiogenesis
- Real-time study with continuous analysis of wash-in and washout
- Ionizing radiation free technology, as compared with contrast-enhanced CT, with the possibility of repeated studies and follow-up

However, CEUS also has several limitations and disadvantages, as follows:

- Increase in the cost of study.
- Transformation of a noninvasive US to an invasive one with regulations on aseptic processing and potential adverse effects.
- Hardware and operator dependency. US scanner with special option for CEUS with low mechanical index is essential; Doppler modes and other options cannot substitute it.
- Increase the time of the study and the need in additional personnel (to make intravenous injection, etc.).

The research data accumulated since introduction of CEUS into practice demonstrate important achievements in a number of complex diagnostic problems and rapid further development.

Fast *computer processing* of US images permits the three-dimensional (3D) reconstruction of the thyroid structure, lesions, the vascular tree, and surrounding tissues (Fig. 1.17). This option may be incorporated into ordinary US scanners as additional software. Data acquisition is achieved by a freehand scan with a

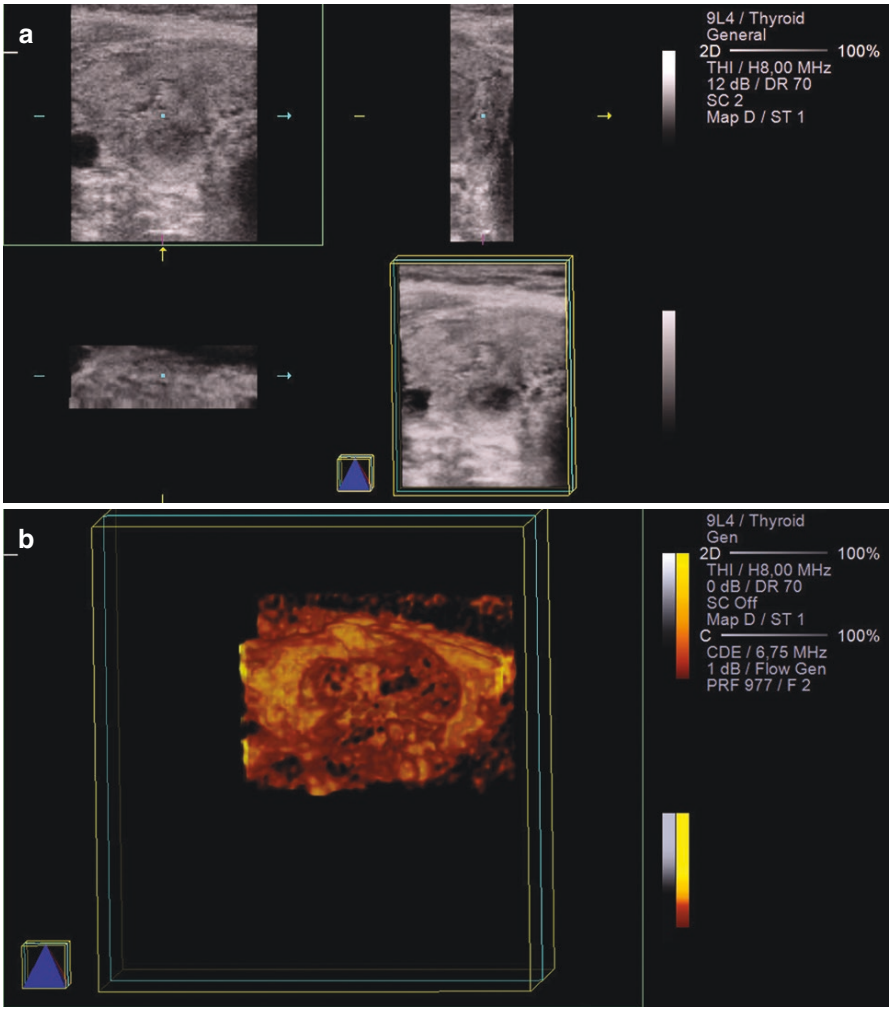

Fig. 1.17 3D image reconstruction. (**a**) Grayscale 3D image reconstruction. (**b**) 3D image reconstruction in power Doppler mode

conventional 2D probe. Such cases demand subsequent computational processing of the data obtained. Some scanners can be equipped with special probes for mechanical 3D scanning.

Real-time 3D ultrasound (4D) needs special US probes and high-class equipment. 3D image acquisition and reconstruction are performed quickly enough to allow real-time 3D visualization. 4D allows the spatial features of the thyroid to be defined more precisely, with a smaller dependence on noise artifacts. 3D imaging confers many advantages, such as the possibility of viewing planes that are usually inaccessible, and improved accuracy of volume estimation. It is useful for archiving US data in an objective form suitable for delayed analysis and digital transfer.

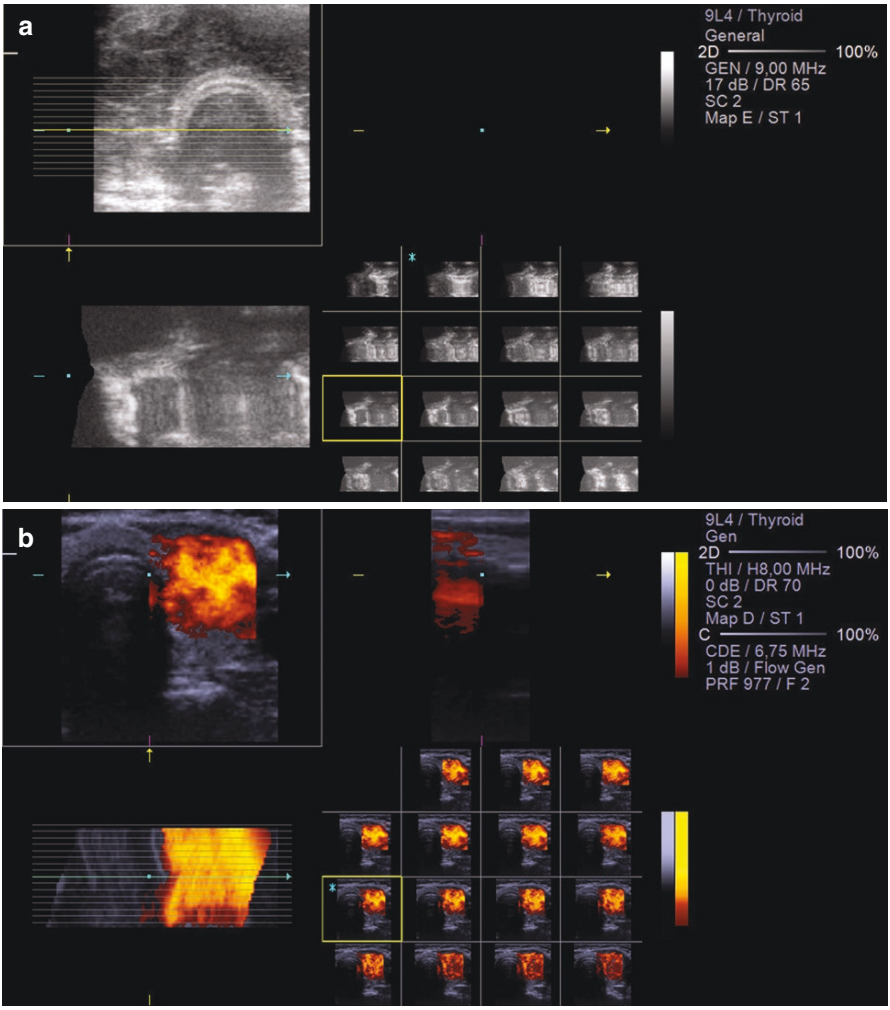

Fig. 1.18 Multislice view. (**a**) Grayscale. (**b**) Power Doppler mode

3D reconstruction of vascular structures (3D power Doppler imaging – 3DPD) enables more specific diagnoses of neoplasms based on the objective visual data for the structure and the intensity of lesion vascularity and the spatial relationships of different vascular structures of the neck (Fig. 1.17b).

In multislice viewing, a 3D US image is converted into a series of consecutive sections corresponding to intervals of 0.5–5 mm in any plane, similar to CT representations (Fig. 1.18). This aids in the analysis of thyroid images and makes it objective.

Panoramic scan is an option that permits an extended field of view, thus simplifying the visualization and measurement of long structures (Fig. 1.19). This helps when attempting to assess the precise dimensions of the thyroid and to calculate the volume of the lobes and the whole gland. It allows complete imaging of the thyroid and surrounding structures, which is especially important in extended affection, invasion, and regional metastases.

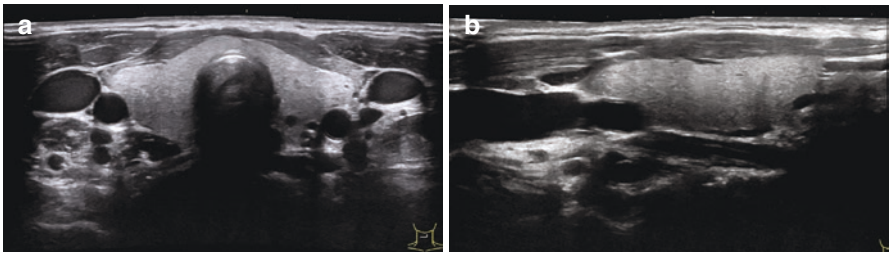

Fig. 1.19 (**a**, **b**) Panoramic scan

Enhancements in traditional procedures and advances in new technologies facilitate continuous improvements in the accuracy and value of diagnostic ultrasound.

References

1. Davydov MI, editor. Thyroid cancer. Oncology. Clinical recommendations. Moscow: Izdatyelskaya gruppa RONTS; 2015. (Book in Russian).
2. Fadeev VV. Nodular lesions of the thyroid gland: international algorithms and domestic clinical practice. Vrach. 2002;7:12–6. (Article in Russian).
3. Kotlyarov PM, Kharchenko VP, Alexandrov YK, et al. Ultrasound diagnosis of the diseases of the thyroid gland. Moscow: Vidar-M; 2009. (Book in Russian).
4. Schenke S, Zimny M. Combination of sonoelastography and TIRADS for the diagnostic assessment of thyroid nodules. Ultrasound Med Biol. 2018;44(3):575–83.
5. Shin JH, Baek JH, Chung J, et al. Ultrasonography diagnosis and imaging-based management of thyroid nodules: revised Korean society of thyroid radiology consensus statement and recommendations. Korean J Radiol. 2016;17(3):370–95.
6. Tessler FN, Middleton WD, Grant EG, et al. ACR thyroid imaging, reporting and data system (TI-RADS): white paper of the ACR TI-RADS committee. J Am Coll Radiol. 2017;14(5):587–95.
7. Baskin HJ, Duick DS, Levine RA, editors. Thyroid ultrasound and ultrasound-guided FNA. Berlin: Springer; 2013.
8. Biersack HJ, Grünwald F. Thyroid cancer. Berlin: Springer; 2005.
9. Choi YM, Kim WG, Kwon H, et al. Changes in standardized mortality rates from thyroid cancer in Korea between 1985 and 2015: analysis of Korean national data. Cancer. 2017;123(24):4808–14.
10. Kouvaraki MA, Shapiro SE, Fornage BD, et al. Role of preoperative ultrasonography in the surgical management of patients with thyroid cancer. Surgery. 2003;134(6):946–54.
11. Paschke R, Cantara S, Crescenzi A, et al. European Thyroid Association Guidelines regarding thyroid nodule molecular fine needle aspiration cytology diagnostics. Eur Thyroid J. 2017;6(3):115–29.
12. Sofferman RA, Ahuja AT, editors. Ultrasound of the thyroid and parathyroid glands. Berlin: Springer; 2012.
13. Cooper DS, Doherty GM, Haugen BR, et al. Revised American Thyroid Association management guidelines for patients with thyroid nodules and differentiated thyroid cancer. Thyroid. 2009;19(11):1167–214.
14. Haugen BR, Alexander EK, Bible KC, et al. 2015 American Thyroid Association management guidelines for adult patients with thyroid nodules and differentiated thyroid cancer: the American Thyroid Association guidelines task force on thyroid nodules and differentiate d thyroid cancer. Thyroid. 2016;26:1–133.

15. Morris LG, Sikora AG, Tosteson TD, Davies L. The increasing incidence of thyroid cancer: the influence of access to care. Thyroid. 2013;23(7):885–91.
16. Kaprin AD, Starinsky VV, Petrova GV, editors. The state of oncological care for the population of Russia in 2017. Moscow: P.A.Hertsen Moscow Oncology Research Center—Branch of Federal State Budgetary Institution National Medical Research Radiological Center of the Ministry of Healthcare of the Russian Federation; 2018. (Book in Russian).
17. Duick DS, Levine RA, Lupo MA, editors. Thyroid and parathyroid ultrasound and ultrasound-guided FNA. Berlin: Springer; 2018.
18. Mitkov VV, Ivanishina TV, Mitkova MD. Shear wave elastography in multiparametric ultrasound diagnosis of thyroid cancer. Ultrazvukovaya i funkcionalnaya diagnostika. 2016;1:13–28. (Article in Russian).
19. Du J, Bai X, Lu Y, et al. Diagnostic efficacy of ultrasonographic characteristics of thyroid carcinoma in predicting cervical lymph node metastasis. Ultrasound Med Biol. 2016;42(1):68–74.
20. Rumyantsev PO, Ilyin AA, Rumyantseva UV, Sayenko VA. Thyroid cancer, modern approaches to diagnosis and treatment. Moscow: GEOTAR-Media; 2009. (Book in Russian).
21. Sencha AN. Ultrasonic visualization of malignant tumors of the thyroid gland. Ultrazvukovaya i funkcionalnaya diagnostika. 2008;2:20–9. (Article in Russian).
22. Howry DH, Holmes JH, Cushman CR, Posakony GJ. Ultrasonic visualization of living organs and tissues; with observations on some disease processes. Geriatrics. 1955;10(3):123–8.
23. Fujimoto Y, Oka A, Omoto R, Hirose M. Ultrasound scanning of the thyroid gland as a new diagnostic approach. Ultrasonics. 1967;5:177.
24. Blum M, Weiss B, Hernberg J. Evaluation of thyroid nodules by A-mode echography. Radiology. 1971;101:651–6.
25. World Health Organization. Assessment of iodine deficiency disorders and monitoring their elimination. A guide for programme managers. 2nd ed. Geneva: WHO; 2002. Available from: http://www.who.int/nutrition/publications/micronutrients/iodine_deficiency/WHO_NHD_01.1/en/.
26. Cui Y, Zhang Z, Li S, et al. Diagnosis and surgical management for retrosternal thyroid mass. Chin Med Sci J. 2002;17(3):173–7.
27. Sciume C, Geraci G, Pisello F. Substernal goitre. Personal experience. Ann Ital Chir. 2005;76(6):517–21.
28. Vlasov PV. Imaging diagnosis of the diseases of the chest. Moscow: Vidar; 2006. (Book in Russian).
29. Pinsky SV, Kalinin AP, Beloborodov VA. Diagnosis of diseases of the thyroid gland. Moscow: Medicine; 2005. (Book in Russian).
30. Ayache S, Mardyla N, Tramier B, Strunski V. Clinical signs and correlation with radiological extent in a series of 117 retrosternal goitre. Rev Laryngol Otol Rhinol (Bord). 2006;127(4):229–37.
31. Mackle T, Meaney J, Timon C. Tracheoesophageal compression associated with substernal goitre. Correlation of symptoms with cross-sectional imaging findings. J Laryngol Otol. 2006;26:1–4.
32. Kazakevich VI. Possibilities of mediastinal ultrasound in substernal spreading of thyroid tumors. Sonoace Int. 2007;16:58–65.. Article in Russian
33. Pishchik VG. Mediastinal neoplasms: the principles of differential diagnosis and surgical treatment. PhD thesis, S-Petersburg. 2008. (Book in Russian).
34. Ignjatovic M. Intrathoracic goiter. Vojnosanit Pregl. 2001;58(1):47–63.
35. Belashkin II, Kulikova AD, Kochetkov AV, Kulikov MP. The value of the second tissue harmonic in the diagnosis of colloid nodes of the thyroid gland. In: Reports of the 4th Congress of the Russian Association of Specialists in ultrasound diagnostics in medicine. Moscow: 2003. p. 209. (Article in Russian).
36. Khadra H, Bakeer M, Hauch A, et al. Is vascular flow a predictor of malignant thyroid nodules? A meta-analysis. Gland Surg. 2016;5(6):576–82.
37. Kahaly GJ, Bartalenab L, Hegedüs L, et al. 2018 European Thyroid Association Guideline for the management of Graves' hyperthyroidism. Eur Thyroid J. 2018;7:167–86.

38. Joish UK, Kavitha Y, Reddy RH, et al. Doppler indices of superior thyroid artery in clinically euthyroid adults. Indian J Radiol Imaging. 2018;28(1):10–3.
39. Palaniappan MK, Aiyappan SK, Ranga U. Role of gray scale, color Doppler and spectral Doppler in differentiation between malignant and benign thyroid nodules. J Clin Diagn Res. 2016;10(8):TC01–6.
40. Ivanishina TV. Diagnostic possibilities of shear wave elastography in thyroid disease. PhD thesis, Moscow: 2017. (Book in Russian).
41. Lindop JE, Treece GM, Gee AH, Prager RW. 3D elastography using freehand ultrasound. J Ultrasound Med Biol. 2006;32(4):529–45.
42. Mitkov VV, Ivanishina TV, Mitkova MD. Ultrasound examination of the unchanged thyroid gland with the use of shear wave elastography technology. Ultrazvukovaya i funkcionalnaya diagnostika. 2014;6:13–20. (Article in Russian).
43. Ophir J, Cespedes I, Ponnekanti H, et al. Elastography: a quantitative method for imaging the elasticity of biological tissues. Ultrason Imaging. 1991;13:111–34.
44. Sencha AN, Mogutov MS, Patrunov YN, et al. Quantitative and qualitative parameters of ultrasonic elastography in the diagnosis of thyroid cancer. Ultrazvukovaya I funkcionalnaya diagnostika. 2013;5:85–98. (Article in Russian).
45. Tanaka K, Fukunari N, Igarashi T, et al. Evaluation of thyroid malignant tumor using real – team tissue elastography. Ultrasound Med Biol. 2006;32(5):93.
46. Zubarev AR, Fedorova VN, Demidova AK, et al. Ultrasonic elastography as a new step in the differential diagnosis of thyroid nodules: a literature review and preliminary clinical data. Medicinskaya Vizualizaciya. 2010;1:11–6. (Article in Russian)
47. Itoh A, Ueno E, Tohno E, et al. Breast disease: clinical application of US elastography for diagnosis. Radiology. 2006;239:341–50.
48. Rago T, Vitti P. Role of thyroid ultrasound in the diagnostic evaluation of thyroid nodules. Best Pract Res Clin Endocrinol Metab. 2008;22:913–28.
49. Park SH, Kim SJ, Kim E, et al. Interobserver agreement in assessing the sonographic and elastographic features of malignant thyroid nodules. AJR. 2009;193(5):W416–23.
50. Cantisani V, Grazhdani H, Ricci P, et al. Q-elastosonography of solid thyroid nodules: assessment of diagnostic efficacy and interobserver variability in a large patient cohort. Eur Radiol. 2014;24:143–50.
51. Fukunari N, Arai K, Naakamura A, et al. Clinical evaluation of elastography for the differential diagnosis of thyroid follicular tumors. Abstracts from the 12th Congress of World Federation for Ultrasound in Medicine and Biology. J Ultrasound Med Biol. 2009;35(S8):230.
52. Vasiliev DA, Kostromina EV, ZA-G R, et al. Ways to improve the diagnostic significance of sonoelastography in differential diagnosis of thyroid nodules. Clin Exp Thyroid. 2014;10(1):38–43. (Article in Russian).
53. Wang Y, Dan HJ, Dan HY, et al. Differential diagnosis of small single solid thyroid nodules using realtime ultrasound elastography. J Int Med Res. 2010;38(2):466–72.
54. Garra BS. Tissue elasticity imaging using ultrasound. Appl Radiol. 2011;2:24–30.
55. Sencha AN, Mogutov MS, Sergeeva ED, Shmelev DM. Sonoelastografiya and the newest technologies of ultrasonic research of a cancer of a thyroid gland. Moscow: Vidar; 2010. (Book in Russian).
56. Borsukov AV, Morozova TG, Kovalev AV, et al. Standardized technique of compression thyroid ultrasound of the thyroid gland. Endocr Surg. 2014;1:55–61. (Article in Russian).
57. Calvete AC, Mestre JD, Gonzalez JM, et al. Acoustic radiation force impulse imaging for evaluation of the thyroid gland. J Ultrasound Med. 2014;33(6):1031–40.
58. Friedrich-Rust M, Sperber A, Holzer K, et al. Real-time elastography and contrast-enhanced ultrasound for the assessment of thyroid nodules. Exp Clin Endocrinol Diabetes. 2010;118:602–9.
59. Monpeyssen H, Tramalloni J, Poiree S, et al. Elastography of the thyroid. Diagn Interv Imaging. 2013;94(5):535–44.
60. Pomortsev AV, Gudkov GV, Degtyareva YS, et al. Possibilities of shear wave elastography in differential diagnostics of focal thyroid pathology. Radiat Diagn Ther. 2011;3:60–6. (Article in Russian).

61. Sebag F, Vaillant-Lombard J, Berbis J, et al. Shear wave elastography: a new ultrasound imaging mode for the differential diagnosis of benign and malignant thyroid nodules. J Clin Endocrinol Metab. 2010;95(12):5281–8.
62. Sencha AN. Ultrasound diagnostics. Surface-located organs. Moscow: Vidar M Publishing House; 2015. (Book in Russian).
63. Osipov LV. Ultrasound diagnostic devices. Modes, methods and techniques. Moscow: Izomed; 2011. (Book in Russian).
64. Magri F, Chytiris S, Capelli V, et al. Shear wave elastography in the diagnosis of thyroid nodules: feasibility in the case of coexistent chronic autoimmune Hashimoto's thyroiditis. Clin Endocrinol. 2012;76(1):137–41.
65. Ma BY, Jin Y, Suntdar PS, et al. Contrast-enhanced ultrasonography findings for papillary thyroid carcinoma and its pathological bases. Sichuan Da Xue Xue Bao Yi Xue Ban. 2014;45(6):997–1000.
66. Sencha AN, Mogutov MS, Patrunov YN, et al. Ultrasound with contrast agents. Moscow: Vidar; 2016. (Book in Russian).
67. Sencha EA. Ultrasound examination with contrast enhancement in the diagnosis of thyroid tumors. REJR. 2017;7(3):44–52. (Article in Russian).
68. Zhang B, Jiang YX, Liu JB, et al. Utility of contrast-enhanced ultrasound for evaluation of thyroid nodules. Thyroid. 2010;20(1):51–7.
69. Zhang Y, Zhou P, Tian SM, et al. Usefulness of combined use of contrast-enhanced ultrasound and TI-RADS classification for the differentiation of benign from malignant lesions of thyroid nodules. Eur Radiol. 2017;27:1527–36.
70. Zhao RN, Zhang B, Yang X, et al. Diagnostic value of contrast enhanced ultrasound of thyroid nodules coexisting with Hashimoto's thyroiditis. Zhongguo Yi Xue Ke Xue Yuan Xue Bao. 2015;37(1):66–70.
71. Gramiak R, Shah P, Cramer D. Ultrasound cardiography: contrast studies in anatomy and function. Radiology. 1969;92:939.
72. Spiezia S, Farina R, Cerbone G. Analysis of time/intensity enhancement curves after echocontrast agents injection in thyroid nodules evaluation: preliminary report. In: Ultrasound in medicine and biology 26(S2). Abstracts from the 9th Congress of WFUMB. Florence. Italy. 2000; p. A181.
73. Schleder S, Janke M, Agha A, et al. Preoperative differentiation of thyroid adenomas and thyroid carcinomas using high resolution contrast-enhanced ultrasound (CEUS). Clin Hemorheol Microcirc. 2015;61(1):13–22.
74. Sencha EA, Sencha AN, Penyaeva EI, et al. The use of quantitative analysis of ultrasound with contrast enhancement in the differential diagnosis of focal changes in the thyroid gland. Ultrazvukovaya i funkcionalnaya diagnostika. 2018;2:12–26. (Article in Russian).
75. Yuan Z, Quan J, Yunxiao Z, et al. Contrast-enhanced ultrasound in the diagnosis of solitary thyroid nodules. J Cancer Res Ther. 2015;11:41–5.
76. Turtulici G, Orlandi D, Fabbro E, et al. Contrast-enhanced ultrasound (CEUS) quantitative evaluation of histologically proven thyroid nodules. In: Radiological Society of North America 2011 Scientific Assembly and Annual Meeting, November 26 - December 2, 2011, Chicago IL. 2011. http://archive.rsna.org/2011/11034465.html.
77. Jiang J, Huang L, Zhang H, et al. Contrast-enhanced sonography of thyroid nodules. J Clin Ultrasound. 2015;43(3):153–6.
78. Sencha AN, Patrunov Yu N, Mogutov MS, et al. Thyroid cancer: US THI-RADS classification, ultrasound qualitative and quantitative elastography, contrast ultrasound. In: Collection of scientific papers "Nevsky Radiologichesky Forum-2015". St. Petersburg: ELBI-SPb; 2015. pp. 605–8. (Book in Russian).
79. Yu D, Han Y, Chen T. Contrast-enhanced ultrasound for differentiation of benign and malignant thyroid lesions: meta-analysis. Otolaryngol Head Neck Surg. 2014;151(6):909–15.

Ultrasound Image of the Normal Thyroid Gland

2

Yury N. Patrunov, Alexander N. Sencha, Ekaterina A. Sencha, Ella I. Peniaeva, Liubov A. Timofeyeva, and Munir G. Tukhbatullin

The thyroid gland is normally located in the midline of the neck about 1–3 cm above the breastbone and clavicle. It consists of right and left lobes and the isthmus (Fig. 2.1a). A pyramidal lobe arising cranially from the isthmus (more often from the left part) toward the hyoid bone may sometimes be observed. The thyroid is usually a butterfly-shaped gland. It can sometimes take a different shape, depending on individual features.

The thyroid surrounds the larynx and trachea, which are situated in the central part of the neck dorsally from the isthmus and medially from the thyroid lobes and

Y. N. Patrunov (✉)
Department of Ultrasound Diagnostics of the Center for Radiological Diagnostics, Non-State Healthcare Institution "Yaroslavl Railway Clinic of JSC "Russian Railways", Yaroslavl, Russia

A. N. Sencha
Department of Visual and Functional Diagnostics of National Research Center for Obstetrics, Gynecology and Perinatology, Ministry of Healthcare of the Russian Federation, Moscow, Russia

E. A. Sencha
Ultrasound Diagnostics Department, Medical Diagnostic Center, Moscow, Russia

E. I. Peniaeva
Department of Ultrasound Diagnostics, Center for Radiological Diagnostics of Non-State Healthcare Institution Yaroslavl Railway Clinic of JSC "Russian Railways", Yaroslavl, Russia

L. A. Timofeyeva
Department for Internal Diseases Propaedeutic, Course of Diagnostic Radiology of Medical Faculty of Federal State Budget Educational Institution of Higher Education "I. N. Ulianov Chuvash State University", Cheboksary, Russia

M. G. Tukhbatullin
Department of Ultrasound Diagnostics, Kazan State Medical Academy – Branch Campus of the Federal State Budget Educational Institution of Further Professional Education, "Russian Medical Academy of Continuing Professional Education" of the Ministry of Healthcare of the Russian Federation, Kazan, Russia

A. N. Sencha, Y. N. Patrunov (eds.), *Thyroid Ultrasound*,
https://doi.org/10.1007/978-3-030-14451-7_2

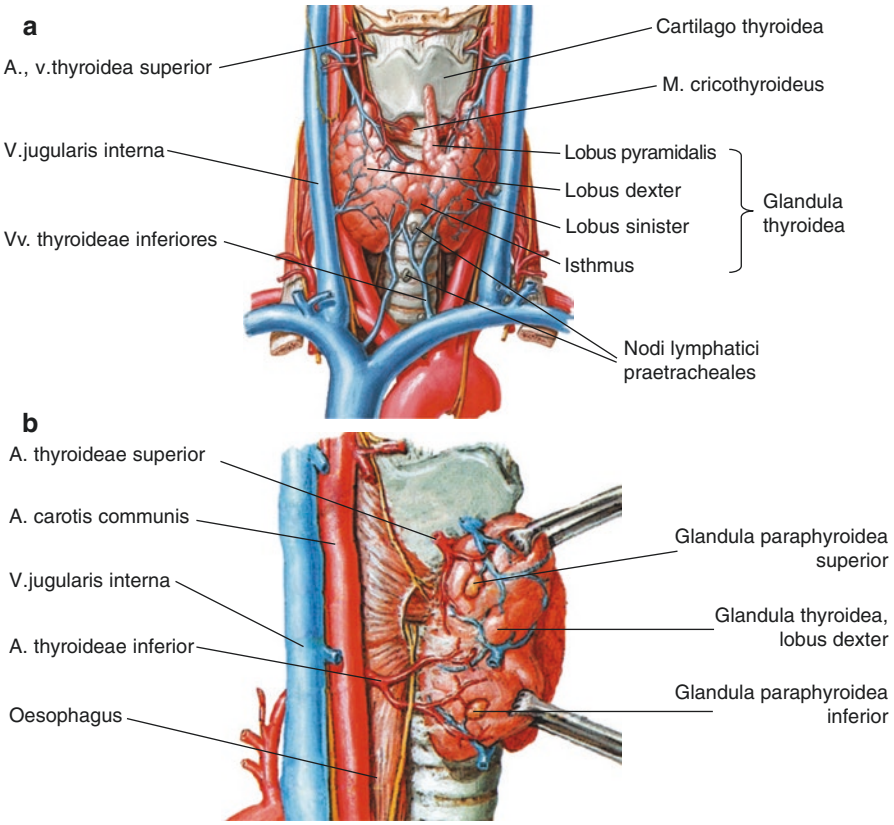

Fig. 2.1 Thyroid location, scheme [1]. (**a**) Front view. (**b**) Sagittal view

imaged as an arch-shaped structure with acoustic shadow. The gland is covered ventrally and laterally by the symmetric prethyroid muscles (sternothyroid, sternohyoid, the superior belly of the omohyoid, and partially by the sternocleidomastoid), subcutaneous fat, and skin.

The vascular bundles of the neck are represented by the symmetric common carotid arteries (CCA) and internal jugular veins (IJV) (Fig. 2.1a, b). The CCA is sonographically detected as a large incompressible vessel laterally adjacent to the thyroid lobes. It shows an arterial spectrum upon PW Doppler interrogation. IJV exhibits venous blood flow, has thinner walls, and can be completely compressed with the US probe. It is located laterally to the CCA.

The esophagus is usually observed neighboring the posterior and medial margins of the left thyroid lobe. It looks like a pipe-shaped stricture with differentiation of the wall layers and a rough inner contour (Fig. 2.2). If the patient turns the head to the left, the esophagus changes its location and can be detected adjacent to the posterior inner aspect of the right thyroid lobe (Fig. 2.3). Swallowing can help to differentiate it from neck lesions. Peristalsis is easily discerned when hyperechoic masses pass caudally through its lumen.

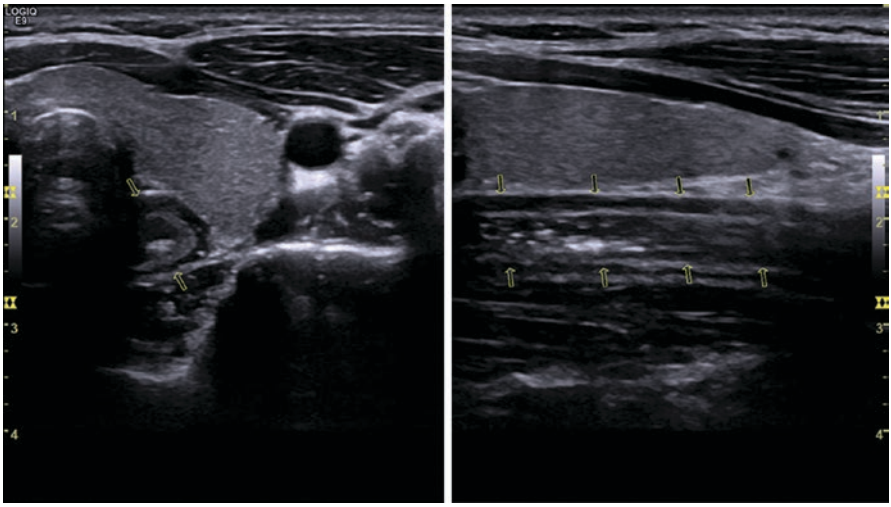

Fig. 2.2 US view of the esophagus (arrows). Transverse and longitudinal scans

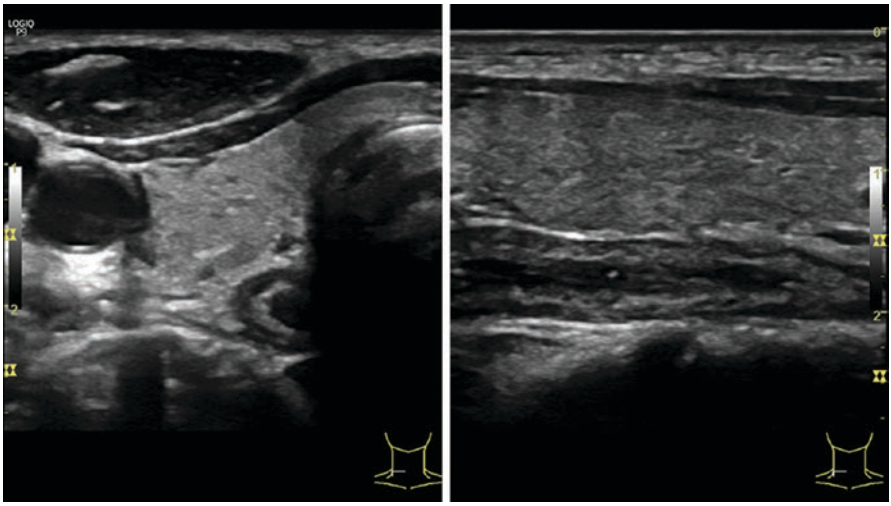

Fig. 2.3 Right-sided location of the esophagus (arrow) on US with the patient's head turned left

Traditionally accepted that the normal volume of the thyroid gland in adults is 7.7–25 cm^3 in men and 4.4–18 cm^3 in women [2]. The width of the thyroid lobe in adults is about 13–18 mm, its depth is 16–18 mm, its length is 45–60 mm, and the depth of the isthmus is 2–6 mm.

Sonographically, normal thyroid shows isoechoic homogeneous echostructure, accurate regular margins, and an echogenic capsule (Figs. 2.4 and 2.5). Echodensity of the thyroid parenchyma is usually compared with the echodensity of the normal submandibular salivary gland and is isoechoic. It has higher echodensity than the

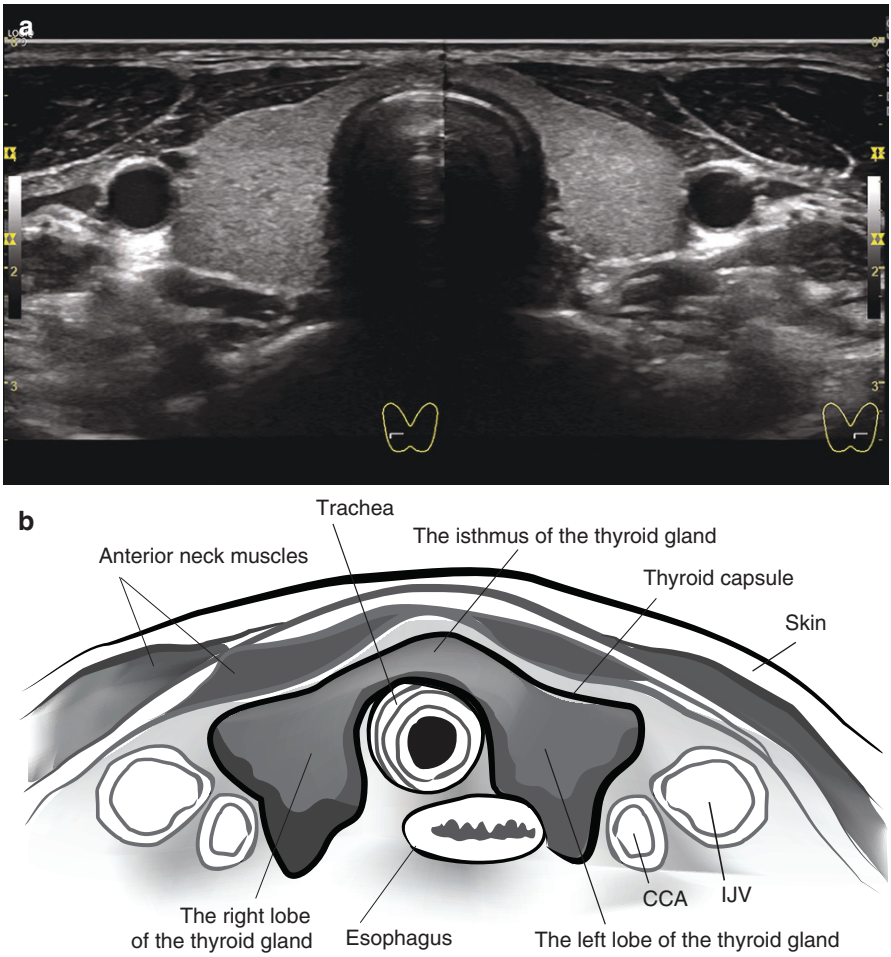

Fig. 2.4 Normal thyroid US. (**a**) Transverse plane grayscale US image. (**b**) Scheme

neck muscles. The structure of the glandular tissue is considered homogeneous in cases with fine granularity that does not exceed 1 mm. The presence of areas that differ in echodensity from the normal background is interpreted as heterogeneous echostructure. This may correspond to diffuse or nodular thyroid pathology.

An anatomical classification that divides the thyroid into segments has been suggested [3]. However, it is reasonable to describe the superior, middle, and inferior segments that correspond to one-third of the length of each lobe in daily sonographic practice. The anterior (ventral) and posterior (dorsal) surfaces, paratracheal and paravasal sites, and the right, left, superior, and inferior segments of the isthmus may be described to specify the locations of lesions.

The thyroid gland has a pyramidal lobe in about 50% of cases. This arises from the upper part of the isthmus or from the adjacent portion of either lobe and courses toward

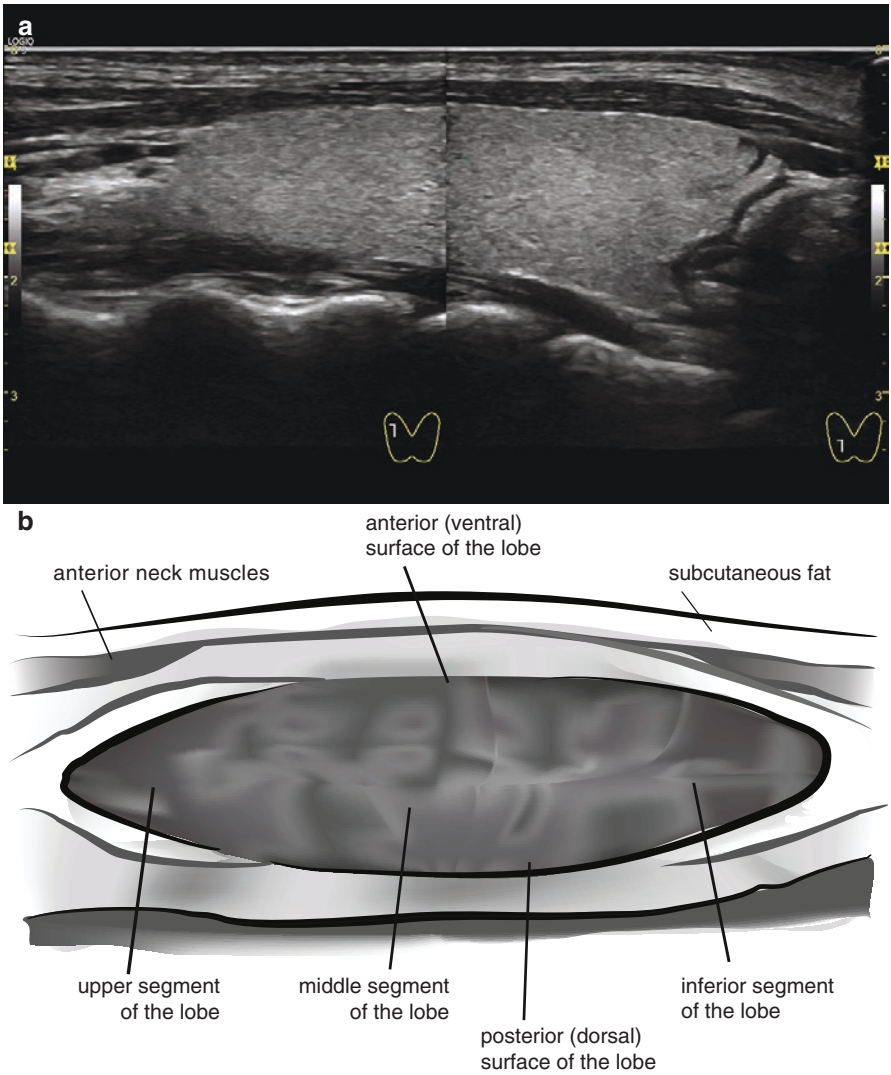

Fig. 2.5 Normal thyroid US. (**a**) Longitudinal plane grayscale US image. (**b**) Scheme

the hyoid bone. However, thyroid US reveals it in only 10–15% of cases. This lobe most often appears similar in echodensity, homogeneity, and vascularity to the isthmus and lobes (Fig. 2.6). The posterior surface of the thyroid lobe, especially in the inferior segment, may have an outpoach, named Zuckerkandl tubercle, separated from the main lobe mass with fibrous hyperechoic posterior septum (Fig. 2.7). It is identical in the structure and vascularity to the parenchyma of the lobe but often exhibits decreased echodensity due to posterior shadowing from the septum. This posterior process may mimic a thyroid or parathyroid lesion and cause difficulties in interpretation.

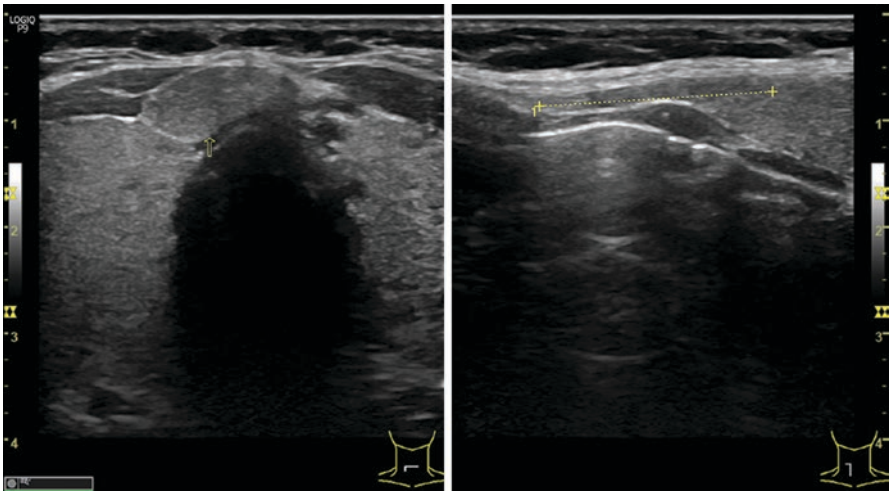

Fig. 2.6 Pyramidal lobe of the thyroid gland. Grayscale US

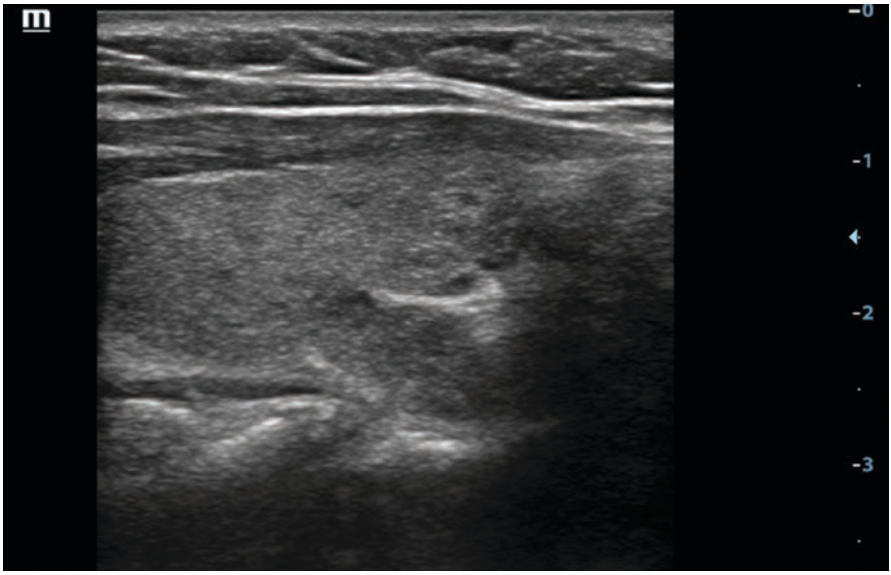

Fig. 2.7 Posterior septum (Zuckerkandl tubercle) of the right thyroid lobe. Grayscale US

The thyroid is supplied with blood from two paired superior thyroid arteries (STA) and inferior thyroid arteries (ITA). The fifth artery, the thyroid ima, which supplies the isthmus with blood, is sometimes defined. The average gauge of the arteries does not exceed 1–2 mm. The STA form the first branch of the external carotid artery. In rare cases, they depart from the common carotid artery. The STA split off at the level of the upper poles of the thyroid lobes into three branches:

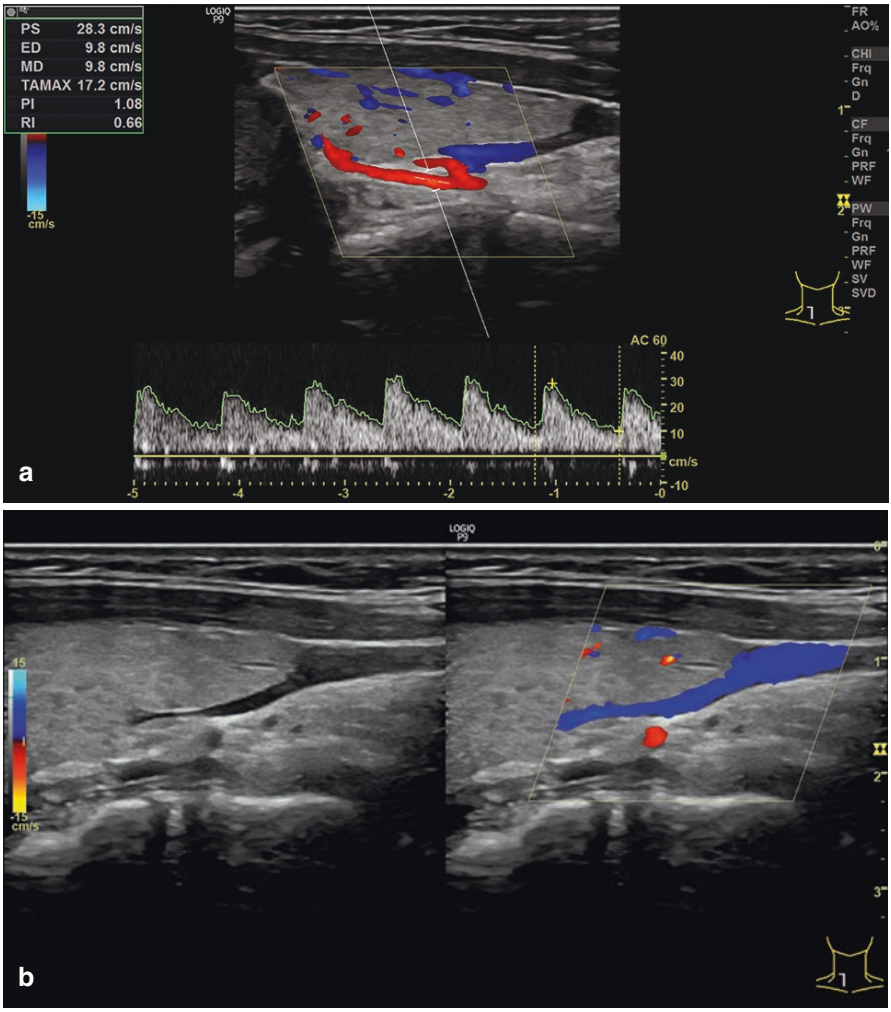

Fig. 2.8 Thyroid vessels. Sonograms. (**a**) Inferior thyroid artery. Grayscale, CDI, and PW Doppler. (**b**) Inferior thyroid vein

anterior, inferior, and internal (the isthmus branch). The ITA usually branches from the thyrocervical trunk, which emerges from the proximal part of the subclavian artery. The ITA divides into three branches (inferior, superior, and deep) close to the back surface of the inferior segment or the inferior pole of the thyroid lobe (Fig. 2.8a). Congenital anomalies, including anomalies in the number and location of the arteries, may be observed in rare cases. Thyroid arteries are well-defined with color mapping.

Statistically significant differences in blood flow velocity with PW Doppler in the STA and ITA in men and women have not been discerned. The following ranges for

blood flow in the thyroid arteries are reported normal: PSV in the STA, 17 ± 1 to 24 ± 6 cm/s; in the ITA, 16 ± 1 to 23 ± 7 cm/s; EDV in the STA, 7 ± 1 to 8 ± 3 cm/s; in the ITA, 6 ± 0.3 to 10 ± 3 cm/s; RI in the ITA, 0.58 ± 0.1; in the STA, 0.56 ± 0.01 to 0.66 ± 0.05; PI in the STA, 0.96 ± 0.34 to 1.06 ± 0.54; and in the ITA, 0.85 ± 0.24 to 0.88 ± 0.26 [4, 5]. Struchkova [6] defines the following norms for blood flow in all four arteries: PSV, 10.4–28.1 cm/s; EDV, 3.1–9.6 cm/s; RI, 0.5–0.75; and PI, 0.7–1.2.

The venous blood from the thyroid is drained via the twin upper, middle, and inferior thyroid veins (Fig. 2.8b). As a rule, they emerge from the venous plexus of the thyroid, accompany the corresponding arteries, and drain into the IJV. The diameters of the thyroid veins do not usually exceed 2–2.5 mm. The blood flow in the thyroid veins is related to breathing. The velocity of the blood flow does not show significant any difference between the left and the right sides. The average blood flow velocity in the thyroid veins registered with PW Doppler ranges from 1.0 to 36.0 cm/s.

Individual color spots in thyroid parenchyma are normally detected with CDI and PDI. They may be of various sizes and are usually rather symmetric with a relatively uniform distribution (Fig. 2.9). The average color pixel density (CPD) in a normal thyroid is 5–15%. The average number of color cartograms of various vessels is 0.4–2.5 in 1 cm^2, and the number of color pixels within the normal thyroid lobe ranges from 5 to 10 [6].

Normal thyroid parenchyma exhibits uniform medium elasticity with compression USE. It is evenly colored with fine- and medium-grained texture, quite symmetrical in all aspects (Fig. 2.10a, b). Quantitatively assessed, it exhibits the average Young's modulus of 12–23 kPa [7–12]. Our own research defined the average value of the Young's modulus in the normal thyroid of 11.3 (9.8–22.0) kPa and an average shear wave velocity of the Virtual Touch Tissue Quantification technology (ARFI) of 2.8 (1.7–3.5) m/s (Fig. 2.10c, d).

Arda et al. [7] and Mitkov et al. [12] reported extremely weak correlation between the indices of stiffness of thyroid tissue with patient's age and sex. No correlation between the stiffness with Doppler data and thyroid volume were detected.

Contrast enhancement is not necessary with normal thyroid ultrasound. Normal thyroid parenchyma exhibits intense, uniform, and symmetrical enhancement. It washes out slowly and regularly (Fig. 2.11).

The Example US Report in the Normal Thyroid

- First name, middle initial, last name:
- Age:
- Date:
- The number of case history:
- US scanner:

The thyroid gland is typically located with regular well-defined margins and homogeneous isoechoic structure. The capsule is uniform and continuous on all extent. Cystic and solid lesions are not detected.

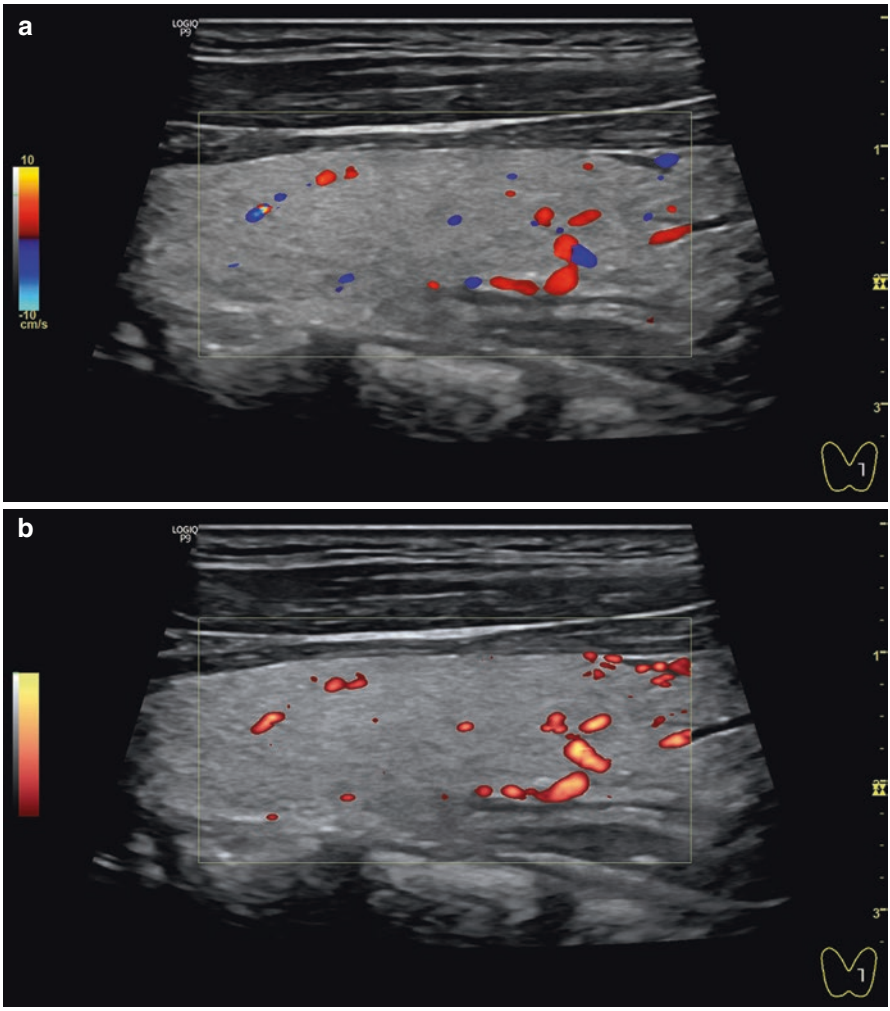

Fig. 2.9 Normal vascular pattern with thyroid US. (**a**) CDI. (**b**) PDI

The depth of the *isthmus*—4 mm			
Right lobe		Left lobe	
Depth	15 mm	Depth	14 mm
Width	17 mm	Width	14 mm
Length	48 mm	Length	47 mm
Volume	5.9 cm^3	Volume	4.4 cm^3

The total volume 10.3 cm^3 does not exceed the upper limit.

The vascular pattern of the parenchyma is normal and symmetric with CDI and PDI. CPD is below 10%.

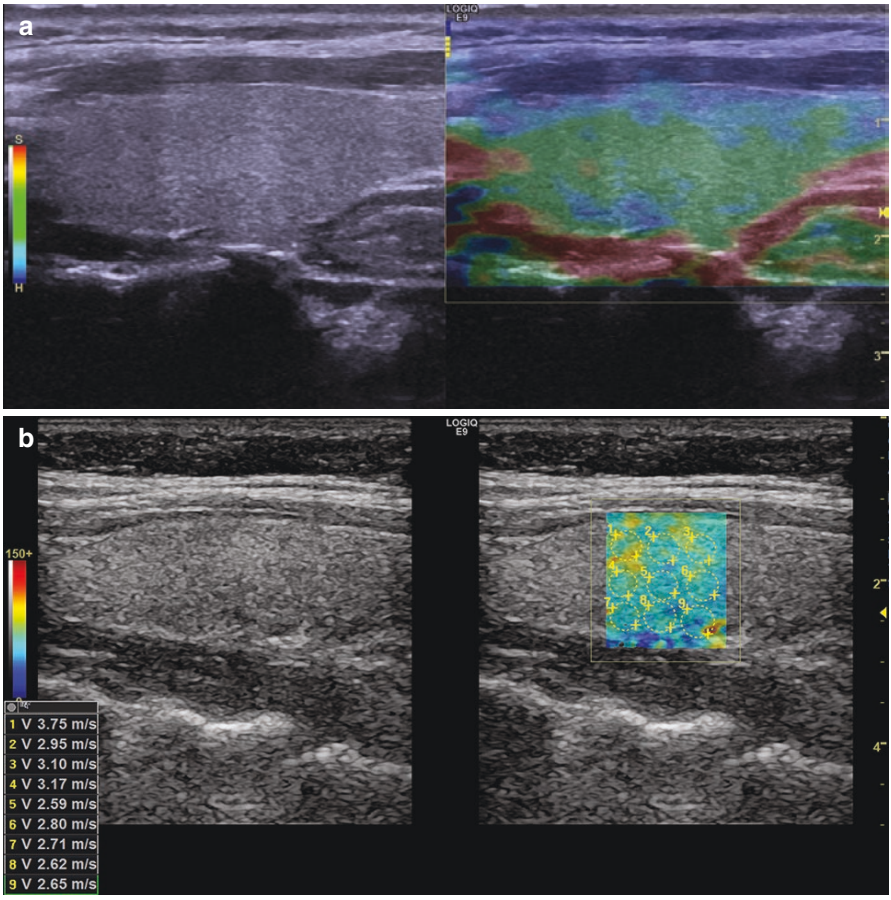

Fig. 2.10 Normal thyroid. (**a**) Regular medium elasticity of the normal thyroid gland with compression USE. (**b**) Normal values of shear wave velocities. (**c**) Young's modulus measurements. (**d**) Normal strain value with ARFI mode

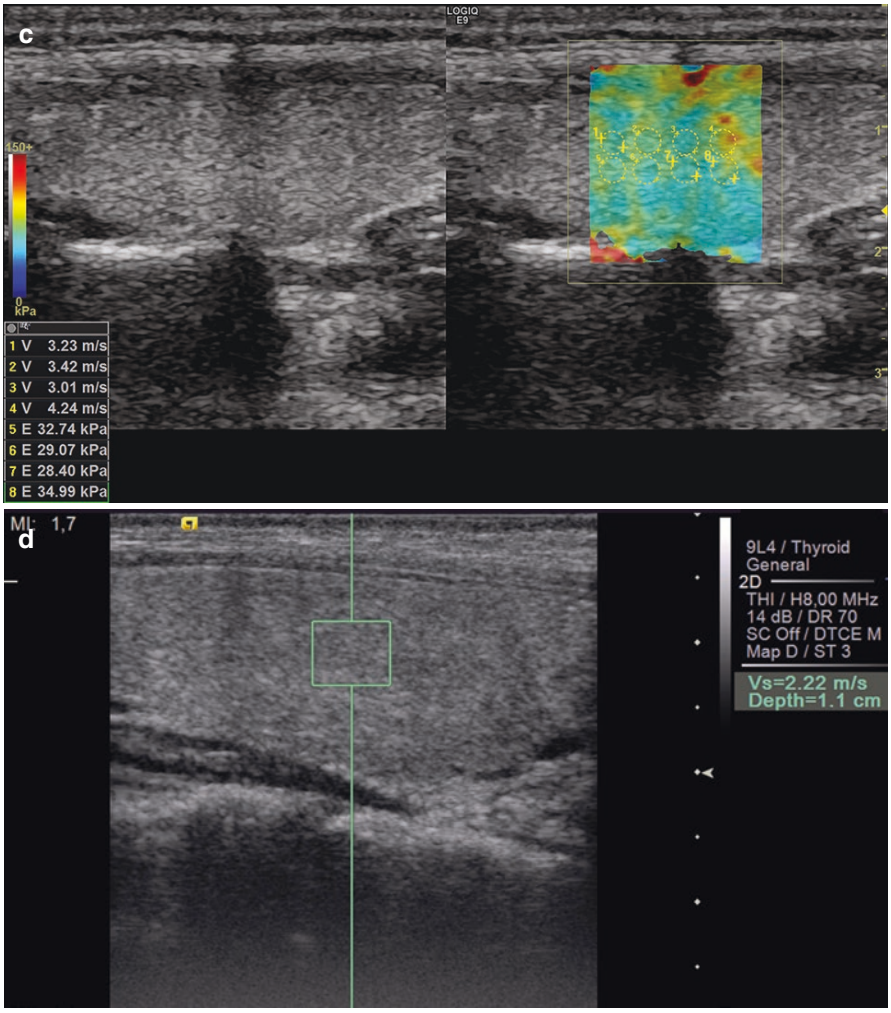

Fig. 2.10 (continued)

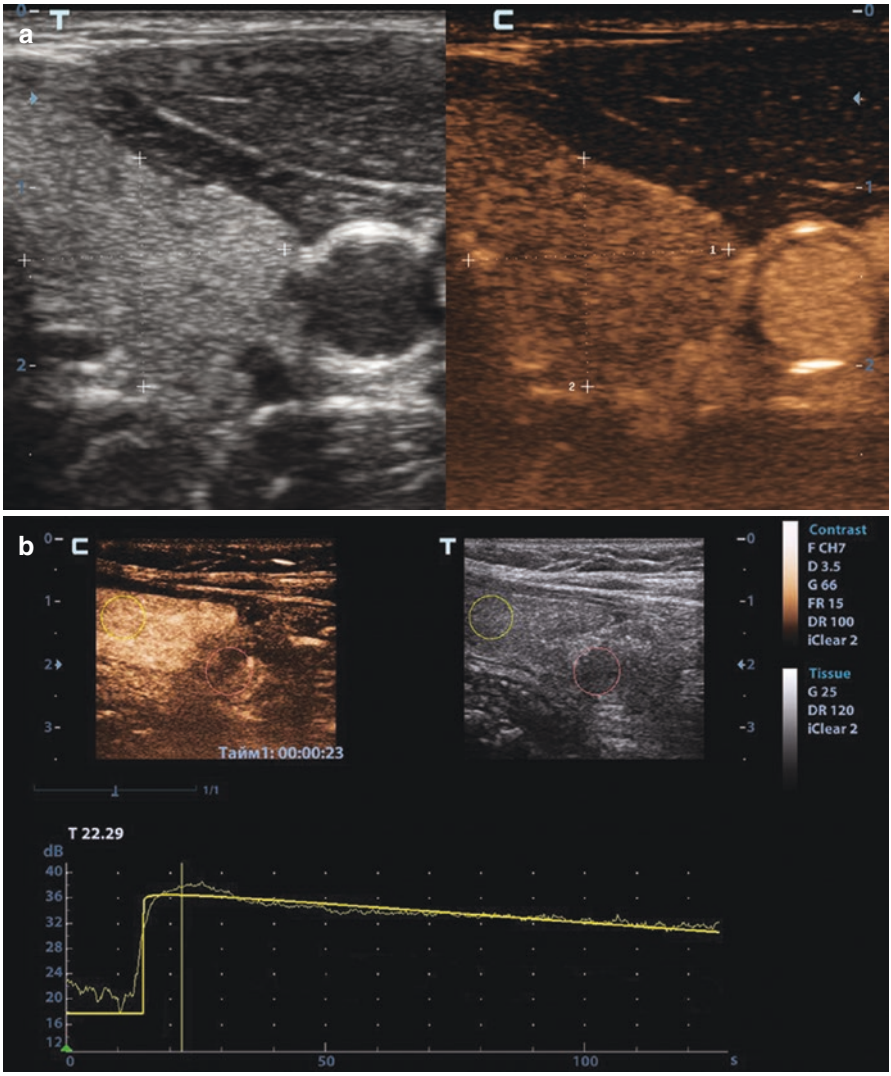

Fig. 2.11 CEUS of the normal thyroid gland with SonoVue®, 2.4 mL. (**a**) Contrast enhancement of the parenchyma. (**b**) Time-intensity curve

The lymph nodes in the neck and supraclavicular areas are not enlarged.
Conclusion: Normal thyroid.
US specialist

References

1. Netter FH, Hansen JT. Atlas of human anatomy. 3rd ed. Teterboro: Icon Learning Systems; 2003.
2. Gutekunst R, Becker W, Hehrmann R, et al. Ultraschalldiagnostik der Schilddrüse. Dtsch Med Wochenschr. 1988;113:1109–12.

3. Parshin VS, Tarasova GP, Glotov PI. Ultrasonic screening in the diagnosis of diseases of the thyroid gland. Methodical aspects and efficiency. Visualizaciya Clinice. 1999;14-15:1–7.
4. Lelyuk VG, Lelyuk SE. Some methodological aspects of complex thyroid ultrasound. Moscow: Springer; 2007.
5. Markova NV. The value of ultrasound angiography in the diagnosis of the main diseases of the thyroid gland. PhD thesis. Moscow; 2001.
6. Struchkova TY. Parameters of blood flow in the lower and upper thyroid arteries. Normative values. In: Abstracts of the 4th Congress of the Russian Association of Specialists in Ultrasound Diagnostics in Medicine. Moscow, 2003. pp. 221–2.
7. Arda K, Ciledag N, Aktas E, et al. Quantitative assessment of normal soft-tissue elasticity using shear-wave ultrasound elastography. AJR Am J Roentgenol. 2011;197(3):532–6.
8. Kim I, Kim EK, Yoon JH, et al. Diagnostic role of conventional ultrasonography and shear wave elastography in asymptomatic patients with diffuse thyroid disease: initial experience with 57 patients. Yonsei Med J. 2014;55(1):247–53.
9. Sebag F, Vaillant-Lombard J, Berbis J, et al. Shear wave elastography: a new ultrasound imaging mode for the differential diagnosis of benign and malignant thyroid nodules. J Clin Endocrinol Metab. 2010;95(12):5281–8.
10. Pomortsev AV, Gudkov GV, Degtyareva YS, et al. Possibilities of shear wave elastography in differential diagnostics of focal thyroid pathology. Radiat Diagn Ther. 2011;3:60–66 (Article in Russian).
11. Monpeyssen H, Tramalloni J, Poiree S, et al. Elastography of the thyroid. Diagn Interv Imaging. 2013;94(5):535–44.
12. Mitkov VV, Ivanishina TV, Mitkova MD. Ultrasound examination of the unchanged thyroid gland with the use of shear wave elastography technology. Ultrazvukovaya i funkcionalnaya diagnostika. 2014;6:13–20.

Congenital Thyroid Anomalies and Thyroid Diseases in Children

3

Alexander N. Sencha and Munir G. Tukhbatullin

The thyroid gland affects the development of a child at any age. Adequate thyroid function is necessary for the development of the brain and other organs and systems, including the immune system and sexual development. Much attention is paid to examining the thyroid gland in children, taking into account the influences of numerous negative factors [1]. The most significant factors are an iodine deficiency, an unfavorable ecological situation, an urbanization, and an intense rhythm of life with stressful influences. In this regard, regular screening has become a medical standard, especially in children suspected of having a thyroid pathology.

The technique of thyroid US in children actually does not differ from that in adults, except for special demands in relation to the accuracy of the volume calculation. Thyroid US in infants is preferably performed with an assistant due to certain difficulties in fixing the baby's head. The assistant places the hand under the baby's neck and upper back and slightly lifts it supporting the jaw with the thumb to prevent the baby from reflex flexing the head.

A change in gland volume accompanies almost all thyroid pathologies in children. Inspection and palpation fail to assess the thyroid volume correctly in about 35% of cases. In areas of mild to moderate iodine deficiency, the sensitivity and specificity of palpation are very poor. Measurement of thyroid size using ultrasound is preferable.

A. N. Sencha (✉)
Department of Visual and Functional Diagnostics, National Research Center for Obstetrics, Gynecology and Perinatology, Ministry of Healthcare of the Russian Federation, Moscow, Russia

M. G. Tukhbatullin
Department of Ultrasound Diagnostics, Kazan State Medical Academy – Branch Campus of the Federal State Budget Educational Institution of Further Professional Education, "Russian Medical Academy of Continuing Professional Education" of the Ministry of Healthcare of the Russian Federation, Kazan, Russia

A. N. Sencha, Y. N. Patrunov (eds.), *Thyroid Ultrasound*,
https://doi.org/10.1007/978-3-030-14451-7_3

The thyroid volume is the sum of the volumes of both lobes. The volume of each lobe is calculated from the measurements of the depth (d), the width (w), and the length (l) by the standard formula: V (mL) = 0.479 × d × w × l (cm). The volume of the isthmus is not included.

The issue of correctly interpreting the US measurements obtained in children and teenagers is a pertinent one. Numerous attempts have been made to define normal values of thyroid volume in different age [2, 3].

WHO [4] proposed the international reference values for goiter screening presented as a function of age, sex, and body surface area (BSA) (Tables 3.1 and 3.2). These were based on the study of Zimmermann et al. [6] that conferred the data of 3529 children from areas of long-term iodine sufficiency in North and South America, Central Europe, the Eastern Mediterranean, Africa, and the Western Pacific. By using the ultrasonography criteria, a thyroid gland will be called

Table 3.1 Median [50th percentile (P50)] and 97th percentile (P97) values for thyroid volume measured by ultrasound according to sex and age in an international sample of 6–12-year-old children from areas of long-term iodine sufficiency

	Boys		Girls	
Age (y)	P50	P97	P50	P97
	mL		mL	
6 (n = 468)	1.60	2.91	1.57	2.84
7 (n = 561)	1.80	3.29	1.81	3.26
8 (n = 579)	2.03	3.71	2.08	3.76
9 (n = 588)	2.30	4.19	2.40	4.32
10 (n = 528)	2.59	4.73	2.76	4.98
11 (n = 492)	2.92	5.34	3.17	5.73
12 (n = 313)	3.30	6.03	3.65	6.59

Table 3.2 Median [50th percentile (P50)] and 97th percentile (P97) values for thyroid volume measured by ultrasound according to sex and body surface area (BSA) in an international sample of 6–12-year-old children from areas of long-term iodine sufficiency

	Boys		Girls	
	P50	P97	P50	P97
BSA[a] (m^2)	mL		mL	
0.7 (n = 138)	1.47	2.62	1.46	2.56
0.8 (n = 493)	1.66	2.95	1.67	2.91
0.9 (n = 592)	1.86	3.32	1.9	3.32
1.0 (n = 640)	2.10	3.73	2.17	3.79
1.1 (n = 536)	2.36	4.2	2.47	4.32
1.2 (n = 445)	2.65	4.73	2.82	4.92
1.3 (n = 330)	2.99	5.32	3.21	5.61
1.4 (n = 174)	3.36	5.98	3.66	6.40
1.5 (n = 104)	3.78	6.73	4.17	7.29
1.6 (n = 77)	4.25	7.57	4.76	8.32

[a]The body surface area is calculated using the formula of Dubois and Dubois: BSA (m^2) = $W^{0.425}$ × $H^{0.725}$ × 71.84 × 10^{-4} [5]

goitrous when its values will be above the 97th percentile of the volume found in an iodine-replete population used as control. Typically, reference values for the 97th percentile for thyroid volume, as a function of both age and sex, are used (Table 3.1). BSA reference (Table 3.2) is potentially useful in countries with a high prevalence of child growth retardation due to malnutrition with both stunting (low height-for-age) and underweight (low weight-for-age). An advantage of the thyroid volume for BSA is that the age of the child is not required, which in some populations is not known with certainty.

The norms listed above for the thyroid volume with respect to age or BSA have been simplified and adapted for US screening. They do not take into account the physical development of a child and puberty in a teenager. Kasatkina et al. [7] suggested a method of defining thyroid hyperplasia and hypoplasia in children, which is linked to anthropometric parameters that depend on age and the presence of puberty. Thoracic circumference at maximal expiration is measured at the ages of 4–6 years, leg length (distance between the greater trochanter and the sole) at 7–9 years of age and in children over 10 years of age who are yet to enter puberty, and body weight in children undergoing puberty. Table 3.3 is used to interpret the obtained data.

Table 3.3 Limits on normal thyroid volume in children as a function of age, anthropometric parameters, and puberty [7]

Prior to puberty						During puberty		
4–6 years			7–9 years			13–15 years		
TC (cm)	LL (mL)	UL (mL)	Leg length (cm)	LL (mL)	UL (mL)	Body weight (kg)	LL (mL)	UL (mL)
46	0.42	2.12	46	0.43	2.93	30	0.42	7.34
47	0.48	2.18	47	0.43	3.01	31	0.43	7.41
48	0.53	2.23	48	0.50	3.08	32	0.43	7.49
49	0.59	2.29	49	0.58	3.16	33	0.50	7.56
50	0.64	2.34	50	0.65	3.23	34	0.58	7.64
51	0.70	2.40	51	0.73	3.31	35	0.65	7.71
52	0.76	2.46	52	0.81	3.39	36	0.73	7.79
53	0.81	2.51	53	0.88	3.46	37	0.80	7.86
54	0.87	2.57	54	0.96	3.54	38	0.88	7.94
55	0.92	2.62	55	1.03	3.61	39	0.95	8.01
56	0.98	2.68	56	1.11	3.69	40	1.03	8.09
57	1.04	2.74	57	1.19	3.77	41	1.10	8.16
58	1.09	2.79	58	1.26	3.84	42	1.18	8.24
59	1.15	2.85	59	1.34	3.92	43	1.25	8.31
60	1.20	2.90	60	1.41	3.99	44	1.33	8.39
61	1.26	2.96	61	1.49	4.07	45	1.40	8.46
62	1.32	3.02	62	1.57	4.15	46	1.48	8.54
63	1.37	3.07	63	1.64	4.22	47	1.55	8.61
64	1.43	3.13	64	1.72	4.30	48	1.63	8.69
65	1.48	3.18	65	1.79	4.37	49	1.70	8.76
66	1.54	3.24	66	1.87	4.45	50	1.78	8.84

(continued)

Table 3.3 (continued)

Prior to puberty						During puberty		
4–6 years			7–9 years			13–15 years		
TC (cm)	LL (mL)	UL (mL)	Leg length (cm)	LL (mL)	UL (mL)	Body weight (kg)	LL (mL)	UL (mL)
67	1.60	3.30	67	1.95	4.53	51	1.85	8.91
68	1.65	3.35	68	2.02	4.60	52	1.93	8.99
69	1.71	3.41	69	2.10	4.68	53	2.00	9.06
70	1.76	3.46	70	2.17	4.75	54	2.08	9.14
71	1.82	3.52	71	2.25	4.83	55	2.15	9.21
72	1.88	3.58	72	2.33	4.91	56	2.23	9.29
73	1.93	3.63	73	2.40	4.98	57	2.30	9.36
74	1.99	3.69	74	2.48	5.06	58	2.38	9.44
75	2.04	3.74	75	2.55	5.13	59	2.45	9.51
76	2.10	3.80	76	2.63	5.21	60	2.53	9.59
77	2.16	3.86	77	2.71	5.29	61	2.60	9.66
78	2.21	3.91	78	2.78	5.36	62	2.68	9.74
79	2.27	3.97	79	2.86	5.44	63	2.75	9.81
80	2.32	4.02	80	2.94	5.51	64	2.83	9.89
81	2.38	4.08	81	3.01	5.59	65	2.90	9.96
82	2.44	4.14	82	3.09	5.67	66	2.97	10.04
83	2.49	4.19	83	3.16	5.74	67	3.05	10.11
84	2.55	4.25	84	3.24	5.82	68	3.12	10.19
85	2.60	4.30	85	3.32	5.89	69	3.20	10.26
86	2.66	4.36	86	3.39	5.97	70	3.27	10.34
87	2.72	4.42	87	3.47	6.05	71	3.35	10.41
88	2.77	4.47	88	3.54	6.12	72	3.42	10.49
89	2.83	4.53	89	3.62	6.20	73	3.50	10.56
90	2.89	4.58	90	3.70	6.27	74	3.57	10.64

TC thoracic circumference at maximal expiration, *LL* lower limit of thyroid volume, *UL* upper limit of thyroid volume. For children of 10–12 years in the absence of puberty, the columns for children of 7–9 years are used (anthropometric parameter: leg length); in the presence of puberty, the columns for children of 13–15 years are used (anthropometric parameter: body weight). At adiposity during puberty (13–15 years), it is necessary to use not the actual body weight value but the upper limit on the normal body weight taken from standard height–weight tables

The isthmus depth is usually neglected. The thickness of the isthmus can be taken into account indirectly if the thyroid volume appears close to the upper limit. The boundary volume of the thyroid gland is reported normal if the isthmus thickness is normal. Alternatively, if the isthmus is enlarged (thicker than 3 mm in children under 10 years of age and more than 5 mm in teenagers), the thyroid is reported enlarged.

The echodensity of thyroid tissue in children, as well as in adults, is compared to that of the salivary gland. Normal thyroid tissue shows homogeneous echostructure (Fig. 3.1). However, in rare cases, the homogeneity of the tissue does not exclude initial stages of sporadic or endemic diffuse euthyroid goiter.

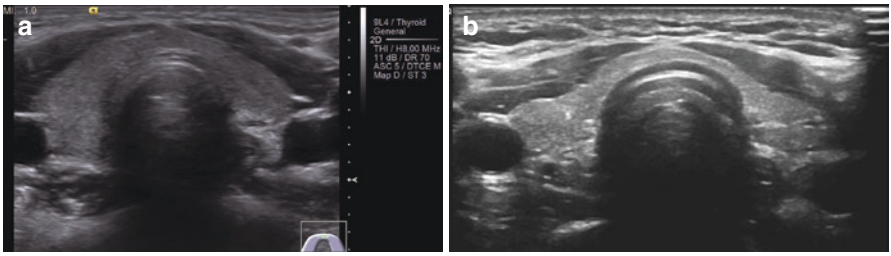

Fig. 3.1 Sonogram of a normal thyroid gland. Grayscale mode. (**a**) A 1-year-old child. (**b**) A 5-year-old child

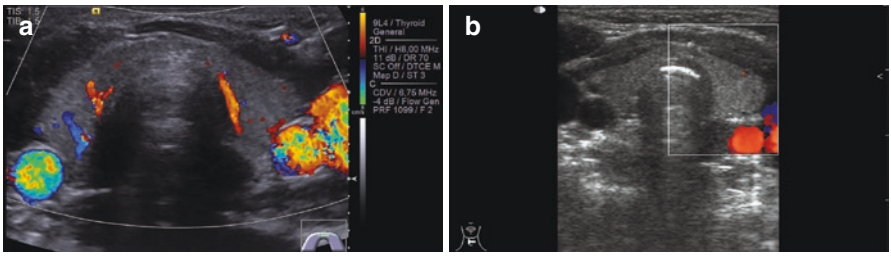

Fig. 3.2 Sonogram of a normal thyroid gland. CDI. (**a**) A 1-year-old child. (**b**) A 5-year-old child

CDI and PDI allow changes in the functional activity of both the thyroid gland and nodules to be gauged and several pathologic conditions to be differentiated based on the vascularization features (Fig. 3.2). However, quantitative assessment with PW Doppler is very subjective, especially for the vessels of the parenchyma, and is not used in everyday practice.

Congenital anomalies of the thyroid occur in <0.3–0.5% of the population. They appear at the stage of prenatal development. The embryonic primordium of the gland descends between weeks 3 and 5 of gestation as a median diverticulum from the floor of the pharynx, which makes its appearance at the level of the second pair of pharyngeal pouches. It evaginates, migrating caudally to the level of the III–IV pairs of pharyngeal pouches, and retains its connection with the pharynx only by a narrow thyroglossal duct at the root of the tongue. It is contributed to by the primordia, which arise laterally from the fourth pharyngeal pouches. The thyroglossal duct obliterates, and the germs of lateral lobes grow quickly and migrate caudally to the inferior part of the fetal neck. The first signs of independent function in the fetal thyroid are observed at week 8 of gestation. Thyroid function becomes apparent between weeks 12 and 14 of gestation.

At the stage of embryogenesis, the thyroid germ migrates from the level of the stomatopharynx to the inferior part of the neck. Various congenital anomalies of the thyroid gland can be formed in cases where the embryo experiences disturbances during histo- or organogenesis resulting in pathology of the thyroid primordium or the thyroid germ fails to successfully migrate. Thus, thyroid anomalies may be divided into size and position anomalies.

Thyroid size anomalies include the following:

- Aplasia (agenesis)
- Hemiagenesis
- Hypoplasia

Thyroid aplasia is the complete absence of thyroid tissue. This is a widespread cause of congenital hypothyroidism, which has been recorded to occur in 1 in every 3000–5000 newborns. Here, the thyroid tissue cannot be sonographically visualized in its typical position or higher up.

Thyroid hemiagenesis is usually a purely sonographic finding and is not accompanied by thyroid disorders. Here, only one thyroid lobe can be detected at its typical site (Fig. 3.3). Its volume, as a rule, does not exceed the standard limits for the total volume of a normal thyroid gland. Echodensity and echostructure of the lobe in grayscale and Doppler modes are normal. The second lobe cannot be visualized.

Congenital hypoplasia of the whole thyroid gland is the second cause of congenital hypothyroidism. Sonography reveals a low thyroid volume, which is more than 2–2.5 times below the lower limit. The gland parenchyma appears normal with normal blood flow. Alternatively, it may exhibit slightly increased echodensity with heterogeneous structure and irregular margins. Hypoplasia of only one thyroid lobe is much more common. Here, the volume of the affected lobe is 2–2.5 times smaller as compared with the contralateral one (Fig. 3.4).

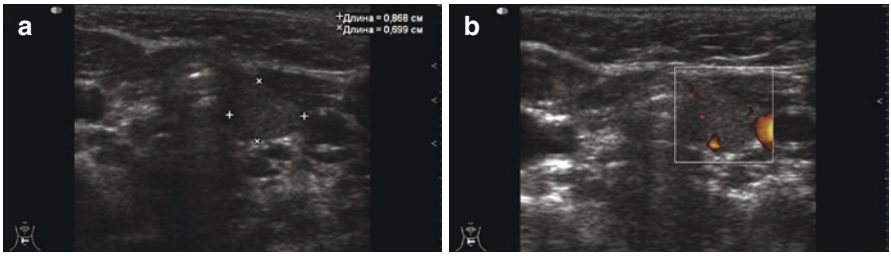

Fig. 3.3 Thyroid sonograms. Hemiagenesia of the right lobe of the thyroid gland. The age of the child is 6 months. (**a**) B-mode and (**b**) PDI

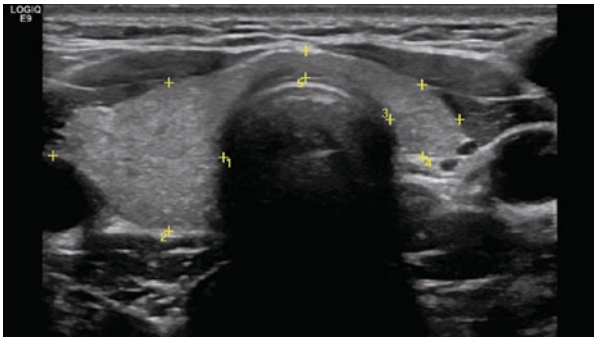

Fig. 3.4 Hypoplasia of the left thyroid lobe. Grayscale sonograms. The age of the child is 15 years

Thyroid gland position anomalies are as follows:

- Dystopia
- Ectopia

Thyroid dystopia and ectopia are sonographically characterized by an absence of thyroid tissue at its typical location. Dystopia refers to the localization of thyroid tissue close to the typical site along the route of natural migration during embryogenesis (within the neck, along the thyroglossal duct). If thyroid tissue is found at an atypical site outside the path of the thyroglossal duct, it is known as thyroid ectopia (aberrant thyroid). An ectopic thyroid gland is at an increased risk of malignant transformation compared to either dystopic or normal thyroid glands.

Thyroid dystopia can take the form of the following variants, depending on the height of location:

- Lingual (goiter of the tongue root)
- Intralingual (lingual goiter)
- Sublingual
- Thyroglossal
- Pre- and intratracheal
- Intraesophageal
- Intrathoracic (truly retrosternal, in cases with an entirely retrosternal location)

Ectopic thyroid can be found in the lateral neck (Fig. 3.5), in an ovary (struma ovarii), in a testicle (struma testis), in pericardium (struma pericardii), etc.

Midline cysts of the neck are similar to dystopia in their pathogenesis. Failed obliteration of the thyroglossal duct during fetal thyroid migration results in the formation of an epithelial cavity with subsequent fluid accumulation. US detects a cystic lesion cranial to the normal thyroid gland.

Thyroid pathology is widespread in children and teenagers. Girls suffer more often. Morbidity increases distinctly with age and reaches its peak in puberty.

Diffuse thyroid diseases in children include pathologic processes characterized by hypertrophy and/or hyperplasia of glandular tissue with thyroid enlargement or by its atrophy with a decrease in thyroid size. Different variants of diffuse euthyroid

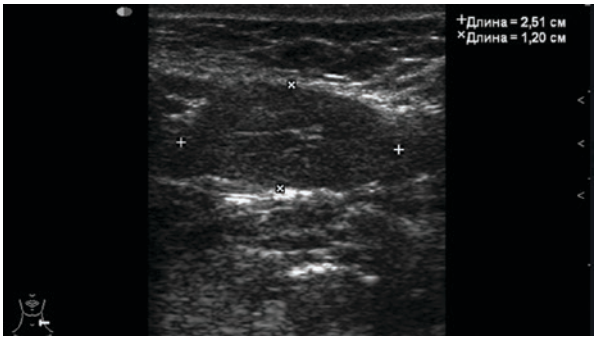

Fig. 3.5 Aberrant thyroid gland in the left supraclavicular area. The age of the child is 13 years. Grayscale US image

goiter dominate among diffuse thyroid diseases in children. Diffuse goiter is a universal pathologic sign of several diseases, such as the following:

- Endemic goiter
- Simple nontoxic (juvenile) goiter
- Iodine-induced goiter
- Idiopathic goiter
- Autoimmune thyroid disease
- Graves' disease
- Pendred syndrome
- Congenital nontoxic goiter

Diffuse endemic goiter is the most common thyroid pathology in children and teenagers. It is associated with iodine deficiency and is identical to the same in adults. Children and adolescents contribute up to 40% of the cases in the total number of diffuse endemic goiter [7]. This disease is sonographically characterized by normal thyroid tissue. Thyroid echostructure remains homogeneous and isoechoic with unchanged tissue vascularity according to color-coded Doppler imaging (Fig. 3.6). The only sign of the disease is an increase in thyroid volume, which thus differentiates it from the norm.

Autoimmune thyroid disease (AITD) in children under 15 years of age reaches 20–25 cases per 100,000. It quite often results in hypothyroidism. The specific features of AITD in children are a consequence of short duration of the disease and minimal changes in the thyroid tissue. Hence, the disease is more difficult to diagnose than it is in adults. The US image is quite variable and is characterized by the heterogeneity of thyroid tissue due to hypoechoic foci (lymphocytic infiltration), which contrast with the normal or slightly hypoechoic surrounding tissue (Fig. 3.7). It may also show the heterogeneous decrease in echodensity of the entire thyroid gland. Increased vascularity of the parenchyma and irregular vascular pattern are registered less often than in adults. Fibrosis is sometimes possible to visualize as echogenic septa. Pseudonules in AITD are often difficult to differentiate with US. Reactive lymph nodes adjacent to lower poles of the lobes tending to upper mediastinum are typical. A specific feature of humoral immune response in

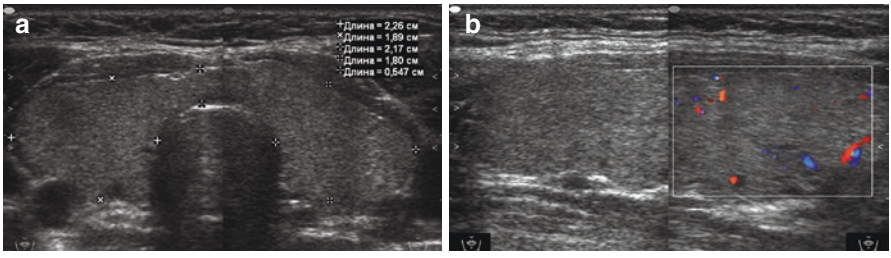

Fig. 3.6 Sonograms. Diffuse thyroid hyperplasia. The age of the child is 13 years. (**a**) B-mode, axial scan. (**b**) CDI, longitudinal scan

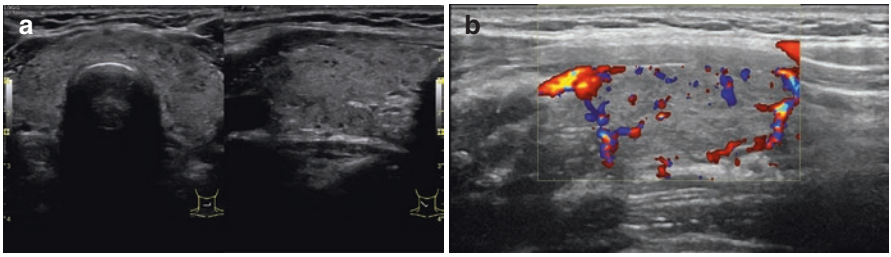

Fig. 3.7 Sonograms. AITD. The age of the child is 10 years. (**a**) B-mode. (**b**) CDI

children with early AITD is a high rate (up to 60%) of cases without any increase in both anti-thyroglobulin (anti-Tg) and antithyroid peroxidase (anti-TPO) antibodies [8]. Such cases of AITD are subject to puncture biopsy and cytology. Expressed autoimmune changes during the initial stages of AITD do not lead to a very big goiter, unlike in adults. The thyroid volume in the majority of children with AITD, as well as those with endemic goiters, is increased by <50–60% compared to the norm [7].

Graves' disease in children and teenagers is a serious endocrine pathology. The annual morbidity is 2–4 cases per 100,000. The disease disproportionately affects girls 10–15 years of age. The clinical symptoms of Graves' disease in children are variable, but they do not develop as quickly as in adults. Organ compression symptoms may arise in cases with a retrosternal thyroid location. However, the degree of thyroid enlargement does not define the severity of thyrotoxicosis. The results of treatment depend on the accuracy and the timeliness of diagnosis. Sonography usually reveals an enlarged thyroid gland with regular, well-defined margins and relatively homogeneous and significantly hypoechoic parenchyma. Blood flow supply in the parenchyma is substantially increased and demonstrates "thyroid inferno" in CDI and PDI. The blood flow velocities in the large arteries with PW Doppler are also significantly increased. Wide veins are often registered with possible arteriovenous shunts.

Thyroid nodules in children and teenagers are noted less often than in the adult population. The incidence of thyroid nodules in children does not exceed 0.5–2% [9]. More than half of the nodules (63.4%) are detected with US screening, and they are more prevalent in elder children. Solitary nodules are detected in about 88.6% of cases [10]. Nodule size, as a rule, does not correlate with age. Thyroid nodules in children do not show specific US features and are similar to such lesions in adults (Fig. 3.8). Specific pitfall in diagnosis of thyroid nodules in children is aberrant thymic tissue within the thyroid gland that may be mistaken for thyroid nodule. Intrathyroid ectopic thymic tissue is usually found incidentally in prepubertal pediatric population, rarely in adults due to age-related involution. It is detected with US in 1% of general pediatric population [11] and is presented by round, oval, or polygonal hypoechoic or hyperechoic lesion, with multiple granular and punctate echogenic foci that are typical for thymus (Fig. 3.9). It is predominantly soft with elastography making no difference as compared to the surrounding thyroid tissue.

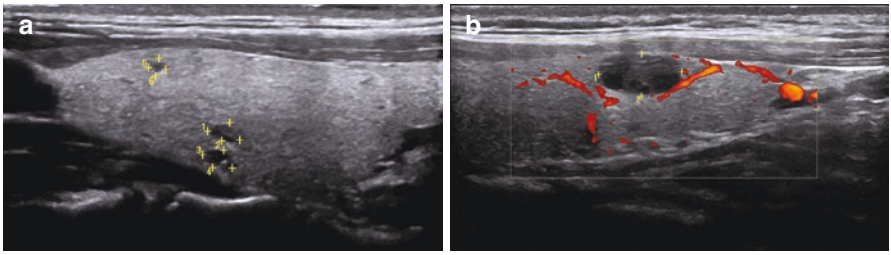

Fig. 3.8 Sonograms. Thyroid nodules. The age of the child is 11 years. (**a**) B-mode. (**b**) PDI

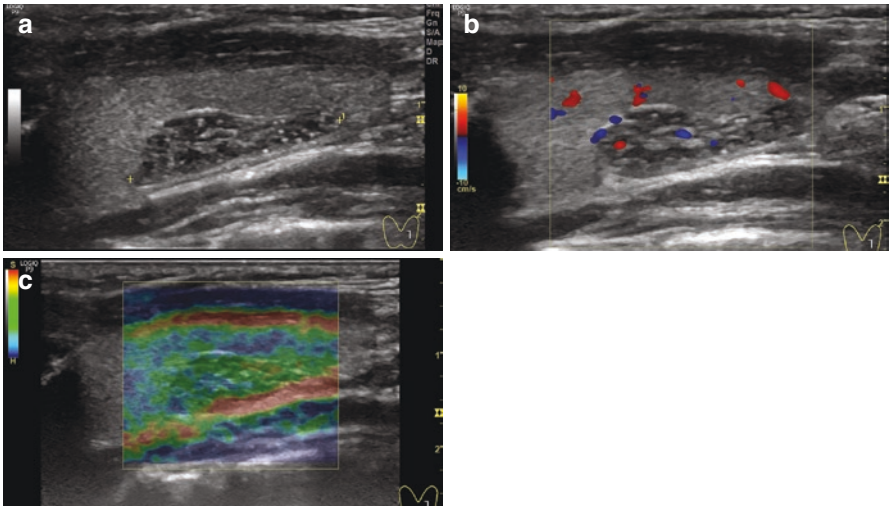

Fig. 3.9 Sonograms. Intrathyroid ectopic thymic tissue in a child of 6 years. (**a**) B-mode. (**b**) CDI. (**c**) Compression elastography

Thyroid cancer is the most widespread tumor of the endocrine system in children. It accounts for up to 45.3% of all malignant neoplasms of endocrine glands at this age [12]. The incidence of pediatric thyroid cancer among all tumors of the head and neck is 8–22% [13, 14]. According to Kiyaev et al. [10], thyroid cancer in children is detected in 11.5% of suspicious thyroid nodules subject to puncture biopsy.

Papillary cancer dominates among all thyroid malignancies in children, as well as in adults. Children 8–14 years of age show the disease more often, with the peak occurring during puberty. The ratio of boys to girls with thyroid malignancy is about 1:1.6. US image of thyroid cancer in children is identical to the same in adults (Fig. 3.10).

The disease is more aggressive in children than in adults. Multicentric growth of thyroid cancer in children is observed in more than half of cases (up to 65%) [12]. Invasion of the tumor through the thyroid capsule is registered in 24–52% of

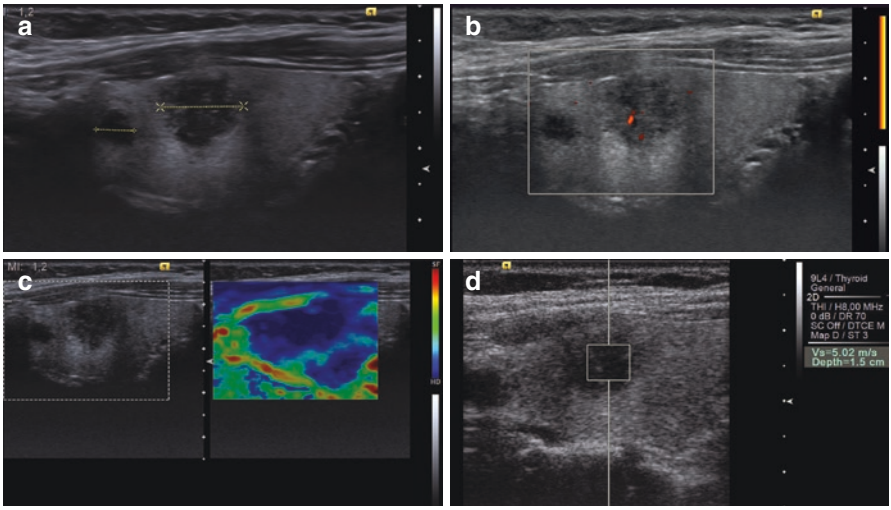

Fig. 3.10 Papillary thyroid cancer. Age of the child is 16 years. Echograms. (**a**) Grayscale image (**b**) PDI. (**c**) Compression elastography. (**d**) ARFI demonstrates high share-wave velocity

patients. The incidence of lymph node metastases in children is 37–93% [15]. More than 30% of children have metastases in cervical lymph nodes before surgery, and up to 28% have distant metastases. Thyroid cancer recurrence occurs more often in children than in adults and constitutes 19–39%. Precise sonography with all accessible options in children with thyroid malignancy before and after surgery permits improved management of thyroid cancer.

References

1. Pykov MI, editor. Children's ultrasound diagnosis. Textbook. Vol 5. Andrology, endocrinology, selected questions. Moscow: Vidar; 2016 (Book in Russian).
2. Delange F, Benker G, Caron P, et al. Thyroid volume and urinary iodine in European schoolchildren: standardization of values for assessment of iodine deficiency. Eur J Endocrinol. 1997;136:180–7.
3. Gutekunst R, Martin-Teichert H. Requirements for goiter surveys and the determination of thyroid size. In: Delange F, Dunn JT, Glinoer D, editors. Iodine deficiency in Europe: a continuing concern. New York: Plenum Press; 1993. p. 109–18.
4. World Health Organization, UNICEF, ICCIDD. Assessment of iodine deficiency disorders and monitoring their elimination: a guide for programme managers. 3rd ed. Geneva: WHO; 2007.
5. Dubois D, Dubois EF. A formula to estimate the approximate surface area if height and weight be known. Arch Intern Med Chic. 1916;17:863–71.
6. Zimmermann MB, Hess SY, Molinari L, et al. New reference values for thyroid volume by ultrasound in iodine-sufficient schoolchildren: a World Health Organization/Nutrition for Health and Development Iodine Deficiency Study Group report. Am J Clin Nutr. 2004;79(2):231–7.
7. Kasatkina EP, Shilin DE, Pykov MI. Ultrasound of the thyroid gland in children and adolescents. Moscow: Vidar; 1998 (Book in Russian).

8. Shilin DE, Pykov MI. Ultrasound examination of the thyroid gland. In: Pykov MI, Vatolin KV, editors. Clinical guidance on ultrasound in pediatrics. Moscow: Vidar; 2001 (Book in Russian).
9. Wang C, Crapo LM. The epidemiology of thyroid disease and implication for screening. Endocrinol Metab Clin N Am. 1997;26:189–218.
10. Kiyaev AV, Fechina LG, Shorikov EV, et al. Thyroid tumors in the structure of nodular goiter in children and the accuracy of fine-needle aspiration biopsy in their diagnosis. Pediatr Oncol. 2008;3:21–4 (Article in Russian).
11. Fukushima T, Suzuki S, Ohira T, et al. Prevalence of ectopic intrathyroidal thymus in Japan: the Fukushima health management survey. Thyroid. 2015;25(5):534–7.
12. Romanchyshen AF. Diagnostics, methods and results of surgical treatment of patients with advanced differentiated thyroid cancer. Vestnik RONTS im NN Blokhin RAMS. 2009;20(2):22 (Article in Russian).
13. Paches AI, Brzhezovsky VZ. Tumors of the thyroid gland. Tumors of the head and neck. Moscow: Practical Medicine; 2013 (Book in Russian).
14. Polyakov VG, Shishkov RV. Local prevalence and metastasis of the thyroid cancer in children and adolescents. Sib Oncol J. 2006;1:89–90 (Article in Russian).
15. Romanchyshen AF, Gostimsky AV. Diseases of the thyroid gland in children and adolescents. Surgical endocrinology. Sankt Petersburg; 2004 (Book in Russian).

Ultrasound Diagnosis in Diffuse Thyroid Diseases

4

Yury N. Patrunov, Alexander N. Sencha, Liubov A. Timofeyeva, Ekaterina A. Sencha, and Ella I. Peniaeva

All thyroid abnormalities that can be detected sonographically are divided into diffuse, nodular, and combined changes.

Diffuse changes confer the following principle pathologies:

- Diffuse nontoxic goiter (diffuse hyperplasia)
- Diffuse toxic goiter (Graves' disease)
- Thyroiditis

4.1 Diffuse Nontoxic Goiter

Diffuse nontoxic goiter (diffuse hyperplasia) is a pathological condition of the thyroid gland, characterized by uniform increase in size of the entire gland without any lesions or focal changes of the parenchyma. It is usually a result of severe iodine

Y. N. Patrunov (✉) · E. I. Peniaeva
Department of Ultrasound Diagnostics, Center for Radiological Diagnostics of Non-State Healthcare Institution Yaroslavl Railway Clinic of JSC "Russian Railways", Yaroslavl, Russia

A. N. Sencha
Department of Visual and Functional Diagnostics of National Research Center for Obstetrics, Gynecology and Perinatology, Ministry of Healthcare of the Russian Federation, Moscow, Russia

L. A. Timofeyeva
Department for Internal Diseases Propaedeutic, Course of Diagnostic Radiology of Medical Faculty of Federal State Budget Educational Institution of Higher Education "I. N. Ulianov Chuvash State University", Cheboksary, Russia

E. A. Sencha
Ultrasound Diagnostics Department, Medical Diagnostic Center, Moscow, Russia

A. N. Sencha, Y. N. Patrunov (eds.), *Thyroid Ultrasound*,
https://doi.org/10.1007/978-3-030-14451-7_4

deficiency and is not associated with hyperthyroidism, hypothyroidism, inflammation, or malignancy. Diffuse hyperplasia alone is observed in 1–5% of the population. In the majority of cases, diffuse thyroid enlargement is a symptom of AITD, Graves' disease, or results from thyroid lesions.

The following US signs are characteristic of diffuse hyperplasia of the thyroid gland (Figs. 4.1, 4.2, 4.3, and 4.4):

- Increase in thyroid volume.
- Homogeneous isoechoic echostructure with a middle- or fine-grained pattern (Fig. 4.1).
- Regular accurate margins. The contours of the poles may sometimes appear rounded.
- A very big thyroid may cause difficulties in visualizing the adjacent organs (vessels, esophagus, etc.) due to their dislocation dorsally or laterally.

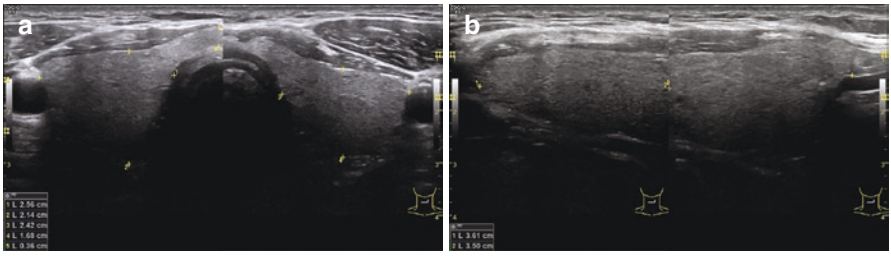

Fig. 4.1 Diffuse thyroid hyperplasia. Echograms. Grayscale mode. (**a**) Transverse scan. (**b**) Longitudinal scan

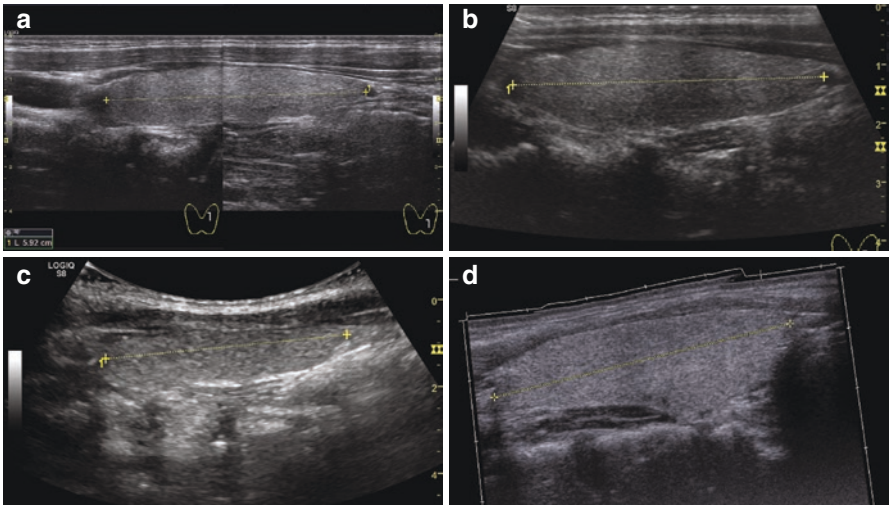

Fig. 4.2 Measurement of large thyroid. Echograms. Grayscale mode. (**a**) Combining two scanning ranges. (**b**) Trapezoid mode. (**c**) Utilizing a convex probe. (**d**) Panoramic scan

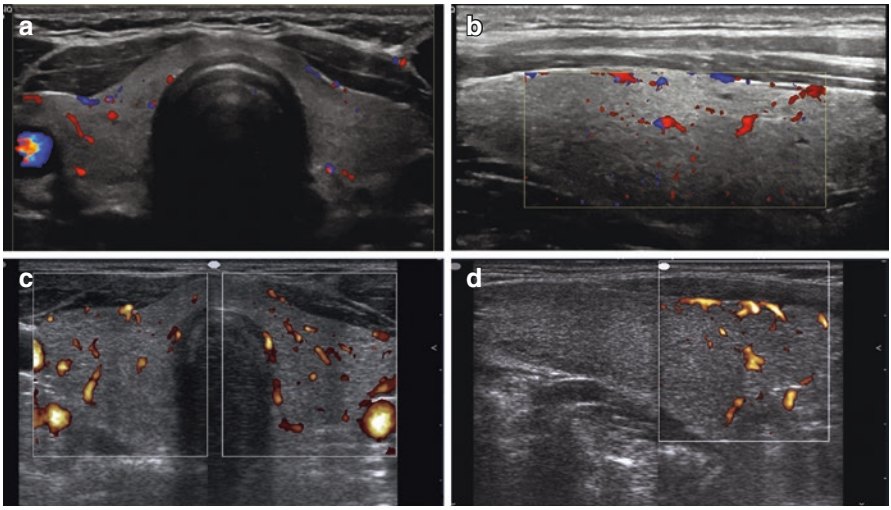

Fig. 4.3 Diffuse thyroid hyperplasia. Echograms. Doppler mapping. (**a**) CDI, transverse scan. (**b**) CDI, longitudinal scan. (**c**) PDI, transverse scan. (**d**) PDI, longitudinal scan

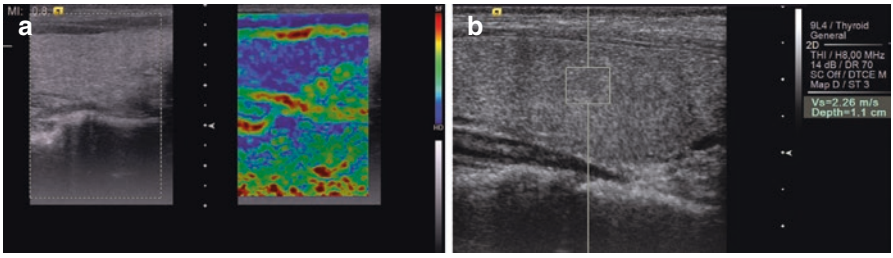

Fig. 4.4 Diffuse thyroid hyperplasia. Echograms. (**a**) Compression elastography. (**b**) ARFI

- CDI and PDI may reveal a negligible symmetric increase in the number of vessels within thyroid lobes with a uniform distribution. A normal color pattern is usually observed (Fig. 4.3).
- Compression elastography demonstrates medium strain with uniform and symmetrical pattern.
- Share-wave elastography reveals Young's modulus values within the normal range of 10–40 kPa.

The volume of a normal thyroid in both adults and children is still the source of debate. Thyroid enlargement is traditionally defined as thyroid volume exceeding 18 ml in women and 25 ml in men [1–3]. The sonographically calculated thyroid volume in adults can be compared with recommended standards that depend on age, height, weight, and body surface area.

It is not entirely clear whether staging of thyroid enlargement based on US calculation of the total thyroid volume is necessary. Figures of calculated volume serve for

follow-up purpose to assess the change during treatment. Extremely large thyroids accompanied with compression of the esophagus, trachea, or other neck organs are subject to surgery. Other cases are treated conservatively. There is no evident data on the influence of the thyroid volume on the choice of conservative treatment.

Big thyroids cause difficulties in assessing the lengths of thyroid lobes. This is a consequence of them being much longer than the length of the US probe, meaning that the whole lobe cannot be viewed in one scanning range. The following techniques can be employed to solve this problem:

- Combining two scanning ranges (Fig. 4.2a)
- Using a "virtual convex" or trapezoid mode (Fig. 4.2b)
- Utilizing a convex probe (Fig. 4.2c)
- Panoramic scan (Fig. 4.2d)

Grayscale US reveals normal structure of thyroid tissue, which looks uniform, homogeneous, and isoechoic (Fig. 4.1). Doppler modalities in diffuse nontoxic goiter do not add any significant data to that afforded by grayscale sonography. The intensity of color pattern and distribution of vessels do not differ from the norm (Fig. 4.3). Diffusely enlarged thyroid in nontoxic goiter is of medium stiffness with compression elastography that is identical to normal thyroid parenchyma. The color pattern is regular, uniform, and symmetric (Fig. 4.4a). Normal stiffness in diffuse thyroid hyperplasia is confirmed by quantitative measurements of share-wave elastography (Fig. 4.4b). The Young's modulus ranges from 10 kPa to 40 kPa with usual figures of 12–23 kPa. CEUS is not applied for diagnosis of diffuse goiter.

The Example US Report in Diffuse Thyroid Hyperplasia

- First name, middle initial, last name:
- Age:
- Date:
- The number of case history:
- US scanner:

The thyroid gland is typically located with regular well-defined margins and homogeneous isoechoic structure. The capsule is uniform and continuous on all extent. Cystic and solid lesions are not detected.

The depth of the *isthmus*—15 mm			
Right lobe		Left lobe	
Depth	28 mm	Depth	26 mm
Width	26 mm	Width	24 mm
Length	62 mm	Length	60 mm
Volume	21.6 cm^3	Volume	17.9 cm^3

The total volume 39.5 cm^3 exceeds the upper limit.

The vascular pattern of the parenchyma is normal and symmetric with CDI and PDI. CPD is 10–15%.

The lymph nodes in the neck and supraclavicular areas are not enlarged.
Conclusion: Diffuse thyroid hyperplasia. TIRADS 1.
US specialist:

4.2 Graves' Disease

Diffuse toxic goiter (Graves' disease) is a diffuse thyroid abnormality that leads to excess production of thyroid hormones and thyrotoxicosis. It is usually accompanied with thyroid enlargement. Its incidence is 20–25 in 100,000 people. Women 30–50 years of age suffer more often than other parts of the population [4].

The basic US features of Graves' disease are as follows (Figs. 4.5, 4.6, and 4.7):

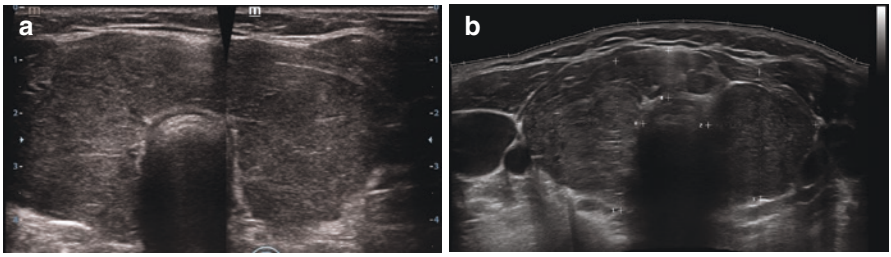

Fig. 4.5 Graves' disease. Echograms. Grayscale mode. (**a**) Conventional transverse scan. (**b**) Panoramic scan

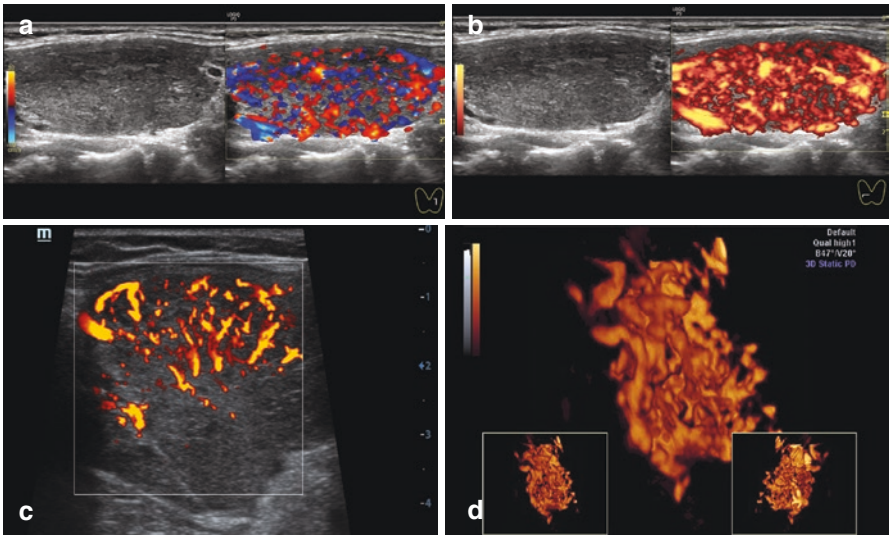

Fig. 4.6 Graves' disease. Echograms. (**a**) CDI, longitudinal scan. (**b**) PDI, longitudinal scan. (**c**) PDI, transverse scan. (**d**) 3DPD

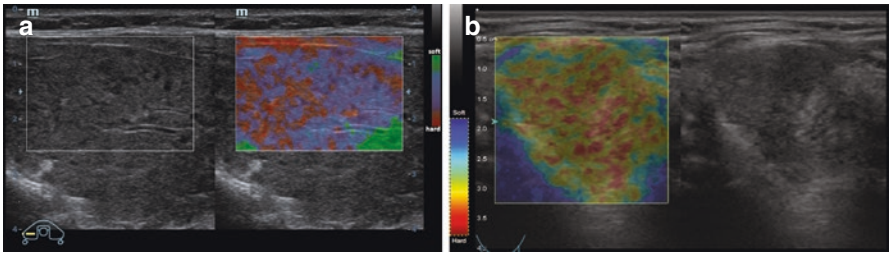

Fig. 4.7 Graves' disease. Echograms. (**a**) Compression USE. (**b**) Compression USE in recurrent Graves' disease

- Volume change (usually symmetric enlargement of the entire thyroid).
- Displacement of vascular bundles of the neck laterally or/and dorsally resulting from the enlargement of the thyroid lobes.
- Protrusion of the anterior surfaces of the lobes, enlargement of the isthmus, rounding of the normal angular outline.
- Diffuse decrease in echodensity.
- Distinct lobular structure of the thyroid with thin septa of stromal component.
- Significant symmetric hypervascularity of the parenchyma in CDI and PDI.
- Heterogeneous stiffness with compression US elastography with irregular color pattern of thyroid parenchyma.
- Share-wave elastography reveals normal or slightly increased stiffness.

In grayscale mode, the ultrasound image of the thyroid parenchyma in Graves' disease may be similar to certain types of autoimmune thyroiditis. Prominent lobulation of hypoechoic thyroid parenchyma with torose anterior surface and thin fibrous septations can be a reason to suspect Graves' disease (Fig. 4.5).

The most spectacular and important changes can be detected with CDI and PDI. The vascularity of the entire thyroid gland appears significantly increased [5]. Extreme hypervascularity is often named "thyroid inferno" (Fig. 4.6). The vessels are usually distributed regularly within the parenchyma and show rectilinear character. The number of detected vessels increases (CPD exceeds 20–50%). The degree of hypervascularization in Graves' disease often depends on the histological type and the clinical development of the disease.

Patients with an active autoimmune process and thyrotoxicosis demonstrate significantly increased blood flow velocity in afferent thyroid arteries with PW Doppler (TAMX is 30–180 cm/s), although the resistance index may be increased (RI is 0.7–0.8) or decreased (RI is 0.3–0.5). According to Donkol et al. [6], CDI and PW Doppler of blood flow in ITA can be used in differential diagnosis of thyrotoxicosis, especially in cases of contraindications for radionuclide scan. PSV of the ITA were reported significantly higher in patients with untreated Graves' disease than in patients with autoimmune thyroiditis [6], subacute thyroiditis, or amiodarone-induced thyrotoxicosis type 2 [7]. Blood flow data from PW Doppler, CDI, and PDI in patients with long-term remission from Graves' disease may remain increased or normal.

Compression US elastography, as a rule, reveals heterogeneous elasticity (stiffness) of thyroid parenchyma with irregular grainy color pattern (Fig. 4.7). CEUS is not used for diagnosis of Graves' disease.

Thyroid lesions of various origins may arise in 10–27% of cases of Graves' disease. They are more often observed in patients over 60 years of age with long-term disease. The total frequency of thyroid carcinoma in Graves' disease is about 3.4–12% [8–10].

The specificity of multiparametric US in the diagnosis of Graves' disease is about 96%; its sensitivity is 80%; and its diagnostic accuracy is 93%.

The Example US Report in Graves' Disease

- First name, middle initial, last name:
- Age:
- Date:
- The number of case history:
- US scanner:

The thyroid gland is typically located.

The depth of the *isthmus*—15 mm			
Right lobe		Left lobe	
Depth	27 mm	Depth	28 mm
Width	26 mm	Width	24 mm
Length	64 mm	Length	58 mm
Volume	21.5 cm^3	Volume	18.7 cm^3

The total volume 40.2 cm^3 exceeds the upper limit.

The thyroid parenchyma is moderately heterogeneous with distinct lobular structure and significantly diffusely decreased echodensity. The margins are irregular and well-defined. The blood flow intensity is significantly increased in CDI and PDI. CPD is 30–40%. Vascular pattern is symmetric.

Cystic and solid lesions are not detected.

The lymph nodes in the neck and supraclavicular areas are not enlarged.

Conclusion: Increase in thyroid volume with diffuse changes of the structure and vascularity of the thyroid gland characteristic of Graves' disease.

US specialist:

4.3 Thyroiditis

Thyroiditis is a generalized term for the group of inflammatory processes in the thyroid gland. All types of thyroiditis are associated with either inflammatory or autoimmune cytotoxic processes in thyroid tissue.

ICD-10 [11] Defines the following types of thyroiditis:

1. Acute thyroiditis
2. Subacute thyroiditis

3. Chronic thyroiditis with transient thyrotoxicosis
4. Autoimmune thyroiditis
5. Drug-induced thyroiditis
6. Other chronic thyroiditis
7. Thyroiditis, unspecified

Various etiologies determine various clinical manifestations and duration of the disease. Any type of thyroiditis implies damage of thyroid follicles resulting in a specific pathological picture that can be imaged with US. However, clinical manifestations and laboratory tests are crucial for correct diagnosis. The commonest types of thyroiditis encountered are autoimmune and subacute thyroiditides.

4.3.1 Autoimmune Thyroiditis

Autoimmune (Hashimoto's) thyroiditis is the most common of the chronic thyroiditides and the most common cause of hypothyroidism. The mechanisms of its development are not fully understood. Partial genetic defect in the immune system is supposed. As a result, thyroid tissue is subject to specific morphological changes ranging from lymphocytic infiltration to fibrous replacement. Autoimmune thyroiditis (AIT) is present in up to 6–11% of the adult population. The rate of clinically significant forms of AIT in the general population is about 1%. The disease disproportionately affects women. The number of women with AITD exceeds the number of men with AIT by 4–8 times. Incidence peaks at 40–60 years of age.

Usually the whole gland is affected. The thyroid gland may be enlarged, but often the size is normal. Hypothyroidism is diagnosed at presentation or subsequently develops in 50% of cases. Most autoimmune thyroiditides initially present with a transient hyperthyroid state [12]. About 1–10% of cases of hyperthyroidism are related to a thyroiditis. Thereafter the thyroid hormone level returns to euthyroidism or falls down to permanent (subclinical or overt) hypothyroidism and requires lifelong replacement therapy. Over 90% of cases of clinical hypothyroidism are a consequence of an autoimmune thyroiditis. In most cases, AIT is diagnosed based on clinical signs and laboratory tests (TSH, T3, T4, antithyroid peroxidase (anti-TPO), antithyroglobulin (anti-Tg) antibodies, and others). In some patients, especially with no symptoms of impaired thyroid function, US is the first diagnostic modality to suspect AIT. In patients with diagnosed AIT, US serves for differential diagnosis with other thyroid diseases, follow-up, and detection of concomitant thyroid diseases.

Transient acute phase typically starts with lymphocytic infiltration in the isthmus and anterior aspects of thyroid lobes represented with homogeneous, uniform hypoechoic spots and areas with ill-defined margins. Spreading infiltration confers all aspects of both lobes in subacute phase accompanied with the enlargement of the entire thyroid gland and irregular hypervascularity (Fig. 4.8).

The common grayscale image of AIT in the majority of patients is registered in chronic phase. It is characterized with the following US signs (Fig. 4.9):

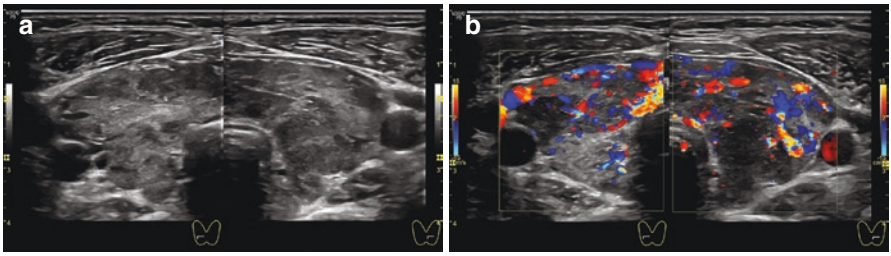

Fig. 4.8 Acute/subacute phase AIT. Sonograms. (**a**) Grayscale US. (**b**) CDI

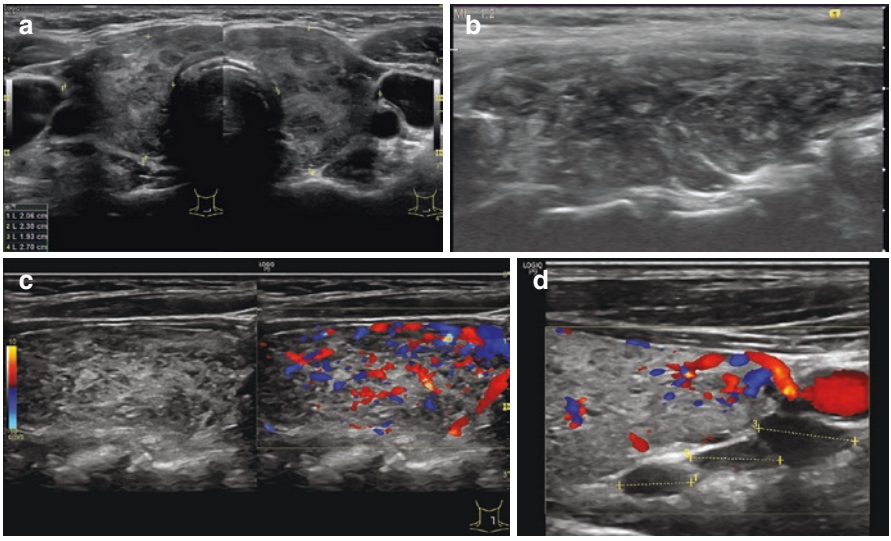

Fig. 4.9 Chronic phase AIT. Sonograms. (**a**) Grayscale US. Transverse scan. (**b**) Grayscale US. Longitudinal scan. (**c**) CDI. (**d**) Enlarged lymph nodes along the posterior surface of thyroid lobe (marked with calipers)

1. Enlargement or normal size of thyroid lobes and isthmus with predominant enlargement of the depth and width of the lobes; the atrophic type of the disease results in a decreased thyroid volume.
2. Irregular decrease in echodensity. Diffuse heterogeneity of the parenchyma (from fine-grained to coarse-grained) resulting from hypoechoic areas of various sizes distributed within the thyroid tissue sometimes merging into each other.
3. Echogenic inclusions with different shapes (more common linear septa or point-like) related to the stromal component.
4. Tuberosity of the posterior surface, blurred, rough margins.
5. Hypovascularity of hypoechoic areas is typical. Diffuse hypervascularization is possible. The blood flow pattern with CDI and PDI is irregular and depends on the type of AIT.
6. Irregular medium-, coarse-grained asymmetric elasticity of the parenchyma with compression US elastography.

7. The stiffness of thyroid parenchyma is usually normal or slightly increased with share-wave elastography.
8. Irregular enhancement of thyroid parenchyma with spots of hypo- or hyperenhancement related to the type/stage of AIT.
9. Common reactive hyperplasia of regional lymph nodes (predominantly of VI and VII levels: prelaryngeal, pre- and paratracheal, anterior/superior mediastinal).

The outcome of AIT with thyroid atrophy and hypothyroidism is characterized with a substantial decrease in the size of the thyroid gland, a decrease in echogenicity, heterogeneous structure, hypovascularity, and dense pattern with US elastography (Fig. 4.10). The margins appear irregular and blurred; the gland is often difficult to distinguish from the surrounding tissue.

Kharchenko et al. [13] proposed the following four types of AIT, based on US features:

1. Diffuse type, characterized by an enlarged thyroid with an ordinary shape, well-defined margins, and diffuse changes in parenchyma.
2. Focal type.
3. Diffuse nodular type, characterized by a lesion or several lesions along with diffuse changes of the whole gland.
4. Mixed with nodules. This type exhibits true colloid nodules along with AIT.

Diffuse type is the most common echographic finding among all types of AIT. The changes of the parenchyma cover the entire enlarged thyroid gland. Prevailing ultrasound features determine the following patterns:

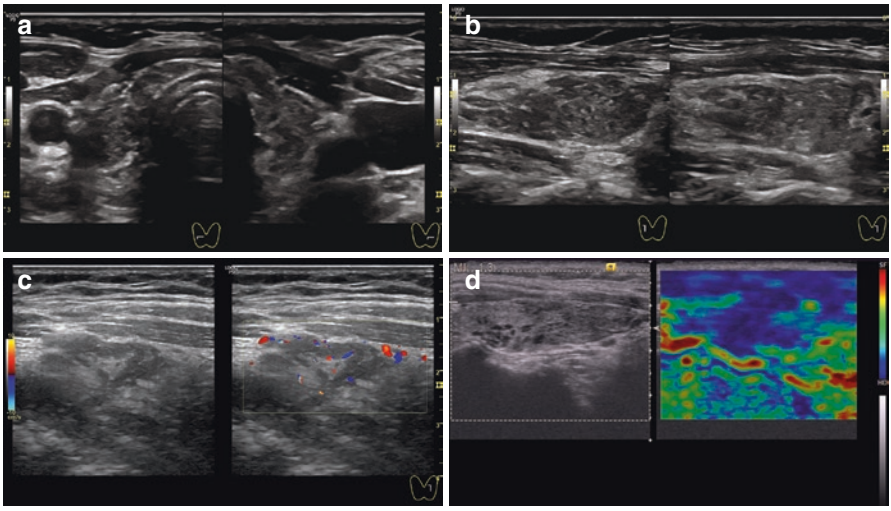

Fig. 4.10 AIT. Atrophic type. Echograms. (**a**) Grayscale US. Transverse scan. (**b**) Grayscale US. Longitudinal scan. (**c**) CDI. Longitudinal scan of the left lobe. (**d**) Compression US elastography. Longitudinal scan of the left lobe

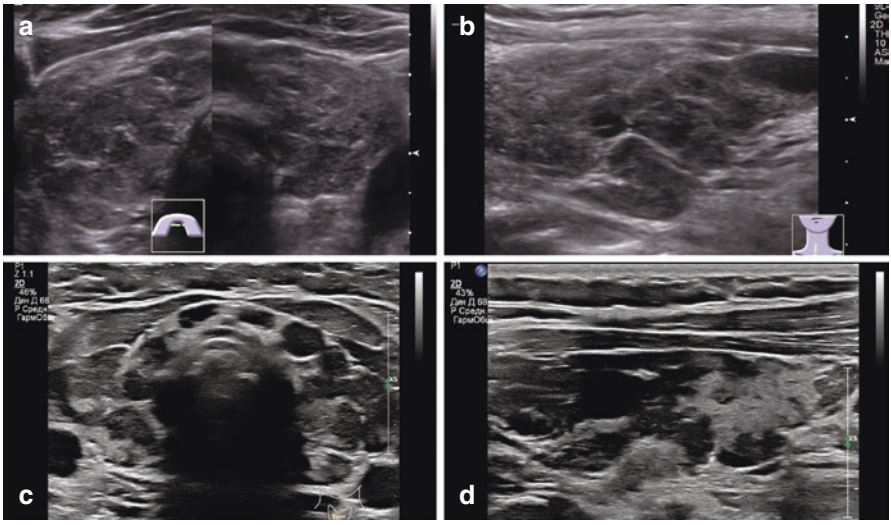

Fig. 4.11 AIT. Echograms. Hypoechoic heterogeneous pattern. Grayscale US. (**a**, **c**) Transverse scan. (**b**, **d**) Longitudinal scan of the left lobe

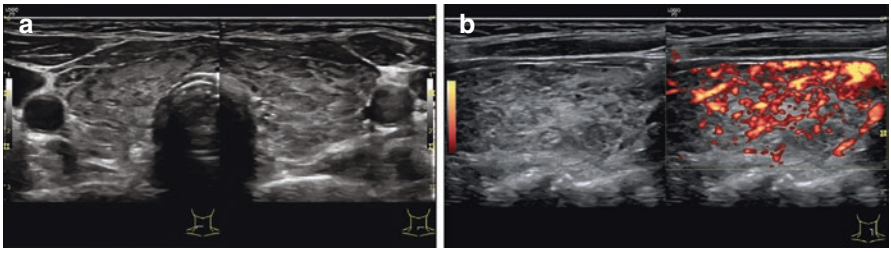

Fig. 4.12 AIT. Echograms. Pseudomicronodular pattern. (**a**) Grayscale US. Transverse scan. (**b**) PDI. Longitudinal scan of the left lobe

- Hypoechoic heterogeneous (Fig. 4.11)
- Pseudomicronodular (Fig. 4.12)
- Pseudomacronodular (Fig. 4.13)
- Significantly hypoechoic (Fig. 4.14)
- With prominent fibrous changes (Fig. 4.15)
- Hyperechoic heterogeneous

In hypertrophic AIT, US determines hypoechoic or isoechoic foci with inaccurate contours, named pseudonodules (false nodes). The term often implies a local hypertrophy of the thyroid parenchyma, which imitates true colloid nodule (Figs. 4.12, 4.13, and 4.17). In cases of enhancing cytotoxic process, they increase in size and heterogeneity and decrease in echodensity with a tendency to merge.

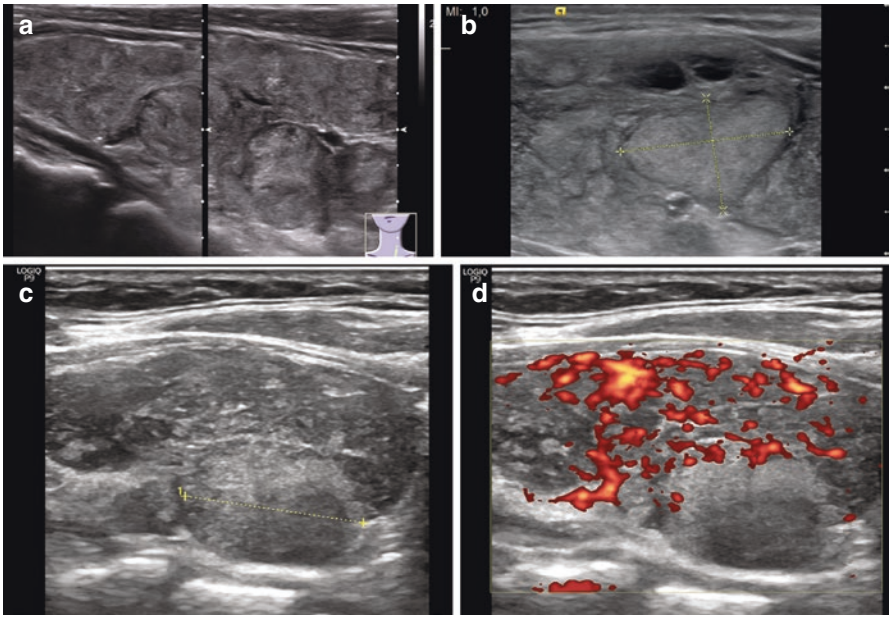

Fig. 4.13 AIT. Echograms. Pseudomacronodular pattern. (**a**, **b**) Grayscale US. (**c**, **d**) Pseudonodule in AIT. Grayscale US and PDI. Longitudinal scan of the left lobe

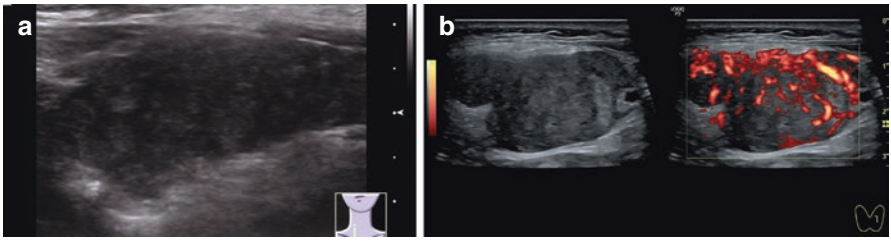

Fig. 4.14 AIT. Echograms. Significantly hypoechoic pattern. Longitudinal scan of the left lobe. (**a**) Grayscale US. (**b**) PDI

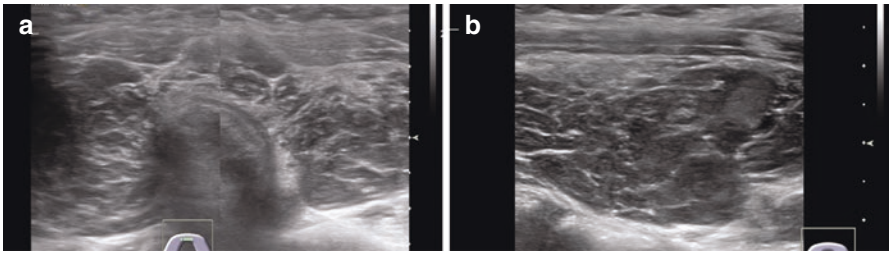

Fig. 4.15 AIT with prominent fibrous changes. Echograms. (**a**) Transverse scan. (**b**) Longitudinal scan of the right lobe

The US image of abnormal thyroid parenchyma in grayscale mode is quite variable. Some figuratively named signs are often mentioned in literature, such as:

- "Swiss cheese" sign is characterized by individual small pseudonodules (hypoechoic foci) (Fig. 4.16a).
- "Honeycomb" sign describes small merging pseudonodules, separated with parenchyma and/or connective tissue septa (so-called stromal component), more common for long-term process (Fig. 4.9c).
- "Cleft" sign is sometimes defined in AIT with prominent fibrous changes and demonstrates fibrous hyperechoic cord (cords) in the structure of the thyroid parenchyma, separating the anterior and posterior aspects (Fig. 4.16b).
- "White knight" sign identifies a lesion of increased echodensity on the background of diffusely decreased echodensity of the thyroid parenchyma. This is a benign regenerative formation, usually larger than 1 cm in size (Figs. 4.13c, d and 4.17).
- "Giraffe" sign refers to multiple thyroid lesions of increased echogenicity separated by thin hypoechoic rims of the parenchyma.

The term "chronic AIT with the formation of nodules" seems incorrect. Any lesion of various natures can occur in the autoimmune thyroid, but this is a different

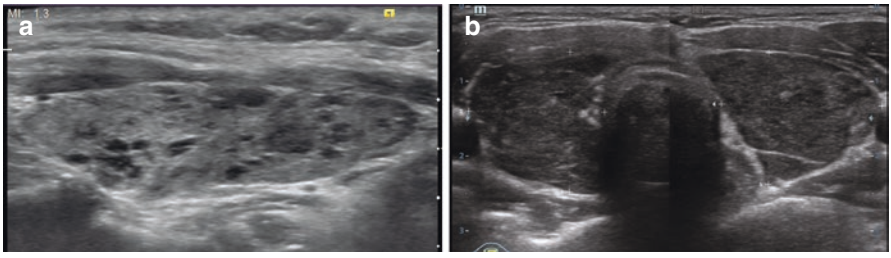

Fig. 4.16 AIT. Grayscale US. (**a**) "Swiss cheese" sign. Longitudinal scan. (**b**) "Cleft" sign. Transverse scan

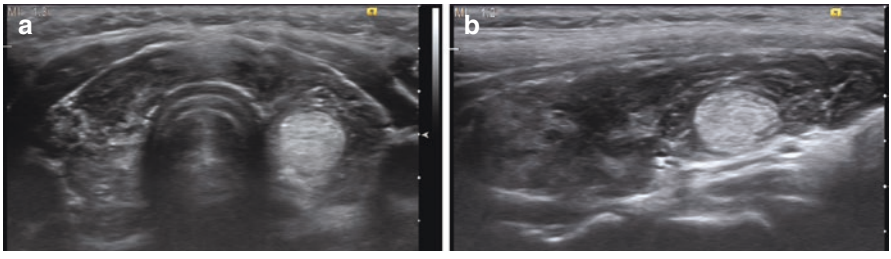

Fig. 4.17 "White knight" sign in AIT. Echograms. Grayscale US. (**a**) Transverse scan. (**b**) Longitudinal scan of the left lobe

disease that often precedes the occurrence of AITD. The differential diagnosis of lesions on the background of AIT is difficult and often impossible. The following principle features of true nodules in autoimmune thyroid may be considered:

- Rounded shape
- Decreased or normal echogenicity
- Homogeneous structure
- Smooth clear margins
- Perinodular vascularization with color-coded Doppler
- Different elasticity of nodules and the surrounding parenchyma with ultrasound elastography
- Different degree of contrast enhancement with CEUS (hyperenhancement is more common)

When analyzing the ultrasound image of irregular diffuse changes of the parenchyma in AIT, it is often difficult to choose the correct term for detected lesions. Commonly used "radiological slang," such as "nodule," "pseudonodule," "locus," "focus," and "emerging nodule," is not accepted by endocrinologists, surgeons, and pathologists. Correct interpretation of such lesions is difficult and often requires additional examinations. Prominent lesions are often described for follow-up purposes.

According to Ahuja [14], affected thyroid parenchyma in AIT is avascular. Hypertrophic AIT with hyperthyroidism exhibits an increase in vascularity of both the parenchyma and the connective tissue septa of the thyroid gland (Figs. 4.8b and 4.18).

An increase in quantitative parameters of blood flow in AIT is reported by Khamzina [15] with the following data: PSV = 0.3–0.75 m/s, RI = 0.44–0.79, and PI = 0.7–1.7. PSV in the inferior thyroid artery was measured in hypothyroidism 0.17 m/s, in euthyroidism 0.4 m/s, and in thyrotoxicosis 0.9–1.17 m/s.

With compression US elastography, the thyroid parenchyma in AIT exhibits medium- or coarse-grained asymmetric pattern of rigidity (Fig. 4.19a, b). With share-wave elastography, the stiffness (elasticity) of the parenchyma is usually normal or slightly increased (depending on the duration of the disease), more asymmetric as compared with normal thyroid gland. According to Ivanishina [16], the mean value of the Young's modulus in diffuse AIT is 16.3 kPa, ranging from 5.2 kPa to 69.4 kPa (Fig. 4.19c, d). It is not suitable for independent use, but allows to take into account the increase in stiffness while performing multiparametric thyroid US.

The initial forms of AIT are often diagnosed with US. In such cases characteristic changes in grayscale mode are not accompanied with changes in color Doppler. Conversely, hypervascularity of thyroid parenchyma may be the only marker of the diffuse AIT even with unchanged grayscale image.

One frequent indirect sign of AITD is enlarged lymph nodes near the inferior poles of the thyroid lobes and isthmus. Lymph nodes in the anterior neck compartment can compose a "chain" that spreads down to the anterior mediastinum. They commonly exhibit homogeneous structure and decreased echodensity, smooth

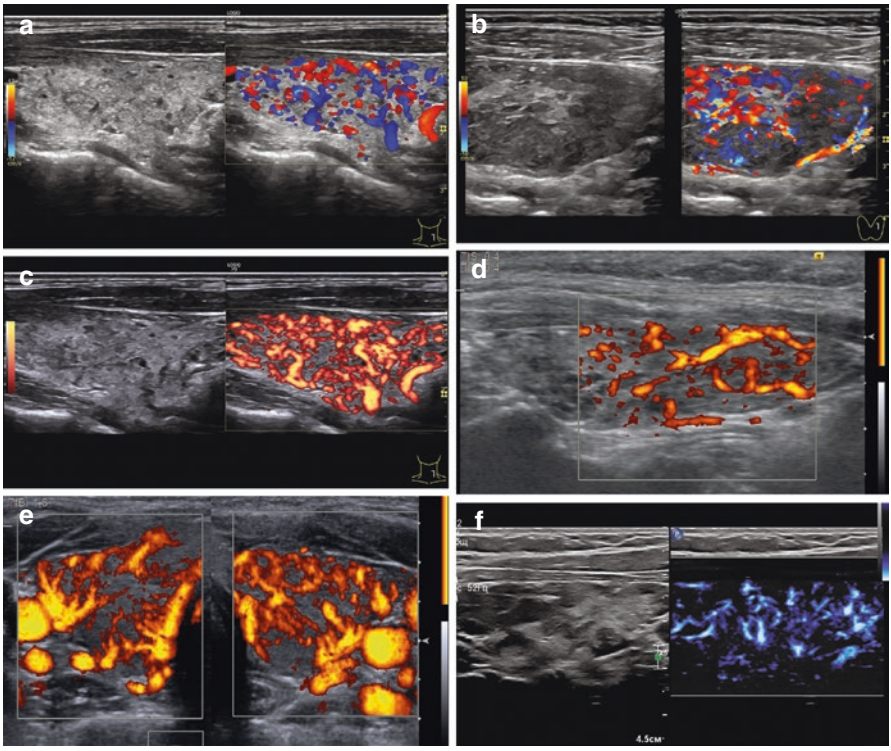

Fig. 4.18 AIT. Diffuse hypervascularization. Echograms. (**a**, **b**) CDI. (**c**–**e**) PDI. (**f**) Microflow imaging

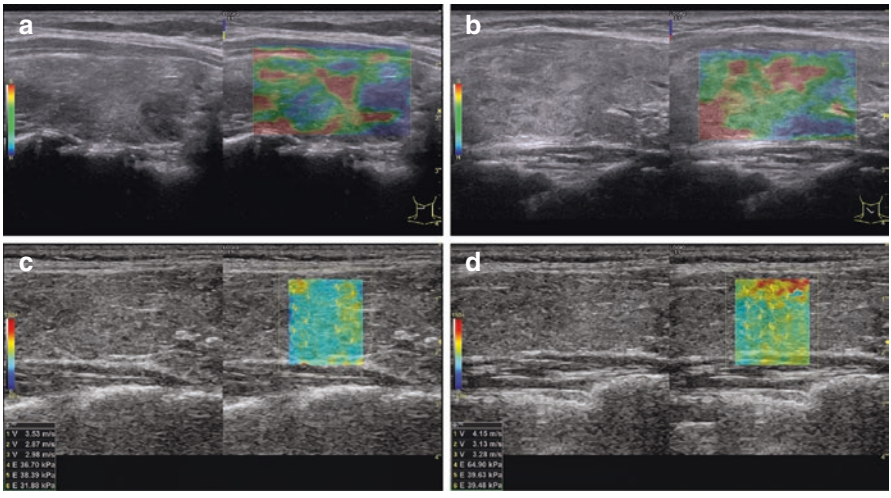

Fig. 4.19 AIT. (**a**, **b**) Compression US elastography. Irregular color pattern. (**c**, **d**) Share-wave elastography. Measurement of Young's modulus

well-defined margins, and oval or roundish shapes (Fig. 4.9d). Lymph node vascularization in CDI and PDI is normally decreased with an unchanged vascular pattern.

The specificity of US for the diagnosis of AIT is about 68–95% with the sensitivity of 54–89% and the diagnostic accuracy of 92%.

The value of CEUS in AIT is doubtful. It may be applied in suspicion of thyroid malignancy, especially for specification of invasion.

FNAB in patients with AIT is unnecessary in the majority of cases. It is reasonable only in suspicion of malignant tumor and lymphoma. A large number of tumors found in combination with AITD correspond morphologically to papillary cancer (87%); follicular thyroid carcinoma is recorded less often. The combination of AITD with medullary and anaplastic cancer is extremely rare.

The Example US Report in AIT

- First name, middle initial, last name:
- Age:
- Date:
- The number of case history:
- US scanner:

The thyroid gland is typically located with irregular and locally blurred margins.

The depth of the *isthmus*—13 mm			
Right lobe		Left lobe	
Depth	29 mm	Depth	24 mm
Width	22 mm	Width	23 mm
Length	54 mm	Length	51 mm
Volume	16.5 cm^3	Volume	13.5 cm^3

The total volume 30 cm^3 exceeds the upper limit.

The echodensity of the thyroid parenchyma is moderately decreased with heterogeneous echostructure and multiple hypoechoic areas of 0.2–0.7 cm in size with irregular indistinct contours. The stromal component is prominent. Vascular architectonics of the parenchyma in CDI and PDI is irregular. Blood flow intensity is increased. CPD is 20–25%.

Cystic and solid lesions are not detected.

Several hypoechoic avascular lymph nodes up to 0.5 × 0.9 cm in size are located close to the inferior poles of both lobes.

The lymph nodes along vascular bundles of the neck are up to 0.3 × 1.0 cm in size, with regular well-defined margins and unchanged differentiation and vascularity. The lymph nodes in supraclavicular areas are not enlarged.

Conclusion: Increase in thyroid volume with diffuse changes of the structure and vascularity of the thyroid gland characteristic of autoimmune thyroiditis.

US specialist:

4.3.2 Subacute Thyroiditis

Subacute (De Quervain's) thyroiditis (SAT) is a thyroid disease induced with upper respiratory tract viral infection, accompanied with inflammatory and destructive changes in thyroid parenchyma. Clinically, patients may present with severe thyroid pain and systemic symptoms of inflammatory disease proven with laboratory blood tests (especially, erythrocyte sedimentation rate). There may be a palpable painful thyroid mass. The disease passes three stages with hormonal status progressively changing from hyperthyroid to hypothyroid returning to euthyroid by the time of recovery.

Unlike acute thyroiditis, SAT is of viral origin. Morbidity relating to SAT corresponds to about 0.16–0.36% of all patients with thyroid pathology. As a rule, the patient's age is 20–50 years, and it is much more prevalent in women, with a ratio of 5:1. The disease is characterized by inflammation and lymphocytic infiltration of thyroid tissue.

The clinical classification of SAT is as follows:

1. SAT with an expressed inflammatory reaction (55%)
2. Slowly progressing SAT (28%)
3. SAT with clinical hyperthyroidism (15%)
4. Pseudoneoplastic SAT (2%)

Thyroid US permits early diagnosis of SAT. SAT is characterized by the following basic US features (Fig. 4.20):

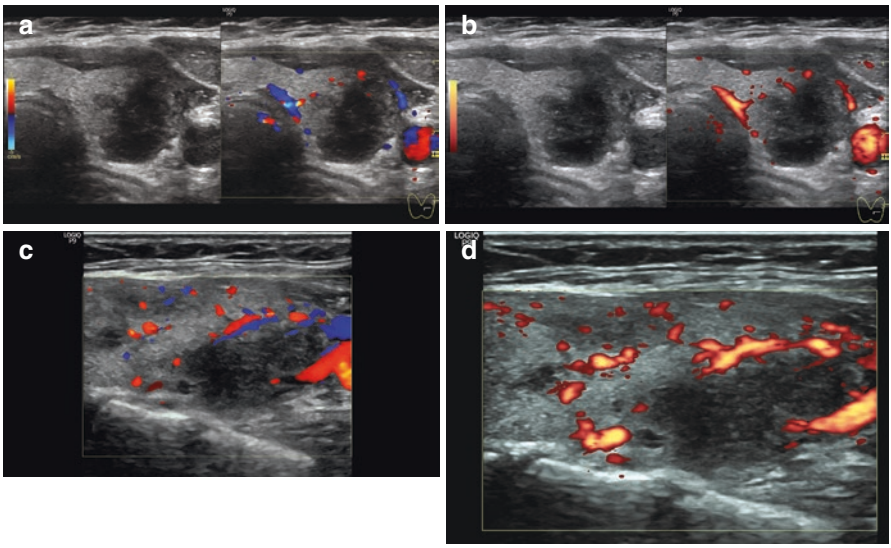

Fig. 4.20 Subacute thyroiditis. (**a**) Grayscale US and CDI, transverse scan of the left lobe. (**b**) Grayscale US and PDI, transverse scan of the left lobe. (**c**) CDI, longitudinal scan of the left lobe. (**d**) PDI, longitudinal scan of the left lobe

1. Thyroid enlargement.
2. Hypoechoic areas with indistinct margins or diffuse decrease in echogenicity of thyroid parenchyma.
3. Pain upon the compression of the thyroid by the US probe, especially at sites where the echodensity decreases.
4. Significant decrease in vascularity in hypoechoic areas with Doppler mapping.
5. Increased rigidity of affected areas with compression US elastography and share-wave elastography.
6. Enlarged cervical lymph nodes can be detected in the acute stage.

Fomina [17] describes the following three sonographic types of SAT:

1. Hypoechoic foci (66%). These are often observed in patients with a slowly progressing form of SAT.
2. Cystiform lobes (27%). This picture is seen in patients with both an expressed inflammatory reaction and clinical hyperthyroidism.
3. Hypoechoic lobes (7%).

Hypoechoic areas appear avascular or significantly hypovascular with CDI and PDI in the acute stage of De Quervain's thyroiditis. At the same time, the vascularity of the surrounding parenchyma is usually not affected or is slightly decreased (Fig. 4.20). According to Fomina [17], the average blood flow velocities in the arteries within the pathological foci decrease twofold or more (PSV of 9.83 ± 2.42 cm/s, EDV of 4.7 ± 2.05 cm/s, RI of 0.52 ± 0.16, and PI of 0.72 ± 0.23). The blood flow velocities and resistance indices observed with PW Doppler in the main thyroid vessels do not differ from the normal thyroid in SAT.

Compression US elastography and share-wave elastography reveal significant rigidity of the affected hypoechoic area, which is substantially stiffer as compared with normal parenchyma (Fig. 4.21).

Recovery phase is sonographically characterized by a gradual decrease in thyroid volume and the restoration of the normal structure and echogenicity of the thyroid parenchyma. Complete restoration may take from 2 months up to 1.5 years. The structure becomes normal again in about 75% of patients. Residual changes can thus be observed in 25% of the patients transforming to AIT.

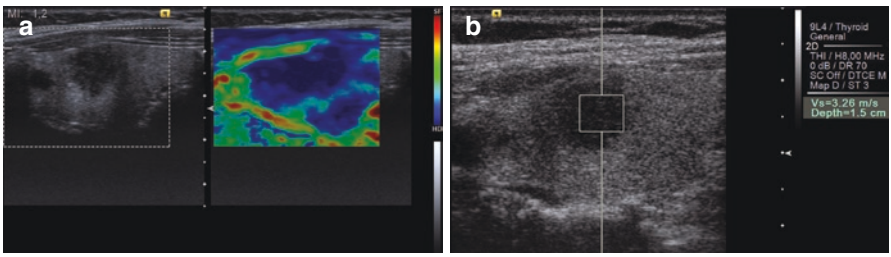

Fig. 4.21 Subacute thyroiditis. (**a**) Stiff pattern with compression US elastography. (**b**) High share-wave velocity with ARFI

SAT recurrence arises in 30–35% of patients and is easily detected sonographically, even in cases with minimal clinical signs. Slow restoration of normal thyroid echostructure is a predictor of SAT recurrence.

The Example US Report in SAT

- First name, middle initial, last name:
- Age:
- Date:
- The number of case history:
- US scanner:

The thyroid gland is typically located with regular well-defined margins and homogeneous isoechoic structure. The capsule is uniform and continuous on all extent.

The depth of the *isthmus*—4 mm			
Right lobe		Left lobe	
Depth	17 mm	Depth	22 mm
Width	15 mm	Width	19 mm
Length	53 mm	Length	54 mm
Volume	6.5 cm^3	Volume	10.8 cm^3

The total volume 17.3 cm^3 close to the edge of the upper limit.

No lesions detected	Significantly hypoechoic focus of 1.8 × 1.6 × 2.4 cm in size with irregular blurred margins, hypovascular, rigid with USE, and moderately painful with compression is located in the inferior segment

The echodensity of the thyroid parenchyma is moderately diffusely decreased. Vascular pattern of the parenchyma out of described areas in CDI and PDI is unchanged. CPD is 10%.

The lymph nodes along vascular bundles of the neck are enlarged up to 0.7 × 1.4 cm, hypoechoic, and heterogeneous with regular well-defined margins and unchanged differentiation and vascularity.

The lymph nodes in supraclavicular areas are not enlarged.

Conclusion: Focal changes of left lobe of the thyroid gland suspicious for subacute thyroiditis.

US specialist:

4.3.3 Acute Thyroiditis

Acute thyroiditis (AT) is a relatively rare disease. Women suffer four times more often than men. The mean age at presentation is 30–40 years. The thyroid gland appears to be relatively resistant to infection [18]. A rich vascular supply and an extended lymphatic drainage, as well as a fibrous capsule and an anatomic

separation from the other structures of the neck by fascial planes, represent protective mechanisms. The high iodine content of the gland may account for some bactericidal effect. AT may be purulent or nonpurulent and further distinguished based on the diffuse or focal involvement of the thyroid parenchyma.

Purulent AT is a consequence of the penetration of bacterial coccal flora into thyroid tissue from sites of infection (abscess, tonsillitis, pneumonia, etc.), mediated by lymphogenous or hematogenous extension. The inflammatory process seldom involves the whole thyroid gland due to structural features (isolation of lobes with the connective tissue septa). Typically, only one lobe is affected. Purulent inflammation leads to thyroid abscess, which may be complicated with a fistula or mediastinitis. In rare cases, the extensive destruction of thyroid parenchyma can result in hypothyroidism.

Nonpurulent AT is associated with aseptic inflammation of thyroid tissue after trauma, radiation therapy, or radioiodine therapy in patients with Graves' disease.

The principal US features of AT are as follows (Fig. 4.22):

1. Asymmetric enlargement of the thyroid, mainly at the expense of one lobe.
2. Local or diffuse decrease in echodensity.
3. Heterogeneous structure with hypoechoic fields.
4. Pain upon the compression of the lobe by the US probe and limited mobility of the thyroid.
5. Hypervascularity of the affected area in CDI and PDI before purulent destruction. In the cases of suppurative process leading to abscess, the area appears avascular.
6. Cervical lymphadenitis.

In rare cases, AT may result in a thyroid abscess. In such cases, sonography shows a hypoechoic heterogeneous lesion of irregular shape along with diffuse changes in the thyroid parenchyma. The abscess contains irregular-shaped fluid collections with an echogenic suspension and is characterized by fast changes in US features (Fig. 4.23). The longer lasts the abscess, the more regular become the cavities and an echogenic capsule arises. Thyroid abscess may result in a cyst. Alternatively, the fibrous changes in the abscess may form in a heterogeneous avascular hypoechoic thyroid lesion with echogenic inclusions that is detected with US lifelong.

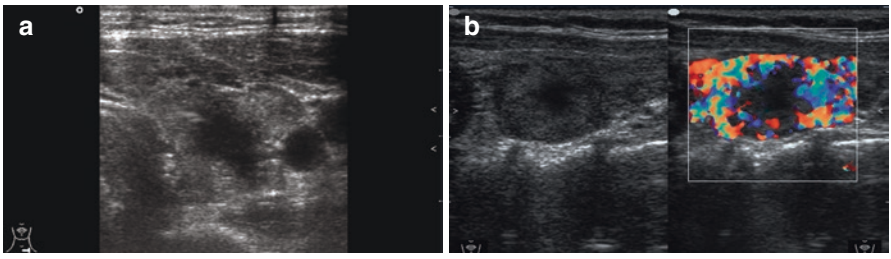

Fig. 4.22 Acute thyroiditis. (**a**) Grayscale US. (**b**) CDI

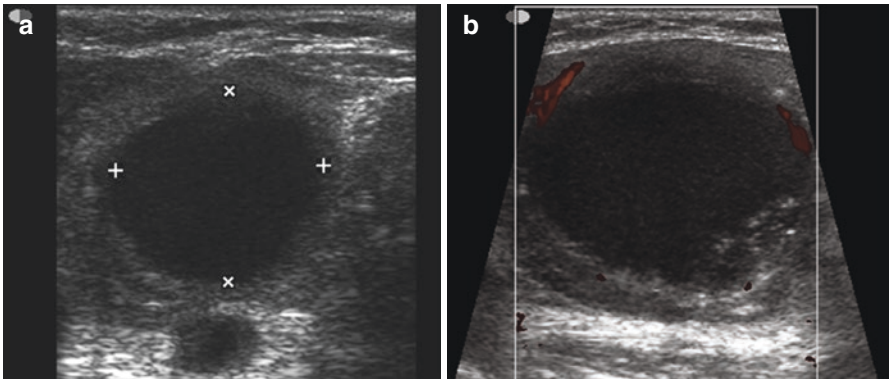

Fig. 4.23 Thyroid abscess. (**a**) Grayscale US. (**b**) PDI

The Example US Report in Acute Thyroiditis

- First name, middle initial, last name:
- Age:
- Date:
- The number of case history:
- US scanner:

The thyroid gland is typically located with regular well-defined margins and homogeneous isoechoic structure. The capsule is uniform and continuous on all extent.

The depth of the *isthmus*—13 mm			
Right lobe		Left lobe	
Depth	27 mm	Depth	15 mm
Width	25 mm	Width	16 mm
Length	57 mm	Length	50 mm
Volume	18.4 cm^3	Volume	5.7 cm^3

The total volume 24.1 cm^3 exceeds the upper limit.

Hypoechoic hypovascular areas of different size and shape with irregular blurred margins and small fluid collections containing homogenous suspension, painful with compression, are located within the middle and inferior segments	No lesions detected

Vascular pattern of the parenchyma out of described areas in CDI and PDI is unchanged. CPD is 10%.

The lymph nodes along vascular bundles of the neck are enlarged up to 0.8 × 2.0 cm, hypoechoic, and heterogeneous with regular well-defined margins, unchanged differentiation, and moderately increased vascularity in hilus and central part. The lymph nodes in supraclavicular areas are not enlarged.

Conclusion: Increase in volume and diffuse changes of the right thyroid lobe suspicious for acute thyroiditis.

US specialist:

References

1. Gutekunst R, Becker W, Hehrmann R, et al. Ultraschalldiagnostik der Schilddrüse. Dtsch Med Wochenschr. 1988;113:1109–12.
2. Smyth PPA, Darke C, Parkes AB, et al. Assessment of goiter in an area of endemic iodine deficiency. Thyroid. 1999;9(9):895–901.
3. World Health Organization. Indicators for assessing iodine deficiency disorders and their control programmes. WHO/NUT/93.1, pp. 12–5; 1993.
4. Dedov II, Troshina EA, Yu YP, et al. Diagnosis of diseases of the thyroid gland. Moscow: Springer; 2001.
5. Kahaly GJ, Bartalenab L, Hegedüs L, et al. 2018 European Thyroid Association Guideline for the management of Graves' hyperthyroidism. Eur Thyroid J. 2018;7:167–86.
6. Donkol RH, Nada M, Boughattas S. Role of color Doppler in differentiation of Graves' disease and thyroiditis in thyrotoxicosis. World J Radiol. 2013;5(4):178–83.
7. Kim TK, Lee EJ. The value of the mean peak systolic velocity of the superior thyroidal artery in the differential diagnosis of thyrotoxicosis. Ultrasonography. 2015;34:292–6.
8. Erbil Y, Barbaros U, Ozbey N, et al. Graves, disease, with and without nodules, and the risk of thyroid carcinoma. J Laryngol Otol. 2008;122:291–5.
9. Romanchyshen AF, Yakovlev PN. Features of surgical treatment of patients with nodal tumors of the thyroid gland on the background of diffuse toxic goiter. Vestnik Khirurgii. 2005;164(1):21–4.
10. Yano Y, Shibuya H, Kitagawa W, et al. Recent outcome of graves, disease patients with papillary thyroid cancer. Eur J Endocrinol. 2007;157:325–9.
11. ICD-10. International statistical classification of diseases and related health problems. 10th revision. 5th ed. Geneva: World Health Organization; 2016.
12. Adamina M, Oertli D. Thyroiditis. In: Oertli D, Udelsman R, editors. Surgery of the thyroid and parathyroid glands. New York: Springer; 2007.
13. Kharchenko VP, Kotlyarov PM, Smetanin LI. Ultrasound diagnosis of thyroid diseases. Moscow: Strom; 1999.
14. Ahuja A. The thyroid and parathyroid. In: Ahuja A, Evans R, editors. Practical head and neck ultrasound. London: Greenwich Medical Media Ltd; 2000.
15. Khamzina FT. Application of color dopplerography in diagnostics. Kazan Med J. 2007;88(3):250–4.
16. Ivanishina TV. Diagnostic possibilities of shear wave elastography in thyroid disease. PhD thesis. Moscow; 2017.
17. Fomina IY. The role of high frequency echography in the diagnosis of subacute De Quervain's thyroiditis. PhD thesis. Nijniy Novgorod; 2003.
18. Oertli D, Udelsman R, editors. Surgery of the thyroid and parathyroid glands. New York: Springer; 2012.

Ultrasound Diagnosis in Benign Thyroid Lesions

5

Alexander N. Sencha, Yury N. Patrunov, Ella I. Peniaeva, Liubov A. Timofeyeva, Munir G. Tukhbatullin, and Ekaterina A. Sencha

Nodular goiter is a clinical concept that does not always coincide with a morphological definition. In clinical practice it is thought to mean a thyroid lesion of any size having a capsule that may be defined by palpation or by means of any imaging modality. A "multinodular goiter" is characterized by the presence of two or more nodules within the thyroid gland.

Thyroid nodules are detected in 4–15% of the population. The nodules are observed in more than 50% of patients with thyroid pathology; the incidence of nodules can reach 98.9% in endemic regions [1]. Thyroid nodules are identified in more than half of all autopsies [2]. The incidence of nodular goiter correlates with age.

Thyroid lesions include both colloid nodules and tumors. The latter are divided into the following groups according to the WHO histological classification (1988):

A. N. Sencha (✉)
Department of Visual and Functional Diagnostics, National Research Center for Obstetrics, Gynecology and Perinatology, Ministry of Healthcare of the Russian Federation, Moscow, Russia

Y. N. Patrunov · E. I. Peniaeva
Department of Ultrasound Diagnostics, Center for Radiological Diagnostics of Non-State Healthcare Institution Yaroslavl Railway Clinic of JSC "Russian Railways", Yaroslavl, Russia

L. A. Timofeyeva
Department for Internal Diseases Propaedeutic, Course of Diagnostic Radiology of Medical Faculty of Federal State Budget Educational Institution of Higher Education "I. N. Ulianov Chuvash State University", Cheboksary, Russia

M. G. Tukhbatullin
Department of Ultrasound Diagnostics, Kazan State Medical Academy – Branch Campus of the Federal State Budget Educational Institution of Further Professional Education, "Russian Medical Academy of Continuing Professional Education" of the Ministry of Healthcare of the Russian Federation, Kazan, Russia

E. A. Sencha
Ultrasound Diagnostics Department, Medical Diagnostic Center, Moscow, Russia

A. N. Sencha, Y. N. Patrunov (eds.), *Thyroid Ultrasound*,
https://doi.org/10.1007/978-3-030-14451-7_5

1. Epithelial tumors
   a. Benign
      - Follicular adenoma
      - Others
   b. Malignant
      - Follicular carcinoma
      - Papillary carcinoma
      - Medullary carcinoma
      - Undifferentiated (anaplastic) carcinoma
      - Others
2. Nonepithelial tumors
   a. Benign
   b. Malignant
3. Malignant lymphomas
4. Miscellaneous tumors
5. Secondary tumors
6. Unclassified tumors
7. Tumorlike lesions

Thyroid lesions are assessed by the following US criteria:

1. Number of nodules
2. Location (in lobes and segments, in relation to the capsule, vascular bundles, or trachea)
3. Dimensions
4. Shape (roundish, oval, irregular)
5. Borders (smooth, rough)
6. Contours (well defined, indistinct)
7. Echodensity
8. Echostructure (the degree heterogeneity)
9. Calcifications (the dimensions, location, and presence of acoustic shadowing)
10. Fluid component (the dimensions and the ratio of fluid to solid components)
11. Peripheral halo
12. Posterior echo change (enhancement or shadowing)
13. Vascularity
14. Elasticity/rigidity with USE and SWE
15. Contrast enhancement, wash-in and wash-out with CEUS

Thyroid nodules may be solitary, multiple (two and more), or conglomeratic (when some nodules merge into one lesion).

The dimensions of nodules are measured in three mutually perpendicular planes. Each dimension (length, width, or depth) is the maximum between the opposite margins of the lesion. Nodule volume is calculated by the standard formula $V = (L \times W \times D) \times 0.52$, where L, W, and D are the length, width, and depth of the nodule, respectively [3]. The calculation of nodule volume in addition to its dimensions is important for precise dynamic follow-up of the thyroid lesions in cases of conservative treatment or minimally invasive modalities.

5.1 Nodular Goiter

Nodular goiter (colloid goiter, nontoxic nodular goiter, simple goiter) is a benign thyroid disease in the form of a nodule (nodules) containing ordinary cells and colloid. It is often associated with iodine deficiency and accounts for 60–75% of all thyroid lesions.

The basic US features of colloid nodules are as follows (Fig. 5.1):

- Oval (or roundish) shape
- Well-defined, smooth margins
- Intact thyroid capsule
- Decreased or unchanged echodensity in most cases
- Heterogeneous structure, often fluid inclusions
- Possible calcifications within the lesion and peripheral "egg-shell" calcification
- Hypoechoic surrounding halo
- Possible posterior echo enhancement
- A- or hypovascularity in CDI and PDI
- Medium elasticity with elastography and elastometry

Obligatory US features of colloid nodule are well-defined margins and intact capsule of both the nodule and thyroid gland. Long-lasting colloid nodules may contain coarse calcifications and shell-shaped or egg-shell peripheral impregnations. A calcium capsule may be observed in 2–4% of cases and can reach 2–3 mm thick (Fig. 5.2). The peripheral calcification significantly differs from microcalcifications and large echogenic inclusions, which are often detected in thyroid cancer.

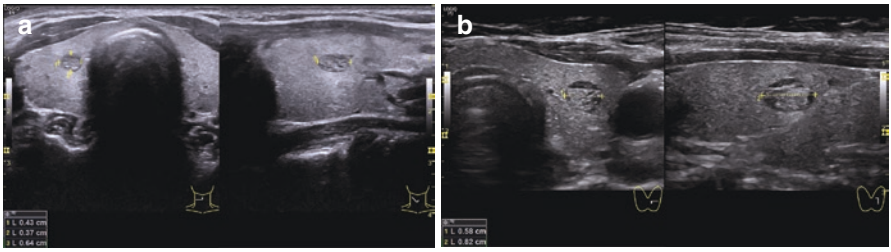

Fig. 5.1 (**a**, **b**) Colloid nodule. Grayscale sonography

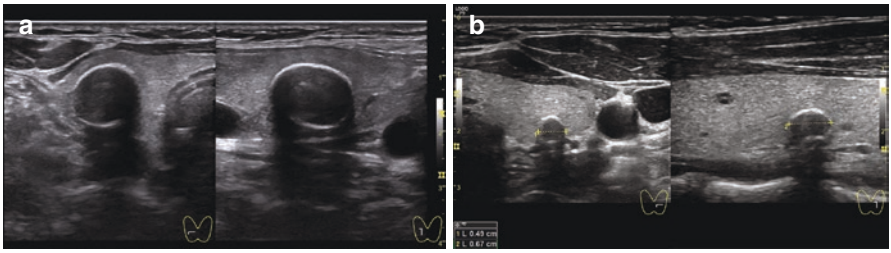

Fig. 5.2 (**a**, **b**) Colloid nodule. Grayscale sonography. "Egg-shell" calcification

Seventy to eighty percent of colloid goiters appear to be multinodular (Fig. 5.3). Multiple nodules often show identical echostructure. Combinations of colloid nodules with cysts, adenomas, or thyroid cancer are less common [4].

Colloid nodules show a peripheral pattern of blood flow with individual vascular signals in CDI in 40–50% of cases. This pattern is associated with the benign character of the nodules. According to Zubarev et al. [5] and Markova [6], CDI and PDI show rectilinear vascular structures that are normally distributed within colloid nodules (Fig. 5.4).

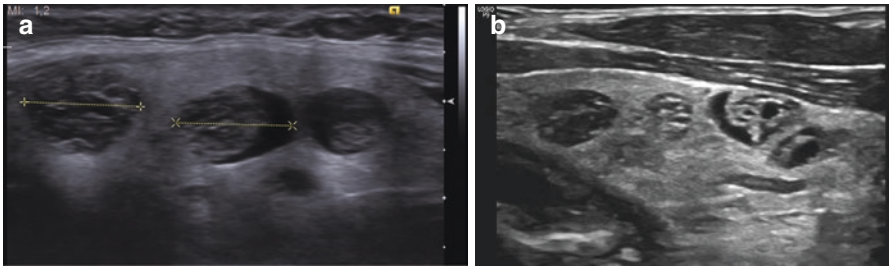

Fig. 5.3 (**a**, **b**) Multiple colloid nodules. Grayscale sonography

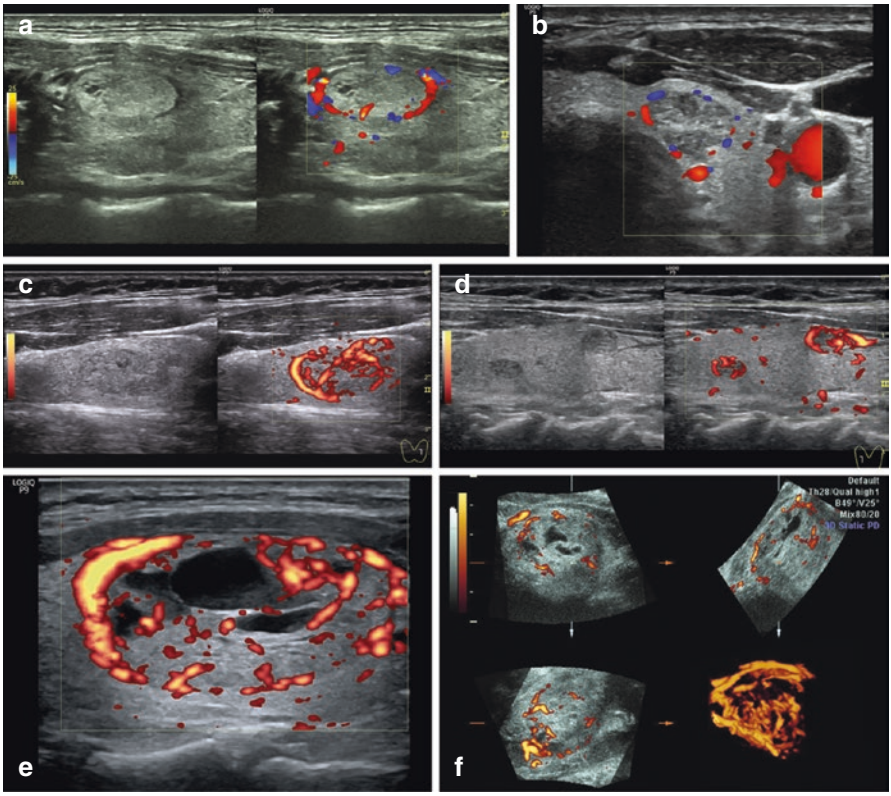

Fig. 5.4 Colloid nodule. Predominantly peripheral blood flow pattern. Sonograms. (**a**, **b**) CDI. (**c**–**e**) PDI. (**f**) 3DPD

Qualitative data of compression USE and quantitative parameters of elasticity (Young's modulus, strain-ratio index, share-wave velocity) in colloid nodes commonly reveal medium stiffness (elasticity), equal to the surrounding unchanged thyroid parenchyma (Fig. 5.5).

There is no need to use CEUS for typical colloid nodules. CEUS in colloid nodules commonly shows hypoenhancement, without any signs of hypervascularity and neoanogenesis (Fig. 5.6). Peripheral ring-shaped contrast enhancement is highly specific for benign thyroid nodules (sensitivity 83%, specificity 94%, positive predictive value 94%, negative predictive value 84%, overall accuracy of 88%) [7].

The specificities of US in grayscale, CDI, PDI, and 3D at diagnosing colloid nodules are 32.1, 47.6, 69.6, and 84.1%; their sensitivities are 70.7, 61.6, 65.5, and 75.7%; and their diagnostic accuracies are 53.1, 56.5, 70.3, and 79.8%, respectively [8]. According to Zubarev et al. [5], Doppler options and 3D reconstruction increase the sensitivity of sonography to colloid nodules by 5% (up to 75.5%), the specificity by 52% (up to 84.1%), and the diagnostic accuracy by 26.7% (up to 79.8%).

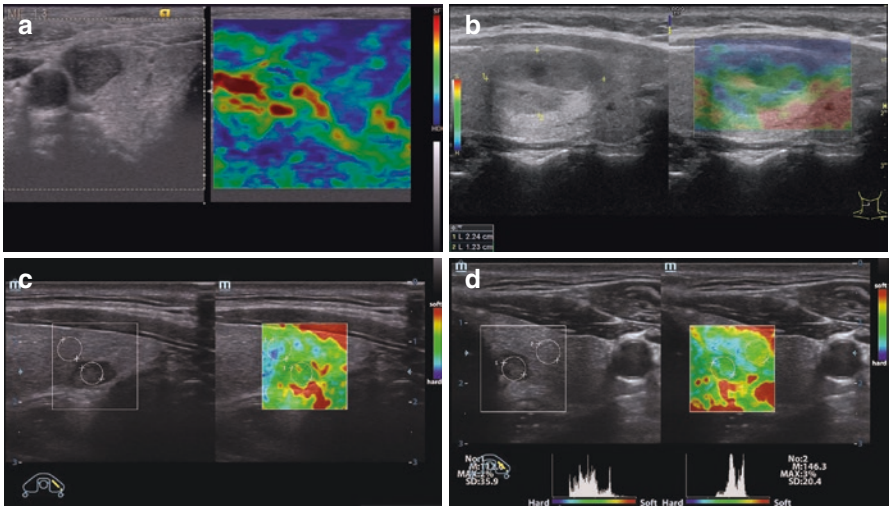

Fig. 5.5 Colloid node. (**a**, **b**) Compression USE. Color pattern similar to the surrounding thyroid parenchyma. (**c**, **d**) Strain-ratio index equal to normal thyroid tissue

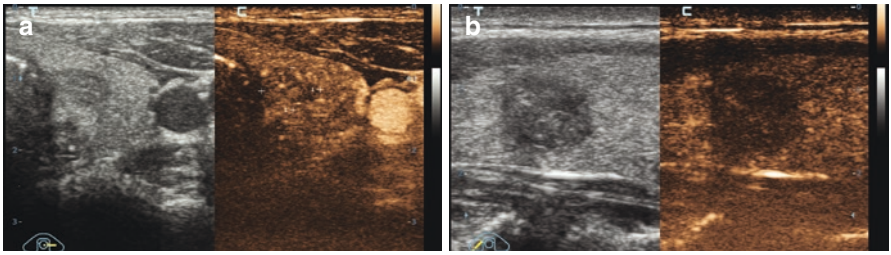

Fig. 5.6 (**a**, **b**) Colloid thyroid nodule. CEUS with SonoVue® 2.4 mL

The Example US Report in Colloid Goiter

- First name, middle initial, last name:
- Age:
- Date:
- The number of case history:
- US scanner:

The thyroid gland is typically located with regular well-defined margins and homogeneous isoechoic structure. The capsule is uniform and continuous on all extent.

The depth of the *isthmus*: 4 mm			
Right lobe		Left lobe	
Depth	16 mm	Depth	15 mm
Width	17 mm	Width	16 mm
Length	51 mm	Length	50 mm
Volume	6.6 cm^3	Volume	5.7 cm^3
The total volume 12.3 cm^3 does not exceed the upper limit			
A hypoechoic heterogeneous hypovascular nodule of 0.5 × 0.5 × 0.6 cm in size of roundish shape with well-defined regular margins, soft with USE, strain ratio 1.1, is located in the middle compartment of the lobe		A hypoechoic homogeneous avascular nodule of 0.8 × 0.7 × 0.9 cm in size with well-defined regular margins, soft with USE, strain ratio 1.1, is located in the inferior segment of the lobe	

The vascular pattern of the parenchyma is normal and symmetric with CDI and PDI. CPD is 10–15%.

The lymph nodes in the neck and supraclavicular areas are not enlarged.

CONCLUSION: Thyroid nodules, TIRADS 2.

US specialist:

5.2 Cyst

Thyroid cysts are thin-walled cavitary lesions filled with fluid (commonly, colloid). Cysts comprise up to 3–5% of all thyroid nodules. True cysts with flat epithelium lining make up <0.5% of all thyroid lesions and, as a rule, are represented by a single cyst. Fluid collections, which are often detected in thyroid nodules, are in most cases a consequence of colloid accumulation or degenerative changes.

Thyroid cysts are sonographically characterized by the following typical features (Fig. 5.7):

- Roundish or oval shape.
- Regular, well-defined margins.
- Anechoic homogenous inner structure; in rare cases the presence of echogenic inclusions or an isoechoic component is possible.
- Dorsal echo enhancement, especially intense in cysts over 5 mm in size.

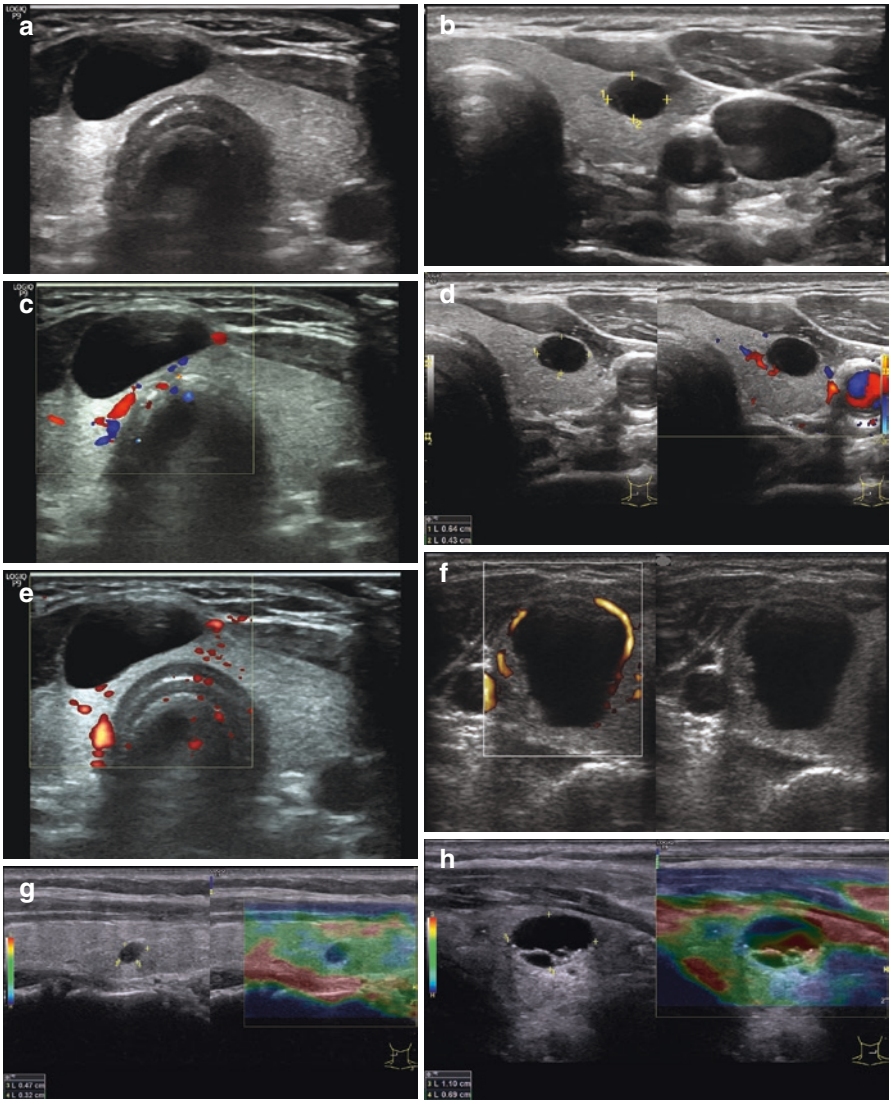

Fig. 5.7 Simple thyroid cyst. (**a**, **b**) Grayscale US. (**c**, **d**) CDI. (**e**, **f**) PDI. (**g**, **h**) Compression USE

- Lateral acoustic shadows, more often associated with cysts over 10 mm in size.
- Avascularity in CDI and PDI and in rare cases vascularization of a solid component.
- Compression US elastography reveals Score 1 according to Ueno-Itoh scale, which corresponds with either a homogeneous elasticity throughout the lesion or the image in three layers produced by reverberation artifacts. No color pattern is often observed. The average strain ratio is 0.5–2.
- Avascularity (perfusion defect) with CEUS.

Thyroid cysts differ in their origins and morphological structures. The following types can be defined [9]:

1. Simple colloid cysts
2. Complex cysts (Fig. 5.8)
   - Result from previous inflammatory processes in thyroid parenchyma
   - Filled with transudate
   - Contain the products of hemorrhages
   - The connective tissue component merges into the lumen
   - Have an epithelial component

Thyroid nodules that contain dense colloid may be observed as anechoic lesions and smooth, well-defined margins. They usually measure up to 1 cm in size and often show distinct point-like echogenic signals with a "comet tail," which

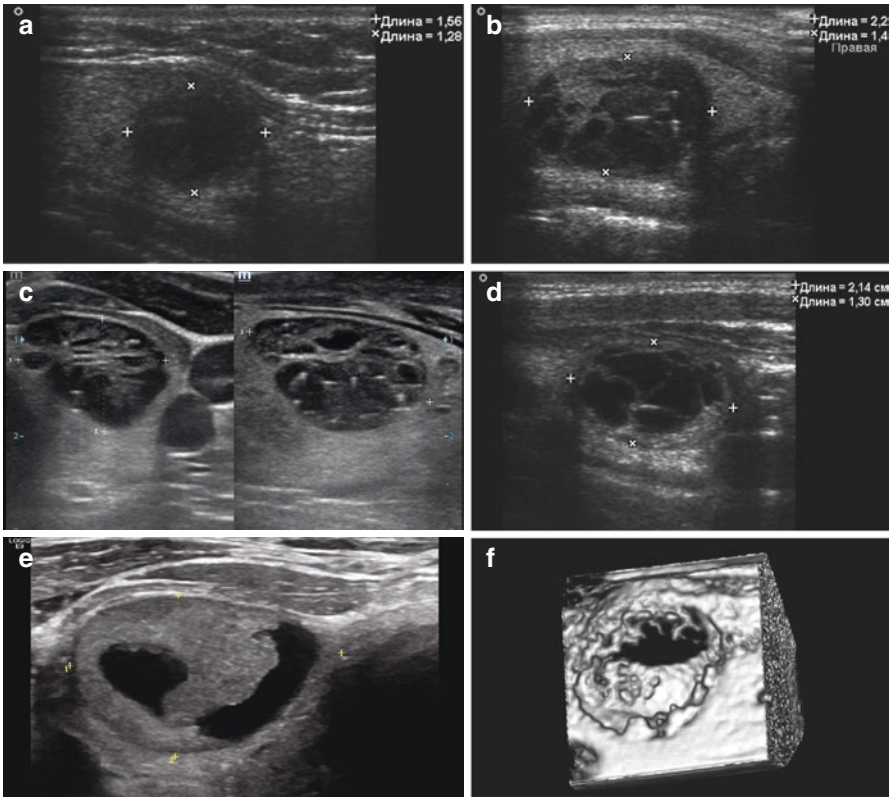

Fig. 5.8 Complex thyroid cyst. (**a**, **b**) Complex thyroid cyst containing products of hemorrhage. Grayscale sonography. (**c**, **d**) Complex thyroid cyst with connective tissue component. Grayscale sonography. (**e**) Complex thyroid cyst with epithelial component. Grayscale sonography. (**f**) 3D reconstruction

characterize dense colloid contents [10]. The "comet tail" is an acoustic phenomenon that results from ultrasound reverberation. It is observed when the US wave is caught between two or multiple reflecting surfaces. Reverberations occurring in grayscale sonography are detected as a short hyperechoic trace ("tail") behind the source of the artifact (Fig. 5.9).

The abovementioned colloid lesions are normally multiple and correspond morphologically to enlarged follicles (macrofollicles) (Fig. 5.10). All cysts, including complex cysts, appear avascular in CDI and PDI (Fig. 5.11).

The incidence of malignancy in cystic lesions is about 7–19% [11]. Up to 20–30% of papillary thyroid cancers demonstrate fluid collections [12]. In cases

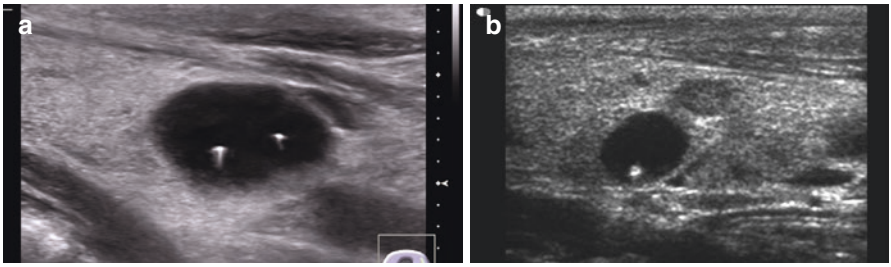

Fig. 5.9 (**a**, **b**) Colloid cyst. "Comet tail" sign. Grayscale sonography

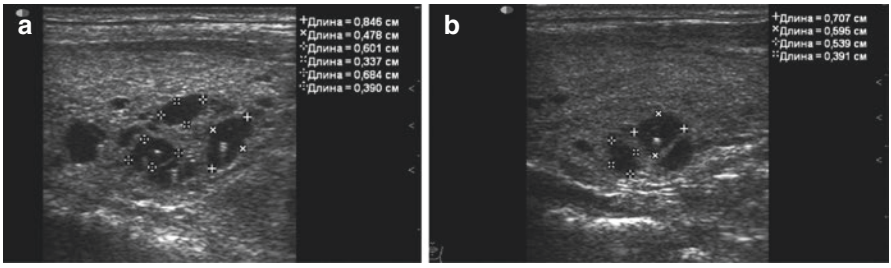

Fig. 5.10 Multiple colloid cysts (macrofollicles). (**a**, **b**) "Comet tail" sign. Grayscale sonography

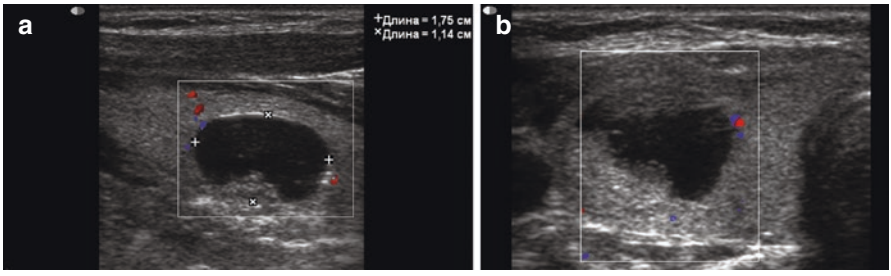

Fig. 5.11 (**a**, **b**) Complex cysts. Avascularity with CDI

with a solid component within the cyst, CDI and PDI are required. Increased vascularity of connective tissue septa and solid components demands further examinations (Fig. 5.12). Avascularity of septa is a reliable sign of a benign process. This is an important feature that permits nodule differentiation. CEUS is very sensitive in the detection of low-velocity blood flow in septa and solid component, thus contributing to differential diagnosis of complex cysts (Fig. 5.13). Solid component of complex thyroid cysts often exhibits the stiffness that is different from fluid component with compression US elastography and share-wave elastography (Fig. 5.14). However, the presence of fluid collections makes these options less reliable.

The specificities of US in grayscale, CDI, PDI, and 3D for thyroid cysts are 26, 63, 63, and 63%, with sensitivities of 96, 90, 90, and 90% and diagnostic accuracies of 64, 80, 80, and 80%, respectively [8].

Sonography permits not only cyst detection but also preliminary assessment of the nature of these lesions. However, it is often impossible to determine the

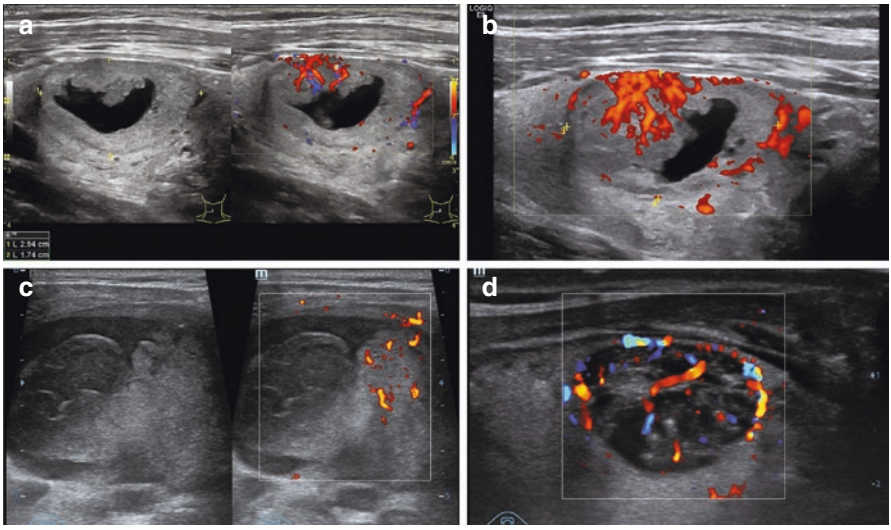

Fig. 5.12 (**a**–**d**) Papillary thyroid cancer with fluid component and hypervascular solid part. Echograms. Gray scale mode, CDI, PDI

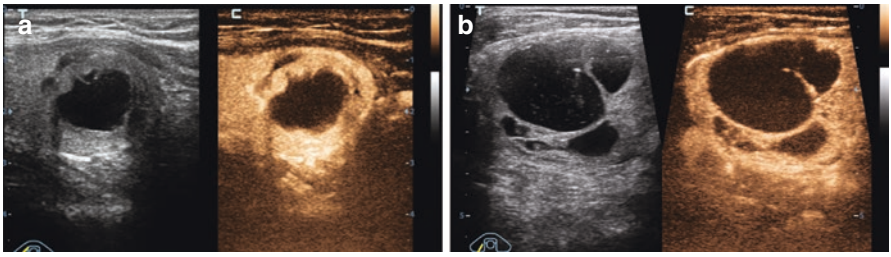

Fig. 5.13 (**a**, **b**) Thyroid lesion with fluid collections and vascularized solid component. Thyroid CEUS with SonoVue® 2.4 mL. FNAB returned colloid nodule, BSRTC 2

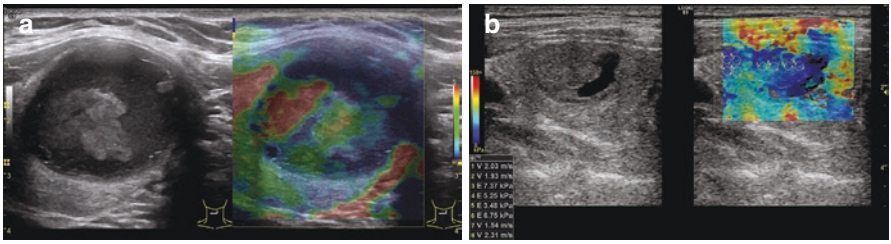

Fig. 5.14 Complex thyroid cyst. (**a**) Compression US elastography. (**b**) Quantitative parameters with share-wave elastography

morphological nature of the solid part of a complex cyst with a single US examination. Therefore, any suspicion of thyroid malignancy should be followed by US-guided FNAB.

The Example US Report in Thyroid Cyst

- First name, middle initial, last name:
- Age:
- Date:
- The number of case history:
- US scanner:

The thyroid gland is typically located with regular well-defined margins and homogeneous isoechoic structure. The capsule is uniform and continuous on all extent.

The depth of the *isthmus*: 3 mm			
Right lobe		Left lobe	
Depth	16 mm	Depth	15 mm
Width	17 mm	Width	16 mm
Length	51 mm	Length	50 mm
Volume	6.6 cm^3	Volume	5.7 cm^3
The total volume 12.3 cm^3 does not exceed the upper limit			
A homogenous anechoic avascular lesion of 0.9 × 0.8 × 0.5 cm in size of roundish shape with well-defined regular thin walls and posterior enhancement is located in the inferior segment of the lobe. Compression US elastography detects no color pattern, strain ratio is 1.0		A homogenous anechoic avascular lesion of 0.9 × 1.0 × 0.8 cm in size with well-defined regular margins and a single echogenic signal within its central compartment is located in the middle segment of the lobe. Compression US elastography detects no color pattern, strain ratio is 1.2	

The vascular pattern of the parenchyma is normal and symmetric with CDI and PDI. CPD is 10–15%.

The lymph nodes in the neck and supraclavicular areas are not enlarged.

CONCLUSION: Fluid (probably, colloid) thyroid lesions. TIRADS 2.

US specialist:

5.3 Adenoma

Adenomas are benign thyroid tumors, which develop as a result of local thyrocyte hyperplasia and proliferation due to genetic abnormality in a single precursor cell. Toxic adenomas (Plummer's disease) autonomously overproduce thyroid hormones and are accompanied by clinical symptoms of thyrotoxicosis.

Adenomas occupy 16–25% of all thyroid lesions [1]. They are typically represented by a solitary nodule. Multiple lesions are rare.

Thyroid adenomas are histologically typed according to the following classification [13]:

a. Follicular adenoma
   1. Simple adenoma (colloid macrofollicular adenoma)
   2. Microfollicular adenoma
   3. Fetal adenoma
   4. Embryonal (trabecular) adenoma
b. Papillary adenoma
c. Variants
   1. Oxyphilic (Hürthle cell) adenoma
   2. Clear cell adenoma
   3. Functioning adenoma (Plummer's disease, toxic multinodular goiter)
   4. Others

Various morphological types of adenomas cannot be sonographically differentiated. Follicular adenoma is the predominant benign thyroid tumor, accounting for over 85% of all benign neoplasms of the gland [14].

Typical US features of thyroid adenoma are as follows (Fig. 5.15):

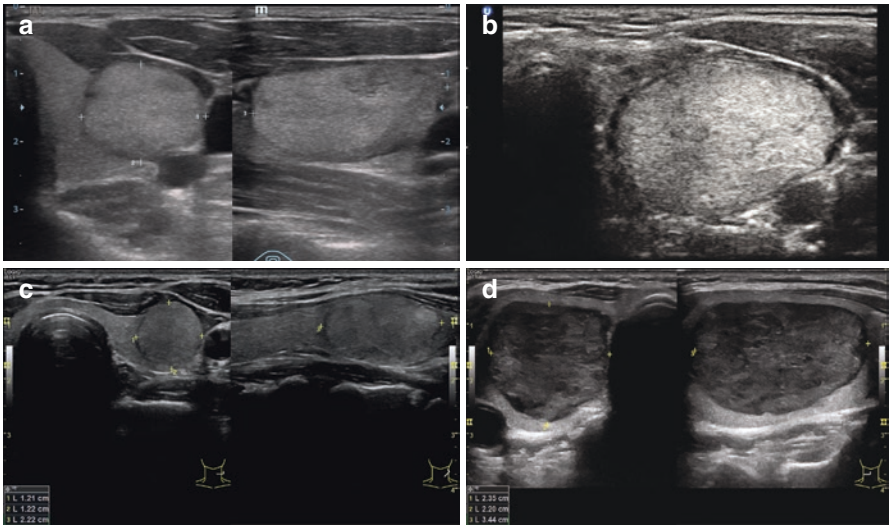

Fig. 5.15 Thyroid adenoma. (**a**–**d**) Grayscale US

- Oval or spherical shape.
- Low echodensity.
- Homogeneous or moderately heterogeneous echostructure.
- Regular, well-defined margins.
- Hypoechoic halo 1–3 mm in width.
- Intact thyroid capsule.
- Absence of calcifications.
- Hypervascularity with a mixed (central and peripheral) pattern and a regular distribution of vessels within the nodule in CDI and PDI is usually seen. A perinodular vascular ring corresponding to a halo is characteristic. Radial centripetal vessels connected to the peripheral ring (a "basketball basket" sign) are commonly detected.
- Compression USE reveals significant increase in lesion elasticity that is substantially different from the surrounding parenchyma. Elastometry detects strain ratio about 3.0 or higher.
- CEUS demonstrates hypervascularity with typical vascular halo and centripetal pattern.

Thyroid adenomas tend to grow fast, so they are normally large (over 2–3 cm in size) by the time they are diagnosed. The majority of adenomas show a peripheral hypoechoic ring (halo) in grayscale sonography. A halo is present in 87% of thyroid adenomas. It corresponds to histological capsule, edema of the surrounding normal parenchyma (especially in fast-growing lesions), or to nodule vessels. Thyroid adenomas show a typical vascular pattern in CDI and PDI (Fig. 5.16) with perinodular

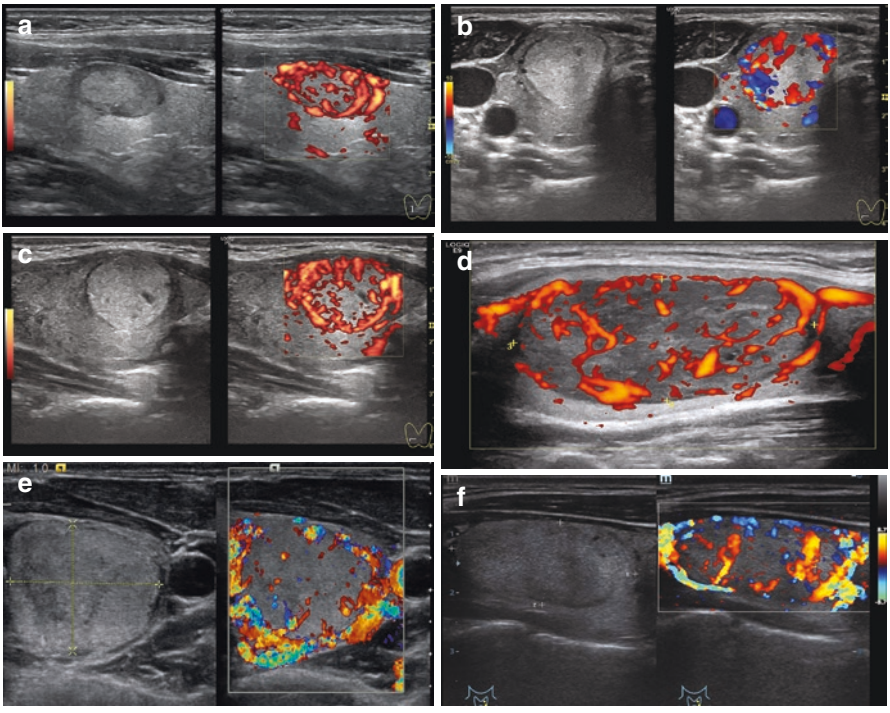

Fig. 5.16 Thyroid adenoma. Typical vascular pattern. (**a**–**f**) Grayscale US, PDI, and CDI

and intranodular hypervascularization: a perinodular vascular ring (corresponding to a halo, which is not always evident in grayscale) with centripetal radial vessels. This pattern was named "basketball basket." According to Sencha [15], this sign is observed in 25% of all thyroid adenomas. The vessels within adenomas appear visually dilated and wavy, with a centripetal direction. Regular vascular pattern without disorganization contributes in differentiation of adenoma from cancer.

Adenomas can undergo degeneration with cystic or hemorrhagic changes or calcination. Adenomas with a significantly decreased echodensity are often difficult to differentiate from colloid nodules and malignant tumors. Hypoechoic areas in adenomas are a consequence of hemorrhages into the nodule. The anechoic component in central or peripheral compartments of the lesion with typical fluid echostructure is thought to be associated with cystic degeneration (Fig. 5.17).

According to Struchkova [16], blood flow velocities in the main thyroid arteries and peripheral vessels of micro- and macrofollicular adenomas, as measured with PW Doppler, are increased compared with micro- and macrofollicular goiters (PSV = 19.3–40.1 cm/s vs. 10.9–30.6 cm/s, EDV = 5.6–13 cm/s vs. 3.3–10.8 cm/s, RI = 0.45–0.6 vs. 0.6–0.8, and PI = 0.8–1.2 vs. 0.7–1.1, respectively). Kotlyarov et al. [17] did not find any significant change in blood flow parameters in the vessels of adenomas with PW Doppler.

Compression USE commonly reveals intense staining of thyroid adenomas that is different from the surrounding parenchyma. The quantitative data of share-wave elastography prove abnormal elasticity of thyroid adenomas (Fig. 5.18).

The use of contrast agents fully demonstrates peripheral and central hypervascularization of thyroid adenomas. The wash-in phase is fast. It clearly reveals the characteristic "basketball basket" sign, which starts from the periphery of the lesion (Fig. 5.19). Follicular adenomas often exhibit the same microvascular architecture as follicular cancer.

According to Schleder et al. [18], thyroid adenomas and carcinomas with CEUS have statistically significant differences in temporal parameters of microvascularity. Thyroid adenomas exhibit very slow overall wash-out or central wash-out with persistent peripheral contrast enhancement in late phase. Thyroid carcinomas are characterized by complete washout. The evaluation of the dynamics of washout is of high diagnostic value (sensitivity, 81%; specificity, 92%; positive predictive value,

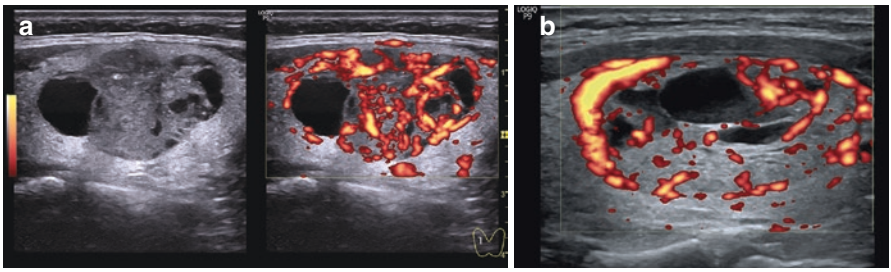

Fig. 5.17 Thyroid adenoma. Cystic degeneration. (**a**–**b**) Grayscale US and PDI

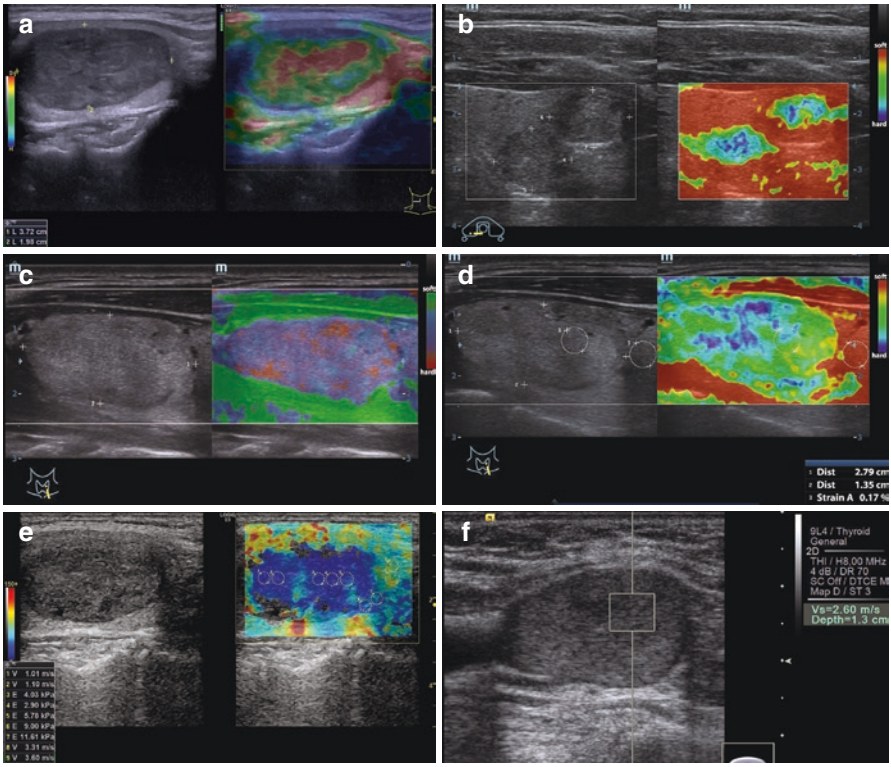

Fig. 5.18 Thyroid adenomas. (**a**–**c**) Compression USE. (**d**) Strain ratio. (**e**) Share-wave elastography. (**f**) ARFI

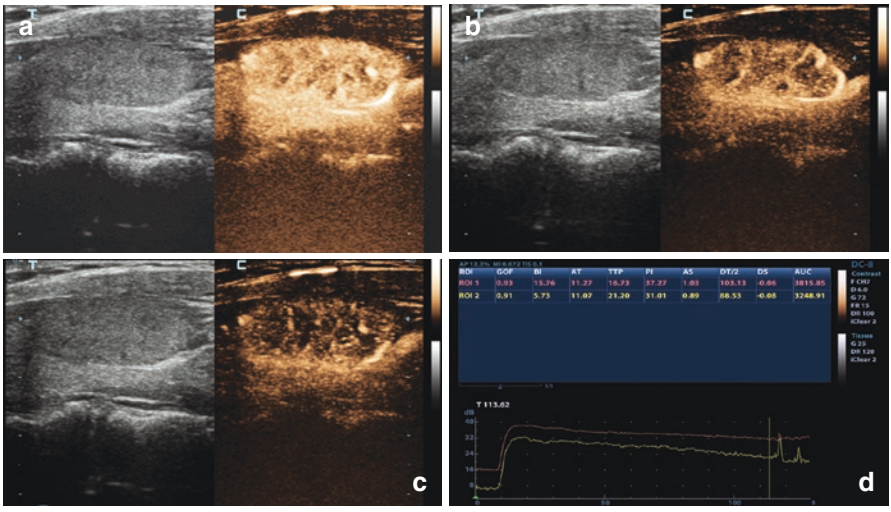

Fig. 5.19 Follicular adenoma of the thyroid gland. Thyroid CEUS with SonoVue® 2.4 mL. (**a**–**c**) Phases of contrast enhancement. (**d**) Time-intensity curve

97%; negative predictive value, 63%). It permits a more reliable differential diagnosis between adenomas and thyroid carcinomas [18].

The specificities of sonography in grayscale, CDI, PDI, and 3D in the diagnosis of thyroid adenomas are about 30, 56.6, 68.7, and 79.2%, with sensitivities of 79.9, 84, 89.5, and 93.4% and diagnostic accuracies of 38.2, 61.5, 72, and 82%, respectively [8]. According to Zubarev et al. [5], combining Doppler options with 3D increases the sensitivity of US to adenomas by 13.5% (up to 93.4%), its specificity by 49.2% (up to 79.2%), and its diagnostic accuracy by 43.8% (up to 82%).

The literature and our own experience prove that none of the features listed above can serve as an absolute criterion of the benign character of a thyroid nodule. Thyroid adenomas commonly belong to the category of TIRADS 4 or TIRADS 3. The role of US is often limited to the selection of the patients with nodules that are suspicious for a tumor and subsequent US-guided FNAB. The cytology often permits the benign nature of the obtained cells to be specified, but this is quite a problem in several cases, such as for follicular tumors and others.

The Example US Report in Thyroid Adenoma

- First name, middle initial, last name:
- Age:
- Date:
- The number of case history:
- US scanner:

The thyroid gland is typically located with regular well-defined margins and homogeneous isoechoic structure. The capsule is uniform and continuous on all extent.

The depth of the *isthmus*: 4 mm			
Right lobe		Left lobe	
Depth	19 mm	Depth	15 mm
Width	19 mm	Width	16 mm
Length	52 mm	Length	50 mm
Volume	9.0 cm^3	Volume	5.7 cm^3
The total volume 14.7 cm^3 does not exceed the upper limit			
A moderately heterogeneous slightly hypoechoic lesion of 1.8 × 1.8 × 3.2 cm in size of roundish shape with well-defined regular margins with halo is located in the lower half of the lobe. The lesion is hypervascular with predominantly peripheral blood flow and regularly distributed centripetal vessels. Compression US elastography detects hard pattern, strain ratio is 4.0		No lesions detected	

The vascular pattern of the parenchyma is normal and symmetric with CDI and PDI. CPD is 10–15%.

The lymph nodes in the neck and supraclavicular areas are not enlarged.

CONCLUSION: A lesion of the right thyroid lobe, suspicious for adenoma. TIRADS 4.

US specialist:

References

1. Vetshev PS, Chilingaridi KE, Gabaidze DI, Saliba MB. Adenomas of the thyroid gland. Khirurgiya. 2005;7:4–8 (Article in Russian).
2. Burch HB. Fine needle aspiration of thyroid nodules. Determinants of insufficiency rate and malignancy yield at thyroidectomy. Acta Cytol. 1996;40:1176–83.
3. Pacella CM, Papini E, Bizzarri G, et al. Assessment of the effect of percutaneous ethanol injection in autonomously functioning thyroid nodules by colour-coded duplex sonography. Eur Radiol. 1995;5:395–400.
4. Tsyb AF, Parshin BC, Nestayko GV, et al. Ultrasound diagnosis of thyroid diseases. Moscow: Medicine; 1997 (Book in Russian).
5. Zubarev AV, Bashilov VP, et al. The value of ultrasonic angiography and three-dimensional reconstruction of vessels in the diagnosis of nodular formations of the thyroid gland. Medicinskaya vizualizaciya. 2000;3:57–62 (Article in Russian).
6. Markova EN. Three-dimensional virtual tomography and ultrasonic angiography in the diagnosis of nodular formations of the thyroid gland [PhD thesis]. Moscow; 2004 (Book in Russian).
7. Zhang B, Jiang YX, Liu JB, et al. Utility of contrast-enhanced ultrasound for evaluation of thyroid nodules. Thyroid. 2010;20(1):51–7.
8. Markova NV. The value of ultrasound angiography in the diagnosis of the main diseases of the thyroid gland [PhD Thesis]. Moscow; 2001 (Book in Russian).
9. Barsukov AN, Konoplev OA, Chebotarev NV, Tolpygo VA. Clinical classification of cystic neoplasms of the thyroid gland. Modern aspects of surgical endocrinology: proceedings of the IX (XI) Russian symposium on surgical endocrinology. Chelyabinsk. 2000:50–52 (Article in Russian).
10. Ahuja A, Chick W, King W, Metreweli C. Clinical significance of the comet tail artifact in thyroid ultrasound. J Clin Ultrasound. 1996;24(3):129–33.
11. Bellantone R, Lombardi CP, Rafaelli M, et al. Management of cystic or predominantly cystic thyroid nodules: the role of ultrasound-guided fine-needle aspiration biopsy. Thyroid. 2004;14(1):143–50.
12. Ahuja A. The thyroid and parathyroid. In: Ahuja A, Evans R, editors. Practical head and neck ultrasound. London: Greenwich Medical Media Ltd; 2000.
13. Yamashita S, Ito M. In: Sigamatsu I, Nagataki S, Foundation for the Promotion of Healthcare, editors. Diagnosis of diseases of the thyroid gland. From the experience of activities to assist in the organization of medical care after the accident in Chernobyl. Sasakawa - Nagasaki; 1996.
14. Bronshtein ME. Thyroid cancer. Probl Endocrinol. 1997;6:33–7 (Article in Russian).
15. Sencha AN. Ultrasonic visualization of malignant tumors of the thyroid gland. Ultrazvukovaya i funkcionalnaya diagnostika. 2008;2:20–29 (Article in Russian).
16. Struchkova TY (2003) Parameters of blood flow in the lower and upper thyroid arteries. Normative values. Abstracts of the 4th Congress of the Russian Association of Specialists in Ultrasound Diagnostics in Medicine. Moscow, pp. 221–222 (Article in Russian).
17. Kotlyarov PM, Kharchenko VP, Alexandrov YK, et al. Ultrasound diagnosis of the diseases of the thyroid gland. Moscow: Vidar-M; 2009 (Book in Russian).
18. Schleder S, Janke M, Agha A, et al. Preoperative differentiation of thyroid adenomas and thyroid carcinomas using high resolution contrast-enhanced ultrasound (CEUS). Clin Hemorheol Microcirc. 2015;61(1):13–22.

Ultrasound Diagnosis of Thyroid Carcinoma

6

Alexander N. Sencha, Ekaterina A. Sencha, Yury N. Patrunov, Yuriy K. Aleksandrov, Munir G. Tukhbatullin, Ella I. Peniaeva, and Liubov A. Timofeyeva

One principle task in US diagnosis of thyroid diseases is detection and ultrasound categorization of malignant tumors.

Thyroid cancer is a malignant tumor developing from follicular or C cells of the thyroid gland. It is a relatively uncommon disease. However, it accounts for about 1.5–2% of all head and neck malignancies and 1–4% of all malignant tumors. It appears to be the cause of death in only 0.3–1% of all cases of malignancy [1].

A. N. Sencha (✉)
Department of Visual and Functional Diagnostics, National Research Center for Obstetrics, Gynecology and Perinatology, Ministry of Healthcare of the Russian Federation, Moscow, Russia

E. A. Sencha
Ultrasound Diagnostics Department, Medical Diagnostic Center, Moscow, Russia

Y. N. Patrunov · E. I. Peniaeva
Department of Ultrasound Diagnostics, Center for Radiological Diagnostics of Non-State Healthcare Institution Yaroslavl Railway Clinic of JSC "Russian Railways", Yaroslavl, Russia

Y. K. Aleksandrov
Department of Surgery, Federal State Budget Educational Institution of Higher Education Yaroslavl State Medical University of the Ministry of Healthcare of the Russian Federation, Yaroslavl, Russia

M. G. Tukhbatullin
Department of Ultrasound Diagnostics, Kazan State Medical Academy – Branch Campus of the Federal State Budget Educational Institution of Further Professional Education, "Russian Medical Academy of Continuing Professional Education" of the Ministry of Healthcare of the Russian Federation, Kazan, Russia

L. A. Timofeyeva
Department for Internal Diseases Propaedeutic, Course of Diagnostic Radiology of Medical Faculty of Federal State Budget Educational Institution of Higher Education "I. N. Ulianov Chuvash State University", Cheboksary, Russia

A. N. Sencha, Y. N. Patrunov (eds.), *Thyroid Ultrasound*,
https://doi.org/10.1007/978-3-030-14451-7_6

Twenty-five to 55 new cases of differentiated thyroid cancer per million are recorded annually. According to the WHO, the incidence of thyroid cancer doubled during the last decade due to the increased detection of "obscure" variants.

6.1 Classification and Staging of Thyroid Malignancies

The classification of thyroid tumors is constantly updating.

The current WHO classification of the tumors of the thyroid gland is as follows (ICD-O codes in brackets) [2]:

- Follicular adenoma (8330/0)
- Hyalinizing trabecular tumor (8336/1)
- Other encapsulated follicular-patterned thyroid tumors
  - Follicular tumors of uncertain malignant potential (8335/1)
  - Well-differentiated tumor of uncertain malignant potential (8348/1)
  - Noninvasive follicular thyroid neoplasm with papillary-like nuclear features (8349/1)
- Papillary thyroid carcinoma
  - Papillary carcinoma (8260/3)
  - Follicular variant of PTC (8340/3)
  - Encapsulated variant of PTC (8343/3)
  - Papillary microcarcinoma (8341/3)
  - Columnar cell variant of PTC (8344/3)
  - Oncocytic variant of PTC (8342/3)
- Follicular thyroid carcinoma (FTC), NOS (8330/3)
  - FTC, minimally invasive (8335/3)
  - FTC, encapsulated angioinvasive (8339/3)
  - FTC, widely invasive (8330/3)
- Hürthle (oncocytic) cell tumors
  - Hürthle cell adenoma (8290/0)
  - Hürthle cell carcinoma (8290/3)
- Poorly differentiated thyroid carcinoma (8337/3)
- Anaplastic thyroid carcinoma (8020/3)
- Squamous cell carcinoma (8070/3)
- Medullary thyroid carcinoma (8345/3)
- Mixed medullary and follicular thyroid carcinoma (8346/3)
- Mucoepidermoid carcinoma (8430/3)
- Sclerosing mucoepidermoid carcinoma with eosinophilia (8430/3)
- Mucinous carcinoma (8480/3)
- Ectopic thymoma (8580/3)
- Spindle epithelial tumor with thymus-like differentiation (8588/3)
- Intrathyroid thymic carcinoma (8589/3)
- Paraganglioma and mesenchymal/stromal tumors
  - Paraganglioma (8693/3)
  - Peripheral nerve sheath tumors

    - Schwannoma (9560/0)
    - Malignant peripheral nerve sheath tumors (9540/3)
  - Benign vascular tumors
    - Hemangioma (9120/0)
    - Cavernous hemangioma (9121/0)
    - Lymphangioma (9170/0)
  - Angiosarcoma (9120/3)
  - Smooth muscle tumors
    - Leiomyoma (8890/0)
    - Leiomyosarcoma (8890/3)
  - Solitary fibrous tumor (8815/1)
- Hematolymphoid tumors
  - Langerhans cell histiocytosis (9751/3)
  - Rosai-Dorfman disease
  - Follicular dendritic cell sarcoma (9758/3)
  - Primary thyroid lymphoma
- Germ cell tumors
  - Benign teratoma (9080/0)
  - Immature teratoma (9080/1)
  - Malignant teratoma (9080/3)
- Secondary tumors

Thyroid tumors may be a part of multiple endocrine neoplasia (MEN) syndromes. The latter are autosomal dominant inherited disorders, in which several endocrine glands develop benign or malignant tumors or grow excessively without forming tumors. The major forms of multiple endocrine neoplasia are called type 1, type 2, and type 4. These types are distinguished by the genes involved, the types of hormones made, and the characteristic signs and symptoms.

Medullary thyroid carcinoma is the most common sign of MEN type 2. Some people with this disorder also develop a pheochromocytoma. MEN type 2 is divided into three subtypes: type 2A, type 2B (formerly called type 3, Wagenmann–Froboese syndrome), and familial medullary thyroid carcinoma (FMTC). These subtypes differ in their characteristic signs and symptoms and risk of specific tumors; for example, hyperparathyroidism occurs only in type 2A, and medullary thyroid carcinoma is the only feature of FMTC.

Almost everyone with MEN type 2A disease (Sipple syndrome) develops medullary thyroid cancer; about 40–50% develop adrenal pheochromocytomas, which are bilateral in 50% of cases. Hyperplasia or adenoma of parathyroid glands occurs in 20–30% of patients.

MEN 2B syndrome (formerly called type 3, Wagenmann–Froboese syndrome, mucosal neuroma syndrome) has clear, easily recognizable phenotypic manifestations. Most people with MEN 2B disease develop neuromas in their mucous membranes (of the conjunctiva, lips, cheeks, digestive, urogenital tracts) and defects of the skeleton and vision. The medullary thyroid cancer that occurs in MEN type 2B tends to develop at an early age (commonly before the age of 5 years). It grows faster and spreads more rapidly than those in type 2A disease.

Papillary and follicular thyroid cancers can be components of hereditary syndromes, most of which are associated with the development of hamartomas. The most famous of them are listed below:

- Multiple endocrine neoplasia type 1 (MEN1), which may include a combination of more than 20 different endocrine and neuroendocrine tumors. It commonly affects the parathyroids (up to 90% of cases), pancreas (80%), pituitary gland (60%), adrenal glands (35%), and thyroid gland (25%). In this case, thyroid cancer may be papillary or follicular, but never medullary. A typical endocrinopathy with MEN1 is primary hyperparathyroidism.
- Cowden syndrome is a combination of breast fibroadenomas and cysts, papillomas, angiomas, lipomas, polyps of the gastrointestinal tract, benign tumors, follicular thyroid tumors, hyperparathyroidism, tumors of the nervous system, endometrial cancer, and macrocephaly.
- Familial adenomatous polyposis and its subtype Gardner syndrome are accompanied with multifocal papillary thyroid cancer in approximately 13% of patients. Classical signs include adenomatosis of the intestines and stomach, skin fibromas, and epidermoid cysts.
- Carney complex is a disease with dominant inheritance, associated with multiple pigment spots on the skin and mucosa, pituitary adenomas, adrenal hyperplasia, and multiple thyroid adenomas. Fifteen percent of patients develop follicular and/or papillary thyroid cancer.
- Werner syndrome is an autosomal recessive condition that manifests in the third or fourth decade of life with symptoms of premature aging: severe atrophy of the skin, cataracts, and hypofunction of the glands. Ten percent of patients develop fibrosarcoma, osteoma, benign thyroid tumors, cancer of parenchymal organs, and thyroid cancer.

Ultrasound imaging of the thyroid gland and other organs and other imaging methods (CT, MRI) along with molecular testing of gene mutations are important components of the differential diagnosis of genetically determined thyroid tumors in inherited multi-tumor syndromes.

For predicting disease-specific survival, TNM staging is used. “T” describes the size of the primary tumor and its invasion to nearby tissue, “N” describes regional lymph nodes, and “M” describes distant metastasis. Current AJCC eighth edition is effective from January 1, 2018. Clinical staging is based on inspection/palpation and imaging (US, PET/CT, etc.) of thyroid gland and regional lymph nodes. Age (cutoff of 55 years) is an essential variable for AJCC staging of differentiated thyroid cancer.

The TNM classification is as follows [2]:

Primary tumor for papillary, follicular, poorly differentiated, Hürthle cell, and anaplastic thyroid carcinomas:

- TX: Primary tumor cannot be assessed.
- T0: No evidence of primary tumor.
- T1: Tumor ≤2 cm in greatest dimension limited to the thyroid.
  - T1a: Tumor ≤1 cm in greatest dimension limited to the thyroid
  - T1b: Tumor >1 cm but ≤2 cm in greatest dimension limited to the thyroid

- T2: Tumor >2 cm but ≤4 cm in greatest dimension limited to the thyroid.
- T3*: Tumor >4 cm limited to the thyroid or gross extrathyroidal extension invading only strap muscles.
  - T3a*: Tumor >4 cm limited to the thyroid
  - T3b*: Gross extrathyroidal extension invading only strap muscles (sternohyoid, sternothyroid, thyrohyoid, or omohyoid muscles) from a tumor of any size
- T4: Includes gross extrathyroidal extension into major neck structures.
  - T4a: Gross extrathyroidal extension invading the subcutaneous soft tissues, larynx, trachea, esophagus, or recurrent laryngeal nerve from a tumor of any size
  - T4b: Gross extrathyroidal extension invading prevertebral fascia or encasing carotid artery or mediastinal vessels from a tumor of any size

Primary tumor for medullary thyroid carcinomas:

- TX–T3: Definitions are similar to the above.
- T4: Advanced disease.
  - T4a: Moderately advanced disease; tumor of any size with gross extrathyroidal extension into the nearby tissues of the neck, including the subcutaneous soft tissue, larynx, trachea, esophagus, or recurrent laryngeal nerve
  - T4b: Very advanced disease; tumor of any size with extension toward the spine or into nearby large blood vessels, invading the prevertebral fascia or encasing the carotid artery or mediastinal vessels

Regional lymph node:

1. NX: Regional lymph nodes cannot be assessed.
2. N0: No evidence of regional lymph node metastasis.
   (a) N0a*: One or more cytologic or histologically confirmed benign lymph nodes
   (b) N0b*: No radiologic or clinical evidence of locoregional lymph node metastasis
3. N1*: Metastasis to regional nodes.
   (a) N1a*: Metastasis to level VI or VII (pretracheal, paratracheal, prelaryngeal/Delphian or upper mediastinal) lymph nodes; this can be unilateral or bilateral disease.
   (b) N1b*: Metastasis to unilateral, bilateral, or contralateral lateral neck lymph nodes (levels I, II, III, IV, or V) or retropharyngeal lymph nodes.

Distant metastasis (M):

- M0: No distant metastasis
- M1: Distant metastasis

*All categories may be subdivided: (s) solitary tumor and (m) multifocal tumor (the largest tumor determines the classification).

Differentiated thyroid cancer is the only thyroid tumor, which has the age an independent stratifying variable. Its predictive power is decisive for staging.

AJCC prognostic stage grouping [2] is provided below.

Differentiated thyroid cancer:

	Age at diagnosis <55 years		
Stage I	Any T	Any N	M0
Stage II	Any T	Any N	M1
	Age at diagnosis ≥55 years		
Stage I	T1	N0/NX	M0
	T2	N0/NX	M0
Stage II	T1	N1	M0
	T2	N1	M0
	T3a/T3b	Any N	M0
Stage III	T4a	Any N	M0
Stage IVA	T4b	Any N	M0
Stage IVB	Any T	Any N	M1

Medullary thyroid cancer:

Stage I	T1	N0	M0
Stage II	T2	N0	M0
	T3	N0	M0
Stage III	T1–3	N1a	M0
Stage IVA	T4a	Any N	M0
	T1–3	N1b	M0
Stage IVB	T4b	Any N	M0
Stage IVC	Any T	Any N	M1

Anaplastic thyroid cancer:

Stage IVA	T1–T3a	N0/NX	M0
Stage IVB	T1–T3a	N1	M0
	T3b	Any N	M0
	T4	Any N	M0
Stage IVC	Any T	Any N	M1

6.2 Ultrasound Imaging of Thyroid Carcinoma

Thyroid cancer is more common in women, with a ratio of 6:1 [3]. Follicular cancer is particularly rare in men (with a ratio of 1:17), although medullary and diffuse sclerosing types of papillary cancer can be observed more often in men. The peak of incidence is between the ages of 41 and 50 years. As a rule, the neoplasm is located in the lateral lobes of the thyroid. The inferior compartments of the lobes tend to be affected more often. Follicular and medullary carcinomas arise twice and

2.5 times as often in the right lobe as they do in the left lobe, respectively. Papillary cancer is more often detected in the isthmus. Solitary lesions in cases of thyroid cancer are often 1–3 cm in size.

Papillary cancer is the most common morphological type of thyroid cancer, accounting for 55–75% of all cases. The most aggressive type, anaplastic thyroid cancer, is registered in <14% of observations. Follicular and medullary carcinomas account for 15–20% and 3–7%, respectively [4]. These data may vary in different populations; however, the increase in the number of cases of thyroid cancer over the past 10–15 years is mainly due to papillary cancer.

The following US features are suspicious for thyroid malignancy (Fig. 6.1):

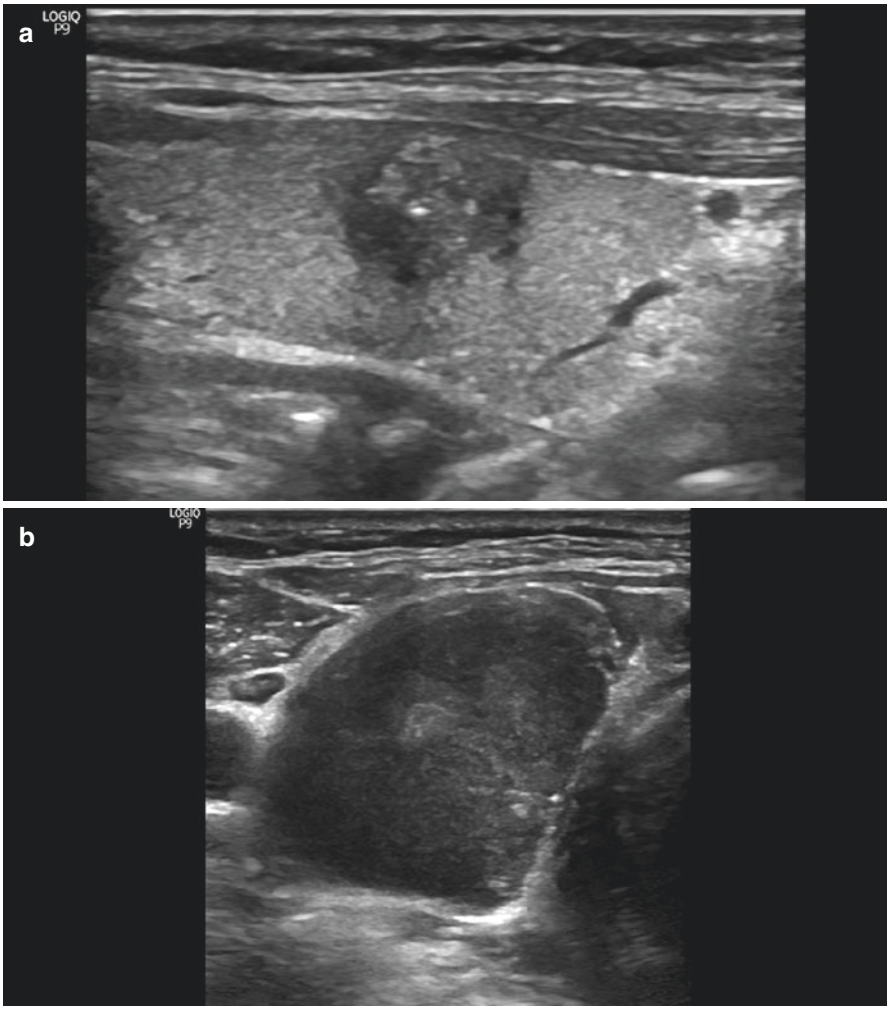

Fig. 6.1 Thyroid cancer. (**a**–**d**) Grayscale US

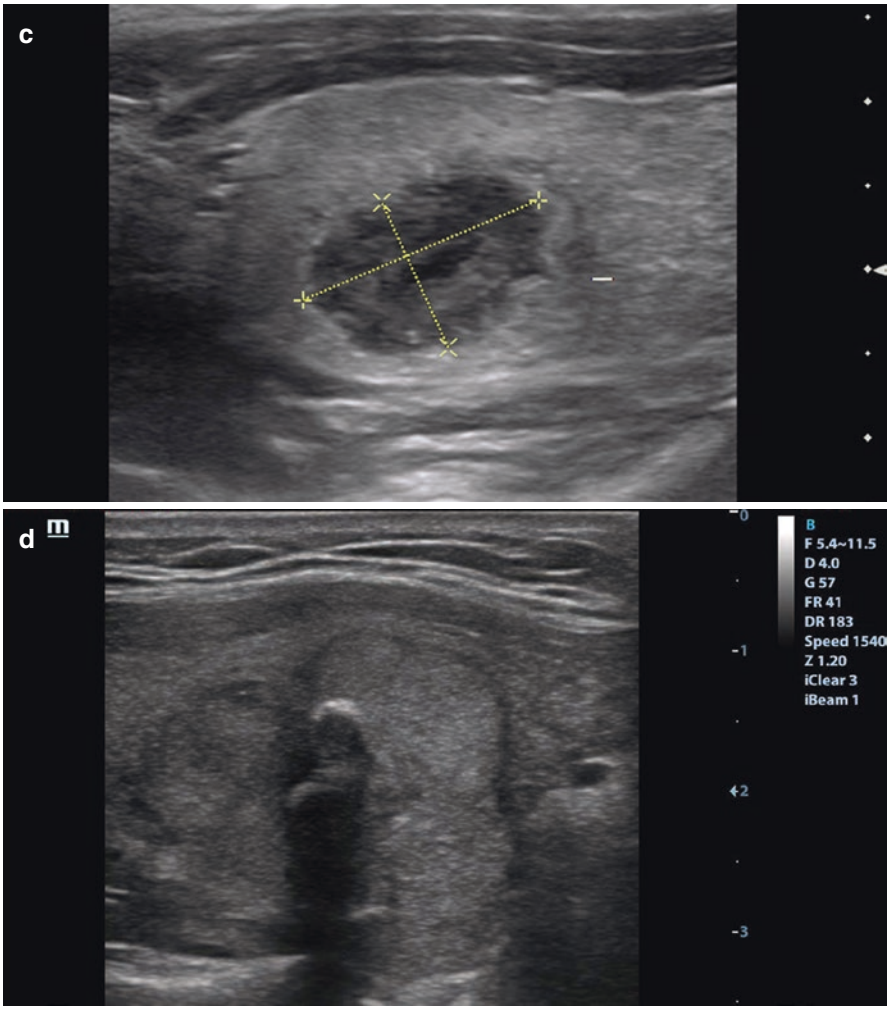

Fig. 6.1 (continued)

1. Single lesion.
2. Irregular shape of the lesion.
3. Tuberous borders.
4. Indistinct contours.
5. Decreased echodensity.
6. Heterogeneity of echostructure.
7. Echogenic inclusions and microcalcifications that are smaller than 2 mm in size, without acoustic shadowing.
8. Posterior shadowing behind the lesion.
9. Absence of the peripheral halo.

10. Hypervascularity of large lesions and hypo- or avascularity of small lesions in CDI and PDI.
11. Irregular distribution of vessels within the lesion, disorganization of the vascular pattern, nonlinear wavy course with a nonuniform gauge, and pathological transformation of the vessels in CDI, PDI, and especially 3DPD.
12. A significant increase in the lesion strain with intense color pattern different from the surrounding parenchyma.
13. Elastometry reveals the average value of the shear-wave velocity in ARFI mode higher than 3 .7m/s; the average value of the strain ratio is 3.4 ± 0.84.
14. Neoangiogenesis and hypervascularity with CEUS.
15. Enlargement of the regional lymph nodes.

Subcapsular nodule location is observed more than in half of thyroid cancers. The following additional sonographic features should lead to a suspicion of carcinoma merging into the thyroid capsule:

1. Adhesion
2. Thyroid deformation
3. Blurred margins of the lesion and the thyroid gland

The echostructure of thyroid cancer can vary: it can be solid hypoechoic, isoechoic, hyperechoic, mixed, or cystic. Sixty to seventy percent of thyroid cancers are characterized by hypoechoic solid structure, 15–25% of neoplasms are isoechoic, 2–4% are hyperechoic, and 5–10% show mixed echostructure.

The tumor margins in thyroid carcinoma are often uniformly or locally indistinct. Microcalcifications and anechoic fields corresponding to necrotic cavities may be observed. The presence of fine echogenic inclusions can be a sign of malignancy, although calcifications of different sizes and shapes may be sometimes detected even in the normal thyroid gland.

Hyperechoic inclusions within thyroid carcinoma are often microcalcifications (up to 2 mm without acoustic shadowing) (Figs. 6.1d and 6.2). Coarse amorphous echogenic calcium (larger than 2 mm with acoustic shadowing) may be sometimes identified. According to Burch [5], peripheral "eggshell" calcification suggests that the nodule is benign. Alternatively, microcalcifications in the central part of the lesion should increase the investigator's suspicion of malignancy. Takashima et al. [6] report that microcalcifications showed the greatest accuracy (76%) and specificity (93%) for diagnosing a malignancy among all US features, but the sensitivity of this approach appeared low, at 36%. According to Moon et al. [3], macro- and microcalcifications are statistically significant features of thyroid cancer and demonstrate sensitivities of 44.2% and 9.7% along with specificities of 90.8% and 96.1%, respectively.

A sonographic study alerts to a suspected thyroid cancer in 65% of cases. The greatest probability (77%) is achieved with the combination of the following four sonographic features: decreased echodensity, irregular shape, indistinct borders, and irregular contours. Indistinct contours and disorganization of the US

architectonics of the affected muscles in cases of invasion of thyroid cancer may serve as accessory signs. The suspicion of a tumor merging into the trachea may arise in cases where more than 10 mm of a malignant lesion appears adjacent to the trachea.

Over 90% of all malignant lesions demonstrate an intranodular blood flow pattern, while Zubarev et al. [7] state that the majority of neoplasms (82%) show perinodular hypervascularization and intranodular hypovascularization with a chaotic disorganized pattern. According to Kotlyarov et al. [8], lesions smaller than 0.8 cm

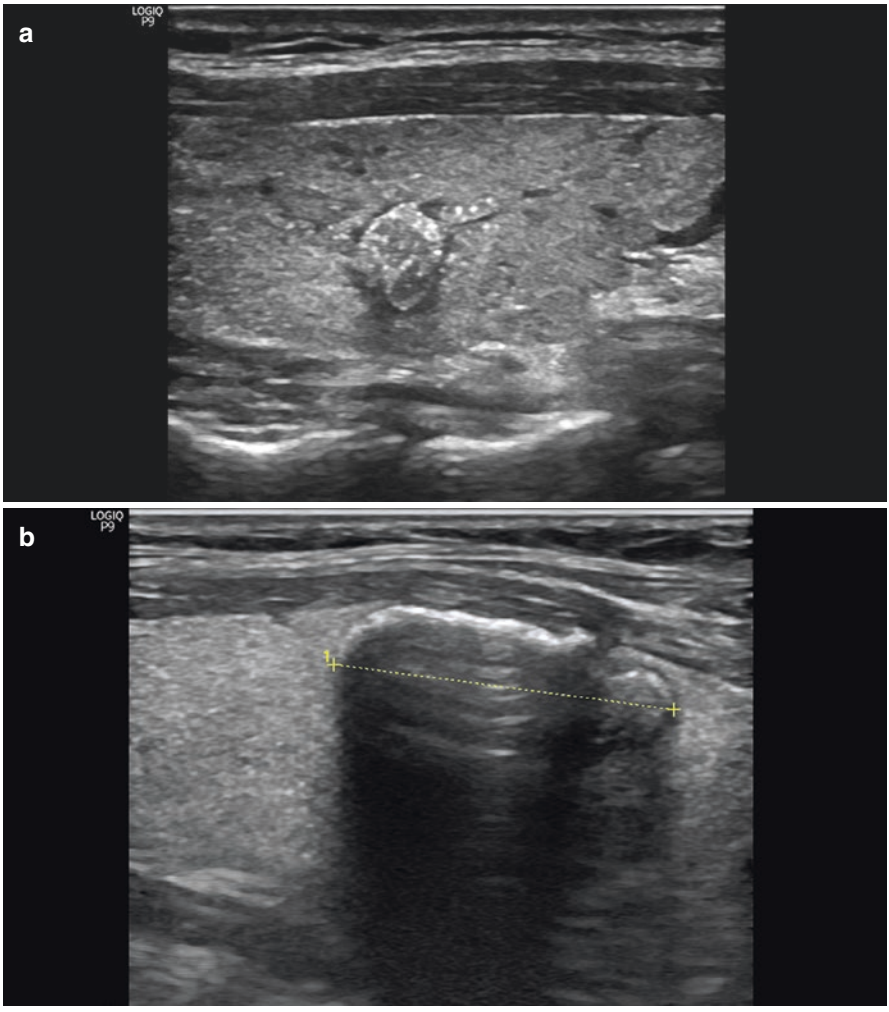

Fig. 6.2 Calcifications in the thyroid gland. Grayscale US. (**a**) Microcalcifications in papillary cancer. (**b**) Benign calcifications in nodular goiter. (**c**) Malignant lesion (BSRTC 6 with FNAB) with typical signs of malignancy emerged from a commonly benign nodule with eggshell calcification. Grayscale longitudinal scan. (**d**) The same lesion as letter "c," CDI

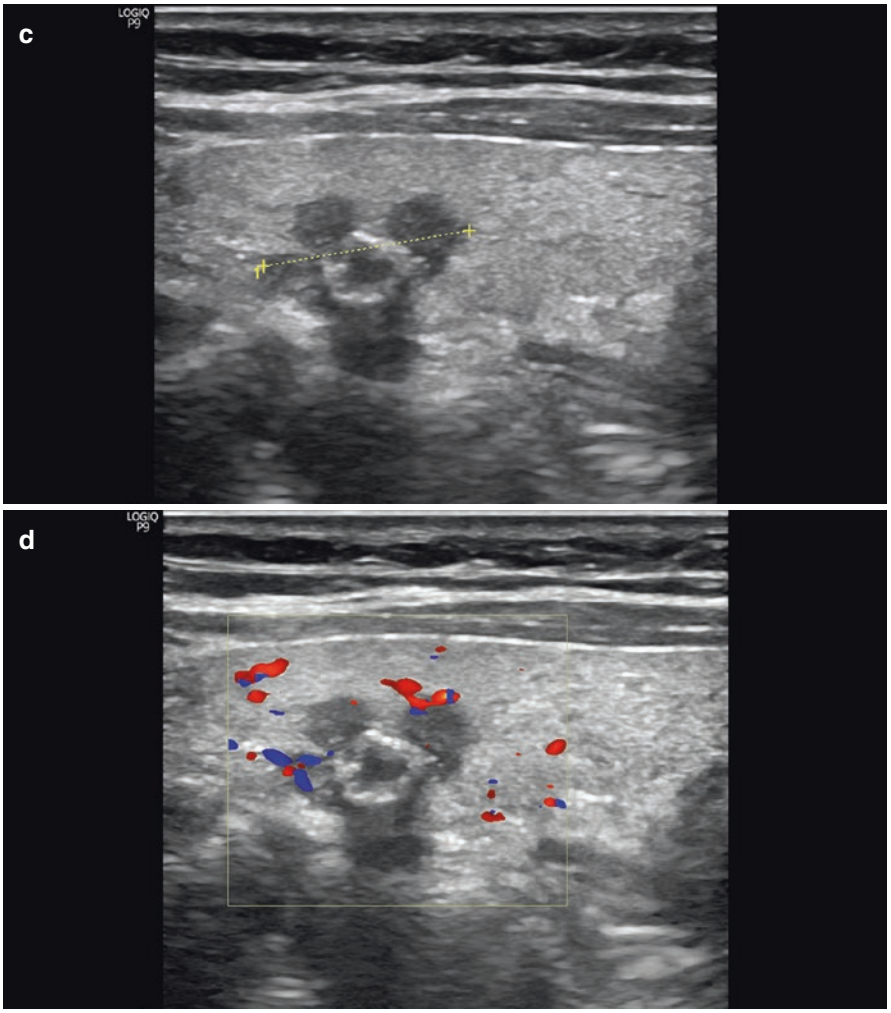

Fig. 6.2 (continued)

in size appear avascular in CDI and PDI in 98%, and lesions of size 0.8–3 cm are hypovascular in 92% of cases. Tumors larger than 3 cm in size corresponded to hypervascular lesions in 99% of cases (Fig. 6.3).

According to Kotlyarov et al. [8], no regularity in blood flow velocity, indices, and other data from PW Doppler was recorded for thyroid cancers of any size.

3D reconstruction increases the diagnostic value of US. It permits an assessment of the number and structure of malignant lesions; allows their location to be specified in relation to the thyroid capsule, vascular bundles, and trachea; enables an analysis of the vascularity, growth, and invasiveness; and can be used to calculate the volume of the affected and intact thyroid tissue. It clearly shows blurred,

irregular, and tuberous margins, calcifications, and interruptions of the thyroid capsule along with merging into adjacent structures. 3D also allows for a more precise follow-up of a lesion of any origin. 3DPD permits accurate assessment of pathological transformations and the density of vessels irregularly distributed within the neoplasm, the definition of the character of and the disturbance to the vascular pattern, and the detection of vessels with corkscrew courses (Fig. 6.4).

Compression US elastography is a valuable tool for differential diagnosis of thyroid lesions and early detection of malignancies. According to Sencha et al. [9], the color pattern in thyroid cancer with USE is hard (clearly different from the surrounding parenchyma) in 79% of cases, intense in 63%, and heterogeneous in 68% (Fig. 6.5).

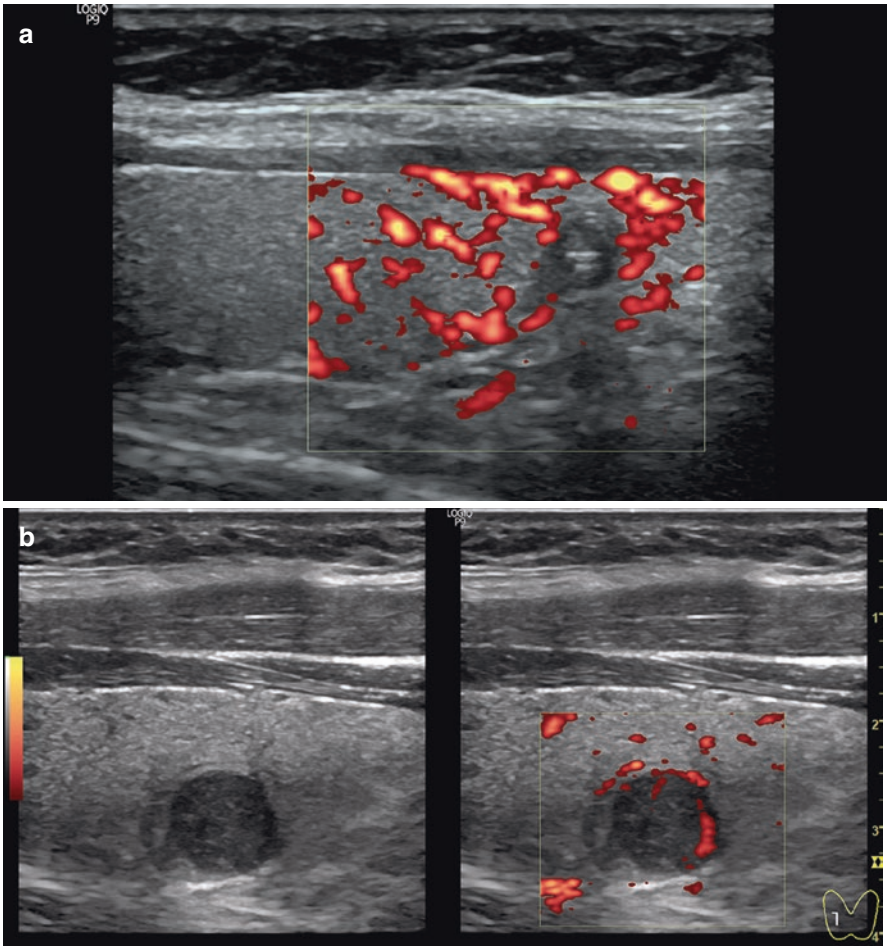

Fig. 6.3 Thyroid cancer. (**a**) Avascular subcentimeter papillary carcinoma. PDI. (**b**) Hypovascular subcentimeter papillary carcinoma. PDI. (**c**, **d**) Hypervascular carcinoma. CDI

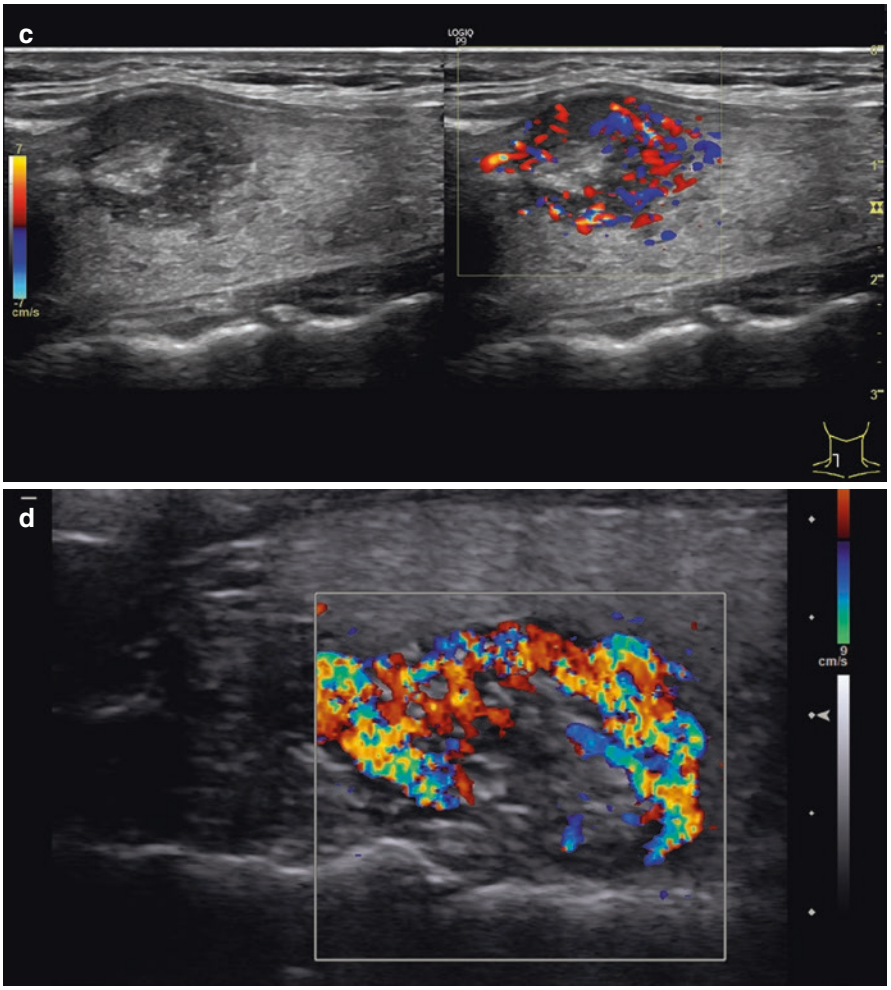

Fig. 6.3 (continued)

Compression USE permitted to obtain additional data crucial for the diagnosis in 14% of thyroid cancers. The following aspects are better analyzed with USE:

- Specification of the size of the lesion due to the imaging of the hard area, which is a consequence of tumor merging into the surrounding structures. The size of the lesion with USE appeared 5–10 mm larger than its grayscale image in 18% of cases. It corresponds to score 5 according to Ueno-Itoh scale (Fig. 6.6a, b).
- Precise analysis of the homogeneity based on elasticity data
- Clarification of the relation of the lesion with the surrounding structures (imaging of invasive process)
- Definition of the tumor origin

USE fails to supply any data in 14% of patients [9] due to the absence of color pattern in a lesion or no obvious difference in color of the lesion and the surrounding structures. Elastometry proves the hard structure of the lesion with quantitative data (Fig. 6.6c, d).

The use of contrast agents is a new promising modality for diagnosis of thyroid cancer [10]. Three types of contrast enhancement may be observed in malignant lesions: homogeneous, heterogeneous, and annular (Fig. 6.7).

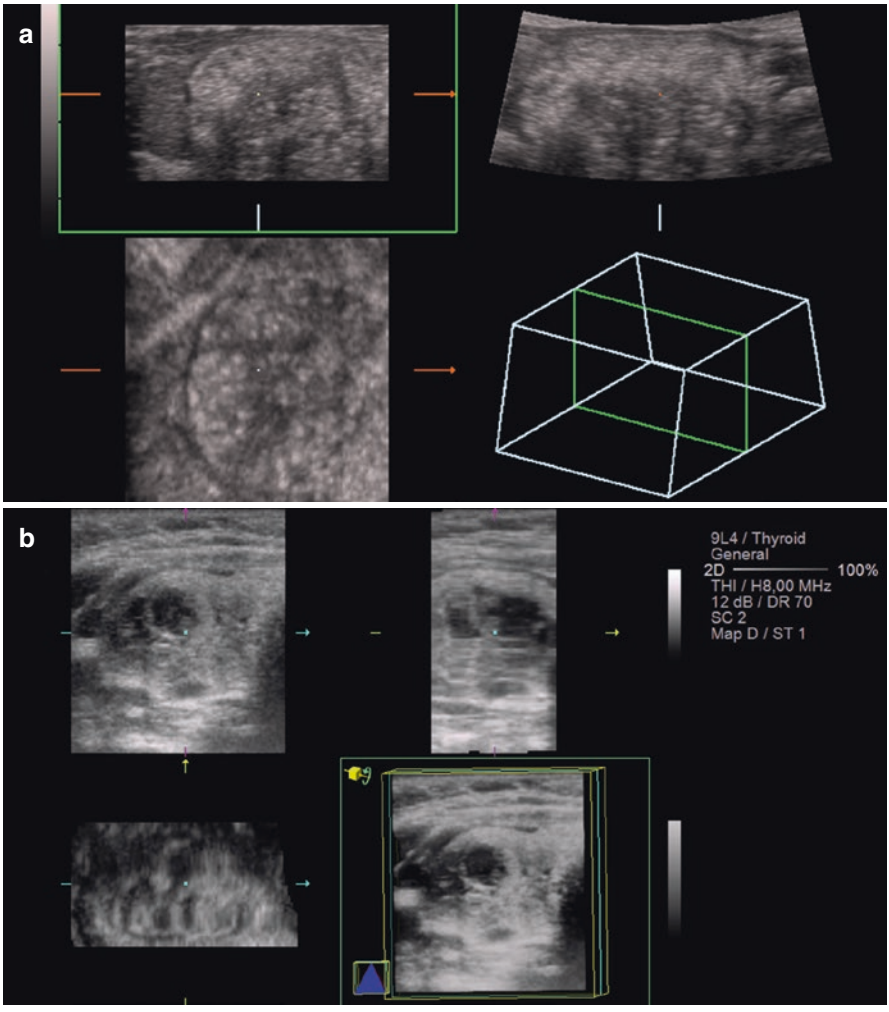

Fig. 6.4 Thyroid cancer. (**a**, **b**) Grayscale 3D imaging. (**c**, **d**) 3DPD

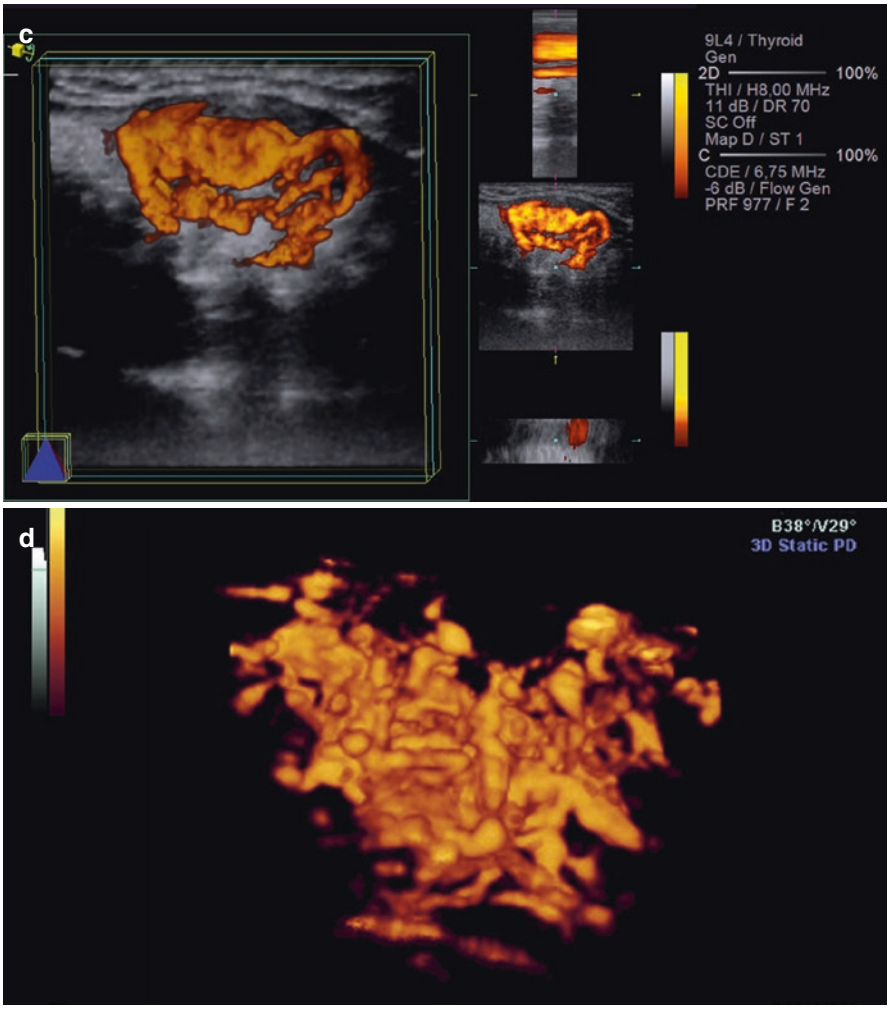

Fig. 6.4 (continued)

Heterogeneous contrast enhancement is a specific sign of a malignant process (sensitivity 88%, specificity 93%, positive predictive value 92%, negative predictive value 89%, and total accuracy 90%) [11, 12].

According to Sencha et al. [10], the most informative indicators in the diagnosis of thyroid cancer are the following: DT/2 index, DV index, and DV difference. The test "DT/2 index > 1.028" exhibits the sensitivity of 86%, specificity of 85%, predictive value of a positive test of 88%, predictive value of a negative test of 83%,

and area under the curve of 0.872. The test "DV index ≤ 0.895" is characterized by the sensitivity of 67%, specificity of 95%, predictive value of a positive test of 94%, predictive value of a negative test of 70%, and area under the curve of 0.840. Tests for differentiation of individual types of thyroid cancer with quantitative analysis of CEUS were not revealed.

The sensitivity of US in the diagnosis of thyroid cancer is 69–98%, and it has a specificity of 50–92% and a diagnostic accuracy of 80–99% [3, 8]. According to [13], the popularization of sonography resulted in an increase in the

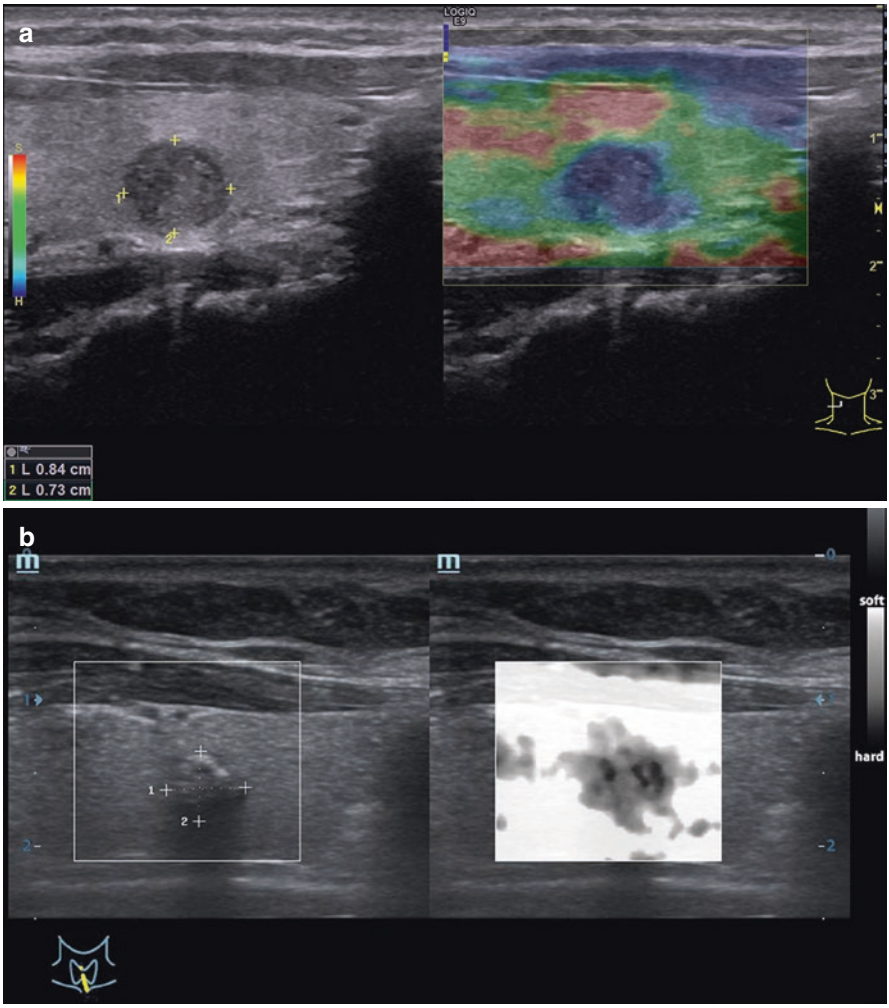

Fig. 6.5 Thyroid cancer. (**a**–**d**) Compression US elastography

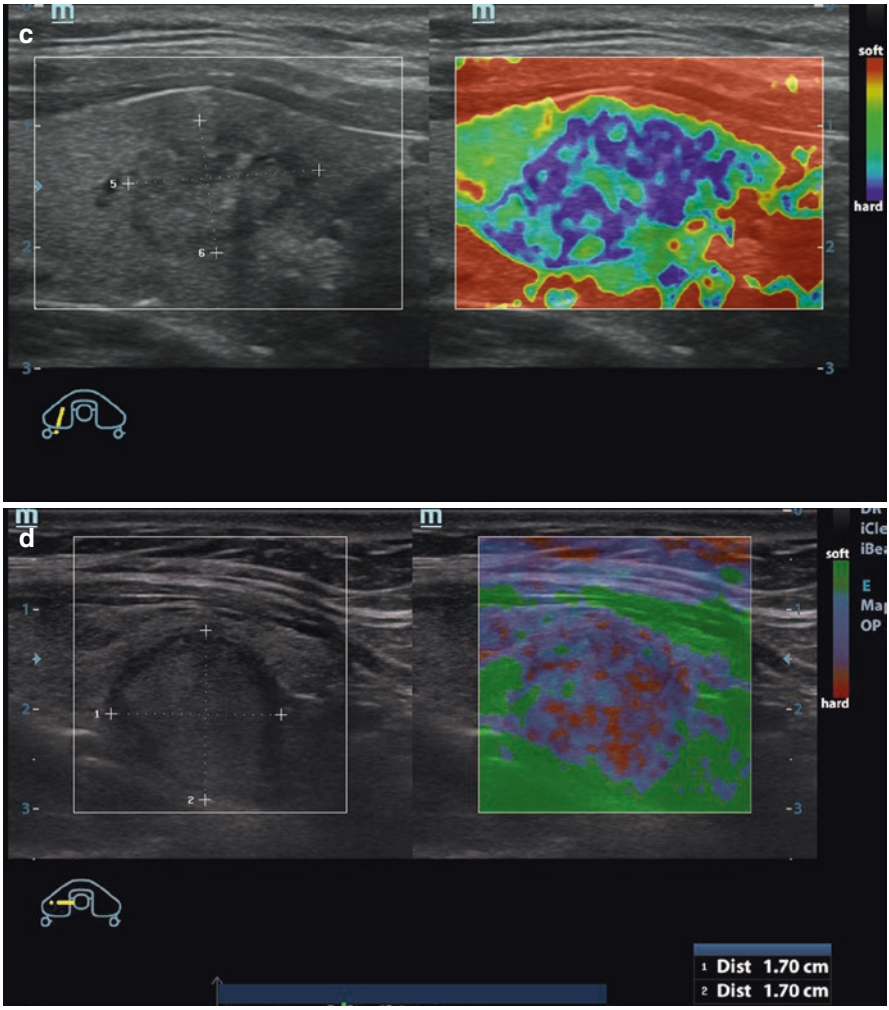

Fig. 6.5 (continued)

proportion of patients with stage T1–2N0M0 thyroid cancer from 57.4% (in 1991) to 70.6% (in 2000). According to Kotlyarov et al. [8], grayscale sonography shows positive predictive value for thyroid cancer in 85% of cases. CDI, PDI, and 3D reconstruction increase the efficacy of US up to 95%. Markova [14] reported that the specificities of sonography in grayscale, CDI, PDI, and 3DPD for the diagnosis of thyroid cancer are 73, 79, 81, and 86%, with sensitivities of 77, 85, 90, and 93% and diagnostic accuracies of 72, 79, 82, and 87%, respectively.

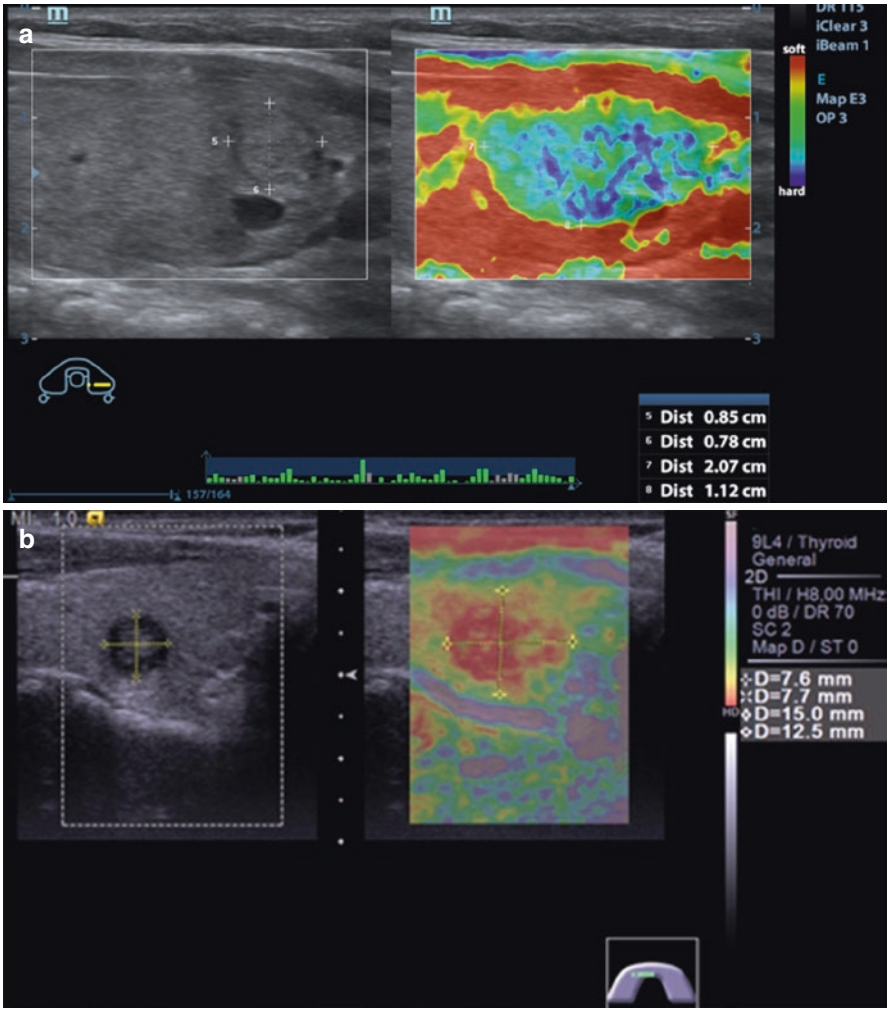

Fig. 6.6 Thyroid cancer. (**a**, **b**) Hard area is larger than grayscale image of the lesion. Compression US elastography. (**c**) Young's modulus with shear-wave elastography. (**d**) Strain-ratio measurement

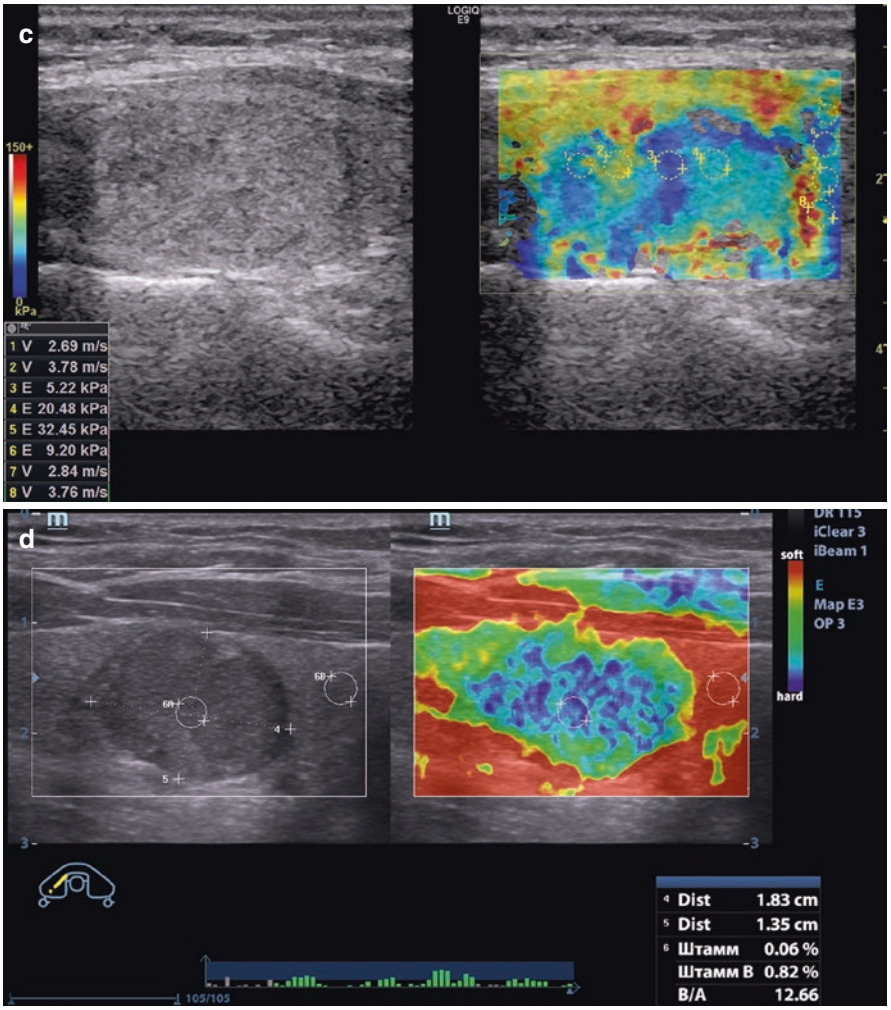

Fig. 6.6 (continued)

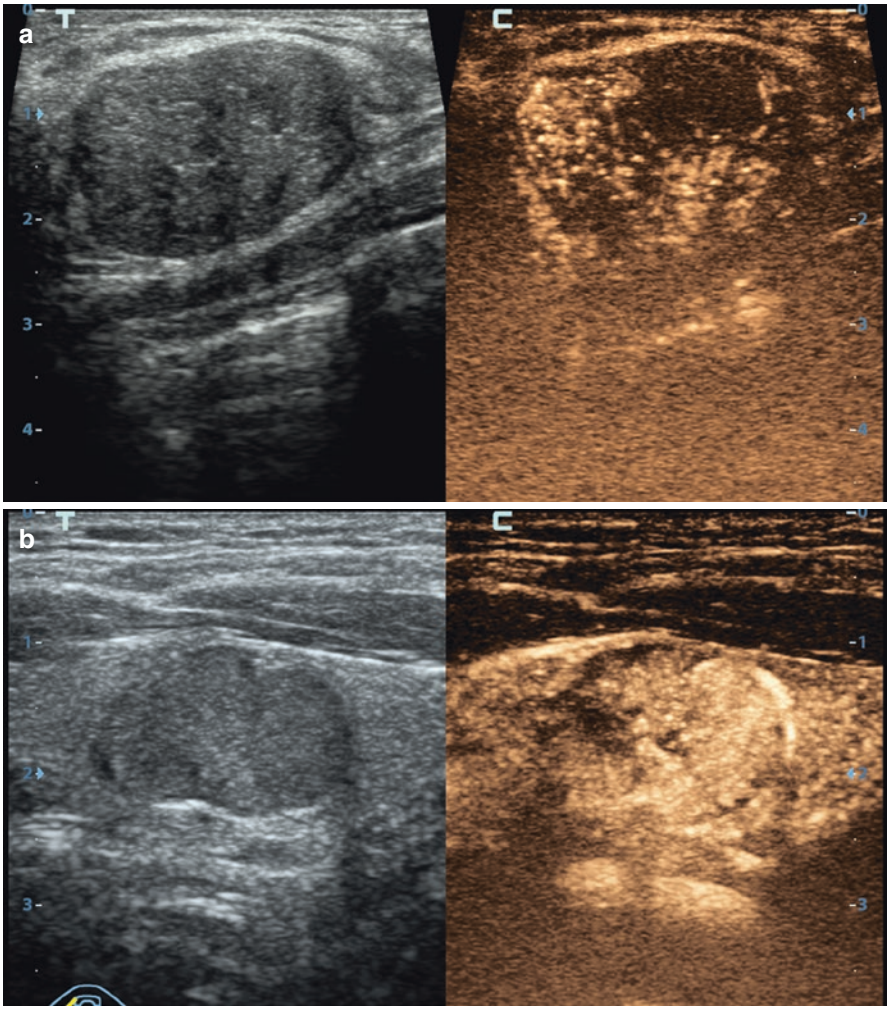

Fig. 6.7 Thyroid cancer. CEUS with SonoVue® 2.4 mL. (**a**, **b**) Irregular hypervascularity of the lesion with neoangiogenesis in the arterial phase. (**c**, **d**) Time-intensity curves

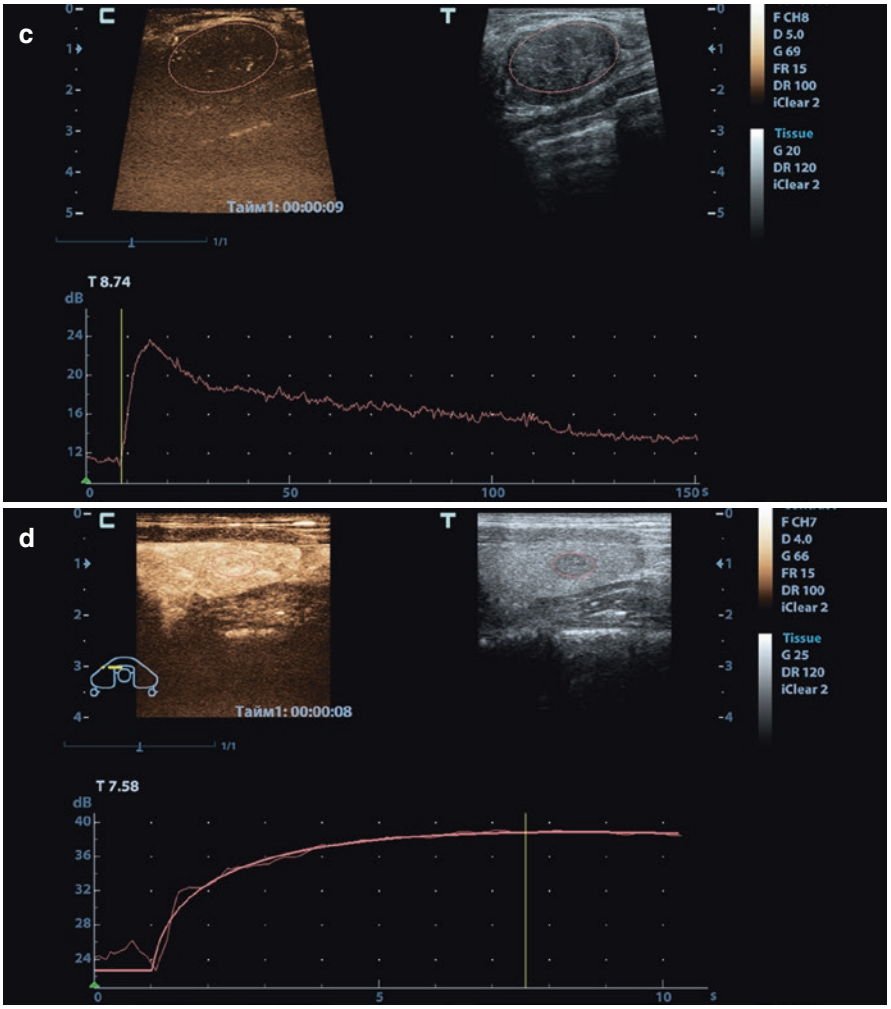

Fig. 6.7 (continued)

Early diagnosis of thyroid cancer is of special importance, since the prognosis depends on the tumor size. In daily practice, early and occult cancers cause certain difficulties.

6.3 Management of Thyroid Microcarcinoma

The clinical significance of subcentimeter thyroid nodules is still the subject of discussion. Some scientists [15–17] deny the need to take into account "small" nodules of the thyroid gland (smaller than 1 cm in size). They point out that such lesions are commonly nodular proliferative colloid goiter; the probability a malignant tumor is small. These nodules do not have any independent clinical significance, hence do not need active detection and treatment. Additionally, in their opinion, thyroid microcarcinoma is a tumor with low malignant potential, low degree of aggressiveness, slow growth, and asymptomatic course [18–21].

Other researchers believe that subcentimeter thyroid nodules have independent clinical significance. The incidence of cancer in palpable and non-palpable thyroid nodules is the same [22–24]. Therefore, the presence of any thyroid lesion, regardless of its size, should be assessed from the point of view of oncological suspicion [25].

Only in 10% of nodules smaller than 10 mm in size are commonly detected by palpation. Therefore, US is the "gold standard" of primary diagnosis of thyroid lesions [9, 24, 26–29]. Its diagnostic capabilities increased the rate of detection of non-palpable thyroid nodules, the so-called incidentaloma.

According to a number of authors [30, 31], an active search with US screening and treatment of occult thyroid carcinomas is associated with significant financial costs and unjustified patient disability. This is argued by the fact that only 3–4% of nodules up to 1 cm can be malignant, and most occult thyroid cancers do not progress to clinically significant stages.

The data on the high efficiency of USE in early and differential diagnosis of thyroid lesions, including thyroid cancer, are rather contradictory [9, 32–37]. A number of researchers [37] believe that the USE allows to determine thyroid tumors up to 5 mm in size and predict the malignancy. In the studies of Dighe et al. [38], the compression USE was demonstrated valuable in the detection of thyroid cancer regardless of size and location. According to Fukunari et al. [34], USE is especially effective in the early and differential diagnosis of follicular tumors, and its specificity and diagnostic accuracy are higher than of color Doppler imaging. Alternatively, other authors believe that USE is of low value in the diagnosis of malignant subcentimeter thyroid lesions. According to Sencha et al. [29], USE fails to differentiate thyroid lesions in several cases, and subcentimeter thyroid nodules compose 83% of such cases. The specificity of USE in thyroid nodules smaller than 1 cm in size is only 21% [29].

US and FNAB complement each other with summing up the diagnostic potential, which is close to 100%. Assessment of the results of these methods is optimal for preoperative diagnosis.

According to the European consensus for the management of patients with differentiated thyroid carcinoma of the follicular epithelium [39], micronodules (≤1 cm) carry a very low risk of morbidity even if malignant and should be submitted to FNAB only in the event of suspicious finding at US (solid hypoechoic with microcalcifications) or personal history.

According to AACE/ACE/AME Guidelines [40], US evaluation is not recommended as a screening test for the general population or patients with a normal thyroid on palpation and a low clinical risk of thyroid disease. US evaluation is recommended for patients who are at risk for thyroid malignancy, have palpable thyroid nodules or goiter, or have neck lymphadenopathy suggestive of a malignant lesion. FNA should be considered for nodules ≤10 mm diameter only when suspicious US signs are present, while nodules ≤5 mm should be monitored rather than biopsied.

However, the final decision on the need of FNAB belongs to clinician, who can consider it necessary even in those cases, where the nodules do not meet the criteria specified in the recommendations.

In about 5% of cases, thyroid cancer exhibits an ultrasound image, which does not correspond to malignant tumors [41]. US imaging only cannot confidently differentiate a malignant nodule from a benign one; the US conclusion is conjectural. However, various US signs have different value for differential diagnosis. Hence, they are grouped to TIRADS categories to facilitate the assessment of the risk of malignancy.

References

1. Mazzaferri EL, Robbins RJ, Spencer CA, et al. A consensus report of the role of serum thyroglobulin as a monitoring method for low-risk patients with papillary thyroid carcinoma. J Clin Endocrinol Metab. 2003;88(4):1433–41.
2. Bychkov A. World Health Organization (WHO) classification. PathologyOutlines.com website. 2018. http://www.pathologyoutlines.com/topic/thyroidwho.html
3. Moon WJ, Jung SL, Lee JH, et al. Benign and malignant thyroid nodules: US differentiation-multicenter retrospective study. Radiology. 2008;247(3):762–70.
4. Valdina EA. Diseases of the thyroid gland. St. Petersburg: Peter; 2001 (Book in Russian).
5. Burch HB. Fine needle aspiration of thyroid nodules. Determinants of insufficiency rate and malignancy yield at thyroidectomy. Acta Cytol. 1996;40:1176–83.
6. Takashima S, Fukuda H, Nomura N, et al. Thyroid nodules: reevaluation with ultrasound. J Clin Ultrasound. 1995;23(3):179–84.
7. Zubarev AV, Bashilov VP, et al. The value of ultrasonic angiography and three-dimensional reconstruction of vessels in the diagnosis of nodular formations of the thyroid gland. Medicinskaya vizualizaciya. 2000;3:57–62 (Article in Russian).
8. Kotlyarov PM, Yanushpolskaya TO, Aleksandrov YK, et al. Ultrasound in the diagnosis of thyroid cancer and its recurrence. Dent Echo. 2001;2(4):349–54 (Article in Russian).
9. Sencha AN, Mogutov MS, Sergeeva ED, Shmelev DM. Sonoelastography and the newest technologies of ultrasonic research of a cancer of a thyroid gland. Moscow: Vidar; 2010 (Book in Russian).

10. Sencha EA, Sencha AN, Penyaeva EI, et al. The use of quantitative analysis of ultrasound with contrast enhancement in the differential diagnosis of focal changes in the thyroid gland. Ultrazvukovaya i funkcionalnaya diagnostika. 2018;2:12–26 (Article in Russian).
11. Ma BY, Jin Y, Suntdar PS, et al. Contrast-enhanced ultrasonography findings for papillary thyroid carcinoma and its pathological bases. Sichuan Da Xue Xue Bao Yi Xue Ban. 2014;45(6):997–1000.
12. Zhang B, Jiang YX, Liu JB, et al. Utility of contrast-enhanced ultrasound for evaluation of thyroid nodules. Thyroid. 2010;20(1):51–7.
13. Agamov AG, Alexandrov YK, Sencha AN. Diagnosis, treatment, and postoperative follow-up of patients with the diagnosis of thyroid cancer. Informatsionniy bulletin, Yaroslavl. 2003;2:18–23 (Article in Russian).
14. Markova NV. The value of ultrasound angiography in the diagnosis of the main diseases of the thyroid gland [PhD Thesis]. Moscow; 2001 (Book in Russian).
15. Dossing H, Bennedæk FN, Hegedus L. Ultrasound-guided interstitial laser thyroid nodule. Thyroid. 2006;13(9):885–8.
16. Vanushko VE, Fadeev VV. Cancer of the thyroid gland. In: Dedov II, Kuznetsov NS, Melnichenko GA, editors. Endocrine surgery. Moscow: Litera; 2011 (Book in Russian).
17. Yang J, Schnadig V, Logrono R, Wasserman PG. Fine needle aspiration of thyroid nodules: a study of 4703 patients with histologic and clinical correlations. Cancer. 2007:306–15.
18. Demidchik YE, Kolobukhov AE, Demidchik EP, et al. Results of treatment of patients with medullary thyroid cancer. Oncol J. 2008;2(3):19–30 (Article in Russian).
19. Ito Y, Miyauchi A. A therapeutic strategy for the papillary microcarcinoma of the thyroid. Nat Clin Pract Endocrinol Metab. 2007;3:240–8.
20. Miccoli P, Minuto MN, Galleri D, et al. Incidental thyroid carcinoma in a large series of consecutive patients operated on for benign thyroid disease. ANZ J Surg. 2006;76(3):123–6.
21. Troshina EA. Diagnosis, treatment and monitoring of nodular forms of thyroid disease [PhD thesis]. Moscow; 2002 (Book in Russian).
22. Barbara D, Simi U, Meucci G, et al. Thyroid papillary cancers: microcarcinoma and carcinoma, incidental cancers and non-incidental cancers - are they different diseases? Clin Endocrinol. 2005;3(5):577–81.
23. Matyanin MV. Optimization of indications and the choice of the scope of surgical intervention in patients with nodular colloid goiter [PhD thesis]. Nijniy Novgorod; 2007 (Book in Russian).
24. Shulutko AM, Semikov VI, Vetshev PS. Non-palpable thyroid nodules. Moscow: Profile-2C; 2011 (Book in Russian).
25. Shevchenko SP, Dymov AA, Dolgova EM, et al. Sonoelastography in the complex of preoperative diagnosis of thyroid cancer. Oncosurgery: Tumors Head Neck. 2011;3:60–3 (Article in Russian).
26. Kharchenko VP, Kotlyarov PM, Mogutov MS, et al. Ultrasound diagnostics of thyroid diseases. Berlin: Springer; 2010.
27. Matyaschuk SI, Naida YN, Shelkova EA. Indications for puncture biopsy (FNAB) of thyroid nodules. Liki Ukraini. 2011;6(152):61–70.
28. Peccin S, de Castsro JA, Furlanetto TW, et al. Ultrasonography: is it useful in the diagnosis of cancer in thyroid nodules? J Endocrinol Investig. 2002;25(1):39–43.
29. Sencha AN, Patrunov YN, Mogutov MS, et al. Elastography and modern technologies of ultrasound examination in diagnosis of thyroid cancer. Moscow: Vidar-M; 2011.
30. Belfiore A, La Rosa GL. Fine-needle aspiration biopsy of the thyroid. Endocrinol Metab Clin North Am. 2001;30:361–400.
31. Wang CC, Friedman L, Kennedy GC, et al. A large multicenter correlation study of thyroid nodule cytopathology and histopathology. Thyroid. 2011;21(3):243–51.
32. Alam F, Naito K, Horiguchi J, et al. Accuracy of sonographic elastography in the differential diagnosis of cervical lymph nodes: comparison with conventional sonography. Am J Roentgenol. 2008;191(2):604–10.
33. Cooper DS, Doherty GM, Haugen BR, et al. American Thyroid Association manager for patients with thyroid nodules and differentiated thyroid cancer. Thyroid. 2009;19(11):1167–214.

34. Fukunari N, Arai K, Naakamura A, et al. Clinical evaluation of thyroid follicular tumors. J Ultrasound Med Biol. 2010;35(8):R230.
35. Ophir J, Cespedes I, Ponnekanti H, et al. Elastography: a quantitative method for imaging of the tissues. Ultrason Imaging. 2000;13(2):111–34.
36. Rago T, Santini F, Scutari M, et al. Elastography: new developments in thyroid nodules. J Clin Endocrinol Metab. 2007;92(8):2917–22.
37. Shevchenko SP. Modern clinical and molecular genetic approaches to the diagnosis and treatment of thyroid cancer [PhD thesis]. Novosibirsk; 2013 (Book in Russian).
38. Dighe M, Bae U, Richardson ML, et al. Differential diagnosis of thyroid nodules with US elastography using carotid artery pulsation. Radiology. 2008;248(2):662–9.
39. Pacini F, Schlumberger M, Dralle H, et al. European consensus for the management of patients with differentiated thyroid carcinoma of the follicular epithelium. Eur J Endocrinol. 2006;154(6):787–803.
40. Gharib H, Papini E, Garber JR, et al. The American Association of Clinical Endocrinologists, American College of Endocrinology, and Associazione Medici Endocrinologi medical guidelines for clinical practice for the diagnosis and management of thyroid nodules – 2016 update. Endocr Pract. 2016;22(Suppl 1):1–60.
41. Sencha AN. Ultrasonic visualization of malignant tumors of the thyroid gland. Ultrazvukovaya i funkcionalnaya diagnostika. 2008;2:20–9 (Article in Russian).

TIRADS Classification as a Malignancy Risk Stratification System

7

Liubov A. Timofeyeva, Ekaterina A. Sencha, Yuriy K. Aleksandrov, Alexander N. Sencha, and Munir G. Tukhbatullin

Experts from the American Association of Clinical Endocrinologists (AACE), the American College of Endocrinology (ACE), and the Associazione Medici Endocrinologi (AME) consider high-resolution ultrasound as the most sensitive test ("gold standard") for detecting thyroid nodules [1]. One more important issue is specification of the lesion character as close to pathology as possible. US reveals a large number of signs that do not have a digital (objective) expression. Hence, there is a great need for systematization of US reports. For example, interpretation and understanding of FNAB is much simpler since the morphologists have been able to come to a consensus on the cytological assessment of thyroid nodules presented in the Bethesda System for Reporting Thyroid Cytopathology.

Attempts to solve the problem by analogy with cytologists led to the fact that several diagnostic stratification systems were developed in different countries [1–5].

L. A.Timofeyeva (✉)
Department for Internal Diseases Propaedeutic, Federal State Budget Educational Institution of Higher Education "I. N. Ulianov Chuvash State University", Cheboksary, Russia

E. A. Sencha
Ultrasound Diagnostics Department of Medical Diagnostic Center No. 9, Moscow, Russia

Y K. Aleksandrov
Department of Surgery, Federal State Budget Educational Institution of Higher Education Yaroslavl State Medical University of the Ministry of Healthcare of the Russian Federation, Yaroslavl, Russia

A. N. Sencha
Department of Visual and Functional Diagnostics, National Research Center for Obstetrics, Gynecology and Perinatology, Ministry of Healthcare of the Russian Federation, Moscow, Russia

M. G. Tukhbatullin
Department of Ultrasound Diagnostics, Kazan State Medical Academy, Federal State Budget Educational Institution of Further Professional Education, "Russian Medical Academy of Continuing Professional Education" of the Ministry of Healthcare of the Russian Federation, Kazan, Russia

A. N. Sencha, Y. N. Patrunov (eds.), *Thyroid Ultrasound*,
https://doi.org/10.1007/978-3-030-14451-7_7

vThese classifications use various complex ultrasound data models to estimate the risk of malignancy thus reducing the influence of subjective factor.

The Thyroid Imaging Reporting and Data System (TIRADS) proposed by Horvath et al. in 2009 for standardization of ultrasound imaging was the first to adopt this approach to the interpretation of US images and the detection of thyroid malignancies [6]. They took as an example the well-known concept of BI-RADS (Breast Imaging Reporting and Data System) mammographic scale, which is successfully adopted worldwide [7]. The main purpose of the system was to develop a unified language with terms for interpreting thyroid images to create recommendations for further tactics.

TIRADS is based on the ranking of a set of ultrasound signs that are most common in various thyroid pathologies. This approach implied ten "images," united in six groups ranged in accordance with the risk of malignancy. The characteristics of thyroid nodules, such as clarity and regularity of margins, echogenicity, echostructure, and presence of macro- and microcalcifications, composed the basic elements of the system. Some new features, e.g., "taller-than-wide" sign, were added later.

TIRADS significantly improved the detection of thyroid tumors [8]. Thyroid nodules TIRADS 2–4a were reported thyroid cancer (BSRTC 6 with FNAB) in 2.3%, suspicious of a malignant tumor (BSRTC 5 with FNAB) in 3.6%, and follicular tumors (BSRTC 4 with FNAB) in 5.0% of cases. In the group of patients with TIRADS 4b–5, thyroid cancer (BSRTC 6 with FNAB) was registered in 42.2%, suspicion for a malignant tumor (BSRTC 5 with FNAB) in 6.3%, and follicular tumors (BSRTC 4 with FNAB) in 18.1%.

In 2017, Horvath et al. published data on the results of the application of the modified TIRADS system (Table 7.1). Thyroid cancer is detected with TIRADS 2 at 0%, with TIRADS 3 at 1.79%, with TIRADS 4 at 76.13% (TIRADS 4a, 5.88%; TIRADS 4b, 62.82%; TIRADS 4c, 91.22%), and 98.85% in TIRADS 5. TIRADS sensitivity in thyroid cancer was 99.6% (95% CI, 98.9–100.0), specificity 74.35% (95% CI, 68.7–80.0), PPV 82.1% (95% CI, 78.0–86.3), NPV 99.4% (95% CI, 98.3–100.0), PLR 3.9% (95% CI, 3.6–4.2), and NLR 0.005% (95% CI, 0.003–0.04).

Based on a meta-analysis of 29,678 thyroid nodules (41 studies), Campanella et al. [11] concluded the following signs with a higher risk of malignancy expressed in odds ratio (OR): nodule height greater than width (OR: 10.15), absent halo sign (OR: 7.14), microcalcifications (OR: 6.76), irregular margins (OR: 6.12), hypoechogenicity (OR: 5.07), solid nodule structure (OR: 4.69), intranodular vascularization (OR: 3.76), family history of thyroid carcinoma (OR: 2.29), nodule size ≥4 cm (OR: 1.63), single nodule (OR: 1.43), history of head/neck irradiation (OR: 1.29), and male gender (OR: 1.22). This provided the basis for integral clinical, ultrasonographic, and cytological scoring system "CUT score" [12] and for determination of tactics in cases with uncertain or repeated nondiagnostic FNAB.

European researchers [3] presented a variant of the system Euro-TIRADS (EU-TIRADS). Unlike TIRADS, the gradations in EU-TIRADS range from 1 to 5. EU-TIRADS 1 corresponds to a normal thyroid, EU-TIRADS 2 to a benign thyroid nodule, and EU-TIRADS 3 to a highly probable benign nodule. Suspicion of

Table 7.1 TIRADS category and US characteristics of thyroid nodules and their malignancy risk [9, 10]

Category	Characteristics	Cancer risk	Recommendations
1	Normal exam		
2	Hashimoto's thyroiditis, typical De Quervain's thyroiditis, Graves's disease; benign colloid lesions (Type 1 and 2 patterns); intraparenchymal calcification without associated nodule; aspirated nodule with benign result, concordant with its US image; small hyperechoic pseudo-nodules in Hashimoto's thyroiditis ("white knight"); old colloid nodule in spontaneous regression (prior exam available that shows the preexistence of a bigger colloid lesion on the same location); situations, such as normal postsurgical control	Benign findings 0.0% malignancy	Follow-up
3	Typical hyperplastic colloid nodules with hyperechoic spots (Type 3 pattern); hypoechoic pseudo-nodules in Hashimoto's thyroiditis that for some reason (size, shape) appear to be different from the other thyroiditis focus dispersed within the parenchyma	Probably benign <5.0% malignancy	Follow-up/FNAC
4a	Solid or mixed hyper-, iso-, or hypoechoic nodule, with a thin capsule. Simple neoplastic pattern. Hypoechoic lesion with infiltrative borders, without calcifications (De Quervain's pattern). Hyper-, iso-, or hypoechoic, hypervascularized, encapsulated nodule with a thick capsule, containing calcifications (coarse or microcalcifications) (suspicious neoplastic pattern)	Low suspicion 5.0–10.0% malignancy	FNAC
4b	Hypoechoic, nonencapsulated nodule, with irregular Shape and margins, penetrating vessels, with or without calcifications (malignant pattern A)	Intermediate suspicion 11.0–65.0% malignancy	FNAC
4c	The presence of micro- and/or coarse calcifications and penetrating vessels increase suspicion (malignant pattern A). Mixed or solid isoechoic nodule, nonencapsulated, vascularized with micro- or macrocalcifications (without hyperechoic spots, malignant pattern C)	High suspicion 66.0–95.0% malignancy	FNAC
5	Nodules with malignant patterns (Types B and C) Adenopathies and ipsilateral suspicious nodules	Suggestive of malignancy >95.0%	FNAC
6	FNAC-confirmed malignancy	100% malignancy	Surgery

malignancy is divided into three categories: EU-TIRADS 4a and 4b correspond to low and high suspicions of malignancy, and EU-TIRADS 5 corresponds to a malignant nodule with two or more cancer criteria. CDI is not regarded (the authors believe that CDI has low reproducibility and efficiency). Innovations include the use of a combination of grayscale mode and US elastography. This improved the sensitivity (98.5%, $P < 0.0001$) and NPV (99.8%) but decreased the specificity (44.7%, $P < 0.0001$) and accuracy (48.3%, $P < 0.0001$). Tugendsam et al. [13] in the study with 45 papillary carcinomas, 8 follicular carcinomas, and 142 benign nodules confirmed the value of EU-TIRADS and recommended its use for stratification of thyroid nodules in Austria in the areas with severe iodine deficiency. The sensitivity for thyroid cancer was reported 85% with the specificity of 45%. The system was effective only in papillary carcinoma (2.98 ± 1.32 vs 1.73 ± 1.18, $P < 0.001$). EU-TIRADS failed to identify follicular cancer. In recent years, studies, based on the use of this classification in the analysis of several thousand thyroid nodules, report the following values of the risk of malignancy: category 2, 0%; 3, <2%; 4a, 2–5%; 4b, 5–50%; and 5, 50–90%.

In the USA, several groups were engaged in the development of stratification systems. The latest AACE/ACE/AME guidelines (2016) emphasize that the requirements for the thyroid ultrasound protocol should be exact and the criteria for the description of the thyroid nodules must be strictly followed. AACE/ACE/AME experts suggest a simplified system of thyroid cancer risk assessment, focusing on a limited number of signs. Gharib et al. [1] proposed to rank the thyroid nodules according to the risk of malignancy as follows: Grade 1, low risk; Grade 2, medium risk; and Grade 3, high risk.

The American College of Radiologists (ACR) proposed an alternative model [5]. A feature of the ACR TIRADS classification is that ultrasound signs have ranking in accordance with their importance for diagnosis. Each sign weights some points, and the ACR TIRADS score directly depends on the total sum of points (Table 7.2). ACR TIRADS does not group ultrasound signs into strict patterns and has a higher nodule size threshold when recommending FNAB in cases of slightly and moderately suspicious lesions.

The American Thyroid Association (ATA) [2] recommended the following five patterns of sonographic image based on a significantly smaller number of ultrasound signs and corresponding with the risk of malignancy: “benign” (purely cystic lesion), “very low suspicion,” “low suspicion,” “intermediate suspicion,” and “high suspicion.”

Consensus statement and recommendations published by Korean scientists [14] implied the concept of the Korean thyroid image reporting and data system (K-TIRADS) [15]. Korean scientists have significantly reduced the number of signs evaluated. Several US features, such as hypoechogenicity, marked hypoechogenicity, microlobulated or irregular margins, microcalcifications, and taller-than-wide shape, were regarded as independent US features of malignancy. In addition, they proposed not only to record the presence of ultrasound signs but to count them. The presence of one of the signs (4a) indicated a low risk of suspected malignancy, two (4b), intermediate; three or four (4c), moderate; and five (5), high risk of malignancy (Table 7.3).

Table 7.2 Chart showing five categories on the basis of the ACR TIRADS lexicon, TR levels, and criteria for fine-needle aspiration or follow-up ultrasound according to Tessler et al. [5]

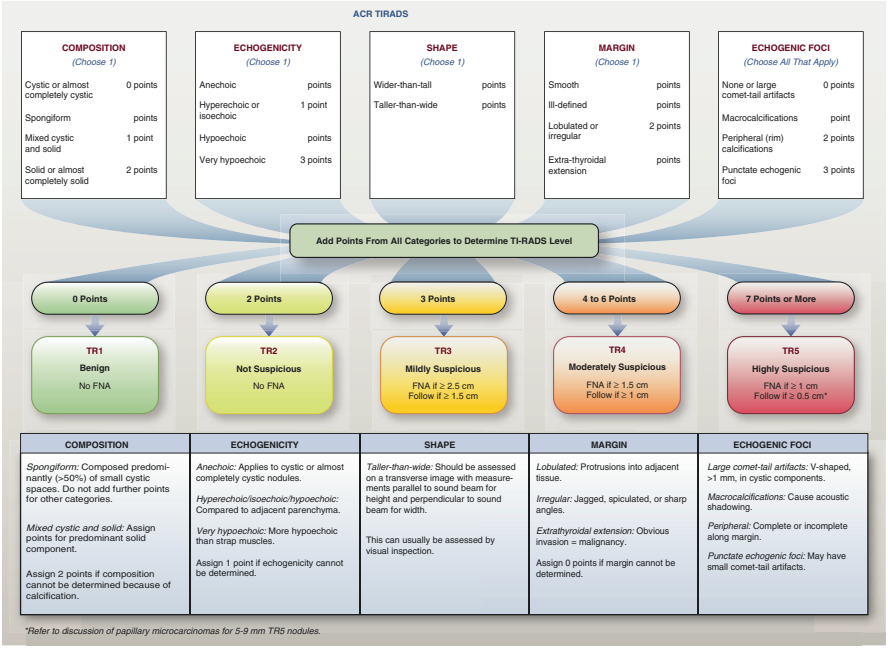

Table 7.3 K-TIRADS category and malignancy risk

Category	Characteristics	Cancer risk	Recommendations
1	Normal exam		
2	Predominantly cystic peripheral halo	Benign 0.0% malignancy	Follow-up
3	No suspicious US features	Probably benign 2.0–2.8% malignancy	Follow-up
4a	One suspicious US feature	Low suspicion for malignancy 3.6–12.7%	FNAC, ≥1.0 cm
4b	Two suspicious US features	Intermediate suspicion for malignancy 6.8–37.8%	FNAC ≥1.0 cm
4c	Three or four suspicious US features	Moderate concern but not classic for malignancy 21.0–91.9%	FNAC ≥1.0 cm
5	Five suspicious US features including solid, hypoechogenicity, microlobulated or irregular margins, microcalcifications, taller-than-wide shape	Highly suggestive of malignancy 88.7–97.9%	FNAC ≥1.0 cm

Sonographic classification of nodules as intermediate to high suspicion by ATA or TIRADS category 4c displayed positive predictive value of 63% and 71%, respectively [16]. Negative predictive values for ATA and TIRADS were 91 and 74%, respectively.

In 2014, a group of scientists from the British Thyroid Association (BTA) published their version of TIRADS—BTA thyroid nodule ultrasound (U) classification. The authors took the South Korean, AACE, and ARC classifications as a basis. In addition, as in some other systems, the authors proposed to summarize the negative signs and by their total score come to the conclusion about the need for FNAB. The principle of classification is similar to the AACE/ACE/AME system, but the groups U1, the norm, and U4, suspicious, are additionally introduced. The authors also expanded the list of features (peripheral eggshell calcification, globular calcification, and others).

Utilization of the TIRADS scale and terms is now a mandatory feature for making US conclusions in many clinics worldwide. It permitted to improve the interpretation of the detected thyroid lesions with better understanding between radiologists, endocrinologists, and surgeons and to standardize diagnostic approach and treatment.

Analysis of US image of the thyroid gland results in the specification of TIRADS category.

Category TIRADS 1 (negative) confers the following variants (Fig. 7.1):

- Normal thyroid gland with complex echography.
- Volume and structure of the thyroid gland correspond to the age, constitution, and physiological state of the patient.
- No both direct and indirect signs of pathological processes of diffuse and focal nature.

Recommendation: A scheduled US examination according to age (commonly once every 1–3 years), FNAB is not appropriate.

Category TIRADS 2 (benign lesions) confers the following variants (Fig. 7.2):

- Simple cysts
- Colloid nodules
- Hashimoto's thyroiditis, typical De Quervain's thyroiditis, Graves's disease
- Isolated calcification
- Nodules after successive minimally invasive treatment

Recommendations: US follow-up, FNAB is not necessary.

Category TIRADS 3 (probably benign lesions). This category includes benign thyroid lesions with a probability of cancer of no more than 2–5% (Fig. 7.3):

- Hyperplastic expansile, vascularized colloid nodules with hyperechoic spots
- Hypoechoic pseudo-nodules in Hashimoto's thyroiditis
- Atypical or complex cysts

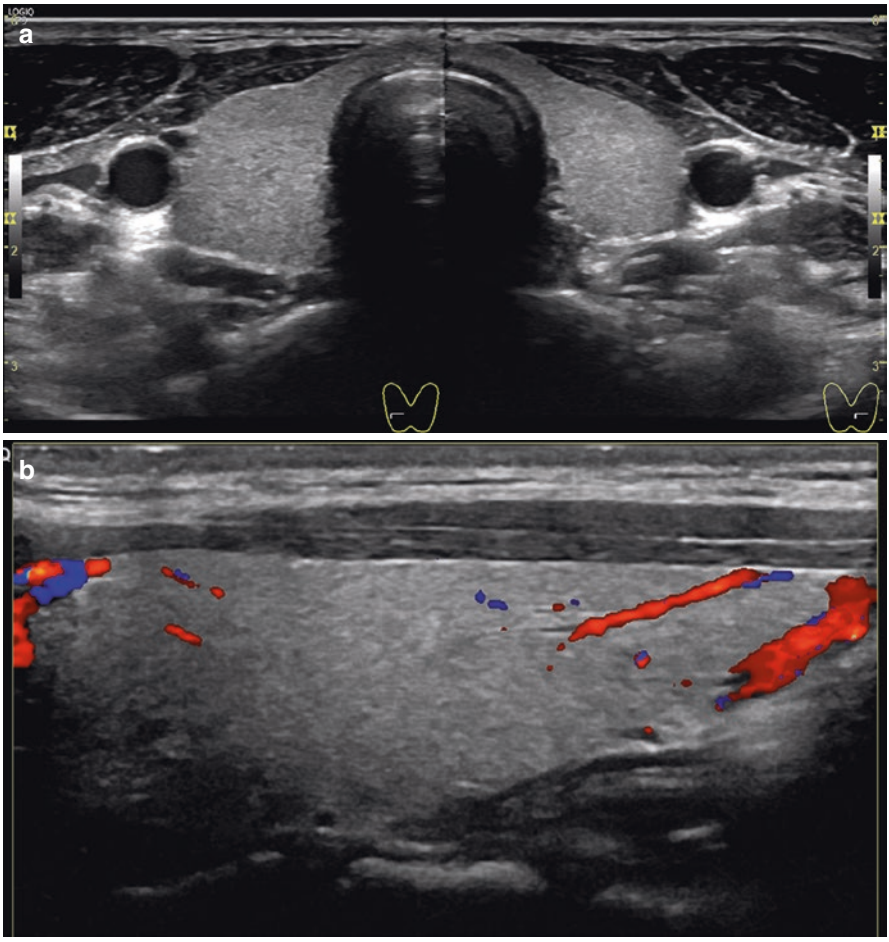

Fig. 7.1 TIRADS 1 category. Normal thyroid gland. (**a**) Grayscale mode. (**b**) CDI

Recommendations: Follow-up every 6–12 months is preferred. If clinical indications arise or at the request of the patient, US-guided FNAB is possible. This group is often transitional. If follow-up reveals suspicion of a malignancy, the case is transferred to the category TIRADS 4. Alternatively, the case is transferred to the category TIRADS 2. If US-guided FNAB reveals benign changes twice, further ultrasound monitoring of cancer risk is not necessary.

Thyroid lesions that significantly change US appearance over a short period of time (6–12 months) are also considered TIRADS 3 [17], such as listed below:

- Increase in volume of more than 30–50%
- Change in grayscale US characteristics (calcifications, fluid component, capsule deformation, etc.)
- Significant change in blood flow with CDI

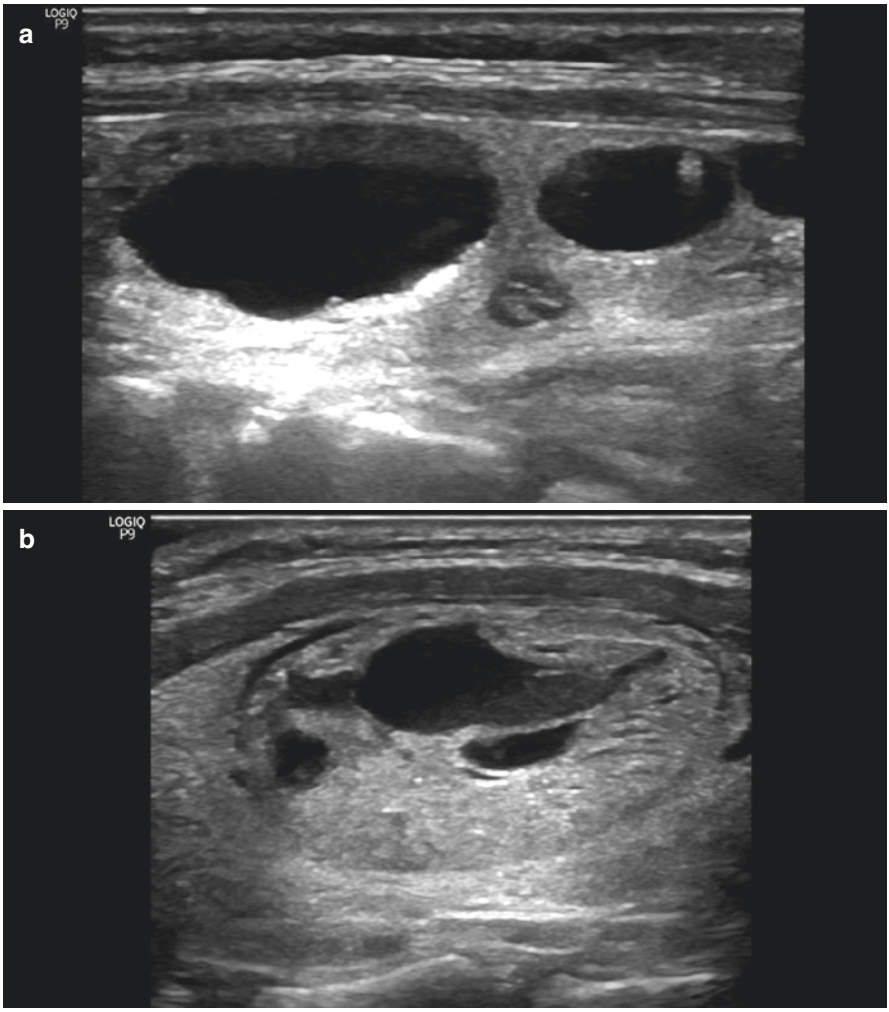

Fig. 7.2 (**a**, **b**) TIRADS 2 category. Colloid thyroid nodule. Echograms. Grayscale mode

- Change in rigidity/elasticity pattern with compression US elastography
- Increase in rigidity with elastometry more than 30–50%
- Appearance of abnormal neck lymph nodes in combination with any thyroid lesion

Category TIRADS 4 (suspected malignancy) (Figs. 7.4, 7.5, and 7.6). Sonographically revealed changes are accompanied with the risk of thyroid malignancy in 5–95% of cases. It confers subcategories 4a, 4b, and 4c that correspond to low, intermediate, and high suspicion of cancer, respectively. These include thyroid lesions, which exhibit the main ultrasound signs of malignancy

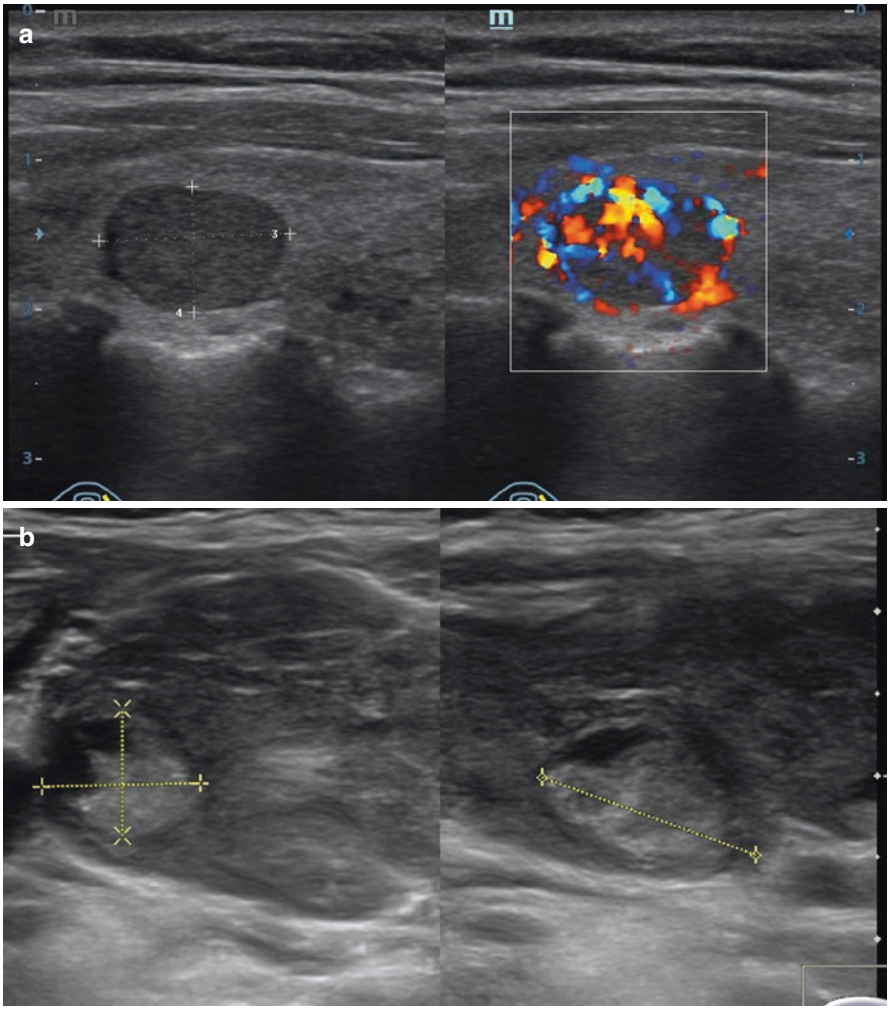

Fig. 7.3 TIRADS 3 category. (**a**) Hypervascular colloid nodule. Grayscale US and CDI. (**b**) Pseudo-nodule in AIT

(ranging from 1 to 4). This group includes solid or mixed colloid nodules with signs of malignancy, such as:

- Infiltrative borders
- Hypervascularization
- Thick capsule
- Coarse or microcalcifications
- Hypoechoic, nonencapsulated nodule
- Irregular shape and margins
- Penetrating vessels

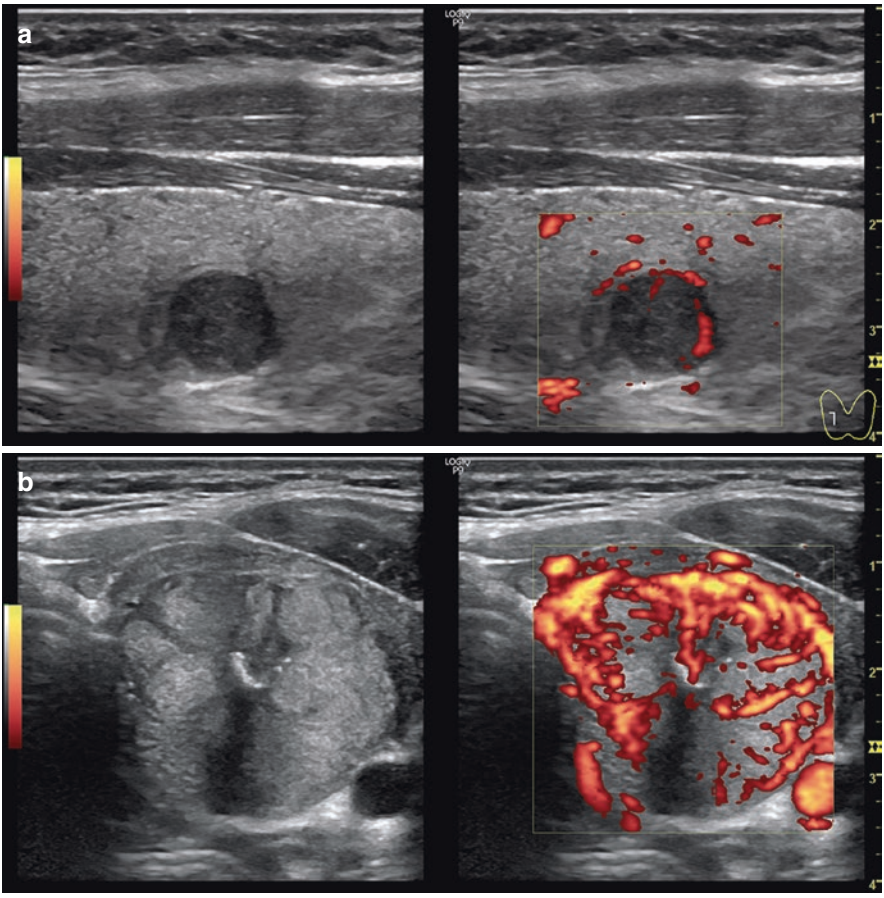

Fig. 7.4 (**a**, **b**) TIRADS 4a category. Grayscale US and PDI

Recommendations: Morphological verification with FNAB is indicated. In the case of benign or doubtful cytology, the lesion is classified as TIRADS 3.

Category TIRADS 5 (suggestive of malignancy) includes the lesions with malignant patterns identical to TIRADS 4c accompanied with enlarged lymph nodes. Thyroid cancer risk is above 95%. US-guided FNAB is indicative.

Category TIRADS 6 includes cases of FNAB-confirmed malignancy (Fig. 7.7). These patients are subject to special treatment, surgery in most cases.

TIRADS permits standardization of thyroid ultrasound reports, thus reducing the subjective aspects in the interpretation of US images. It helps to improve the communication and cooperation of radiologists and clinicians. It contributes to a clear definition of indications for FNAB of thyroid lesions and decrease in the number of unnecessary interventions. One advantage of TIRADS is a good correlation with the Bethesda System for Reporting Thyroid Cytopathology, since FNAB is the most important diagnostic method for thyroid lesions.

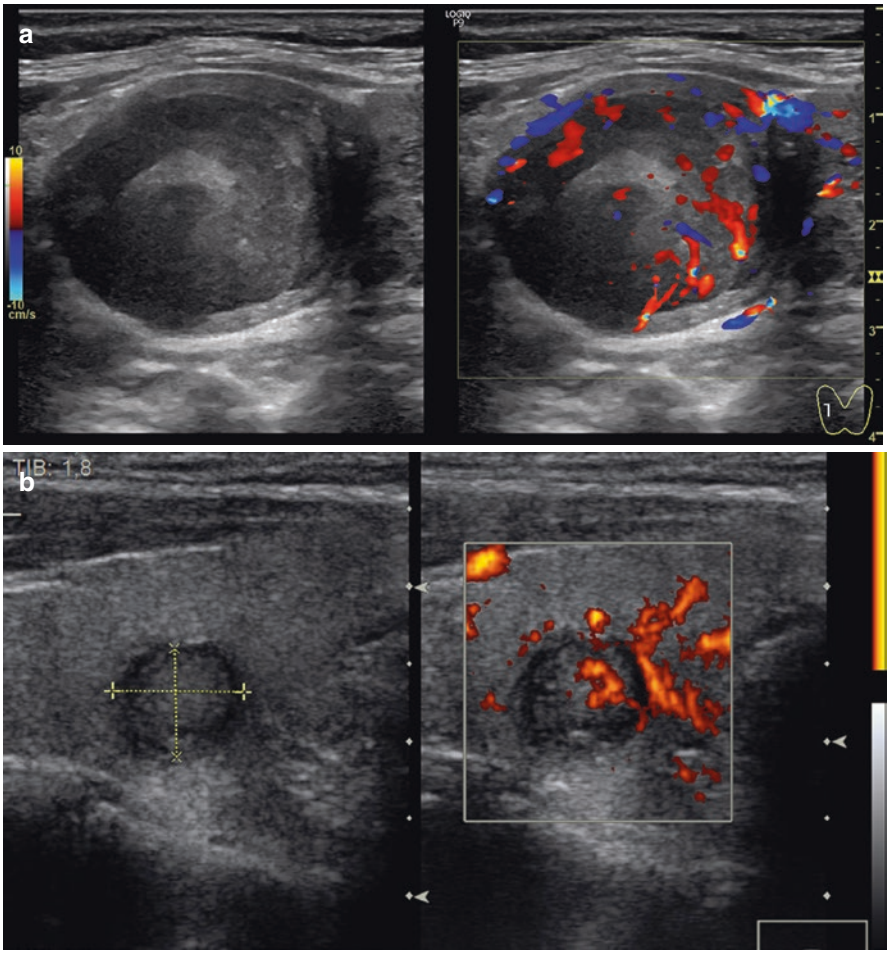

Fig. 7.5 (**a**, **b**) TIRADS 4b category. Grayscale US, CDI, and PDI

The work on improving the efficiency of stratification systems is still in progress. In particular, several approaches have already been proposed, such as quantitative assessment of echogenicity [18] and the use of sonoelastography and contrast agents, but there is no comprehensive information about the value of such systems yet.

The Example US Report in Thyroid Cancer
First name, middle initial, last name:
Age:
Date:
The number of case history:
US scanner:

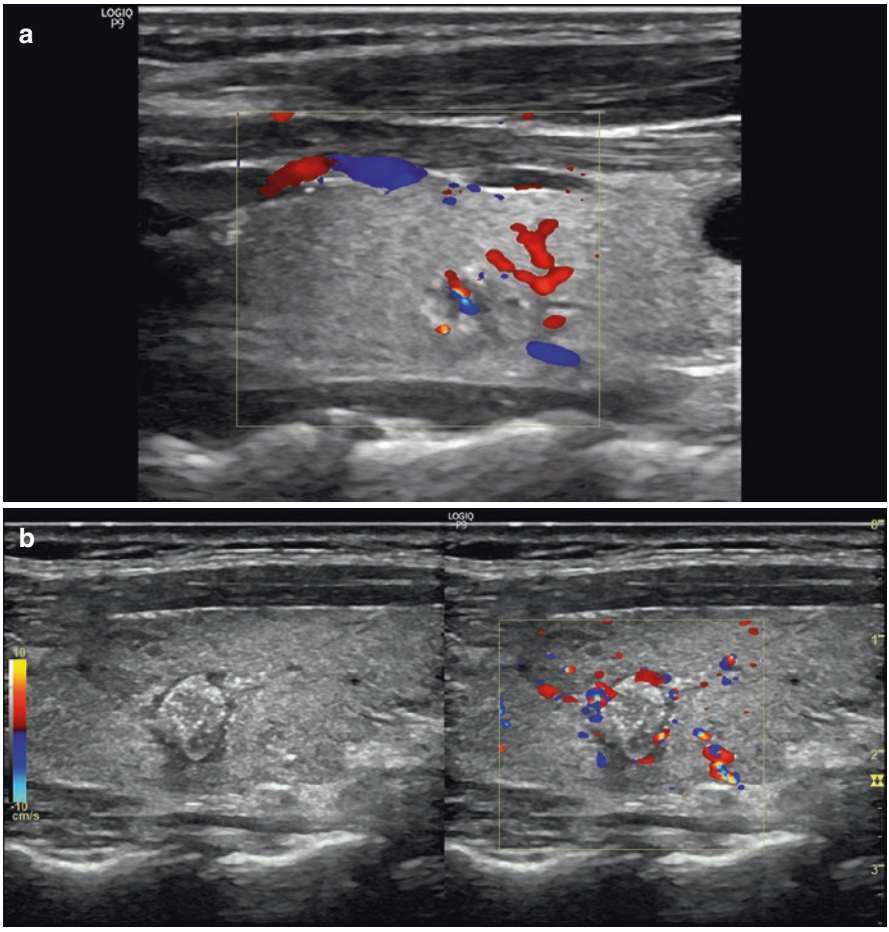

Fig. 7.6 (**a**, **b**) TIRADS 4c category. Grayscale US and CDI

The thyroid gland is of irregular shape, asymmetric with partially substernal location of the left lobe. The contours of the left lobe are irregular, locally indistinct. The capsule of the upper and middle segments of the left lobe is not detected; the echostructure of the adjacent muscles is heterogeneous with general decrease in echogenicity and indistinct contours.

The depth of the *isthmus*, 4 mm					
Right lobe			Left lobe		
Depth	19	mm	Depth	52	mm
Width	11	mm	Width	72	mm
Length	42	mm	Length	80	mm
Volume	4.2	cm^3	Volume	143.5	cm^3
The total volume 147.7 cm^3 significantly exceeds the upper limit					

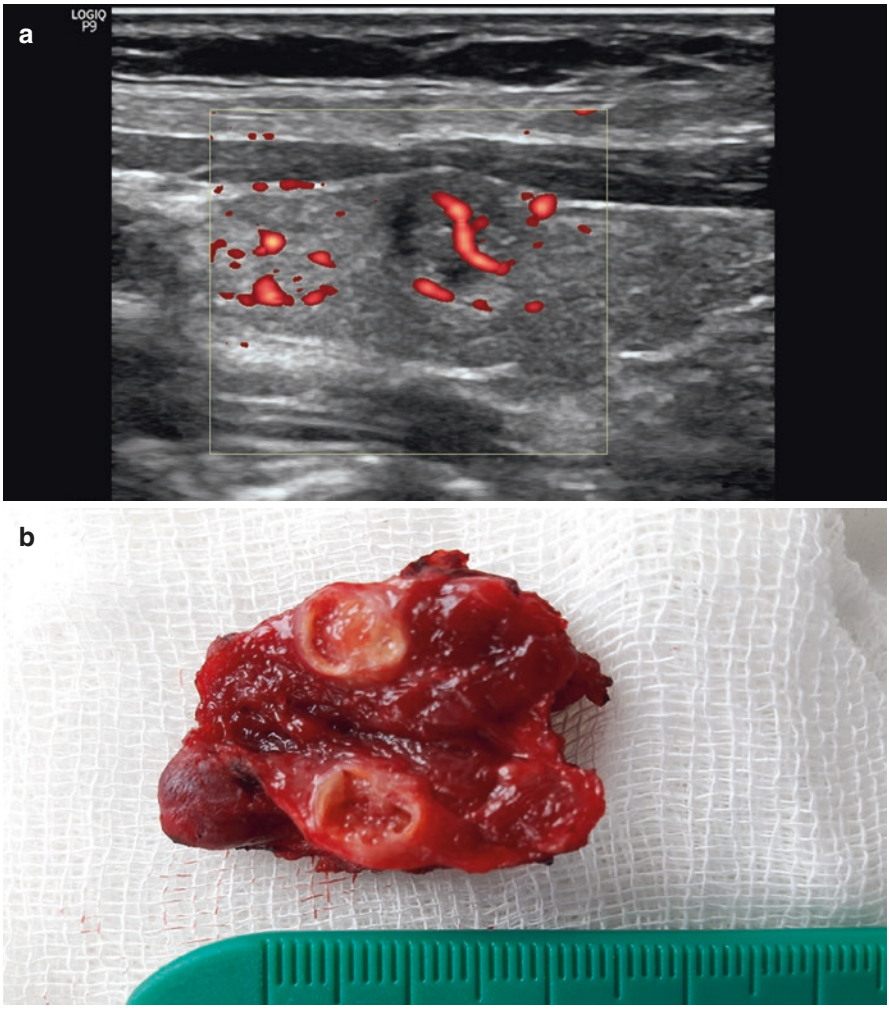

Fig. 7.7 TIRADS 6 category. FNAB-verified papillary thyroid carcinoma, BSRTC 6. (**a**) Sonogram, PDI. (**b**) Macroscopic view of the excised thyroid lobe

The depth of the *isthmus*, 4 mm	
Right lobe	Left lobe
No lesions detected	The lobe is substituted with a heterogeneous predominantly hypoechoic lesion with microcalcifications and locally indistinct uneven margins. It exhibits asymmetric disorganized vascularity and hypervascular areas with CDI and PDI, irregular hard pattern with compression USE, and the average strain ratio of 5.4 with elastometry. CEUS reveals intense fast asymmetric washin and fast washout; DT/2 index is 1.035

The trachea and esophagus are moderately pressed right. The left internal jugular vein is moderately compressed by the above described lesion, collapses with additional compression with US probe, but has spontaneous blood flow echocontrast phenomenon. The vascular bundle on the right side is normal.

Left inferior jugular and paratracheal lymph nodes are enlarged up to 1.0*2.3 cm in size, hypoechoic, heterogeneous, and with disorganized vascular pattern.

Conclusion: *A lesion of the left thyroid lobe, highly suspicious for invasive carcinoma. Left neck lymphadenopathy. TIRADS 5.*

US specialist:

References

1. Gharib H, Papini E, Garber JR, et al. American Association of Clinical Endocrinologists, American College of Endocrinology, and Associazione Medici Endocrinologi medical guidelines for clinical practice for the diagnosis and management of thyroid nodules – 2016 update. Endocr Pract. 2016;22(Suppl 1):1–60.
2. Haugen BR, Alexander EK, Bible KC, et al. American Thyroid Association management guidelines for adult patients with thyroid nodules and differentiated thyroid cancer: the American Thyroid Association guidelines task force on thyroid nodules and differentiated thyroid cancer. Thyroid. 2016;26(1):1–133.
3. Russ G, Bonnema SJ, Erdogan MF, et al. European thyroid association guidelines for ultrasound malignancy risk stratification of thyroid nodules in adults: the EU-TIRADS. Eur Thyroid J. 2017;6:225–37.
4. Shin JH, Baek JH, Chung J, et al. Ultrasonography diagnosis and imaging-based management of thyroid nodules: revised Korean Society of thyroid radiology consensus statement and recommendations. Korean J Radiol. 2016;17:370–95.
5. Tessler FN, Middleton WD, Grant EG, et al. ACR thyroid imaging, reporting and data system (TI-RADS): white paper of the ACR TI-RADS committee. J Am Coll Radiol. 2017;14:587–95.
6. Fernández-Sánchez J. TI-RADS classification of thyroid nodules based on a score modified according to ultrasound criteria for malignancy. Rev Argent Radiol. 2014;78(3):138–48.
7. American College of Radiology, BI-RADS Committee. ACR BI-RADS breast imaging and reporting data system: breast imaging atlas. 4th ed. Reston: American College of Radiology; 2003. p. 1–86.
8. Aleksandrov YK, Shulutko AM, Sencha AN, et al. Diagnostic tactics for thyroid nodules based on the TIRADS system. Mosc Surg J. 2015;3(43):24–6 (In Russian).
9. Horvath E, Silva CF, Majlis S, et al. Prospective validation of the ultrasound based TIRADS (thyroid imaging reporting and data system) classification: results in surgically resected thyroid nodules. Eur Radiol. 2017;27(6):2619–28.
10. Horvath E, Majlis S, Rossi R, et al. An ultrasonogram reporting system for thyroid nodules stratifying cancer risk for clinical management. J Clin Endocrinol Metab. 2009;94(5):1748–51.
11. Campanella P, Ianni F, Rota CA, et al. Quantification of cancer risk of each clinical and ultrasonographic suspicious feature of thyroid nodules: a systematic review and meta-analysis. Eur J Endocrinol. 2014;170:R203–11.
12. Ianni F, Campanella P, Rota CA, et al. A meta-analysis-derived proposal for a clinical, ultrasonographic, and cytological scoring system to evaluate thyroid nodules: the "CUT" score. Endocrine. 2015;52(2):313–21. https://doi.org/10.1007/s12020-015-0785-5.
13. Tugendsam C, Petz V, Buchinger W, et al. Ultrasound criteria for risk stratification of thyroid nodules in the previously iodine deficient area of Austria - a single centre, retrospective analysis. Thyroid Res. 2018;11:3.

14. Moon WJ, Baek JH, Jung SL, et al. Korean Society of Thyroid Radiology (KSThR); Korean Society of Radiology. Ultrasonography and the ultrasound-based management of thyroid nodules: consensus statement and recommendations. Korean J Radiol. 2011;12:1–14.
15. Kwak JY, Han KH, Yoon JH, et al. Thyroid imaging reporting and data system for US features of nodules: a step in establishing better stratification of cancer risk. Radiology. 2011;260:892–9.
16. Grani G, Lamartina L, Ascoli V, et al. Ultrasonography scoring systems can rule out malignancy in cytologically indeterminate thyroid nodules. Endocrine. 2017;57:256–61.
17. Sencha AN, Patrunov YN, Mogutov MS, et al. Thyroid cancer: US THI-RADS classification, ultrasound qualitative and quantitative elastography, contrast ultrasound. Collection of scientific papers "Nevsky Radiologichesky Forum-2015". St. Petersburg: ELBI-SPb; 2015. p. 605–8 (In Russian).
18. Grani G, D'Alessandri M, Carbotta G, et al. Grey-scale analysis improves the ultrasonographic evaluation of thyroid nodules. Medicine. 2015;94:1129.

Ultrasound of the Parathyroid Glands and Neck Masses

8

Yuriy K. Aleksandrov and Yury N. Patrunov

A large variety of neck masses is possible to diagnose with US. Some of them are listed below:

- Primary tumors (organ-specific tumors (the thyroid gland, salivary glands, ENT organs, parathyroids, etc.) and non-organ-specific neck tumors)
- Lymphadenopathy (reactive, metastatic, lymphoma, etc.)
- Congenital anomalies (median and lateral neck cysts, thyroid ectopia, teratoma, etc.)
- Vascular abnormalities (aneurysm, hemangioma, lymphangioma, paraganglioma, etc.)
- Inflammatory processes (thyroiditis, sialoadenitis, etc.).

Multiparameter US permits to determine the relation of the neck lesion to organs, characterize the structure and vascularity, and differentiate many typical neck abnormalities.

Soft tissues in the neck can develop more than 70 types of tumors. Most soft tissue tumors are benign and asymptomatic, grow slowly with no compression effects on nearby organs, and cause only cosmetic concern. However, some tumors (e.g., parathyroid tumors) induce severe disorders due to their specific features.

Y. K. Aleksandrov (✉)
Department of Surgery, Federal State Budget Educational Institution of Higher Education Yaroslavl State Medical University of the Ministry of Healthcare of the Russian Federation, Yaroslavl, Russia

Y. N. Patrunov
Department of Ultrasound Diagnostics, Center for Radiological Diagnostics of Non-State Healthcare Institution Yaroslavl Railway Clinic of JSC "Russian Railways", Yaroslavl, Russia

A. N. Sencha, Y. N. Patrunov (eds.), *Thyroid Ultrasound*,
https://doi.org/10.1007/978-3-030-14451-7_8

8.1 Ultrasound of the Parathyroid Glands

Parathyroid gland pathologies are the third most common of all endocrine diseases. The incidence of primary hyperparathyroidism (HPT) ranges from 1:200 to 1:2000 within the population depending on age and gender, with a ratio of men to women of 1:4. Patients who are diagnosed early with primary HPT constitute less than 10% of all those with the actual morbidity. The diagnosis of HPT bases on laboratory data, such as blood PTH, Ca++, and others. The cause of HPT is an abnormal parathyroid gland (or several glands) in most cases. Precise localization of these glands is necessary for successive treatment. Modern approaches to surgical treatment of hyperparathyroidism, which aim to remove or destroy abnormal parathyroid glands, are impossible without multiple confirmation of tumor location. Imaging techniques that are used for their detection are based on functional (radionuclide scan with 99mTc-sestamibi and SPECT) and anatomical (US, CT, MRI, etc.) principles. As a rule, a combination of two localizing modalities is utilized.

US is successfully applied for imaging abnormal parathyroid glands in orthotopic location [1]. US of the neck and mediastinum is now included in all protocols of examination of patients with hypercalcemia and hyperparathyroidism. In addition, US is often used as an alternative rather than an auxiliary method when other methods (such as scintigraphy with ^{99m}Tc-sestamibi, CT, and MRI) are ineffective or limited.

Absolute indications for US in patients with high blood PTH and hypercalcemia at the stage of topical diagnosis are as follows:

- Primary HPT due to parathyroid tumor not accumulating ^{99m}Tc-sestamibi
- Concomitant thyroid and parathyroid pathology
- Concomitant pathology of parathyroid glands and lymph nodes
- Recurrent primary HPT
- Several foci of increased uptake of the sestamibi agent in patients with primary HPT
- Differential diagnosis of secondary HPT and tertiary HPT
- Multiple parathyroid lesions
- Prior to fine needle aspiration with cytology and PTH analysis in the needle washout
- Before minimally invasive US-guided treatment of parathyroid diseases
- Impossibility to perform scintigraphy with ^{99m}Tc-sestamibi
- Refusal of a patient to undergo scintigraphy with ^{99m}Tc-sestamibi (radiophobia)
- MEN 1 (Wermer's syndrome) and MEN II (Sipple's syndrome)
- Family PHPT.

Conventional neck US with some auxiliary procedures which improve parathyroid gland imaging is utilized to diagnose parathyroid pathology. The technique of parathyroid US is similar to that of thyroid US. It is performed without special preparation of the patient, with the patient in a supine position with the neck hyperextended. Linear probes with a frequency of 7.5 MHz and higher are used for the

examination. A bolster may be put under the patient's shoulders to facilitate the acoustic access to the inferior neck and mediastinum. Parathyroid glands in the majority of cases are located on the parietal leaf of the third fascia, which helps to apply different techniques to differentiate neck masses by their shift in relation to surrounding tissues. To facilitate the examination of the right half of the neck, the patient may be asked to turn their head to the left and vice versa. Swallowing and deep breathing can supply some additional information. Mobility of the parathyroid glands in these cases helps to differentiate them from neck muscles and lymph nodes. Compression of the neck with a probe enables better assessment of the structure of deeply located paratracheal and paraesophageal masses and facilitates differentiation of intrathyroid and extrathyroid lesions by the peculiarities of their displacement. Abnormal parathyroid glands in some cases can be squeezed out from blind zones (retrotracheal area, etc.) by means of the compression test. The soft consistency of normal and pathologic (in hyperplasia and adenomas) parathyroid glands should be taken into account. The parathyroid gland can change its shape under pressure with the probe and when the patient turns his or her head. Compression may be applied to neck areas with the hand at a certain distance from the probe. Corresponding displacement of neck structures may be of benefit for differential diagnosis.

The probe is positioned on the anterior surface of the neck and moved consistently from the submandibular area to the suprasternal fossa and supraclavicular area. Special attention should be paid to the dorsal aspects of thyroid lobes and the fat close to the inferior poles of thyroid lobes between ITA branches (orthotopic sites of the parathyroids). A prior radionuclide scan facilitates the search.

US report should contain the following data:

- Number of lesions
- Location in relation to the thyroid, neck vascular bundles, trachea, esophagus, larynx, or hyoid
- Dimensions (in three mutually perpendicular planes) and volume
- Shape (spherical, oval, or irregular)
- Borders (smooth or irregular)
- Contours (accurate or indistinct)
- Echodensity
- Echostructure
- Calcifications (dimensions, location, and posterior acoustic shadowing)
- Fluid component (dimensions and fluid/solid ratio)
- Posterior echo pattern (enhancement or shadowing)
- Vascularity.

The majority of studies devoted to hyperparathyroidism underline the fact that US is effective only if the parathyroid glands are located within the neck. Some other researchers consider that US is suitable for diagnosis of the tumors and cysts in the mediastinum.

Eighty-four percent of people have four parathyroids (two on each side). Five to six glands are observed in 3–13% of cases, 2–3 glands in 1–7%, and in rare cases up to 12 parathyroids may be observed [2]. The length of each gland is 2–7 mm, its width is 2–4 mm, its thickness is 0.5–2 mm, and its weight is 35–55 mg.

Twin superior and inferior parathyroids are located on the back surfaces of the thyroid lobes. Superior parathyroids are normally detected in the middle of the posterior margin of the thyroid lobes and are projected at the level of the cricoid plate. About 80% of all superior parathyroids can be found within a circle 2 cm in diameter that is shifted 1 cm cranially from this site [3]. Inferior parathyroids are usually located near the inferior poles of the thyroid lobes close to the ITA (as a rule, dorsally from it). However, their location is more variable than that of the superior parathyroids. They may be detected deep in the thyroid parenchyma, between two capsules, outside the surgical capsule of the thyroid gland, close to the CCA bifurcation, or in the upper mediastinum. Ectopic parathyroid glands occur in 15–20% of patients. They may also be found in a number of unusual locations.

The possibility of and the reliability of the visualization of normal parathyroid glands are somewhat dubious. Normal adult parathyroids contain a large amount of adipocytes. Thus, unlike thyroid parenchyma, they are practically invisible against the surrounding fatty tissue. According to most authors, they are normally not detected by anatomical visualizing modalities (US, CT, or MRI). However, modern US equipment permits imaging of normal parathyroid glands in more than one half of patients. But their detection with US takes a great deal of time and effort, and requires a certain level of experience of the US specialist. The inferior normal parathyroid gland may be detected more often. There are no indications to seek for normal parathyroid glands. The need for their description is mentioned in none of the published world protocols for neck US.

A normal parathyroid can be identified as a structure with the following attributes (Fig. 8.1):

- Structure, more often adjacent to the inferior segment/pole of thyroid lobe or to the dorsal surface of the middle segment of the thyroid lobe, sometimes partially or completely within the thyroid
- Size of 0.2–0.7 cm
- Roundish or oval shape
- Isoechoic or slightly increased echodensity
- Homogeneous structure
- Well-defined, regular margins
- Avascular in CDI, PDI, and 3DPD
- No special pattern with compression elastography, soft with elastometry.

Normal parathyroid glands are more often revealed in the sites of their typical location. Superior parathyroid glands are usually seen at the level of the middle segments of the thyroid lobes in the paratracheal position, close to or pressed into thyroid tissue from the medial or posterior side in the area of the terminal branches of inferior thyroid artery. The inferior parathyroid glands are usually detected behind

the inferior poles of the thyroid lobes or lower along the blood vessels. In the latter case, they are often located 1–2 cm below the inferior poles of the thyroid lobes, between the leaves of the fascia. The site of the superior parathyroid glands is less variable, but the inferior parathyroid glands can be detected more often. One or two inferior parathyroid glands can be revealed with US in 60–70% of patients. It is extremely difficult to reveal blood vessels within normal parathyroid glands. Imaging of normal parathyroid glands may be complicated due to concomitant pathology of the thyroid gland or lymph nodes of the neck. Thyroid nodules, heterogeneity of thyroid tissue in patients with autoimmune thyroid disease, enlargement

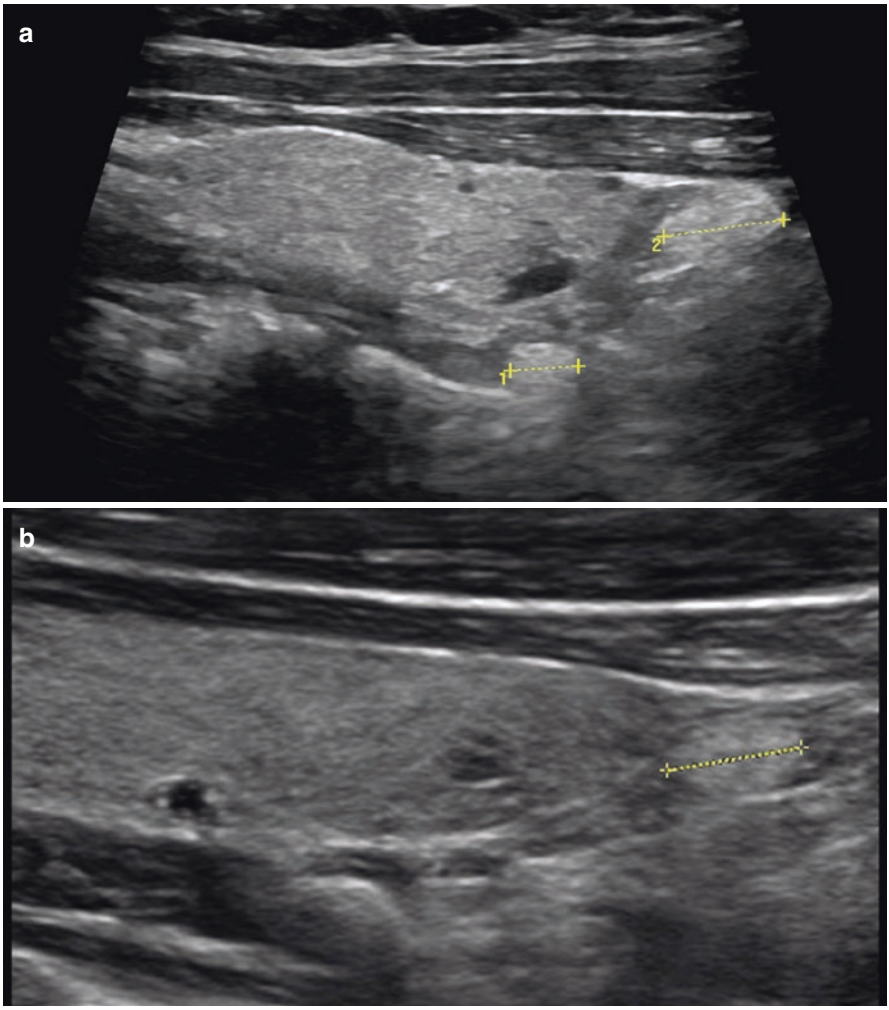

Fig. 8.1 Normal parathyroid gland. (**a**) Superior and inferior parathyroid glands with normal appearance. Grayscale US. (**b**) Normal inferior parathyroid gland. Grayscale US. (**c**) CDI. (**d**) PDI. (**e**) Compression ultrasound elastography. (**f**) Elasticity quantification with ARFI

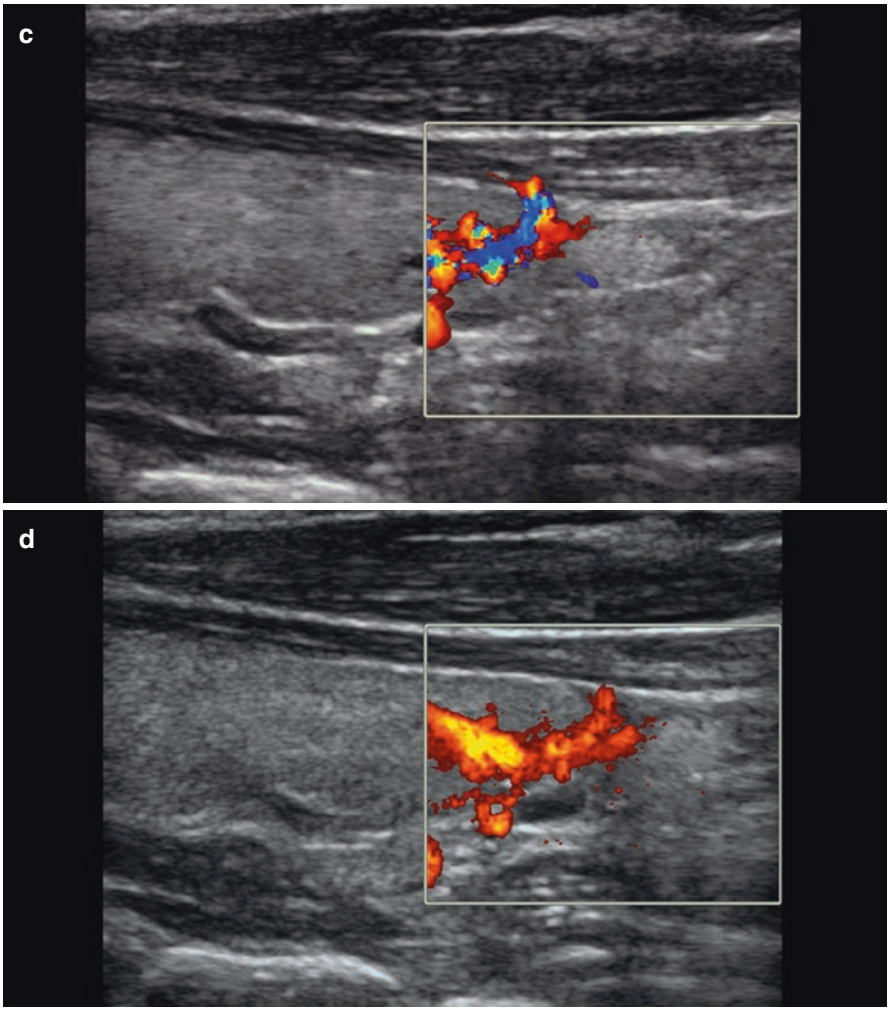

Fig. 8.1 (continued)

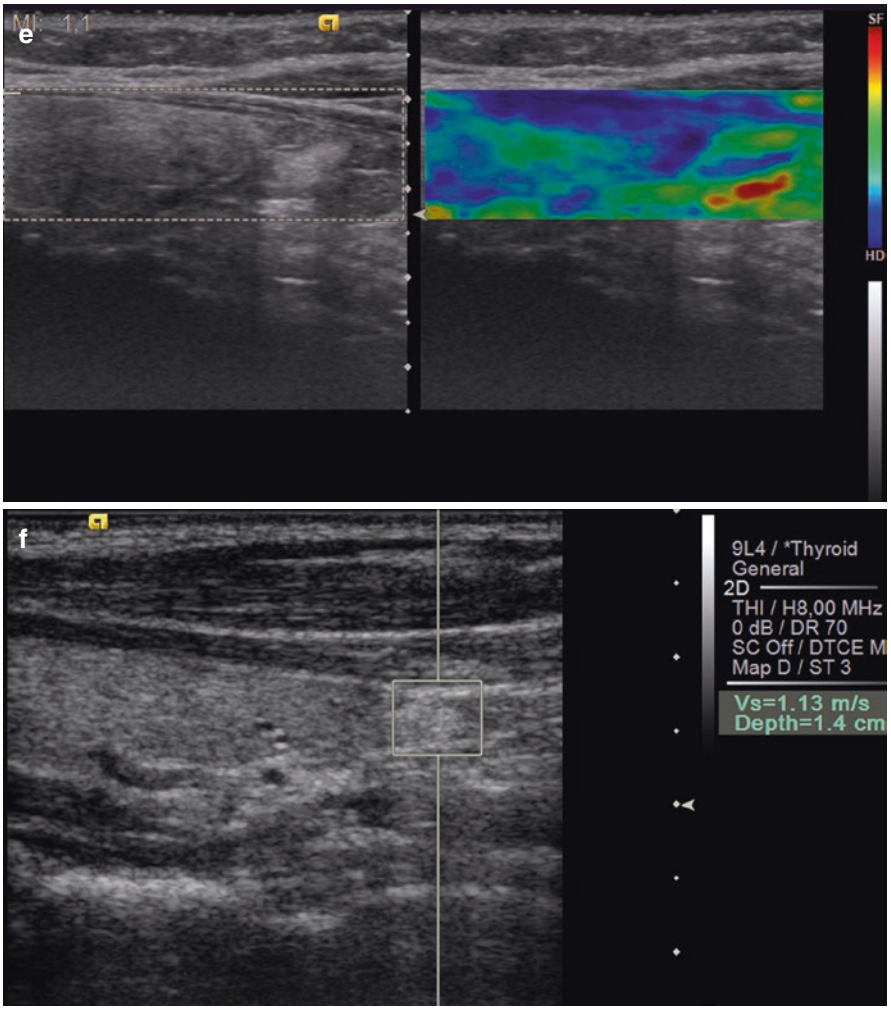

Fig. 8.1 (continued)

in the thyroid size, and other disorders deteriorate parathyroid gland imaging and often make it impossible.

An abnormally enlarged parathyroid is often much more accessible to US visualization. According to Nazarenko et al. [4], parathyroid lesions are found incidentally during thyroid US in 37% of cases, while focused search increases the chance to reveal a parathyroid lesion in up to 63%. Abnormal parathyroid glands are mainly observed in adults.

Successful imaging of a parathyroid adenoma and hyperplasia is a consequence of the peculiarities of their histological structure with a large number of chief and oxyphil cells. The ratio of adipose cells to chief and oxyphil cells decreases. Additionally, functional hyperactivity results in enlargement of the chief and oxyphil cells. It makes the parathyroid gland more permeable to US and visible (at the expense of low echodensity) against the background of the surrounding fat. As the changes are similar in adenomas and hyperplasia, the appearance of the parathyroid gland with US is practically identical in both types of pathology.

Ultrasound has been proven to detect the following parathyroid abnormalities:

- Adenoma
- Hyperplasia
- Cyst
- Cancer.

PTH hyperproduction is often a consequence of one (83%) or several (5%) parathyroid adenomas, or of parathyroid hyperplasia (11–20%), or malignant hormone-releasing parathyroid tumor (1%) [4]. The sensitivity of US for the diagnosis of parathyroid abnormalities is 63–78%. Its sensitivity to parathyroid hyperplasia is lower than it is for adenomas: 24–50% [5]. It is even lower in cases with prior neck surgery.

Adenoma of the superior parathyroid is usually detected with a longitudinal scan along the back margin of the middle segment of the thyroid lobe in the projection of the recurrent nerve and ITA branch. Adenoma of the inferior parathyroid is most often located below the inferior pole of the thyroid lobe or in the initial part of the thyrothymic ligament. Parathyroid adenoma is observed with a transverse scan dorsally from thyroid lobes, in paratracheal or paravasal (medially and dorsally from the CCA) sites.

Parathyroid adenomas commonly exhibit the following features (Figs. 8.2 and 8.3):

- Extended, triangular, dumbbell-like, or oval shape. Parathyroid adenomas of a small size (up to 10 mm) are oval or oblong in shape. During the process of enlargement, the tumor becomes more elongated and extended
- Decreased echogenicity in comparison with thyroid tissue
- Relatively homogeneous echostructure. In some cases the echostructure can be moderately or significantly heterogeneous due to small areas of increased echodensity, echogenic inclusions, or anechoic fluid collections. Fluid component

does not influence the expression of HPT. It does not reflect the "age" of the adenoma either, and does not allow its development to be predicted.
- CDI and PDI often reveal a feeding vessel with branching within the lesion and circumflexing vessels.
- Soft structure with compression US elastography and elastometry.

The shape of a lesion serves as a criterion for differential diagnosis between thyroid and parathyroid tumors. Thyroid lesions are characterized by a roundish shape in all scans. Parathyroid adenomas in the majority of cases exhibit stretched, flattened shapes. This especially refers to superior parathyroid glands typically

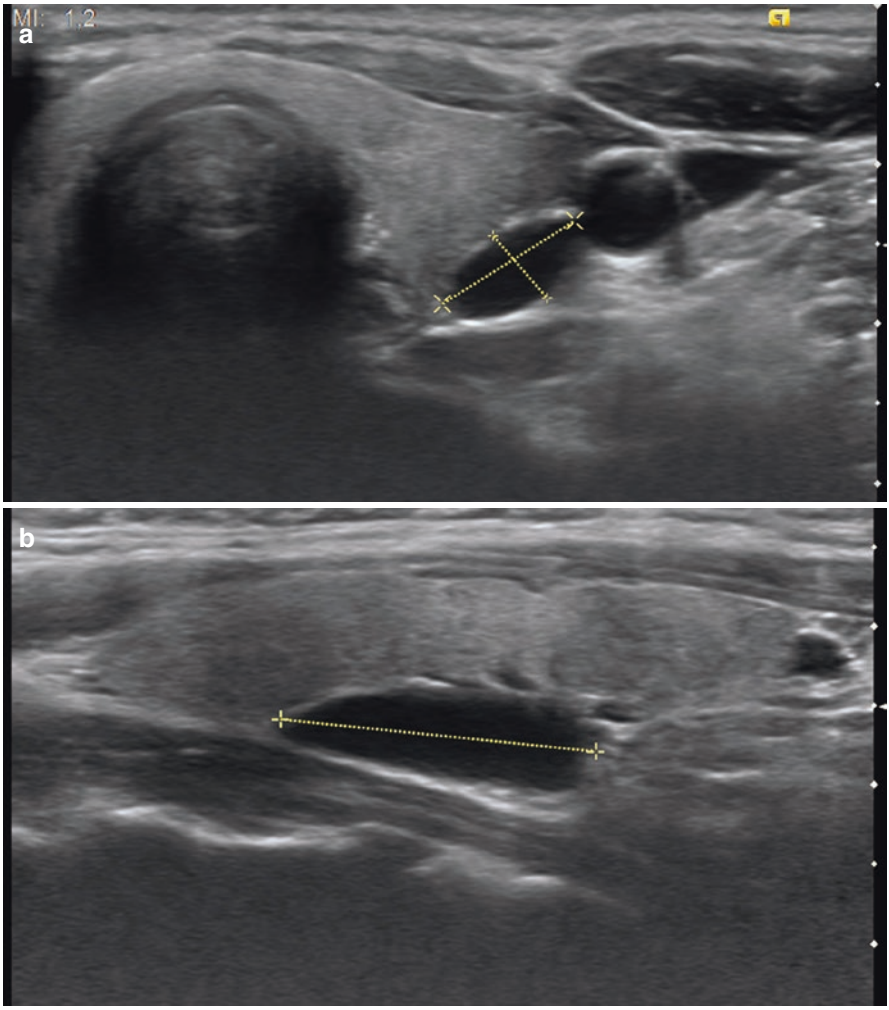

Fig. 8.2 Adenoma of the left superior parathyroid gland. (**a**) Grayscale US. Transverse scan. (**b**) Grayscale US. Longitudinal scan. (**c**) CDI. (**d**) Compression ultrasound elastography

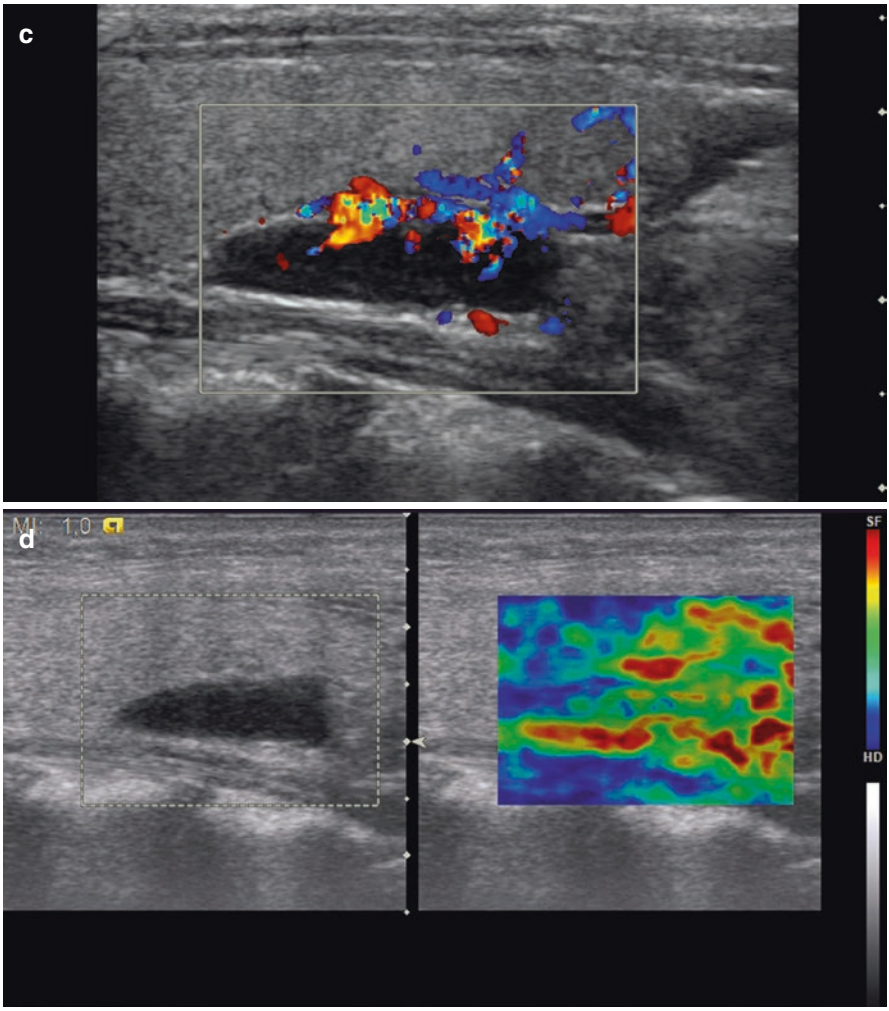

Fig. 8.2 (continued)

located near the posterior thyroid surface. Adenomas of the inferior parathyroid gland are often observed as elliptical or spherical lesions taken by mistake for thyroid lesions.

The pulsing afferent artery of the parathyroid gland is identified with CDI and PDI in 83% of patients (Fig. 8.4a). Lane et al. [6] consider the afferent arteries the "road maps," which lead to parathyroid adenomas regardless of their size and location. Therefore, the search for afferent arteries is a mandatory element of US examination in patients with PHPT.

CDI and PDI in the majority of cases of parathyroid adenomas reveal a "branching" sign: the afferent artery branches into smaller vessels on entering the gland.

This sign permits differentiation of parathyroid adenomas from thyroid lesions. Another sign, which is specific for parathyroid adenomas [7], is a "vascular arch." It can be observed as a vessel that partly embraces the adenoma around its circumference (Fig. 8.4b). This arch is detected in 63% of patients with parathyroid adenomas. The intensity of vascularization in parathyroid adenoma is often higher than in neck lymph nodes.

Contrast enhanced ultrasound permits detailed assessment of blood flow of parathyroid adenoma and demonstrates its high vascularity (Fig. 8.5a). It permits

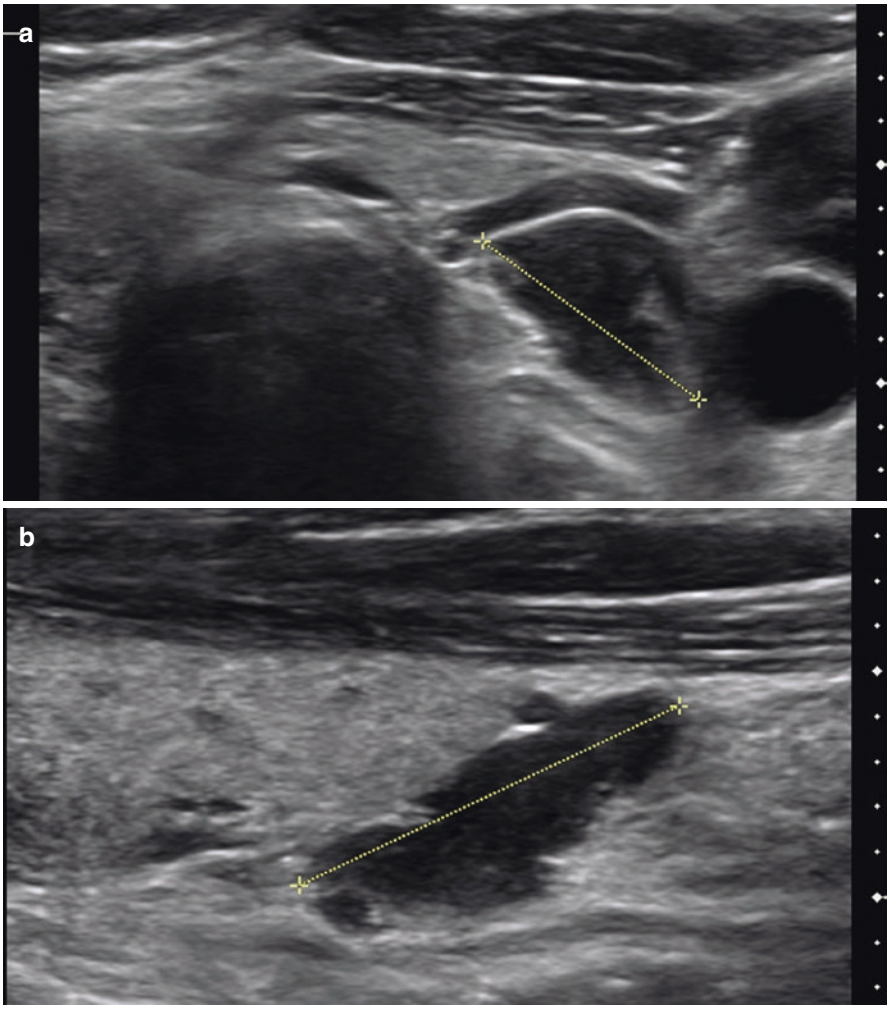

Fig. 8.3 Adenoma of the left inferior parathyroid gland. (**a**) Grayscale US. Transverse scan. (**b**) Grayscale US. Longitudinal scan. (**c**) CDI. (**d**) PDI. (**e**) Compression ultrasound elastography. (**f**) Elasticity quantification with ARFI

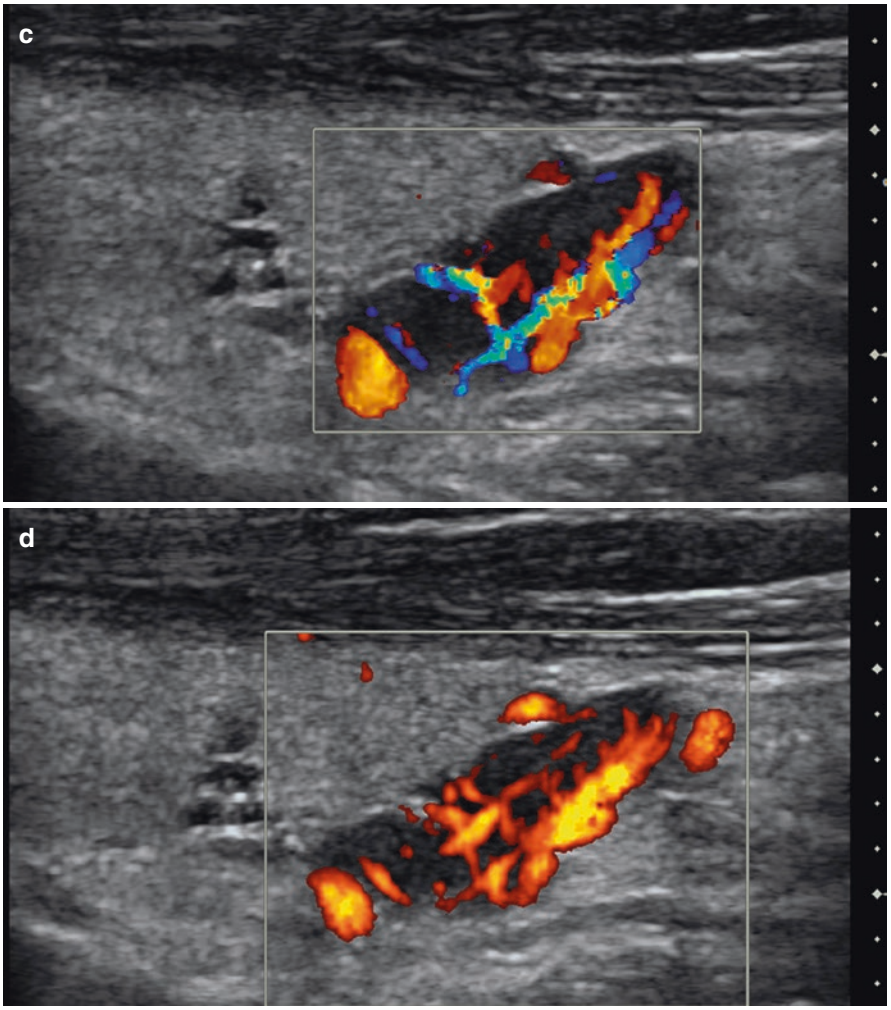

Fig. 8.3 (continued)

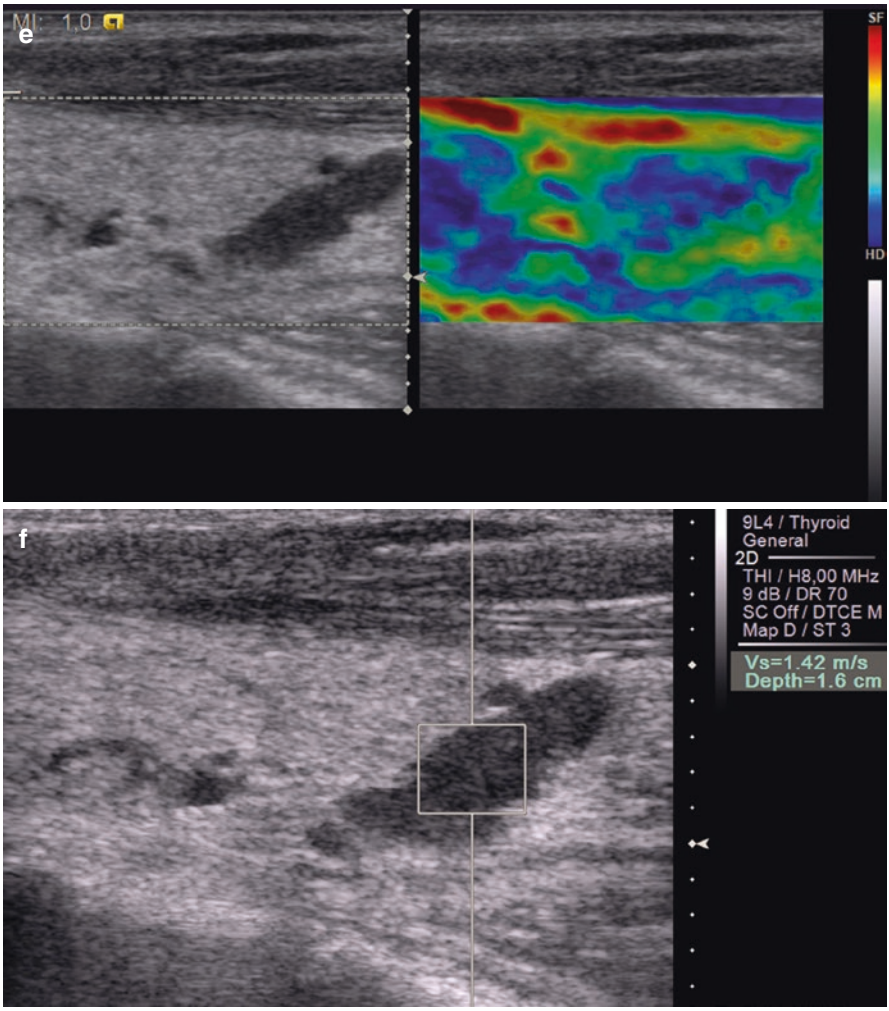

Fig. 8.3 (continued)

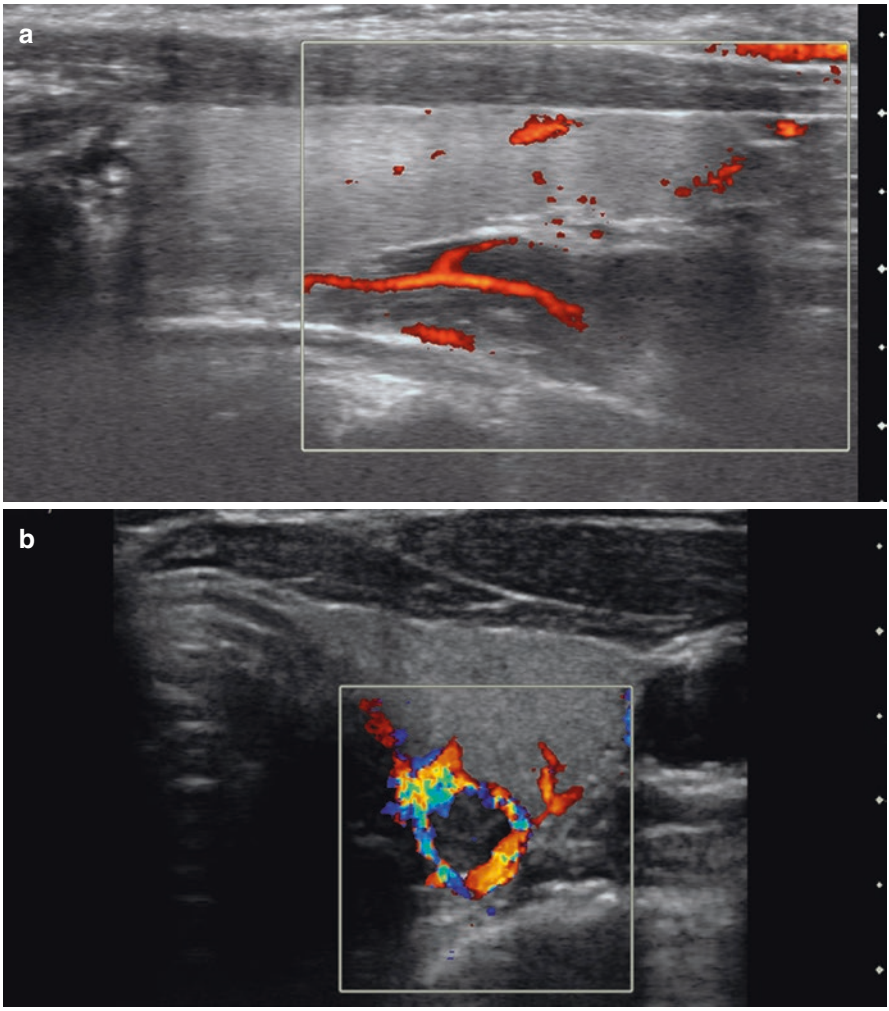

Fig. 8.4 (**a**) Afferent vessel in parathyroid adenoma. PDI. (**b**) "Vascular arch" sign. CDI

reliable differentiation of vascularized lesions, such as adenoma, from cysts (Fig. 8.5b). In our study, it was effective to demonstrate avascularity of parathyroid adenoma after successive percutaneous laser ablation. No data on the value of CEUS for the differential diagnosis of solid parathyroid lesions is available yet.

Assessment of elasticity is an auxiliary tool. Parathyroid adenomas are commonly soft with compression US elastography or cannot be differentiated from the surrounding tissues based on strain pattern (Fig. 8.2d and 8.3e). Elastometry with ARFI or SWE proves soft character of parathyroid adenoma (Fig. 8.3f). This fact helps to sort out hard lesions that are not likely to be adenomas.

Ultrasound detection of a neck lesion with sonographic signs of a parathyroid adenoma should be followed by thorough search for other parathyroid glands. This

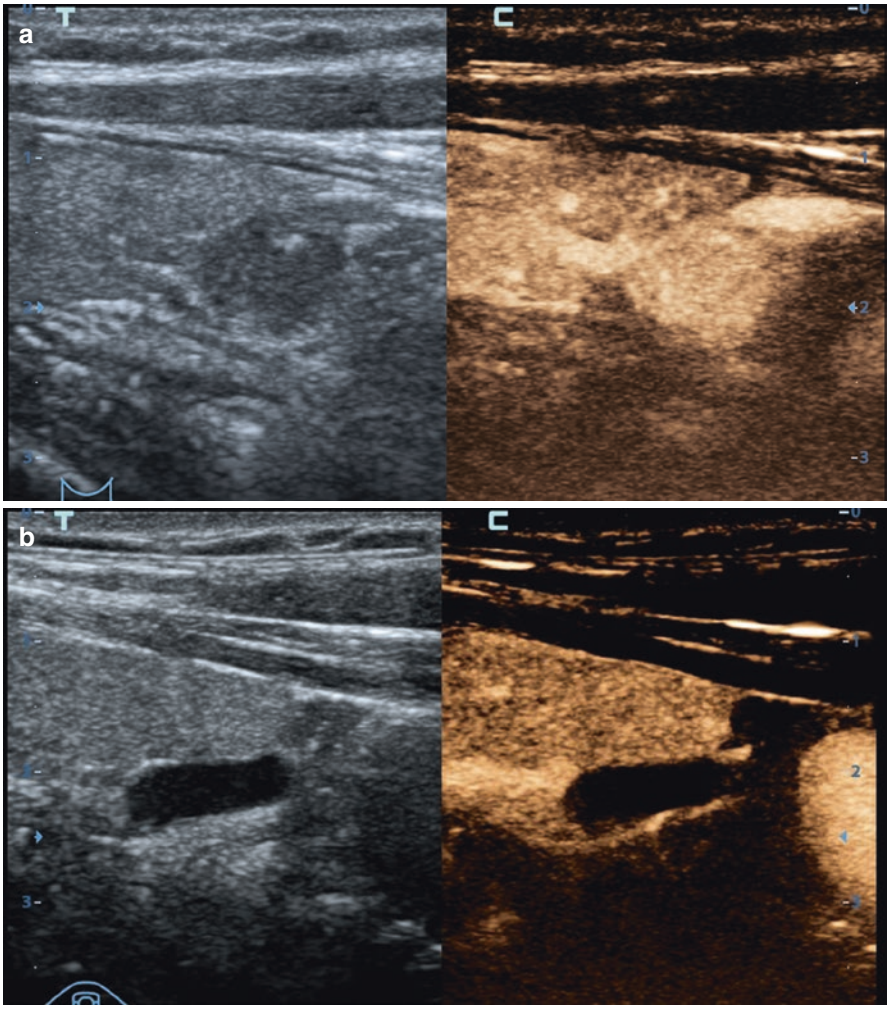

Fig. 8.5 Parathyroid lesion. CEUS with SonoVue® 4.0 ml. (**a**) Parathyroid adenoma exhibits homogeneous enhancement in arterial phase. (**b**) Parathyroid cyst demonstrates no contrast enhancement

necessity is associated with possible "double" parathyroid adenomas that are not always registered with sestamibi scan.

An atypical location of a parathyroid adenoma, such as intrathyroid, intrathymic, paravasal, or along the anterior thyroid surface, remains a diagnostic problem. US fails to differentiate adenomas in the majority of such cases. Lymph nodes, lipomas, or other neck masses are usually misinterpreted as adenomas in HPT patients. In some cases, when there is no information about serum PTH and Ca^{2+}, atypically located parathyroid adenomas are mistaken for thyroid lesions. One should be aware of possible hyperparathyroidism, especially in patients in a high-risk group.

Intrathyroid location of a parathyroid adenoma causes special diagnostic difficulties because the capsule of the gland is very thin and hard to distinguish. Nevertheless, US is considered to be advantageous as compared with other imaging modalities in cases of intrathyroid and antethyroid locations of the parathyroid gland.

Large parathyroid adenomas can be mistaken for thyroid masses. Such adenomas displace other organs (first of all the thyroid gland) and occupy their "official" places. This significantly hampers differential diagnosis regardless of positive sestamibi scan. Abnormalities of the surrounding organs and tissues also result in difficulties in topical diagnosis of parathyroid adenomas. False-positive results (6–15%) are often caused by thyroid nodules and to a lesser degree, by abnormal lymph nodes or esophageal pathology. Multinodular goiter that is characterized by several thyroid nodules of different echodensity can mask a parathyroid adenoma. Normal serum Ca^{2+} (normocalcemic HPT) and absence of clinical symptoms of HPT (asymptomatic HPT) can sometimes lead to a parathyroid adenoma being left undetected. Special difficulties arise if the patient has a history of neck surgery and recurrent goiter. Pitfalls may arise with concomitant pathology of the parathyroid gland and lymph nodes, especially of metastatic character. Malignant lymph nodes demonstrate special US signs: enlargement, spherical shape, rough margins, decreased echodensity, heterogeneous echostructure, barely differentiated hilum, and disorganized vascular pattern. CDI and PDI facilitate detection of subcapsular and aberrant vessels, which are highly suspicious for malignancy. Alternatively, reactive lymph nodes are elongated with hilar vascular pattern. The above-mentioned "vascular arch" may be the sign that helps to differentiate a parathyroid adenoma from lymph nodes, the latter being devoid of it.

In doubtful cases, US-guided FNA with a test for PTH in the needle washout is of benefit. The needle is washed with 1 ml of saline, the way this is usually done to assess thyroglobulin in FNA samples from lymph nodes suspicious for metastases of thyroid carcinoma. A PTH test of the needle washout serves as a qualitative rather than a quantitative test, but a level higher than 1000 pg/ml is typical for a parathyroid adenoma. The level of thyroglobulin (a marker of thyroid tissue) in the needle washout is also assessed to achieve more reliable results. This test demonstrates higher sensitivity and diagnostic value than FNA cytology. Cytologic material obtained from parathyroid lesions with FNAB is frequently misinterpreted as a follicular neoplasia of the thyroid gland [8]. The sensitivity and specificity of US with FNA are equal to those of scintigraphy with ^{99m}Tc-sestamibi. Certain difficulties are associated with localizing parathyroid adenomas in patients with concomitant AITD. Heterogeneity of thyroid tissue with pseudonodules and a high incidence of local lymph nodes make the detection of parathyroid adenomas difficult.

Indirect data about parathyroid adenomas can be obtained from serum Ca^{2+} and PTH. This is based on a correlation between the size and volume of parathyroid adenoma, on the one hand, and indices of homeostasis and hormonal status, on the other. Some researchers think that levels of Ca^{2+} and PTH permit prediction of the weight and volume of a parathyroid adenoma [9].

Parathyroid hyperplasia is commonly characterized by the enlargement of two or more glands. Hyperplasia of a single parathyroid gland is rare. Multiple hyperplasias are observed in 15–20% of patients. Parathyroid hyperplasia often develops in

patients with chronic renal failure on chronic hemodialysis, as a consequence of hyperphosphatemia and hypocalcemia, leading to the secondary HPT.

Both parathyroid hyperplasia and parathyroid adenoma are associated with an increased weight of parathyrocytes and a significant decrease in adipocytes. It facilitates US identification of abnormal parathyroid glands. However, similar morphologic changes in the parathyroid glands of patients with hyperplasia and adenoma practically exclude the possibility of US differentiation between these conditions (Fig. 8.6). One can suspect parathyroid hyperplasia in cases of several detected

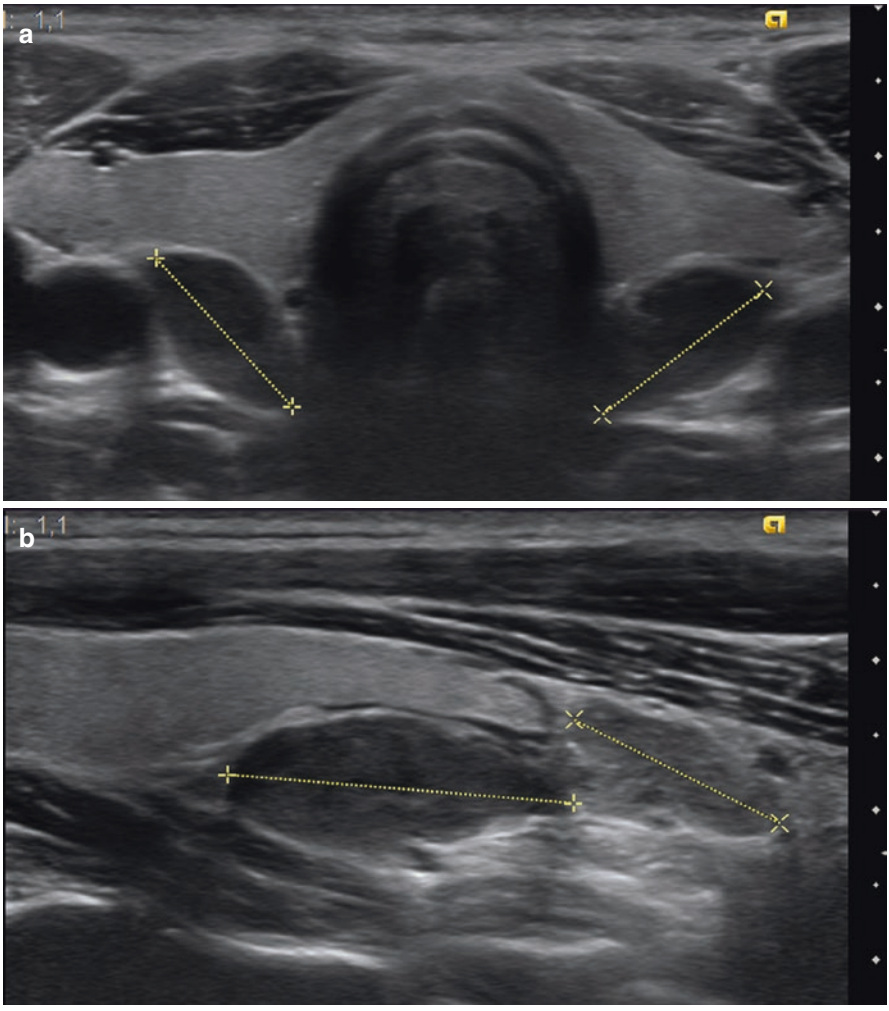

Fig. 8.6 Hyperplasia of four parathyroid glands in a patient with secondary HPT. (**a**) Grayscale US. Transverse scan. (**b**) Grayscale US. Longitudinal scan along the right thyroid lobe. (**c**) Grayscale US. Longitudinal scan along the left thyroid lobe. (**d**) Compression ultrasound elastography. Longitudinal scan along the right thyroid lobe

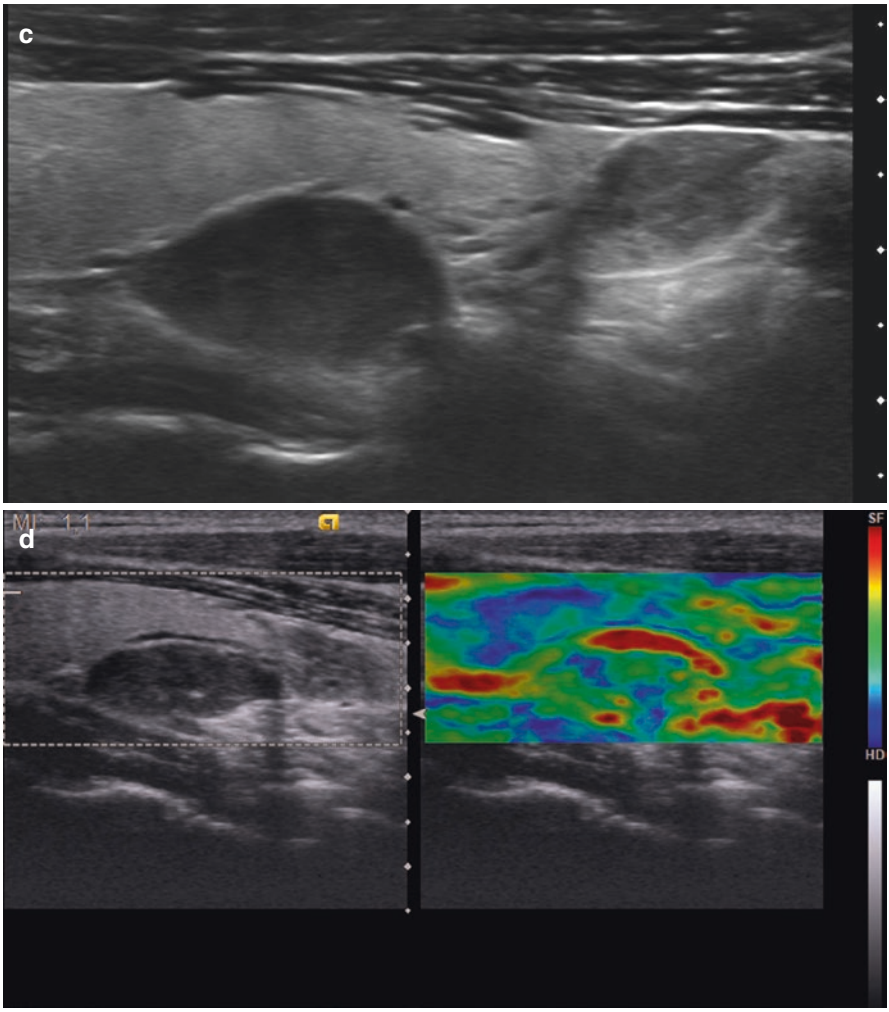

Fig. 8.6 (continued)

abnormal parathyroid glands. Calcifications, inclusive of spherical "egg shell" type, are more common for parathyroid hyperplasia in secondary HPT (Fig. 8.7a). The larger grow the glands, the more weird shaped they become (Fig. 8.7b). The differential diagnosis of parathyroid hyperplasia and adenoma is difficult, and not only for ultrasound specialists. Most often, they cannot be distinguished visually during surgery either. The final conclusion is drawn based only on morphological examination. The differential diagnosis of diffuse and nodular types of parathyroid hyperplasia in secondary HPT is a challenge for an ultrasound specialist. In most cases, the areas of early nodular hyperplasia in parathyroid tissue are small and are difficult to spot with US. Parathyroid echostructure in such cases becomes two-layered,

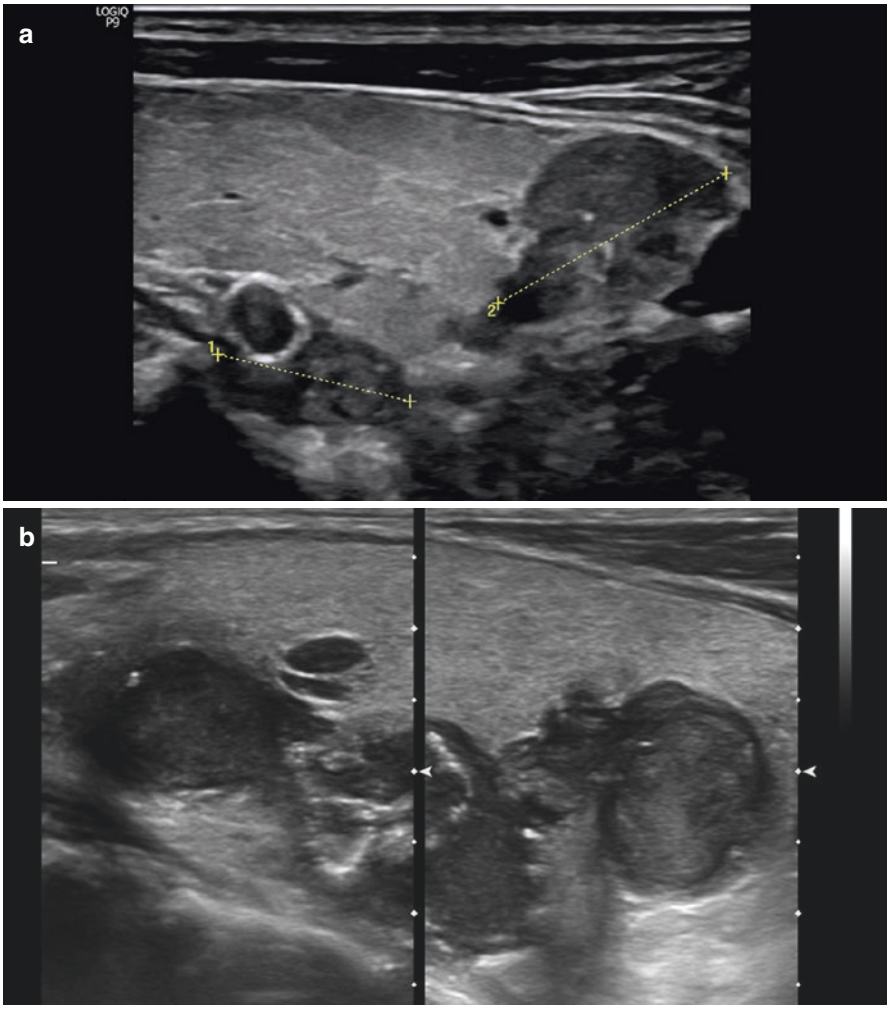

Fig. 8.7 Hyperplasia of four parathyroid glands in a patient with secondary HPT. (**a**) Grayscale US. Longitudinal scan along the right thyroid lobe. Egg-shell calcification within the hyperplased superior parathyroid. Inferior parathyroid devoid of calcifications. (**b**) Grayscale US. Longitudinal scan along the right thyroid lobe. Significantly enlarged parathyroid glands of weird shape with calcifications in a patient with terminal stage of chronic renal failure and programmed hemodialysis for more than 6 years

with a roundish hypoechoic center of hyperplasia and isoechoic periphery with preserved adipose tissue (Fig. 8.8) that may result in erroneous interpretation of these lesions as lymph nodes.

Diffuse or nodular hyperplasia of the parathyroid glands in patients with chronic renal failure may affect a different number of parathyroid glands—up to all of them. Hyperplastic parathyroid glands may be quite large (a length of

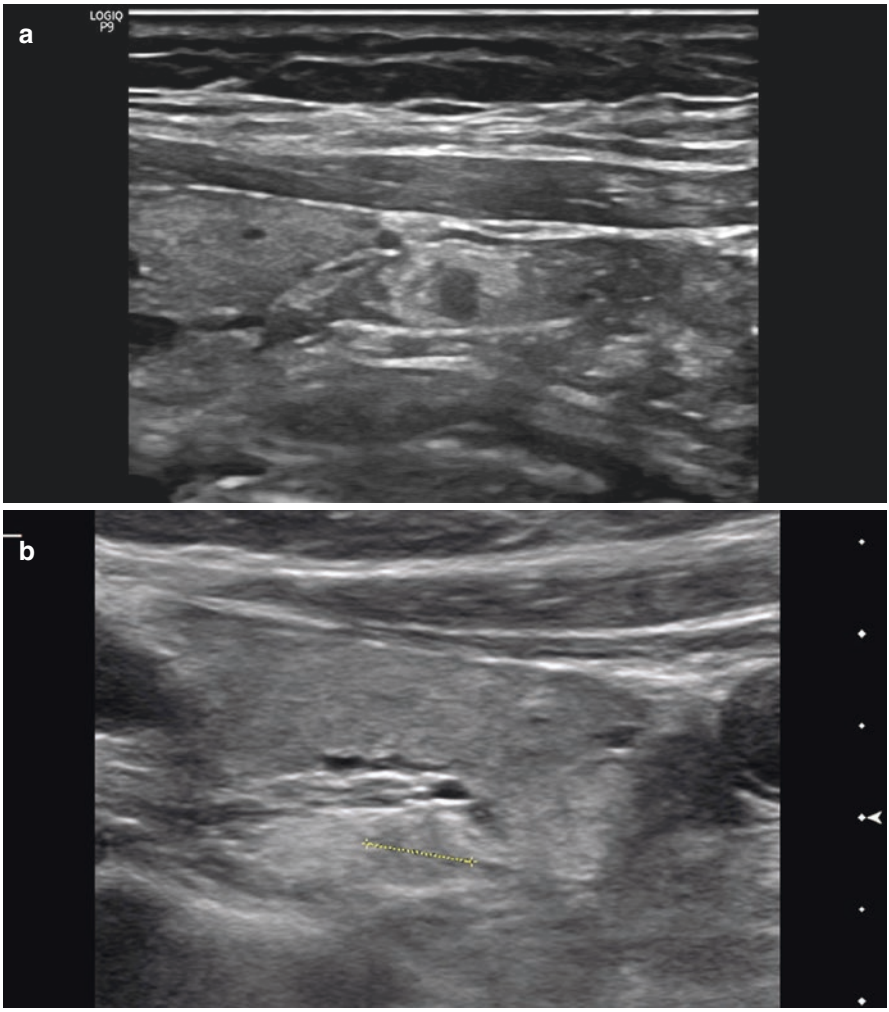

Fig. 8.8 (**a**, **b**) Early nodular hyperplasia of a parathyroid gland in a patient with secondary HPT

10–50 mm and weight of 500–6000 mg). US of patients with secondary HPT aims not only to detect abnormal parathyroid glands but also to define the volume of all affected parathyroid glands that is necessary for choosing the correct treatment.

Parathyroid cysts are observed quite rarely. In the majority of cases, they are called incidentalomas, as they are nonfunctional and revealed by chance during neck US. Functional parathyroid cysts, which lead to primary HPT, are extremely rare [10]. Nonfunctioning cysts are always located in the inferior parathyroid glands. The location of a functioning cyst is less predictable, they can be detected in the range from the angle of the mandible to the mediastinum [11].

Parathyroid cysts demonstrate the following US features (Fig. 8.9):

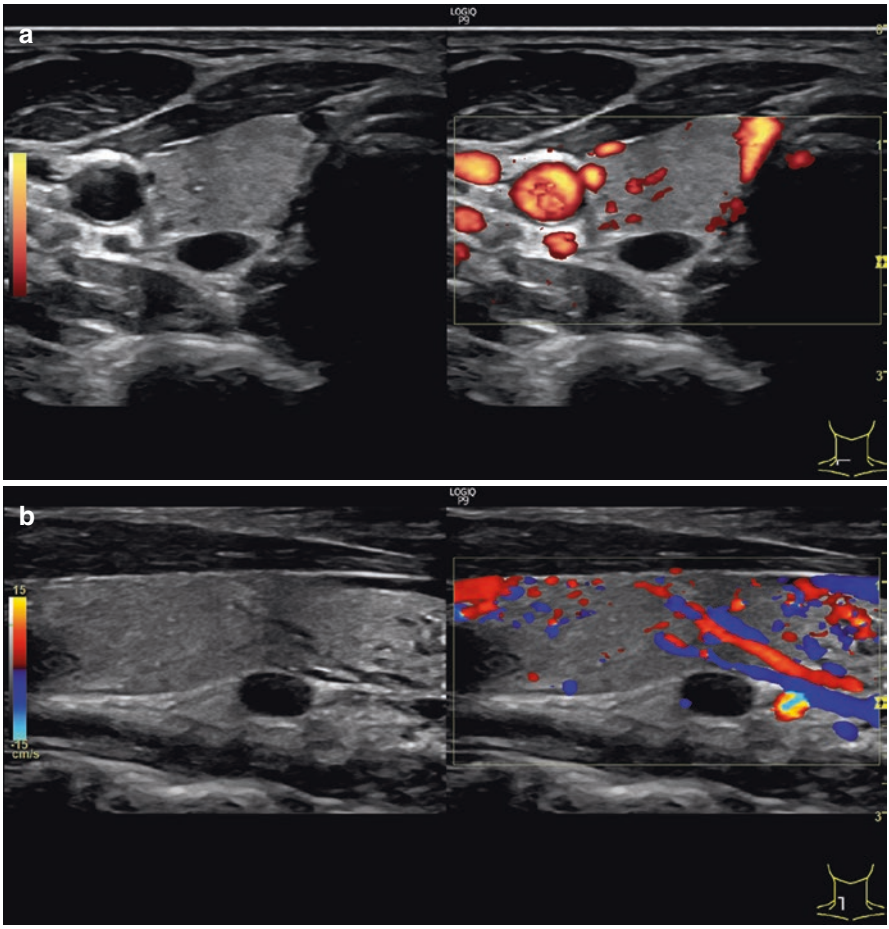

Fig. 8.9 Parathyroid cyst. Sonograms. (**a**) Transverse cans. Grayscale US and PDI. (**b**) Longitudinal scan. Grayscale US and CDI

- Anechoic lesion located at the sites of parathyroid glands
- Roundish or oval shape
- Regular accurate margins
- Capsule is thin, echogenic, or sometimes not visualized by conventional sonography
- Avascular with CDI and PDI. Peripheral blood around the cyst or the afferent artery may be identified
- No special pattern with compression US elastography or three-layer fluid pattern.

Parathyroid cysts should be differentiated from fluid nodules and true cysts of the thyroid gland, median and lateral neck cysts, and metastases of well-differentiated thyroid cancer into neck lymph nodes. Parathyroid cysts do not demonstrate any specific US features. Therefore, US-guided FNAB should be utilized to assess the PTH

level and the parathyrocytes in the aspirate [12]. Typical content of a parathyroid cyst is water-like colorless and transparent, whereas that of both thyroid cysts and cystic thyroid adenomas is dark-brown, black, yellow, or amber colored. The content of the lateral and median neck cysts is dense (thick), turbid, and white or yellow colored.

Parathyroid cancer is a rare disease accounting for only 1–2% of all primary HPT cases. In the opinion of Kinoshita et al. [13], malignant tumors demonstrate increased echodensity due to the large number of connective tissue septations, which make them similar to colloid thyroid nodules. Unlike parathyroid hyperplasia and adenomas, which have an elongated shape and distinct capsule as they grow, the malignant neoplasm retains its round or oval shape. Parathyroid cancer is also characterized by irregular, rough, indistinct margins, and the absence of a hyperechoic capsule (Fig. 8.10). Irregular asymmetric vascularity with CDI and PDI assists in

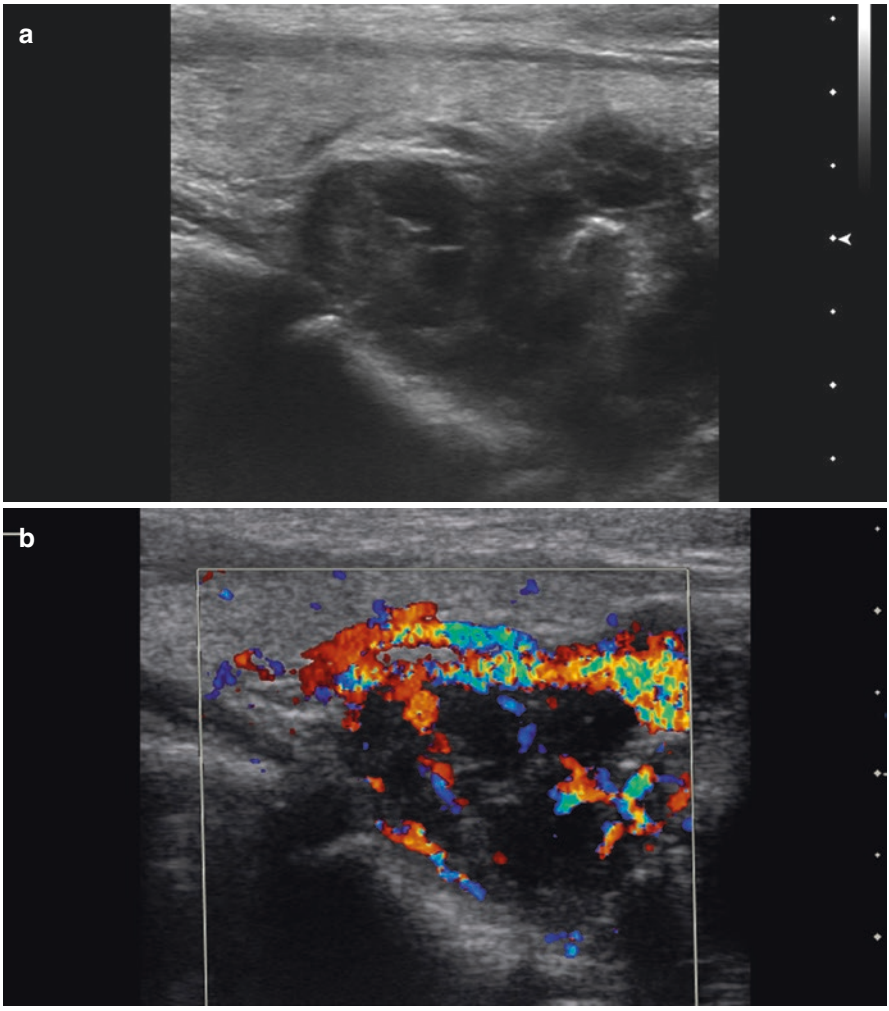

Fig. 8.10 Parathyroid cancer. Sonograms. Longitudinal scan. (**a**) Grayscale US. (**b**) CDI. (**c**) PDI. (**d**) Compression ultrasound elastography

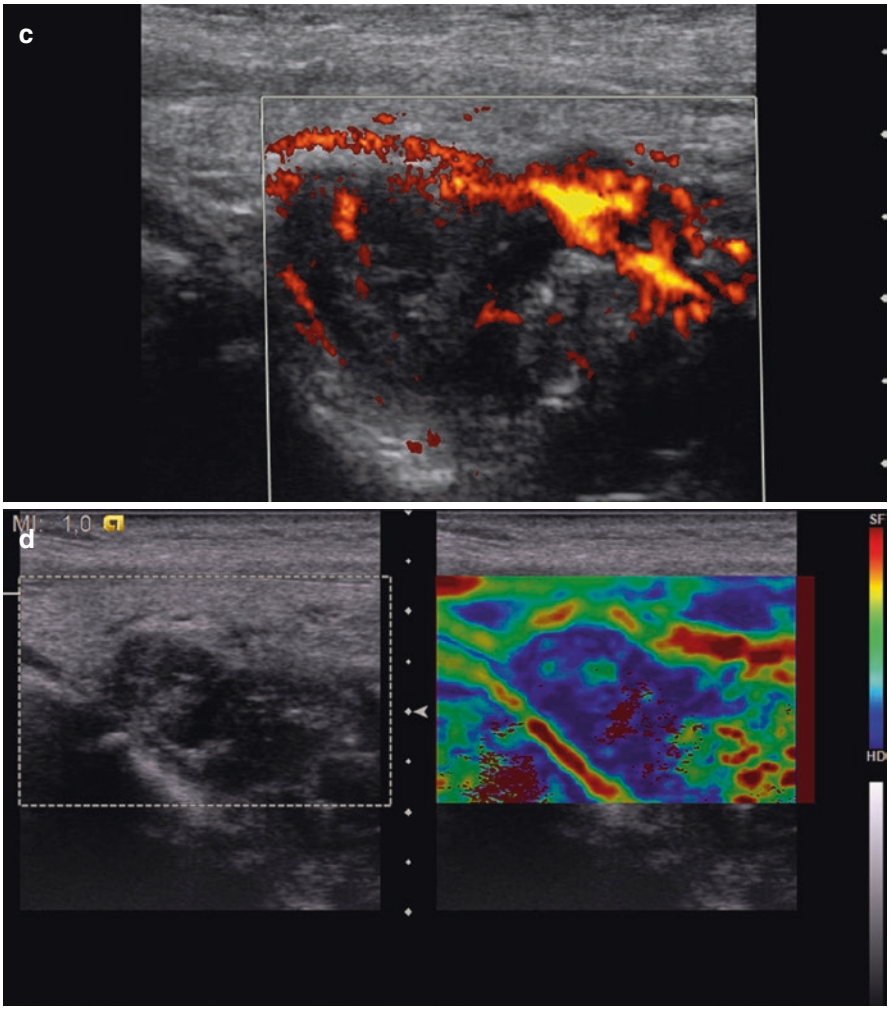

Fig. 8.10 (continued)

differential diagnosis. Compression US elastography reveals hard pattern, and elastometry with ARFI detects share-wave velocity of 3.0 m/s and higher. It is sometimes difficult to differentiate parathyroid adenomas and parathyroid cancer using US. Large size and weight (up to 15–200 mg) are suspicious for parathyroid cancer. Extremely high blood PTH and Ca^{2+} are also typical for parathyroid cancer. US detection of metastases in the lymph nodes can serve as an additional sign of parathyroid cancer in the absence of malignancies in the other organs of the head, neck, and mediastinum. Alternatively, they can easily mask the abnormal parathyroid, which appears to have a similar echostructure on US.

Tumor size is an important aspect in US of HPT patients. Small tumors are difficult to detect. US is often negative or doubtful in retrotracheal, retroesophageal, mediastinal, and intrathymic locations of abnormal parathyroids. In these cases, US

efficiency is low and yields to that of sestamibi scan, CT, and MRI. One significant disadvantage of US is high operator dependency. Kairys et al. [14] showed that the sensitivity of parathyroid US conducted by an experienced specialist is higher as compared with that of a general practitioner in an outpatient department (79 vs. 33%, respectively).

Despite a large number of publications concerning the advantages and opportunities of sonography in topical diagnosis of abnormal parathyroid glands, some studies deny the necessity of "routine" imaging of parathyroid glands with US.

8.2 US of Neck Masses

The fourth edition of the WHO head and neck tumor classification presents tumor entities in accordance to the sites of their most common occurrence and presentation [15]. Chapters devoted to the oropharyngeal and the neck region are established.

Extra-organ primary tumors account for 1.25% of all human neoplasms. Neck tumors of mesenchymal origin constitute 52.4% of all extra-organ primary tumors, cysts—34.9%, and tumors of neuroectodermal origin—12.7%. Extra-organ tumors arising from soft tissues of the neck comprise a small but highly polymorphous group of lesions.

Extra-organ neck tumors can be grouped as follows:

1. Tumors of mesenchymal derivatives
   - Adipocytic (lipoma and liposarcoma)
   - Fibroblastic (fibroma, desmoid, and fibrosarcoma)
   - Vascular (lymphangioma, hemangioma, and angiosarcoma)
   - Muscular (rhabdomyosarcoma and leiomyosarcoma)
   - Rare tumors (chondrosarcoma, synovioma, mesenchymoma, and others)
2. Dysembryonic tumors
   - Branchial cyst (or branchial cancer)
   - Thyroglossal neck cyst (or cyst cancer)
   - Rare tumors (chordoma, teratoma, and others)
3. Tumors of neuroectodermal origin
   - Paraganglioma (carotid, vagal, atypical)
   - Neurinoma and ganglioneuroma
   - Meningioma
4. Lymphadenopathy (metastatic, inflammatory, and hemoblastoses).

Diagnostic methods that are utilized to diagnose neck masses can be classed as either visualizing (US, CT, radionuclide scan, MRI, PET, etc.), morphological (cytological and histological examination), or auxiliary (serological, laboratory, etc.). In most cases, US aids in achieving an exact diagnosis or, at least, in determining the relation of the lesion to one or another neck organ, as well as its size, structure, margins, and vascularity. Morphological examination is necessary in cases

with suspected Hodgkin's disease, malignancy of any neck site, or conglomeratic lesions. If the neck lesion is large, extends to sonographically inaccessible sites, or contacts with octal structures, CT is recommended. MRI is feasible for detailed assessment of soft tissues and blood vessels in particular. Chest X-ray, abdominal US, scintigraphy of bones, and other methods are performed to rule out remote metastases in cases of malignant neoplasm.

Extra-organ neck tumors are sonographically characterized according to their locations in the following anatomical neck regions:

- Submental triangle
- Submandibular triangle
- Hyoid area
- Carotid triangle (the area of CCA bifurcation)
- Sternocleidomastoid area
- Lateral neck triangle
- Back surface of the neck.

Neck lesions that contain fluid are cysts. These are grouped into median and lateral types.

A *median neck cyst* (thyroglossal cyst) of the neck is an embryonic dysplasia resulting from a failure to obliterate the thyroglossal duct. It can occur anywhere from the base of the tongue to the thyroid gland, but is usually located under the deep cervical fascia between the hyoid bone and the upper edge of the thyroid cartilage, and sometimes in the submandibular triangle. It is midline or just off the midline and necessarily connected to the hyoid bone. It is represented by a painless fluid structure of flattened or roundish shape that moves up and down upon swallowing (Fig. 8.11). It exhibits a thin regular capsule and homogeneous anechoic fluid contents. A certain amount of suspension may be detected. It may grow slowly. Up to half of all thyroglossal cysts are not diagnosed until adulthood. The size of the cyst can change periodically if the connection with the oral cavity through the thyroglossal duct is preserved. If the cyst is infected, the inflammation manifests as pain at swallowing and a painful midline infiltrate. Sonographically, this corresponds to the dilation of the cyst with an increase in suspension. The margins appear indistinct and thickened (Fig. 8.12). Thin septa may arise within the cyst. The empyema of the cyst often results in the destruction of the capsule and overlaying soft tissues with the formation of a fistula.

Lateral cysts of the neck are a consequence of congenital developmental defects arising from branchial arches, clefts, and pouches. Lateral cysts may be divided according to their origin into lymphogenous (inflammatory and dysembryogenic) and branchial. Upper lateral cysts are located at the level of the mandible angle and are usually of inflammatory origin. Inferior lateral cysts are located in supraclavicular areas and are dysembryogenic. Second branchial cleft cysts are most common. They are found in the upper neck along the anterior border of the sternocleidomastoid at the level of carotid bifurcation, more often on the left side. The position ahead of the sternocleidomastoid muscle at the level of the angle of the mandible is

the basic feature for differential diagnosis. The cyst is, as a rule, unilateral. Bilateral cysts still occur in 2% of cases. They may develop branchial cancer, which is morphologically represented by either squamous cell carcinoma or adenocarcinoma. The incidence of this disease is higher in people over 50 years of age and is equal in men and women. Unless infected, these cysts can exist in a dormant state for a long time. Infected cysts may result in fistulas.

Lateral and median cysts are sonographically defined among the neck muscles. They demonstrate the below listed characteristic features (Fig. 8.13):

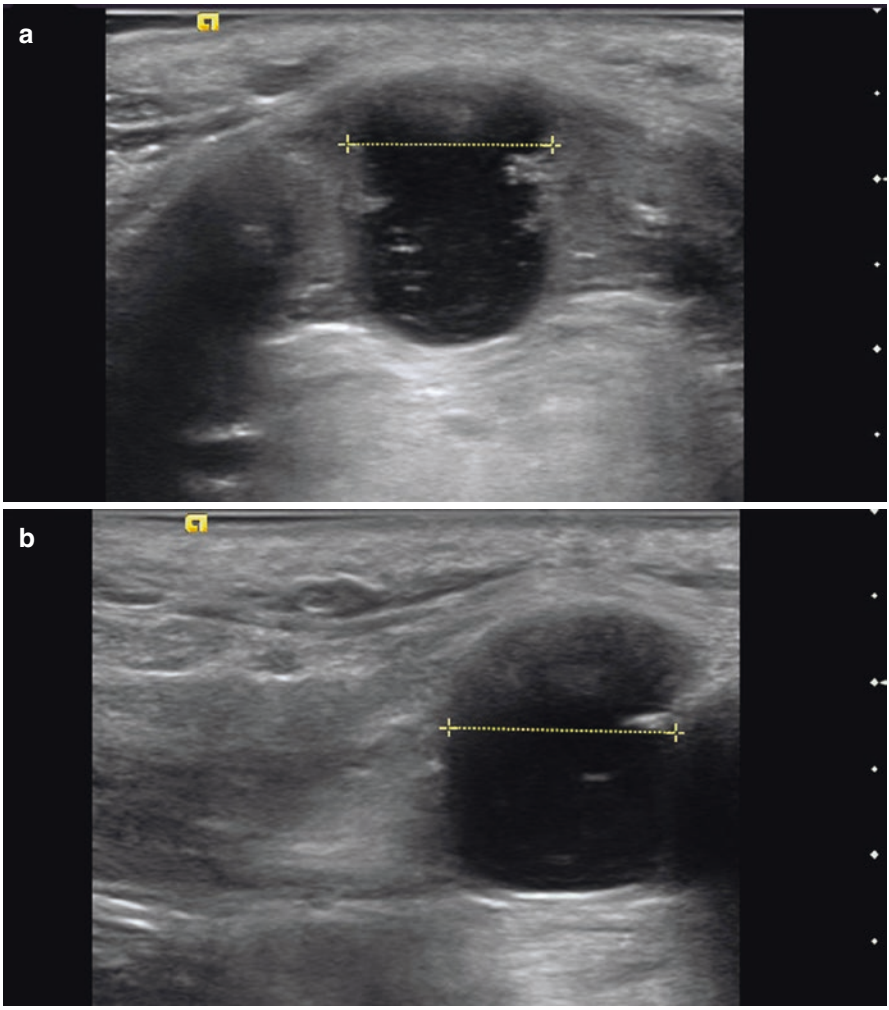

Fig. 8.11 Median neck cyst. Grayscale US (**a**) Transverse scan. (**b**) The same cyst as letter a, longitudinal scan. (**c**) Cyst with homogeneous suspension, transverse scan. (**d**) The same cyst as letter c, longitudinal scan

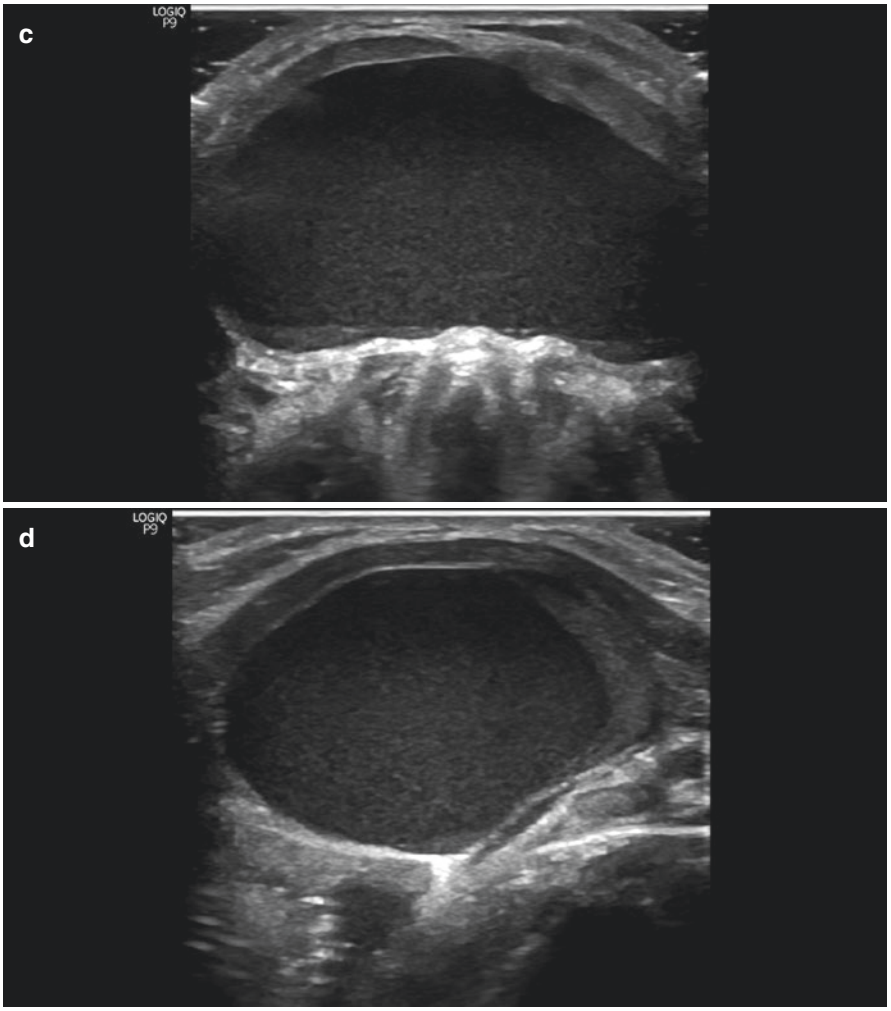

Fig. 8.11 (continued)

- Roundish or oval shape
- Regular, well-defined margins
- Homogeneous structure, commonly with suspension at the time of presentation, or anechoic, sometimes with echogenic inclusions or solid component
- Posterior echo enhancement
- Avascularity in CDI and PDI
- Limited mobility
- No special pattern with compression US elastography or three-layer fluid pattern
- Elasticity with palpation.

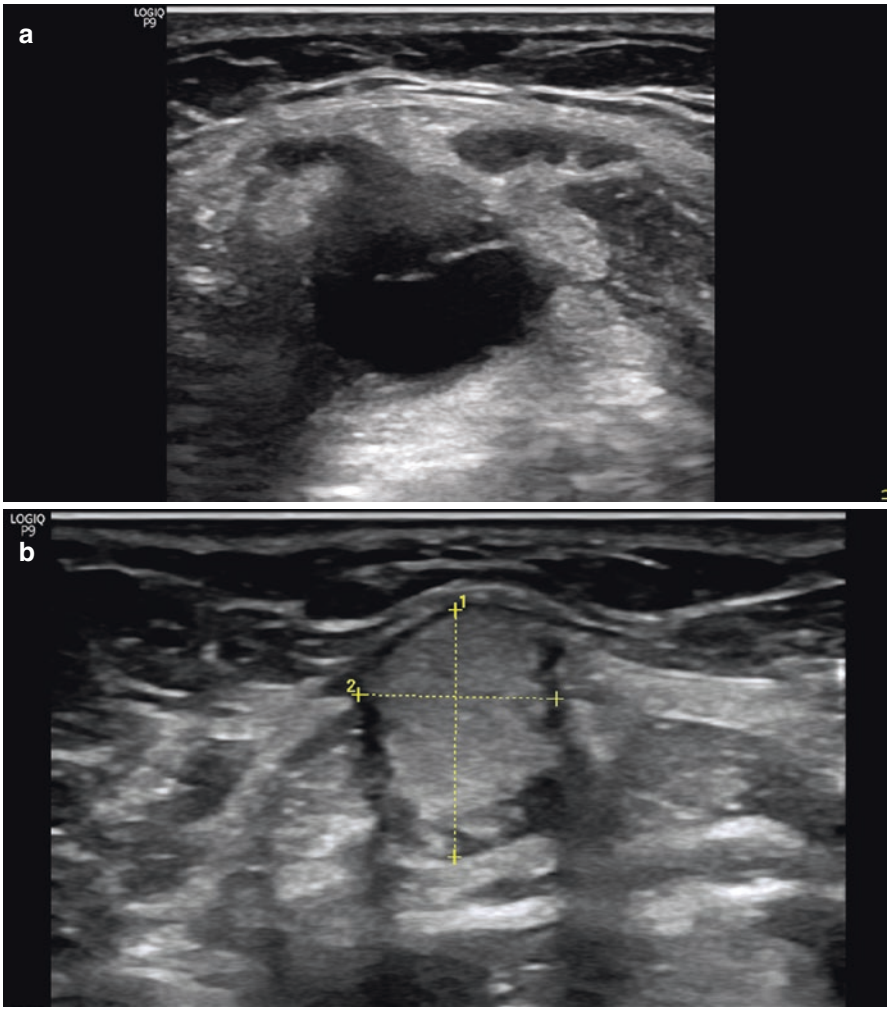

Fig. 8.12 (**a**) Infected median neck cyst. Grayscale US. Transverse scan. (**b**) Infected median neck cyst with dense contents after conservative treatment

The capsule of the cyst is usually easily identified as the echogenic linear avascular margin of the thickness up to 1–2 mm (depending on whether the cyst is infected). Inflammation leads to cyst dilation with much suspension, clots, and changes in the capsule. The capsule of the cyst becomes thicker or thinner (and sometimes cannot be differentiated). Edema and infiltration of the surrounding tissues may accompany the inflammation in some cases. This is sonographically observed as a decrease or increase in echodensity, protruding heterogeneity, and a blurring of the differentiation of the structure. Lymph node enlargement associated with inflammation may occur.

Neuroectodermal tumors of the neck are represented by *paragangliomas* (chemodectomas, glomus tumors). These form part of the extra-adrenal neuroendocrine system. There are two main location-specific types of neck paraganglioma: carotid and vagal paragangliomas. Carotid paragangliomas—also called carotid body glomus tumors—are the most common of the head and neck paragangliomas. They occur at the bifurcation of the CCA and arise from the tissue of the normal carotid body. Vagal paragangliomas are the least common of the head and neck paragangliomas. Paragangliomas are more often observed in women 40–45 years old. They usually appear as solitary lesions, although multiple lesions at multiple sites may be

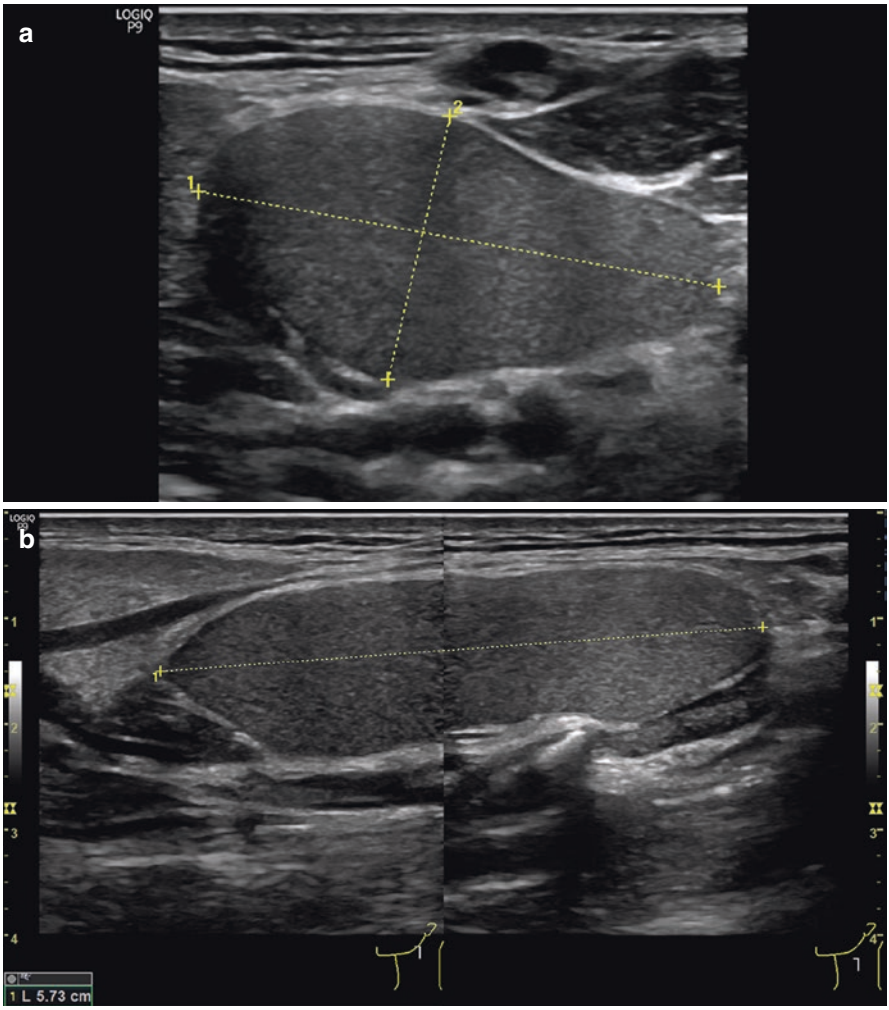

Fig. 8.13 (**a**) Lateral neck cyst. (**a**) Grayscale US. Transverse scan. (**b**) Grayscale US. Longitudinal scan. (**c**) CDI. (**d**) PDI

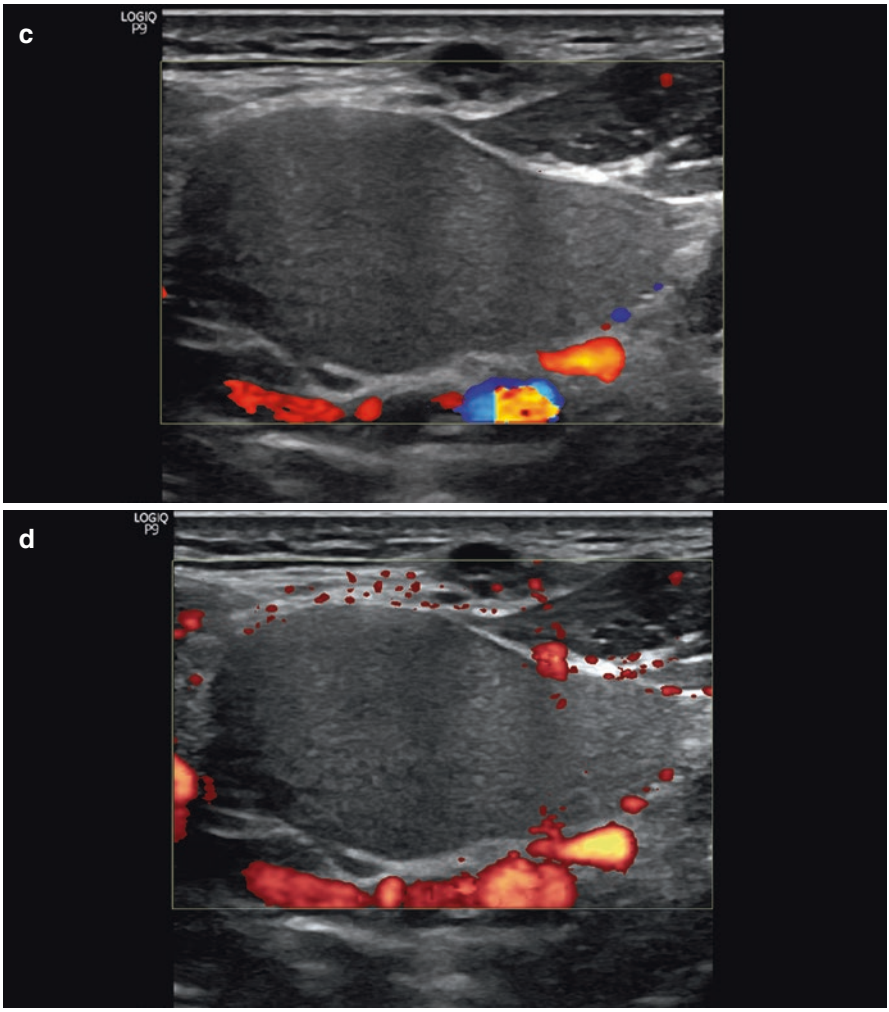

Fig. 8.13 (continued)

seen in 3–5% of cases. The vast majority of glomus tumors are benign and slow to grow. In rare cases they may become active and secrete catecholamines, which can lead to clinical manifestations similar to pheochromocytoma. Carotid paragangliomas are found at the site of CCA bifurcation and are tightly connected to the vessels. The tumor is sonographically represented by a large lesion (up to 10 cm) of oval or roundish shape, iso- or hypoechoic homogeneous structure, with accurate regular contours (Fig. 8.14). It shows very limited mobility and appears dense upon compression by the US probe. Because it is part of the neuroendocrine system, this tumor is highly vascularized. A large amount of arterial and venous vessels is rather characteristic. Doppler examination is also necessary in such patients to assess both

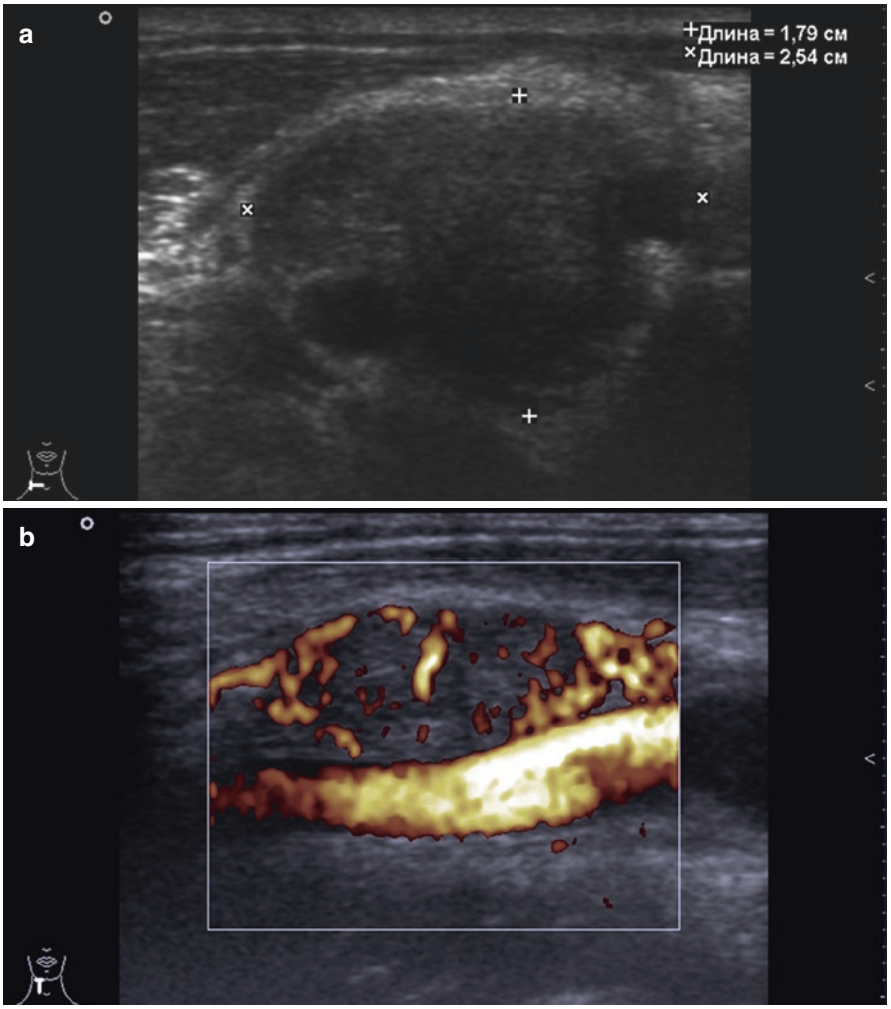

Fig. 8.14 Right carotid paraganglioma. (**a**) Grayscale US, transverse scan. (**b**) PDI, longitudinal scan

the anatomical course and hemodynamic changes in the carotid artery. In cases of malignant tumor, metastases in regional lymph nodes are possible.

US permits the differentiation of *malignant pathology of the larynx*. Laryngeal cancer is the most common malignancy of the larynx (50–60%), and one that mainly affects men 40–70 years old. Larynx sarcomas are most often represented by rhabdomyosarcomas, liposarcomas, fibrosarcomas, and angiosarcomas. Carcinosarcomas are rare. Malignant tumors of the larynx show different clinical signs that complicate the differential diagnosis. They exhibit sonographic features similar to cancers of other neck organs (e.g., the thyroid or

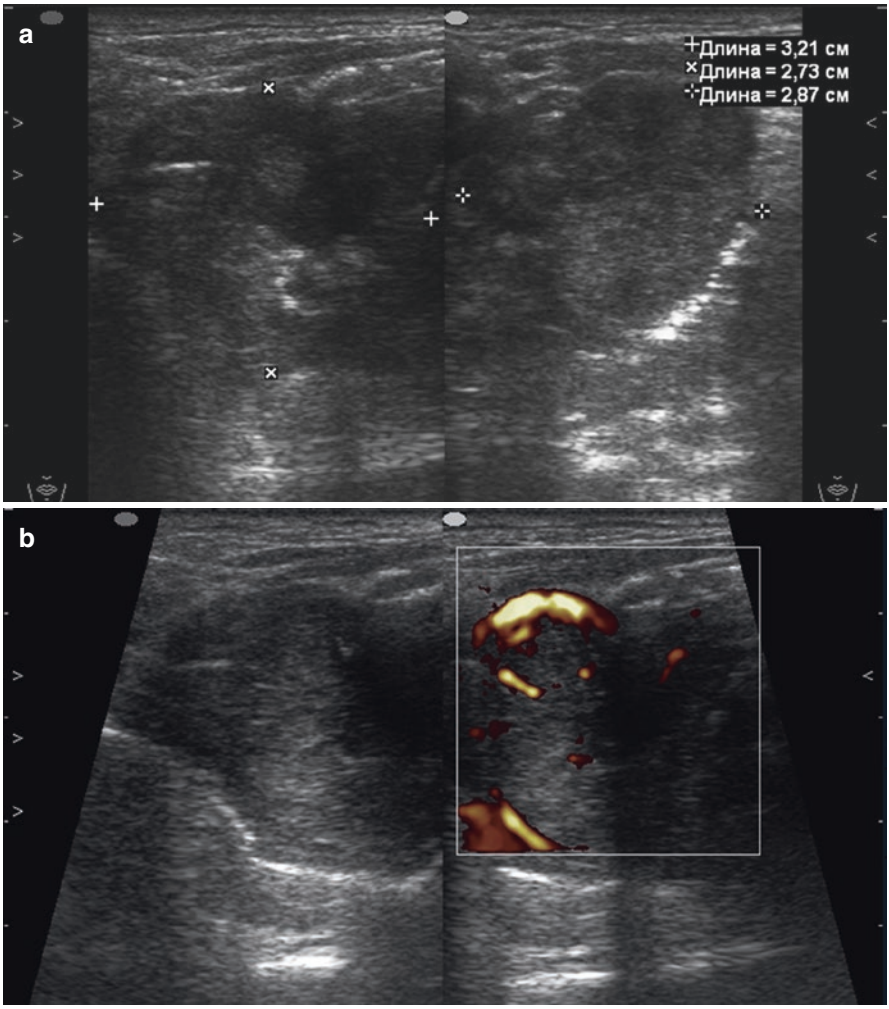

Fig. 8.15 Laryngeal cancer. (**a**) Grayscale US. (**b**) PDI

salivary glands), and are characterized by lesions in the projections of median structures of the neck with the following features (Fig. 8.15):

- Decreased echodensity
- Irregular shape
- Indistinct contours
- Heterogeneous structure often with echogenic inclusions
- Immobility, incompressibility, painlessness with compression
- Heterogeneous disorganized vascularity with CDI and PDI in large-sized tumors
- Frequent enlargement of regional lymph nodes.

CT of the larynx is always needed in order to assess the lesion more precisely.

Hodgkin's lymphoma is a type of malignancy originating from lymphocytes. It affects cervical lymph nodes in 60–70% of cases. It commonly arises in combination with abnormal axillary, mediastinal, inguinal, retroperitoneal, or other groups of lymph nodes. The disease is more often observed in males and exhibits two peaks in incidence: at 20–30 years and over 60 years of age. During the initial stage of the disease, the lymph nodes show the following US picture (Fig. 8.16):

- Enlarged size of 1–3 cm
- Roundish, oval, or irregular shape
- Regular or irregular accurate margins
- Decreased echodensity
- Frequent heterogeneity of echostructure

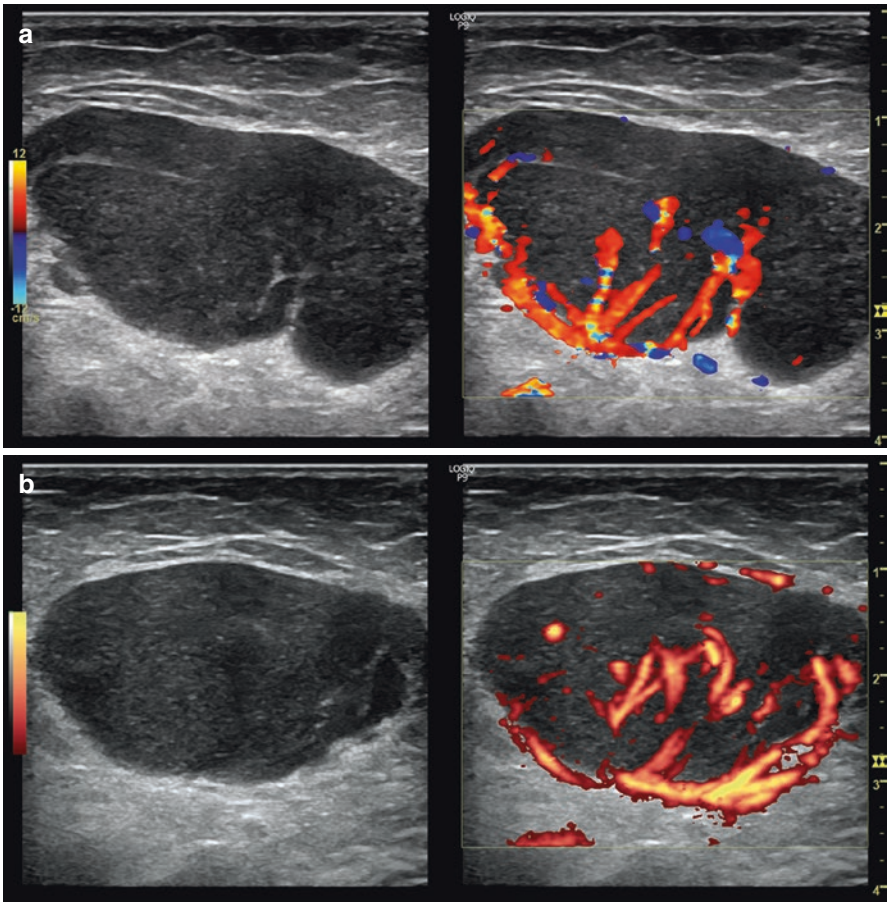

Fig. 8.16 Enlarged neck lymph node in Hodgkin's disease. (**a**) Grayscale US and CDI. (**b**) Grayscale US and PDI. (**c**) Compression US elastography, high strain ratio. (**d**) CEUS

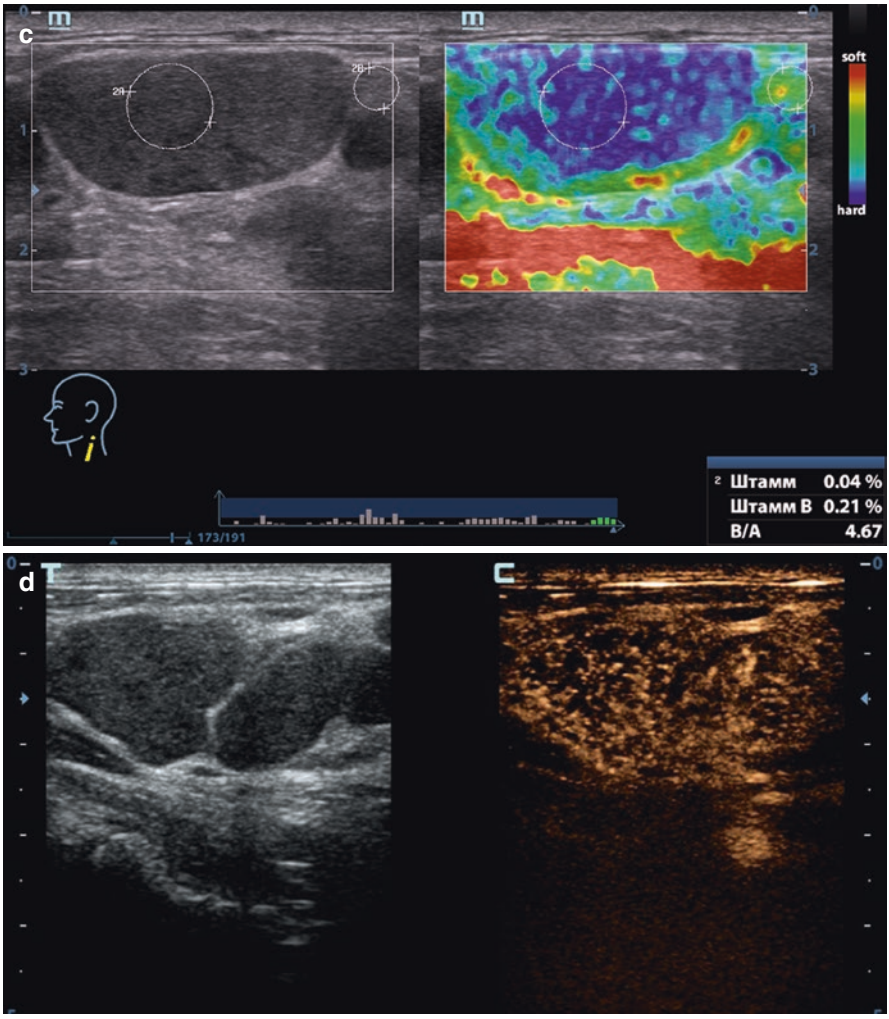

Fig. 8.16 (continued)

- Hypovascularization or hypervascularization with a hypertrophic hilar blood flow pattern with CDI and PDI
- Low mobility, incompressibility, painlessness with compression
- Dense with compression US elastography and elastometry
- CEUS reveals fast regular grainy contrast enhancement of the medulla and cortex.

Further development of the disease is characterized by conglomerations of lymph nodes of various sizes and densities. The natural course of the disease is characterized by spontaneous remissions and flares. As the disease progresses, new groups of

lymph nodes become affected and the disease generalizes. Abnormal lymphatic nodes in Hodgkin's disease are differentiated from metastases of thyroid cancer or malignant tumors of other head and neck organs.

Abnormalities of submandibular *salivary glands* may be identified in the upper neck area. Inflammatory diseases (sialadenitis), salivary gland stones, and tumors (e.g., adenoma, Fig. 8.17) are most common conditions.

Cervical esophageal diverticulum is a rare diagnostic finding with US (Fig. 8.18). Esophageal diverticulum is a diversely shaped evagination of the esophageal wall that is connected with the esophageal lumen. True and false types of diverticula can be distinguished. The walls of the first type contain all of the layers of the normal

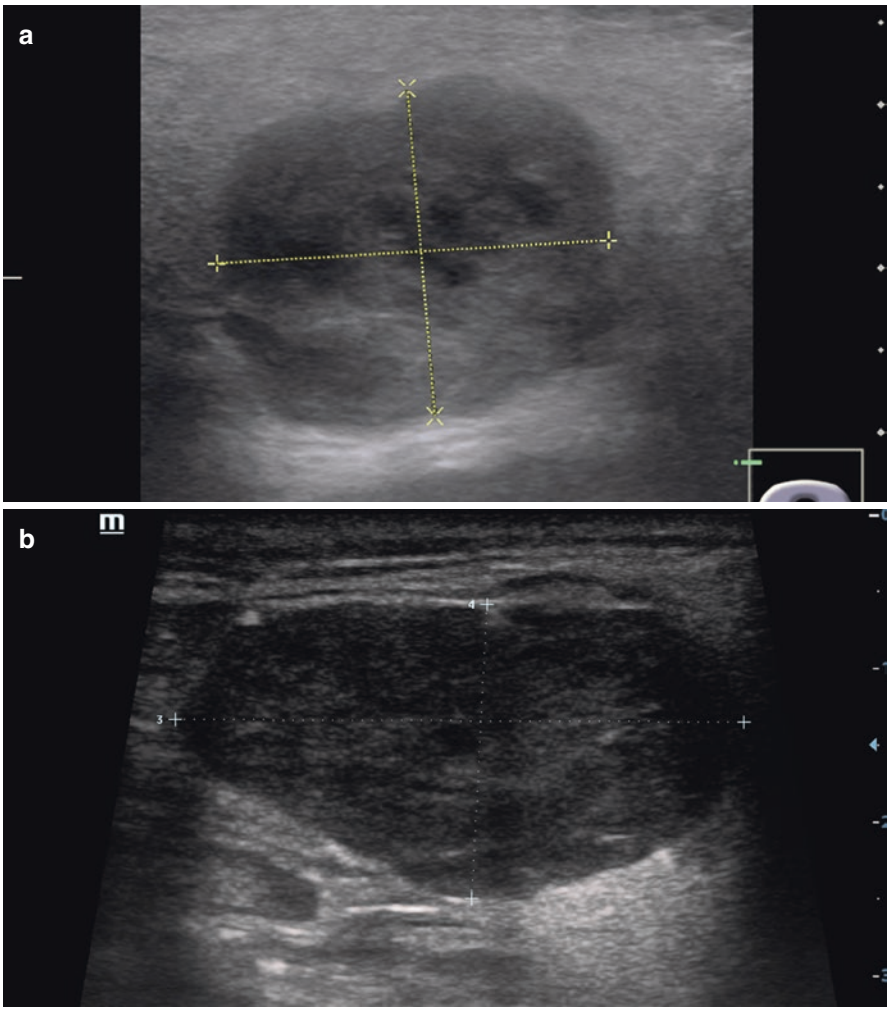

Fig. 8.17 Pleomorphic adenoma of a salivary gland. (**a**, **b**) Grayscale US. (**c**) CDI. (**d**) PDI

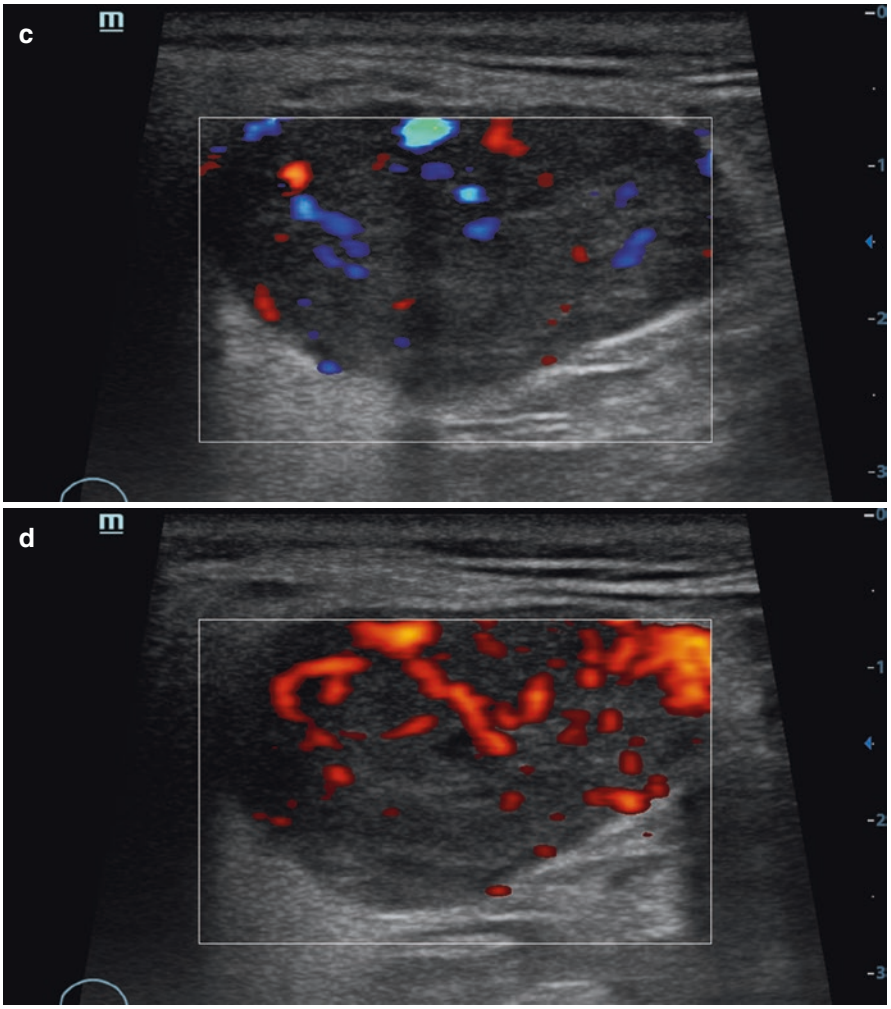

Fig. 8.17 (continued)

esophageal wall. The walls of the latter type consist of the mucosa that outpouches through the defect in the muscular layer. Esophageal diverticulum may have a congenital or acquired origin. The latter develop due to the following mechanisms: pulsion (appears with an increase in pressure within the esophagus resulting from a disturbance to its motility or distal stenosis), traction (arises as a result of adhesion between the esophageal wall and the surrounding structures due to an inflammatory process, etc.), and pulsion-traction (mixed). Diverticula may exist in any part of the esophagus and be solitary or multiple. Esophageal diverticulum is sonographically visualized as a roundish isoechoic or hypoechoic lesion of regular shape with accurate margins and a length of 0.5 to 2–3 cm that is avascular in CDI and PDI. It

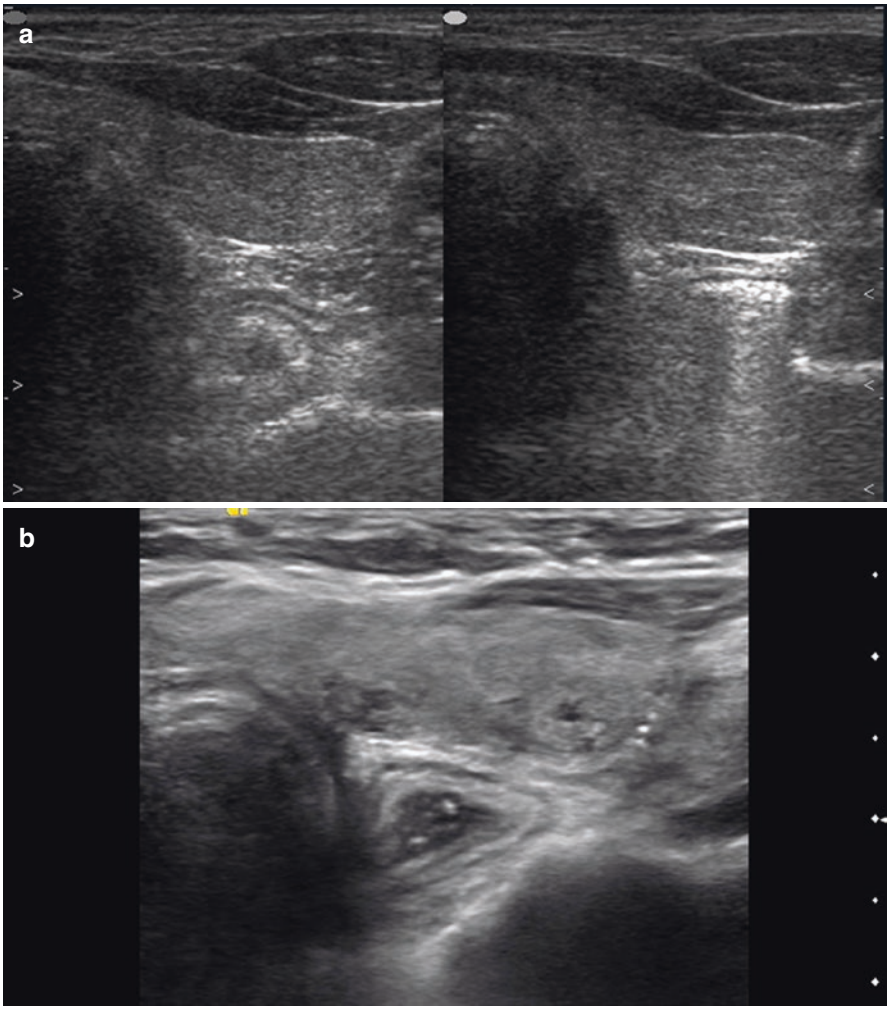

Fig. 8.18 Grayscale US (**a**) Cervical esophageal diverticulum. (**b**) Esophageal achalasia

contains heterogeneous, mostly hyperechoic, inclusions in the central part that are similar to those of a microcalcification or an arc-shaped calcification, and which move and change shape upon swallowing. The lesion may change in size and content depending on the patient's head or body position. The esophageal wall is most often differentiated as a hypoechoic boundary structure up to 2 mm thick that surrounds the lesion. The echodensity and echostructure of the wall may differ from homogeneous and hypoechoic to heterogeneous and mostly hyperechoic depending on the morphological structure and the type of diverticulum. Careful examination can reveal its connection with the adjacent esophageal wall. Esophageal diverticula can easily be misdiagnosed as thyroid nodules, since they often occur on the

posterior portion of the thyroid gland, especially on the left side. Turning the patient's head maximally results in the esophagus changing position. It is normally located close to the dorsal part of the left thyroid lobe. Upon turning the head to the left, the esophagus moves to the right and appears adjacent to the right thyroid lobe. The diverticulum, if not fixed, may change position. Swallowing also helps to distinguish the diverticulum from a thyroid nodule. Sometimes it is difficult to differentiate a diverticulum with esophageal achalasia—diffuse and uniform expansion of its lumen—based on only US image (Fig. 8.18b).

The location and spread of *inflammatory processes* in the soft tissues of the neck are defined by the complexity of the anatomy of the neck, with tender fat separated by multiple fascias, muscles, neck internals, and other structures. The following sonographic stages of inflammation are generally identified: edema, infiltrate, preabscess, and hypo- and anechoic abscesses. They represent the transition of serous inflammation to purulent, resulting in an abscess. Neck inflammation may lead to phlegmons and abscesses at different locations, which imply a high risk of descent into the mediastinum, sepsis, purulent blood vessel destruction with bleeding, development of venous thrombosis, thrombosinusitis, and brain abscess. US allows the type of inflammation and its stage of development to be specified. The site, volume, structure, margins, relation to blood vessels, and surrounding organs should be outlined to follow up the infiltrate during treatment. Purulent inflammation can be identified precisely, and pus collections can be located to assist the surgery.

US is a valuable imaging modality for neck lesions. It has a number of advantages. The main ones are undoubtedly availability, harmlessness, high diagnostic value, accuracy in localizing neck structures, easy follow-up, and real-time guidance for minimally invasive procedures.

References

1. Kalinin AP, Pavlov AV, Alexandrov YK, et al. The parathyroid glands. imaging and surgery. Berlin: Springer; 2013.
2. Wang C. The anatomic basis of parathyroid surgery. Ann Surg. 1976;183(3):271–5.
3. Randel SB, Gooding GAW, Clark OH, et al. Parathyroid variants: US evaluation. Radiology. 1987;165:191–4.
4. Nazarenko GI, Krasnova TV, Zykova NA, et al. Technological aspects of diagnosis of parathyroid tumors by means of radiological methods. Ultrazvukovaya i funkcionalnaya diagnostika. 2004;4:15–22.. (Article in Russian)
5. Wakamatsu H, Noguchi SM, Yamashita H, et al. Parathyroid scintigraphy with ^{99m}Tc-MIBI and ^{123}I subtraction: a comparison with magnetic resonance imaging and ultrasonography. Nucl Med Commun. 2003;24(7):755–62.
6. Lane MJ, Desser TS, Weigel RJ, Jeffrey RB. Use of color and power Doppler sonography to identify feeding arteries associated with parathyroid adenomas. Am J Roentgenol. 1998;171(3):819–23.
7. Wolf RJ, Cronan JJ, Monchik JM. Color Doppler sonography: an adjunctive technique in assessment of parathyroid adenomas. J Ultrasound Med. 1994;13(4):303–8.
8. Weymouth MD, Serpell JW, Chambers D. Palpable parathyroid adenomas presenting as clinical solitary thyroid nodules and cytologically as follicular thyroid neoplasms. ANZ J Surg. 2003;73(1–2):36–9.

9. Bindlish V, Freeman JL, Witterick IJ, Asa SL. Correlation of biochemical parameters with single parathyroid adenoma weight and volume. Head Neck. 2002;24(11):1000–3.
10. Sugimoto K, Umekawa T, Kurita T. A case of functioning parathyroid cyst. Hinyokika Kiyo. 1997;43(12):903–6.
11. Pinney SP, Daly PA. Parathyroid cyst: an uncommon cause of a palpable neck mass and hypercalcemia. West J Med. 1999;170(2):118–20.
12. Birnbaum J, Van Herle AJ. Immunoheterogeneity of parathyroid hormone in parathyroid cysts: diagnostic implications. J Endocrinol Investig. 1989;12:831–6.
13. Kinoshita Y, Fukase M, Uchihashi M, et al. Significance of preoperative use of ultrasonography in parathyroid neoplasms: comparison of sonographic textures with histologic findings. J Clin Ultrasound. 1985;13(7):457–60.
14. Kairys JC, Daskalakis C, Weigel RJ. Surgeon performed ultrasound for preoperative localization of abnormal parathyroid glands in patients with primary hyperparathyroidism. World J Surg. 2006;30:1658–63.
15. El-Naggar AK, JKC C, Grandis JR, et al., editors. WHO classification of head and neck tumours. 4th ed. Lyon: IARC; 2017.

Neck Ultrasound After Thyroid Surgery

9

Yuriy K. Aleksandrov, Yury N. Patrunov,
Alexander N. Sencha, Ella I. Peniaeva, Ekaterina A. Sencha,
and Munir G. Tukhbatullin

9.1 General Assessment of the Postoperative Neck and the Thyroid Gland

The volume of neck surgery in thyroid diseases ranges from the resection of a lobe fragment to total thyroidectomy with radical neck dissection. Each type of surgery has certain advantages and disadvantages that may be accompanied with specific complications and side effects. Despite modern surgical techniques, several types of complications remain quite common, such as recurrent laryngeal nerve injury, postoperative bleeding, hypoparathyroidism, and laryngotracheal edema, which occur with a frequency of 2–15%. Patients' age and constitution, the size and location of goiter, the quality of preoperative imaging, the experience of the surgeon, and other factors

Y. K. Aleksandrov (✉)
Department of Surgery, Federal State Budget Educational Institution of Higher Education Yaroslavl State Medical University of the Ministry of Healthcare of the Russian Federation, Yaroslavl, Russia

Y. N. Patrunov · E. I. Peniaeva
Department of Ultrasound Diagnostics of the Center for Radiological Diagnostics, Non-State Healthcare Institution Yaroslavl Railway Clinic of JSC "Russian Railways", Yaroslavl, Russia

A. N. Sencha
Department of Visual and Functional Diagnostics of National Research Center for Obstetrics, Gynecology and Perinatology, Ministry of Healthcare of the Russian Federation, Moscow, Russia

E. A. Sencha
Ultrasound Diagnostics Department, Medical Diagnostic Center, Moscow, Russia

M. G. Tukhbatullin
Department of Ultrasound Diagnostics, Kazan State Medical Academy – Branch Campus of the Federal State Budget Educational Institution of Further Professional Education, "Russian Medical Academy of Continuing Professional Education" of the Ministry of Healthcare of the Russian Federation, Kazan, Russia

A. N. Sencha, Y. N. Patrunov (eds.), *Thyroid Ultrasound*,
https://doi.org/10.1007/978-3-030-14451-7_9

influence the rate of complications. Recently, minimally invasive video-assisted thyroidectomy and robotic thyroid surgery have been promoted and analyzed.

Patients with operated thyroid may not notify the sonographer about the previous thyroid surgery. Modern surgery leaves minimally visible scars or no signs of operation on the neck skin. Therefore, a correct US study should begin with a visual inspection of the neck (Fig. 9.1) and acquiring data of case history.

Neck US after thyroid surgery considers the time after surgery, the volume of intervention, and the data of pathology of the excised structures. Patients are commonly aware of the diagnosis and can supply the necessary information. Multiparametric echography of the postsurgical neck and evaluation of the operated thyroid gland are performed with high-frequency (7.5–15 MHz) linear probes following the standard technique.

Below is a guide to interpreting the US changes in the region of the operation:

1. Detection of thyroid tissue in the thyroid bed (residue or fragments)
   - Number of thyroid fragments
   - Location of each fragment and relations to surrounding structures
   - Size
   - Margins
   - Echodensity and echostructure
   - Vascularity of the thyroid residue and fragments
   - Elasticity with compression USE and elastometry

Fig. 9.1 Status after thyroid surgery. View of the neck

2. Detection of lesions in the remaining thyroid tissue (location, size, shape, borders, contours, echodensity, echostructure, vascularization, and relations to surrounding organs and tissues)
3. Mutual relations of neck organs and structures
4. Status of cervical and supra- and subclavicular lymph nodes
5. Status of postoperative scar zone

The US image of the thyroid bed depends largely on the volume of the thyroid tissue removed, the technique of surgery, and on the time after the operation. In the first days and weeks after thyroid surgery, as a rule, there is no need for an ultrasound scan of the neck. Early studies and follow-up are necessary only in the cases of suspected postoperative complications (bleeding, suture failure, suppuration, etc.). The study in the first week after surgery can be difficult because of the swelling of the neck tissue and pain, when pressed with US probe. The immediate postsurgical period is characterized by the infiltration of the thyroid bed and subcutaneous fat, with possible visualization of hematomas and suture material. Granulomas, calcifications, and fluid structures may appear later. This may lead to US hyperdiagnosis of disease recurrence.

Sonography within the first 2 months may normally reveal the following features:

- Thickening and heterogeneity of fat with a decrease in echodensity due to edema and infiltration. These changes may be misinterpreted as preserved thyroid tissue, or they can also mask the thyroid residue (its margins are poorly differentiated against the changes in the structure of the surrounding tissue).
- Hemorrhages can be seen as hypoechoic lesions in the thyroid bed (Fig. 9.2). They are most often observed as heterogeneous structures with hypo- and hyperechoic areas, often with anechoic fluid collections of different shapes and sizes. They show fast changes in US appearance, which are also typical of hematomas with other localizations.
- Suture material is often visualized as dot-shaped echogenic inclusions with indistinct or absent acoustic shadows located in the bed of the thyroid lobe or attached to the capsule of the thyroid residue.

Sonography of the thyroid bed more than 3 months after surgery reveals full or partial absence of thyroid tissue. The site shows diffuse fibrous changes with vascular bundles displaced medially (Fig. 9.3). The fields of hemorrhage, as a rule, disappear. Organizational features can be detected at the locations of former hematomas, and these show an increase in echodensity, heterogeneous structure, and indistinct and irregular contours. Three months after surgery, sutures and ligatures can only be defined in a few cases. Fine, roundish fields of increased echodensity up to 5 mm in size with regular distinct margins may be noted in some patients at the locations of former sutures. These may be regarded as suture granulomas. Anechoic lesions, such as fine cysts and organized fluid collections, may be seen in rare cases.

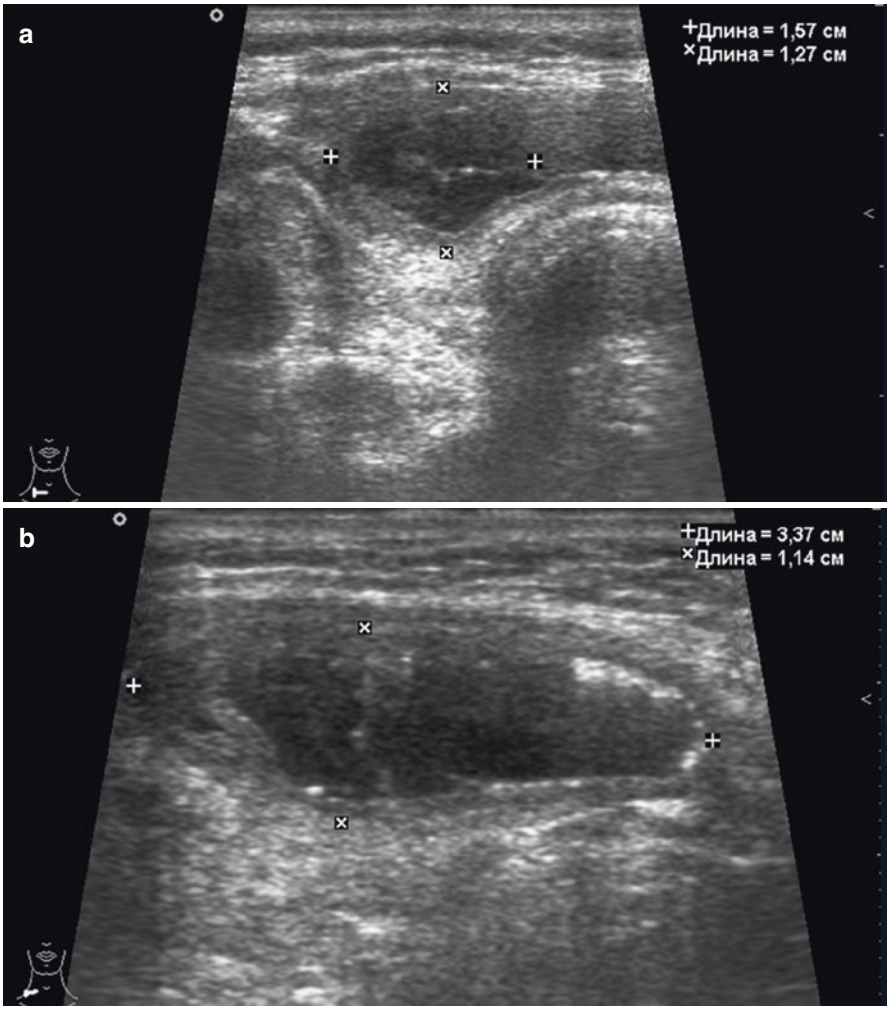

Fig. 9.2 (**a**, **b**) Status 1 month after thyroid surgery. Postoperative hematomas. Grayscale US

The US image of the thyroid bed 3 months after organ-preserving operations (subtotal resection, hemithyroidectomy) depicts the thyroid residue with regular margins, homogeneous structure, and unchanged or slightly decreased/increased echodensity (Fig. 9.4). The vascular bundle on the operated side is displaced medially toward the trachea.

Fibrotic changes are often seen in the bed of the removed lobe. The remnants of organized hematomas may be detected in rare cases as dense heterogeneous inclusions with indistinct contours, calcifications, suture granulomas, or individual cysts.

Central neck dissection leads to specific changes in sonograms. The trachea contours appear indistinct, and vascular bundles migrate superficially close to the trachea. Fibrous changes in the tissues adjacent to the thyroid bed are prominent.

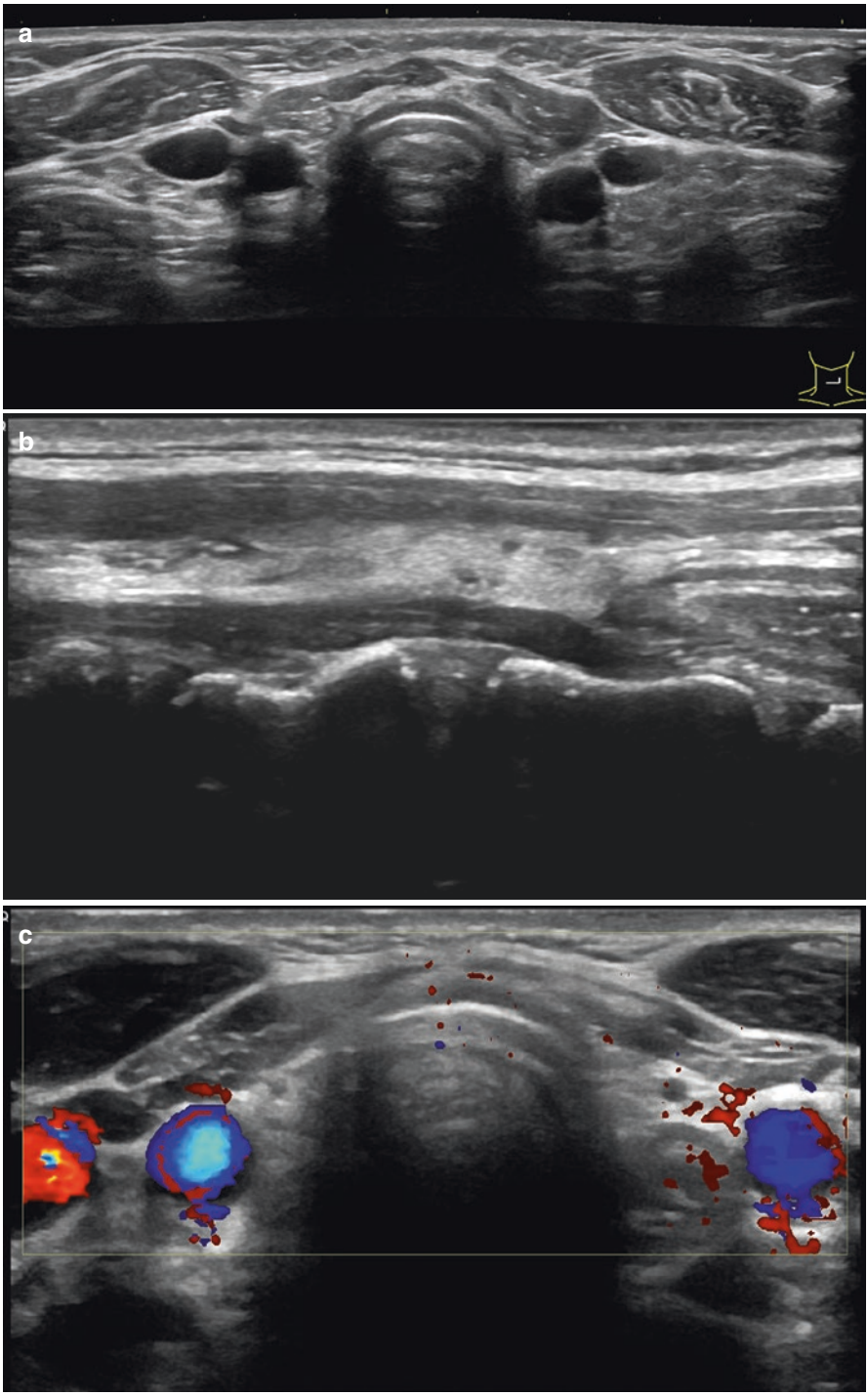

Fig. 9.3 Status 3 months after thyroid surgery. Imaging of the thyroid bed. (**a**) Grayscale transverse panoramic scan. (**b**) Grayscale US. Longitudinal scan. (**c**, **d**) CDI

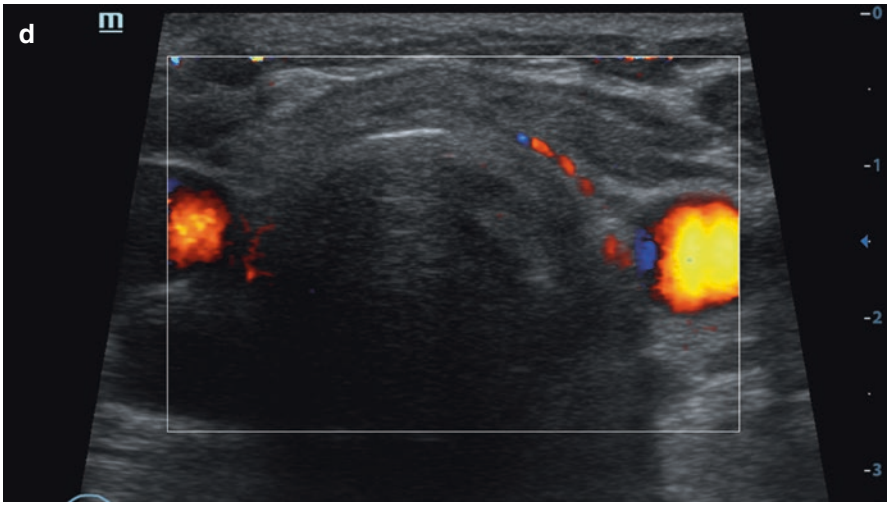

Fig. 9.3 (continued)

Several operations for thyroid cancer and malignant tumors of the head and neck require the removal of different neck structures. In some cases, cervical and supraclavicular lymph nodes, the submandibular salivary gland, sternomastoid and omohyoid muscles, or the internal jugular vein is/are excised, resulting in corresponding sonographic changes.

Five years or more after the resection of more than half of the thyroid lobe, its volume usually remains unchanged (Fig. 9.5); in the case of the resection of one-half to one-third of the thyroid lobe, it usually recovers to its full size as a rule. The thyroid remnant shows well-defined margins, normal or slightly increased echodensity, and possible heterogeneity. A decreased or normal parenchymal blood flow pattern is seen with CDI and PDI.

In some patients who have undergone total thyroidectomy, the thyroid bed may subsequently display thyroid remnants of various sizes, shapes, and vascularities upon US and radionuclide scans. According to Salvatori et al. [1] and Sencha and Belyaev [2], scintigraphy after total thyroidectomy and radioiodine therapy did not detect any residual thyroid tissue in the thyroid bed in only 7% of patients.

Radioiodine (^{131}I) treatment and remote gamma therapy after thyroidectomy lead to some distinctive sonographic features. The thyroid remnant, if any, after the treatment is poorly differentiated from the surrounding tissues (Fig. 9.6). It appears to have indistinct and irregular margins, heterogeneous echostructure, and decreased vascularity. Areas of increased echodensity and fibrous changes in the surrounding tissues may arise [3].

Sometimes, the interpretation of the presence (or absence) of thyroid residual fragments in thyroid bed is ambiguous. Opinions of several US specialists can be radically different. In some cases, the identification of a typical parenchymatous

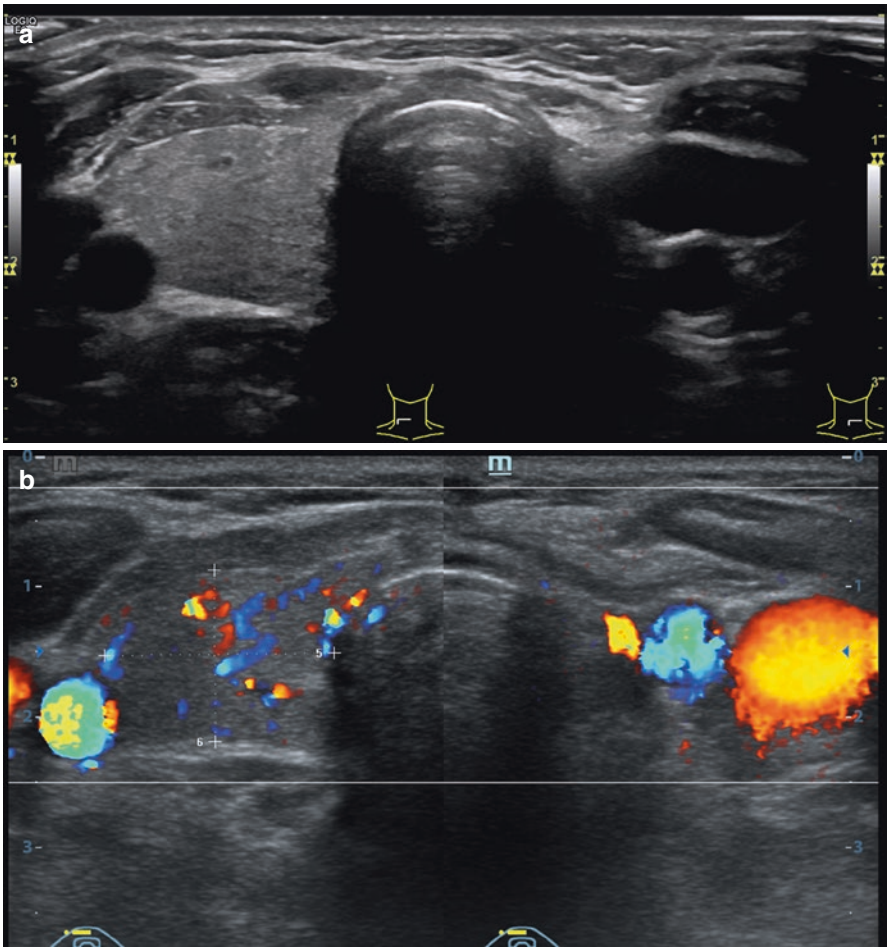

Fig. 9.4 Status 3 months after hemithyroidectomy. Imaging of the thyroid remnant. (**a**) Grayscale US. Transverse scan. (**b**) CDI

thyroid blood flow with CEUS helps to differentiate the thyroid tissue against the background of severe diffuse changes in thyroid bed (Fig. 9.7). Commonly, determination of functional activity of the thyroid residue with radionuclide scan and blood tests (e.g., thyroglobulin) is of benefit.

Patients who have been operated on for thyroid malignancy should be examined sonographically at the following intervals:

- Once every 3 months during the first postoperative year
- Once every 6 months for the next 5 years
- Once a year after that

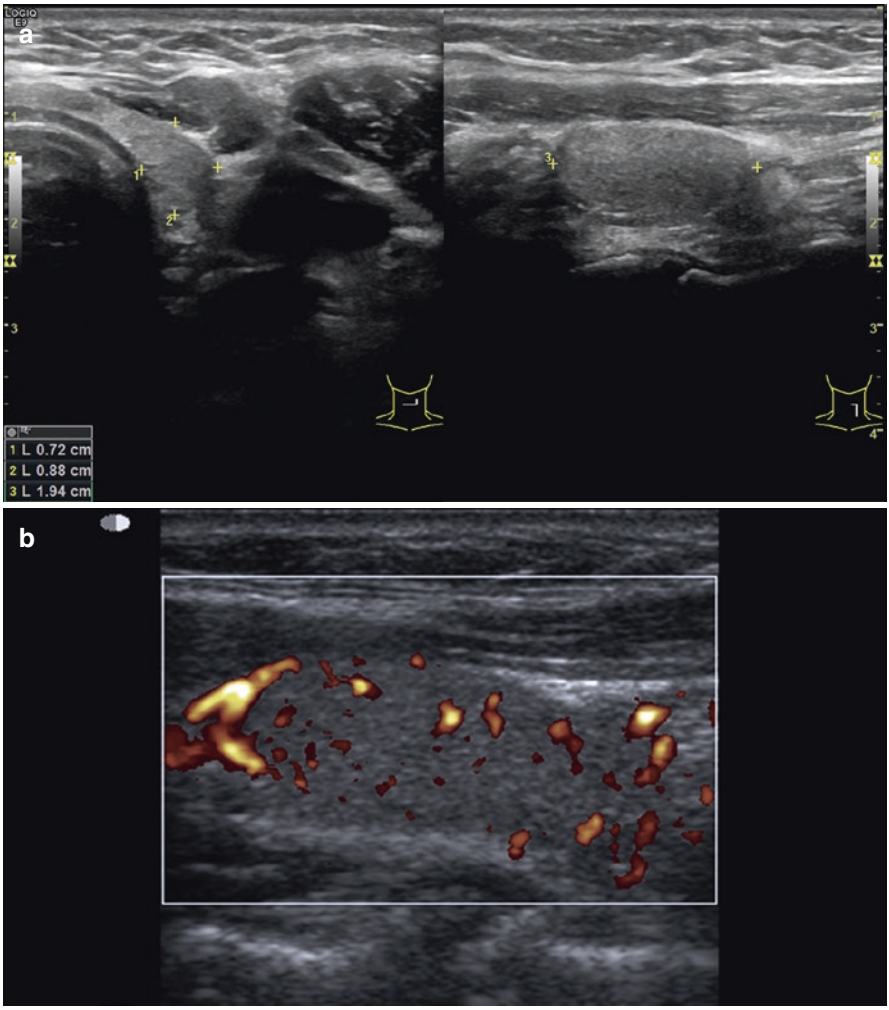

Fig. 9.5 Status 5 years after thyroid surgery. Thyroid remnant. (**a**) Grayscale US image. Transverse and longitudinal scans. (**b**) PDI

After surgery for benign thyroid diseases, patients should undergo thyroid US at 3, 6, and 12 months after the operation during the first year and once a year after that.

Each scheduled US follow-up permits the precise characterization of the thyroid bed and residue, allowing the potential for future recurrence to be determined.

The Example of US Report in Postoperative Neck

- First name, middle initial, last name:
- Age:
- Date:
- The number of case history:
- US scanner:

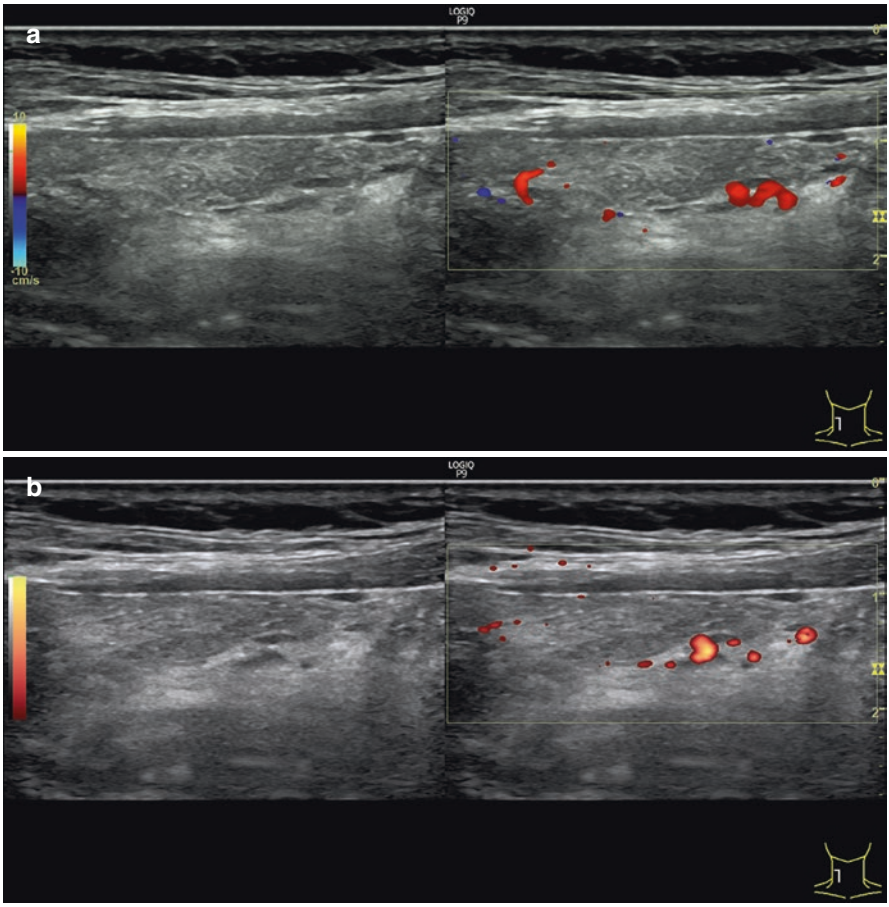

Fig. 9.6 Status 1 year after radioiodine (^{131}I) treatment. Sonogram, longitudinal scan. (**a**) Grayscale US and CDI. (**b**) Grayscale US and PDI

The thyroid is operated on (the surgery, 2010; pathology, unknown).

The *isthmus* is removed		
Right lobe		*Left lobe*
Depth	20 mm	Is removed. Thyroid tissue, cystic, and solid lesions are not detected in the bed of the lobe. The vascular bundle is displaced medially
Width	19 mm	
Length	42 mm	
Volume	8.0 cm^3	

The *total volume* 8.0 cm^3 does not exceed the upper limit.

The echodensity of parenchyma of the thyroid residue is slightly diffusely decreased and heterogeneous. The lesions are not detected. Vascular pattern intensity of the parenchyma is slightly decreased in CDI and PDI. CPD is up to 5–10%.

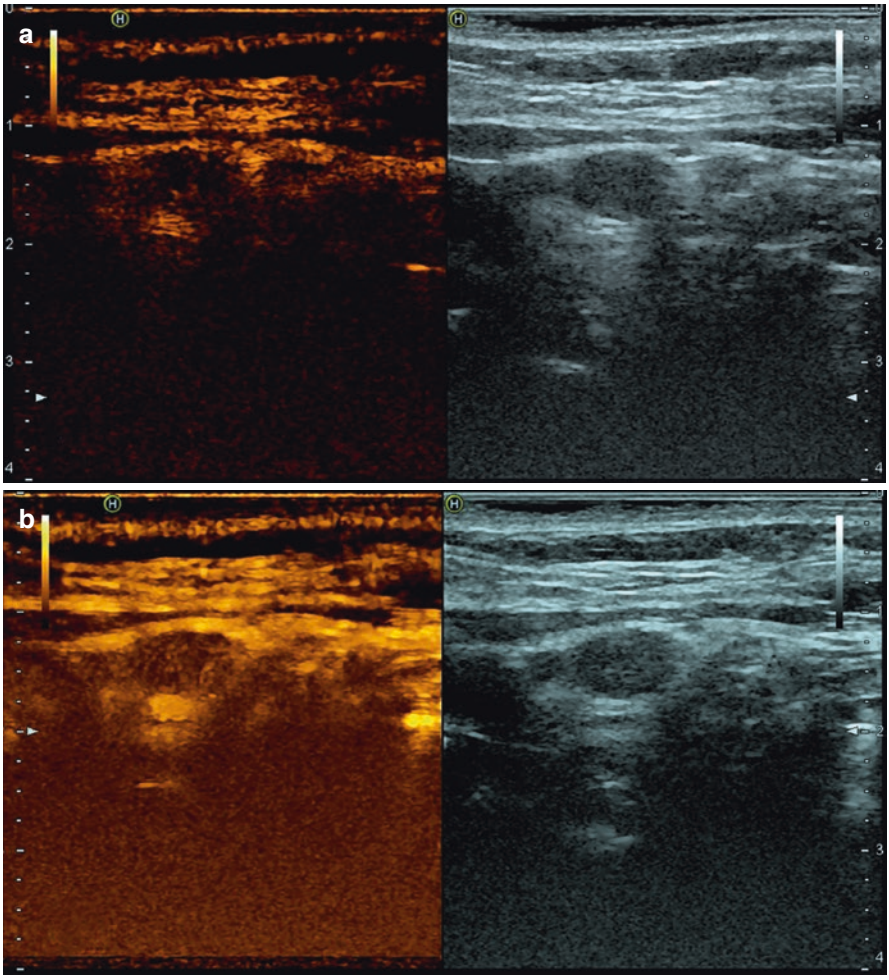

Fig. 9.7 (**a**, **b**) Detection of a thyroid remnant in the thyroid bed. CEUS with SonoVue® 2.4 ml

The lymph nodes in the neck and supra- and infraclavicular areas are not enlarged. *Conclusion: The status after hemithyroidectomy. No recurrence is determined.* US specialist:

9.2 Recurrent Thyroid Lesions

Postoperative recurrent goiter is characterized by the reappearance of thyroid pathology in patients who have previously been operated on for this condition. Recurrence is considered to be the thyroid disease that was observed prior to the surgery and was the reason for the operation. According to Akinchev and Romanchishen [4], 89% of the diseases in a thyroid remnant are primary thyroid diseases. However, diseases

that are different from the preoperative abnormality arise in some patients. Such cases should be considered new diseases of the thyroid remnant. The rates of recurrence for various thyroid diseases are as follows: multinodular nontoxic goiter 54.7%, Graves' disease 14.5%, nodular nontoxic goiter 13.1%, multinodular toxic goiter 6.8%, thyroid cancer 1.3%, cancer with another pathology 2.8%, AIT 2.3%, nodular toxic goiter 1.7%, and undifferentiated thyroid cancer 0.8% [4].

Some authors differentiate between false and true recurrences. False recurrences are detected soon after surgery. A false recurrence is actually associated with inadequate revision during the operation, which results in some remnant of the lesion being left in the thyroid gland. True recurrence appears much later, in the unchanged tissue of the thyroid residue, and has the same causes as the primary lesion.

US is the main visualizing method used for the early diagnosis of recurrent goiter. The most frequent US features of recurrent nodular goiter are as follows (Fig. 9.8):

- Lesion in the thyroid bed or thyroid residue
- Roundish or oval shape of lesion
- Hyper- and hypoechodensity
- Heterogeneous echostructure
- Regular, well-defined margins
- Additional lesions during the course of lymphatic drainage of the neck (in cases with thyroid cancer recurrence and metastases)
- Different types of vascularity in CDI and PDI
- Any elasticity with compression US elastography

It is not correct to use the term "recurrence" in relation to AITD, because autoimmune diseases initially affect the whole thyroid gland, so the part that remains after the surgery is sure to be affected, as surgical treatment does not interrupt the pathogenesis of the disease (Fig. 9.9).

In accordance with the American Joint Committee on Cancer [5], cancer in the thyroid residue and metastases in regional lymph nodes that are detected within 3 months of surgery and remote metastases found within 6 months of surgical treatment are regarded as cancer recurrences.

The frequency of long-term recurrent nodular goiter (relative to all operated patients) after surgery is 1.8–88%. The incidence of thyroid cancer in recurrent goiter is 10–31.7%, including 6.8–30% for well-differentiated cancer and 30–88% for poorly or undifferentiated cancer [3, 6]. According to Akinchev and Romanchishen [4], the incidence of new cases of thyroid cancer in recurrent goiter is about 4.9%.

Thyroid cancer recurrence is usually diagnosed 2–10 years (up to 30%) after the operation, with the ratio of men to women affected is 1:4, with an average age of 31–60 years [7]. It is usually seen on the side of the primary lesion (43.8%), on the opposite side in 30.2%, and on both sides in 26%.

Recurrent cancer is usually characterized by the same US features as the primary tumor. However, it exhibits rare calcifications, often an increased vascularity, and invasion into the surrounding organs (Fig. 9.10).

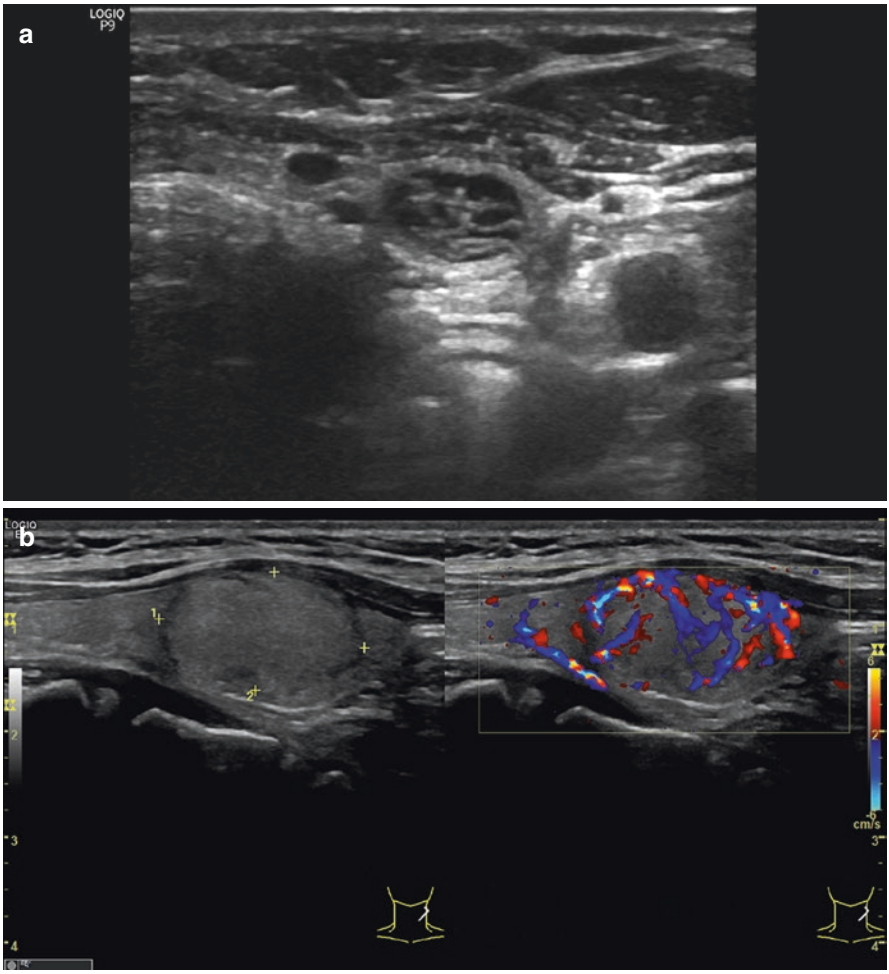

Fig. 9.8 Status after thyroid surgery. Recurrent nodular goiter. (**a**) Grayscale. (**b**) Grayscale US and CDI

Recurrent thyroid cancer is represented by the following histological types: papillary, 50–80%; follicular, 15–40%; and poorly or undifferentiated carcinoma, 2–5% of cases [8]. The diagnosis of thyroid cancer in recurrent goiter is extremely complex and demands the use of a combination of all diagnostic options and technologies. The sensitivity of US to local recurrence of thyroid cancer is 83–93.6%; its specificity is 90.2–92% and its diagnostic accuracy is 90–91% [8]. Publications on new ultrasound methods, such as US elastography, 3D image reconstruction, multiplanar scanning, and CEUS, are mainly related to the diagnosis of primary thyroid cancer; their efficacy in diagnosis of thyroid cancer recurrence is expected. Suspicion for recurrent thyroid cancer is an indication for US-guided FNAB.

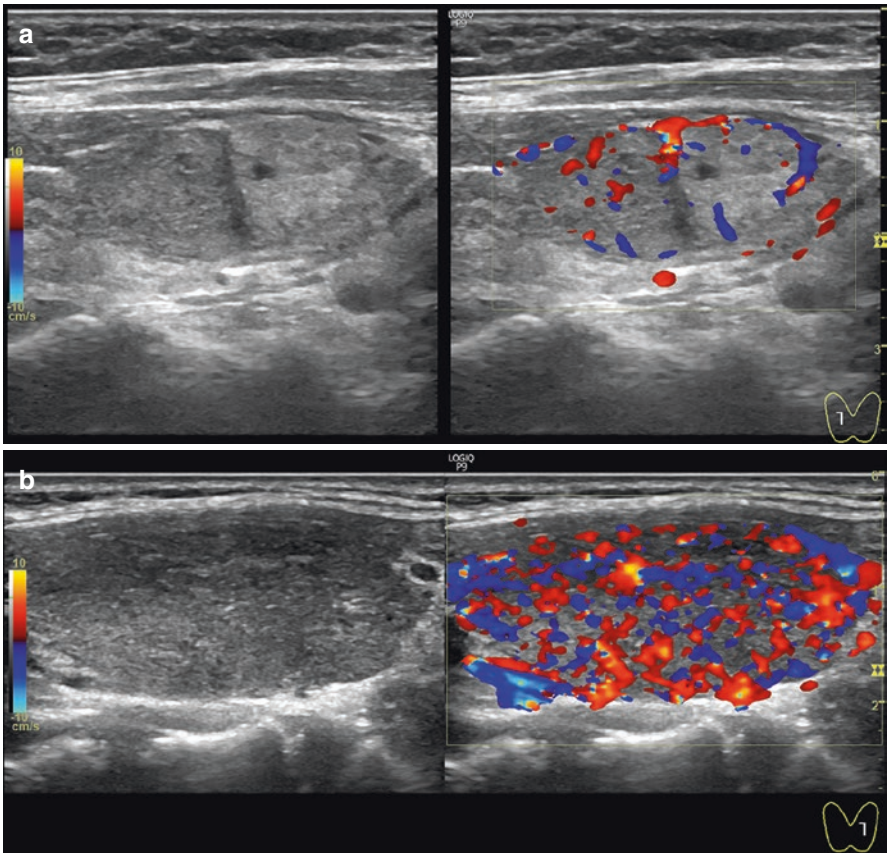

Fig. 9.9 Status after thyroid surgery. Grayscale US and CDI. (**a**) AIT. (**b**) Graves' disease

The Example of US Report in Recurrent Nodular Goiter

- First name, middle initial, last name:
- Age:
- Date:
- The number of case history:
- US scanner:

The thyroid is operated on (the surgery, 2001; pathology, simple colloid goiter).

The *isthmus* is removed		
Right lobe		*Left lobe*
Depth	17 mm	Is removed. Thyroid tissue, cystic, and solid lesions are not detected in the bed of the lobe. The vascular bundle is displaced medially
Width	17 mm	
Length	38 mm	
Volume	5.3 cm^3	

The *total volume* 5.3 cm^3 does not exceed the upper limit.

Two isoechoic heterogeneous avascular nodules of 0.6 × 0.5 × 1.0 cm and 0.6 × 0.9 × 1.0 cm in size with well-defined regular margins and small fluid inclusions are located in the middle compartment of the lobe.

The structure and vascularity of the parenchyma of the thyroid residue is normal. CPD is up to 5–10%.

The lymph nodes in the neck and supra- and infraclavicular areas are not enlarged.

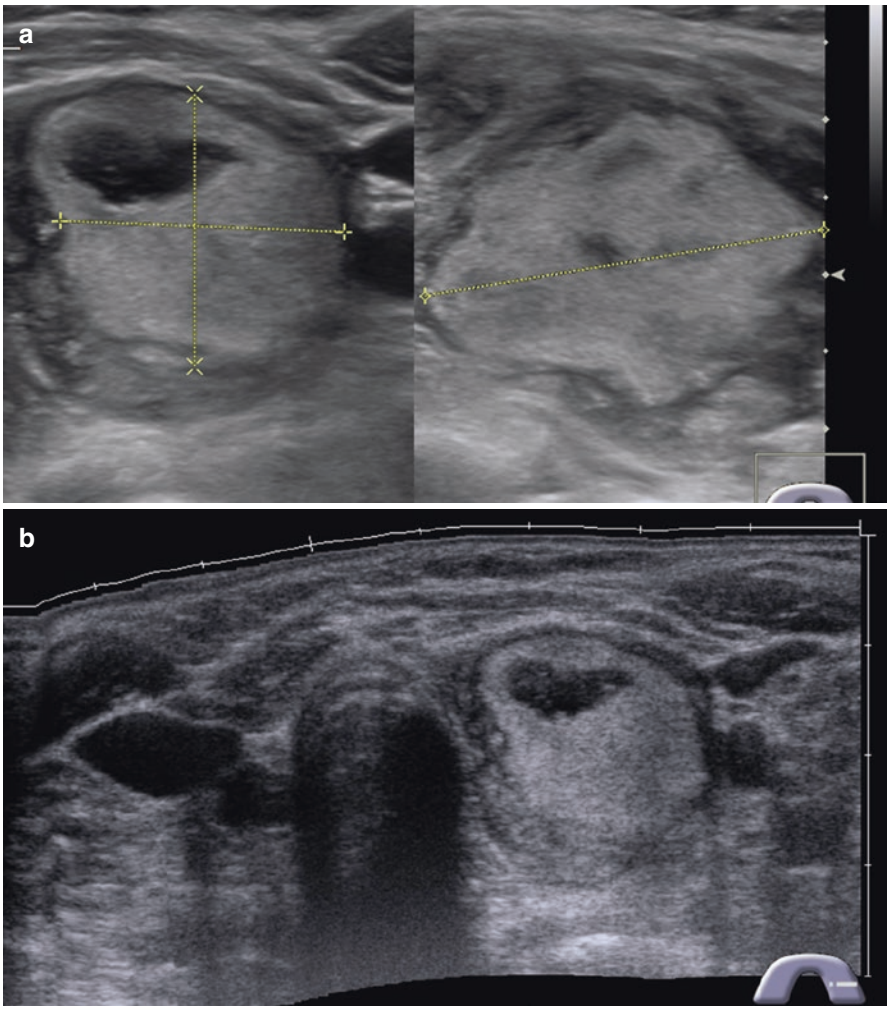

Fig. 9.10 Status after thyroid surgery. Recurrent thyroid cancer. (**a**) Grayscale US. (**b**) Panoramic scan. (**c**) 3D power Doppler reconstruction. (**d**) Measurement of elasticity with ARFI

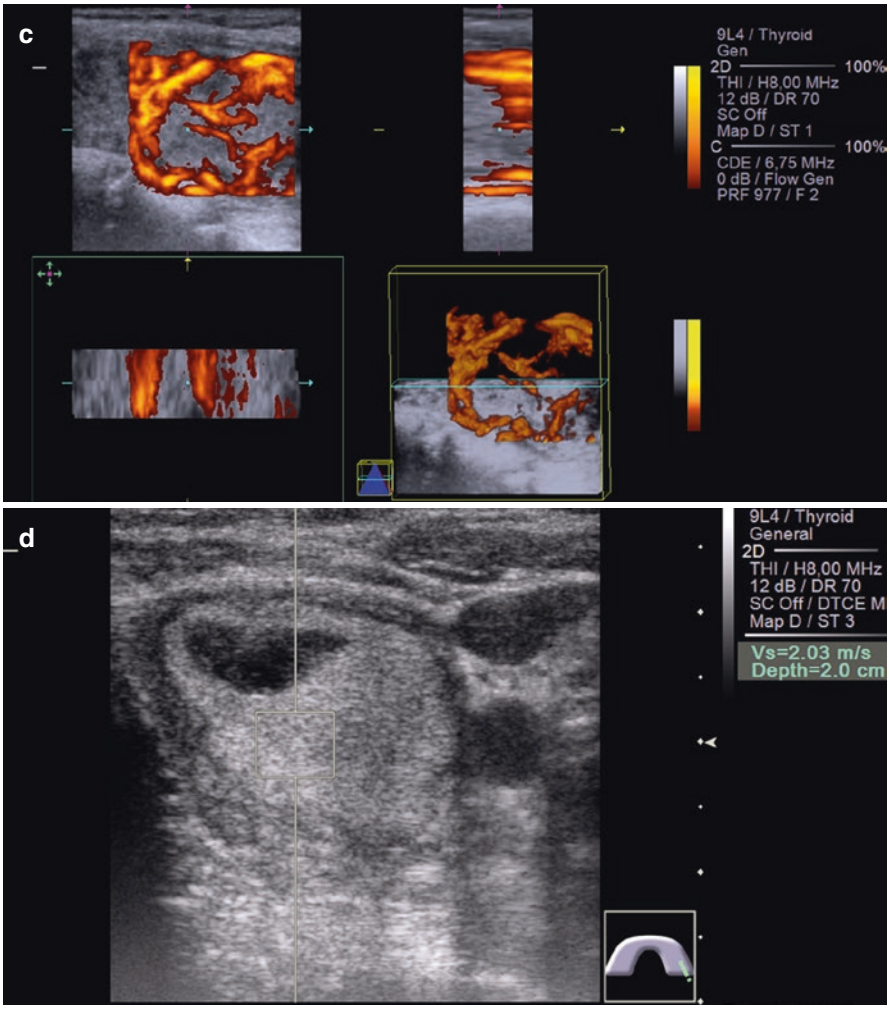

Fig. 9.10 (continued)

Conclusion: The status after hemithyroidectomy. Nodules of the right lobe remnant, TIRADS 2.

US specialist:

The Example of US Report in Recurrent Thyroid Cancer

- First name, middle initial, last name:
- Age:
- Date:
- The number of case history:
- US scanner:

The thyroid gland is removed (the surgery, 2012; histopathology, papillary carcinoma).

A heterogeneous hypoechoic lesion of 2.3 × 2.2 × 3.6 cm in size of irregular shape, with indistinct margins and small anechoic areas, hypervascular in CDI and PDI is located in the right thyroid lobe bed.

No lesions are detected in the left lobe bed and isthmus site.

The left vascular bundle is displaced medially.

Bilateral enlarged lymph nodes along IJV are located: at the right side up to 0.6 × 1.9 cm hypoechoic, heterogeneous, avascular; at the left side up to 0.7 × 2.4 cm, hypoechoic, heterogeneous, hypovascular with moderate chaotic vascularity throughout the cortex, of irregular shape with the tendency to merging. The lymph nodes in supra- and infraclavicular areas are not enlarged.

Conclusion: The status after thyroid surgery. Right neck lesion, the image suggests thyroid carcinoma recurrence. Suspicion for bilateral metastases in the lymph nodes of the neck.

US specialist:

References

1. Salvatori M, Raffaelli M, Castaldi P, et al. Evaluation of the surgical completeness after total thyroidectomy for differentiated thyroid carcinoma. Eur J Surg Oncol. 2007;33:648–54.
2. Sencha AN, Belyaev DV. Ultrasonic analysis of the thyroid gland after total thyroidectomy. Medicinskaya visualizaciya. Special issue. Materials 2 of the All-Russian National Congress of Radiation Diagnostics and Radiotherapists “Radiology-2009”. 2009;S363–S364 (Article in Russian).
3. Altunina VS. Ultrasound diagnosis of recurrence of thyroid cancer. PhD thesis. Obninsk (Book in Russian); 1996.
4. Akinchev AL, Romanchishen AF. Postoperative recurrent goiter. Vestn Khir Im II Grek. 2005;5:43–46 (Article in Russian).
5. Amin MB, Edge S, Greene F, editors. AJCC cancer staging manual. Basel: Springer; 2017.
6. Paches AI, Propp RM. Thyroid cancer. Moscow (Book in Russian); 1995.
7. Sencha AN. Diagnosis of thyroid cancer by ultrasound. PhD thesis. Moscow (Book in Russian); 2001.
8. Sencha AN. Ultrasonic visualization of malignant tumors of the thyroid gland. Ultrazvukovaya Funkc Diagn. 2008;2:20–29 (Article in Russian).

Thyroid Disorders and Female Reproductive System Diseases: The Thyroid Gland and Pregnancy

10

Antonina A. Smetnik, Alexander N. Sencha, and Stanislav V. Pavlovich

The condition and function of the thyroid gland and the reproductive system of the female body are closely interrelated with each other due to common central regulation. Thyroid diseases are more typical for fertile women than for any other population [1]. Thyroid function influences all stages of development and function of the female reproductive system, inclusive of menstrual cycle regulation, fertility, gestation, and postpartum period.

Pregnancy has a significant effect on the thyroid gland and its functional activity. During pregnancy, the thyroid gland increases in volume up to 10% in women of iodine sufficient areas and by 20–40% in areas with iodine deficiency. Normal pregnancy is accompanied with an increase in renal excretion of iodine, the level of thyroxin-binding proteins, and thyroid hormone production. Stimulating effect of human chorionic gonadotropin (hCG) on the thyroid gland during pregnancy leads to decrease in serum thyroid-stimulating hormone (TSH). According to Alexander et al. [2], thyroxine production can increase by 40–50% to maintain euthyroidism during pregnancy.

All types of thyroid pathology in regard to female reproduction system may be divided into the following two groups: dysfunction of the gland (hypothyroidism and thyrotoxicosis) and abnormalities of thyroid structure (increase in volume and

A. A. Smetnik (✉)
Department of Gynecological Endocrinology, National Medical Research Centre for Obstetrics, Gynecology and Perinatology, Ministry of Healthcare of the Russian Federation, Moscow, Russia

A. N. Sencha
Department of Visual and Functional Diagnostics, National Research Center for Obstetrics, Gynecology and Perinatology, Ministry of Healthcare of the Russian Federation, Moscow, Russia

S. V. Pavlovich
Academic Council of National Research Center for Obstetrics, Gynecology and Perinatology, Ministry of Healthcare of the Russian Federation, Moscow, Russia

A. N. Sencha, Y. N. Patrunov (eds.), *Thyroid Ultrasound*,
https://doi.org/10.1007/978-3-030-14451-7_10

thyroid lesions). Thyroid dysfunction has the most important influence, since it directly affects menstrual cycle, ovulation, conception, and gestation.

Autoimmune thyroid disease occurs in 10% of fertile women and is the main cause of thyroid dysfunction. Currently, active research is underway to determine whether the autoimmune process itself can affect the reproductive system and the ability to conceive and carry pregnancy without affecting the thyroid function. Perminova [3] reports the association of AITD with idiopathic infertility, endometriosis, and endocrine infertility (Fig. 10.1). According to Alexander et al. [2], euthyroid women with infertility more often have an increased level of anti-TPO antibodies, compared to fertile women of the same age group. According to Quintino-Moro et al. [4], infertility was registered in 47% of women of 18–50 years with AITD.

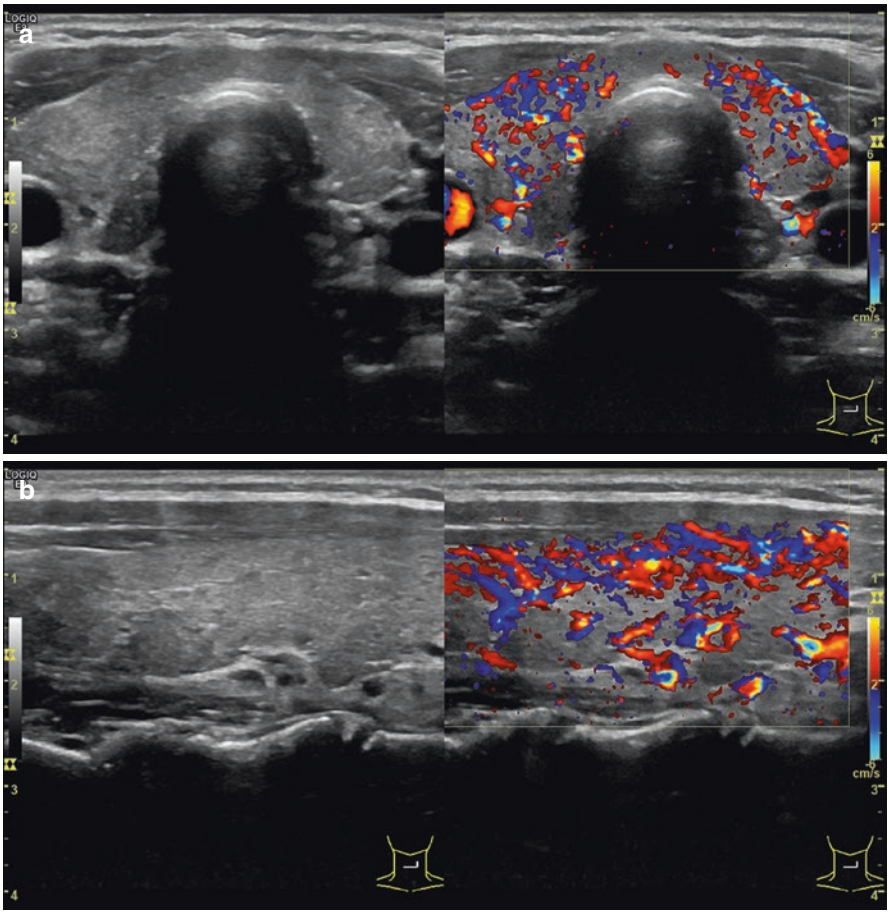

Fig. 10.1 AIT in a patient with diffuse type of chronic adenomyosis and secondary infertility. Grayscale US and CDI. (**a**) Transverse scan. (**b**) Longitudinal scan

According to Kachuei et al. [5], higher prevalence of increased levels of antithyroid antibodies is observed in women with polycystic ovary syndrome. Antithyroid antibodies were also detected in the ovarian follicles in women with AIT and their level correlated with the level of antibodies in the serum [6]. However, their effect on oocytes remains unknown.

The data on the outcomes of assisted reproductive technology programs depending on the presence of antithyroid antibodies is contradictory. Some researchers propose to prescribe thyroxin therapy to women without identified hypothyroidism, but with highly normal levels of TSH, to improve the prognosis of IVF, but not all support this tactic [7–12]. A number of studies with meta-analyses indicate an increase in pregnancy loss rates, including habitual miscarriages, in women with an increased level of antithyroid antibodies [13, 14], as well as the relationship between AIT and preterm delivery [15]. Some studies report increased perinatal mortality [16]. However, not in all publications support this data [17, 18]. In several groups of patients, an increased risk of placental abruption was observed in women with AIT without clinical hypothyroidism [17, 19]. AIT was also associated with postpartum depression [20] and neonatal respiratory distress syndrome [18].

Hypothyroidism can have a significant impact on the reproductive system of a woman. This condition is easily detected and, unlike autoimmune status, is well managed with drug therapy. Both manifest (TSH ≥ 10 mIU/L and/or low free thyroxin) and subclinical (TSH 4–10 mIU/L and normal free thyroxine) hypothyroidisms are a well-studied risk factor for chronic anovulation and infertility. According to Alexander et al. [2], 68% of women with hypothyroidism (with TSH >15 mIU/L) had irregular menstrual cycle, in contrast to the control group with 12% of menstrual disorders. In a retrospective study, Yoshioka et al. [21] reported that 84% of women with infertility and subclinical hypothyroidism successfully became pregnant after a short period of treatment with levothyroxine.

According to van den Boogaard et al. [22] and Alexander et al. [2], manifest hypothyroidism increases the risk of complications in existing pregnancy, such as premature birth and miscarriage, and negatively affects neurocognitive development of the fetus (Fig. 10.2). In this regard, such patients should immediately get the replacement therapy.

The controversial issue remains the effect of subclinical hypothyroidism on pregnancy, since the reference values of TSH may vary depending on the population, iodine deficiency, and associated risk factors, the level of antithyroid antibodies, in particular. The American Thyroid Association (ATA) in 2011 and European Thyroid Association (ETA) in 2014 suggested the trimester-specific reference values of TSH (Table 10.1) to therapy hypothyroidism regardless of the levels of anti-TG and anti-TPO antibodies [23, 24].

In 2017, ATA, in contrast to previous recommendations, proposed a new approach. It recommends not to prescribe levothyroxine to women during the first trimester with TSH 2.5–4.0 mIU/L and low levels of antithyroid antibodies. With the increase in the level of antibodies and TSH of 2.5–4.0 mIU/L, as well as at low levels of antibodies and TSH of 4.0–10 mIU/L, the decision on starting replacement therapy is taken individually [2]. Currently, there are active discussions on this issue, since the

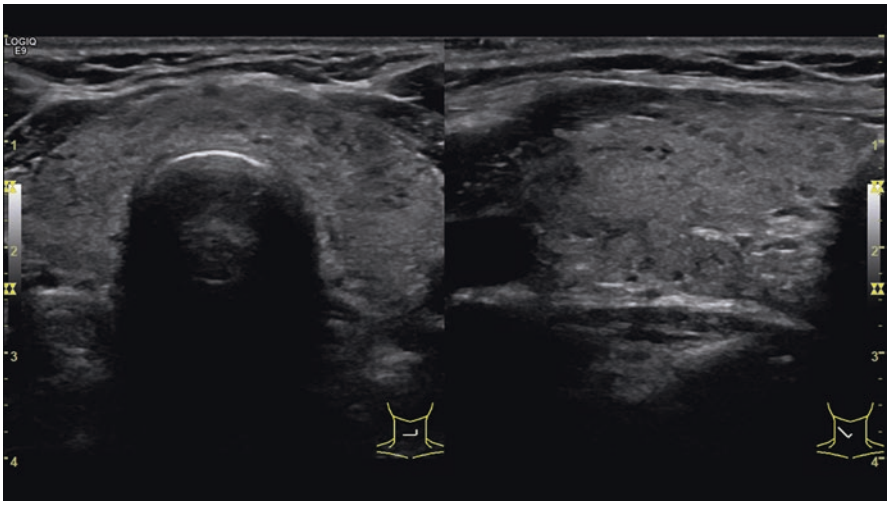

Fig. 10.2 Primary hypothyroidism associated with AIT in a 36-week pregnant woman. Grayscale US

Table 10.1 Trimester-specific reference values of TSH, mIU/L

	American Thyroid Association, 2011	European Thyroid Association, 2014
1st trimester	0.1–2.5	0.1–2.5
2nd trimester	0.2–3.0	0.2–3.0
3rd trimester	0.3–3.0	0.3–3.5

data of research on the effect of mild subclinical hypothyroidism on pregnancy outcomes are ambiguous. A number of studies demonstrated that women with subclinical hypothyroidism and AIT are at risk of early miscarriage [25]. Chan and Boelaert [26] and Maraka et al. [27] showed a correlation between subclinical hypothyroidism and preterm delivery, gestational diabetes, gestational hypertension, eclampsia, fetal growth retardation, and low birth weight. However, the results of Bernardi et al. [28] showed no significant differences in the number of newborns between the groups of patients with euthyroidism and treated and untreated subclinical hypothyroidism.

The same contradictory data is also available for prediction of cognitive function in children. According to Shan et al. [29], subclinical mother's hypothyroidism is a significant predictor of a decrease in the intellectual and physical development in children aged 25–30 months. However, the data of Krassas et al. [30] on the effects of subclinical hypothyroidism of mothers on the IQ score in their 9–10-year-old children suggests otherwise.

Thyrotoxicosis, regardless of the cause, can lead to menstrual cycle disorders. According to Krassas et al. [30], women with hyperthyroidism had irregular menstrual cycle in 22%, which is higher as compared with 8% of women of the control group with euthyroidism.

However, thyrotoxicosis is not a cause of infertility. According to Alexander et al. [2], the incidence of hyperthyroidism (both subclinical and manifest) was

similar in the group of infertile women and the control group of women with normal fertility. Unlike hypothyroidism, in which treatment is practically independent of the cause, clarifying the etiology of thyrotoxicosis is of fundamental importance, since tactics may vary significantly.

Thyrotoxicosis may be the result of the following conditions:

- Hyperproduction of thyroid hormones (Graves' disease, toxic adenoma, iodine-induced thyroiditis type 1)
- Destruction of the thyroid gland (thyrotoxic phase of AIT, subacute or postpartum thyroiditis, iodine-induced thyroiditis type 2)
- Other specific causes (e.g., a TSH-secreting tumor of the pituitary gland, transient gestational hyperthyroidism, cystic skid, etc.)

The management directly depends on the cause. Destruction of the thyroid gland commonly requires no specific treatment. Planning of pregnancy should begin after the finalization of the destructive process and adequate correction of hypothyroidism.

Gestational hyperthyroidism associated with the excessive effect of hCG on TSH receptors in early pregnancy, in fact, is not a disease. It does not require specific treatment, despite the fact that it can worsen the condition of pregnant women, leading to weight loss, tachycardia, toxicosis, and sometimes the indomitable vomiting of pregnant women.

The most common cause of hyperthyroidism in women of childbearing age is Graves' disease. It is registered in 0.4–1.0% of women before pregnancy and approximately in 0.2% during pregnancy [31]. The stimulating antibodies to TSH receptors play a key role in the pathogenesis of Graves' disease. They are also able to penetrate the placental barrier, stimulate the thyroid gland of the fetus, and cause transient thyrotoxicosis.

The US image of the thyroid gland in Graves' disease during pregnancy is the same as in nonpregnant patients. The main features are as follows: decreased echogenicity of the thyroid parenchyma, heterogeneity of the echostructure due to multiple hypoechoic areas, and increased vascularization (Fig. 10.3).

Unlike Graves' disease, thyrotoxicosis due to toxic adenoma proceeds more favorably during pregnancy, since antibodies to the TSH receptors are not produced in the mother's body. Therefore, the thyroid gland of the fetus is not stimulated, as in Graves' disease. However, the risks in both untreated thyrotoxicosis and with thyrostatic therapy remain. Therefore, solving the problem of thyrotoxicosis before pregnancy is the best approach. In most cases surgical treatment or radioiodine therapy is indicated. Toxic adenoma exhibits typical ultrasound signs (Fig. 10.4).

The enlargement of the thyroid gland in the case of normal thyroid function does not affect the female reproductive system. If a pregnant woman is diagnosed of a thyroid nodule, two aspects need to be discussed concerning the thyroid hormonal disorders and benign/malignant nature of the lesion. Lesions smaller than 1 cm without ultrasound signs of malignancy and with unchanged function of the gland commonly do not require clinical attention and imply only ultrasound and biochemical follow-up. Larger lesion with US signs that are suspicious of a tumor should be further examined regardless of whether they were detected before or during

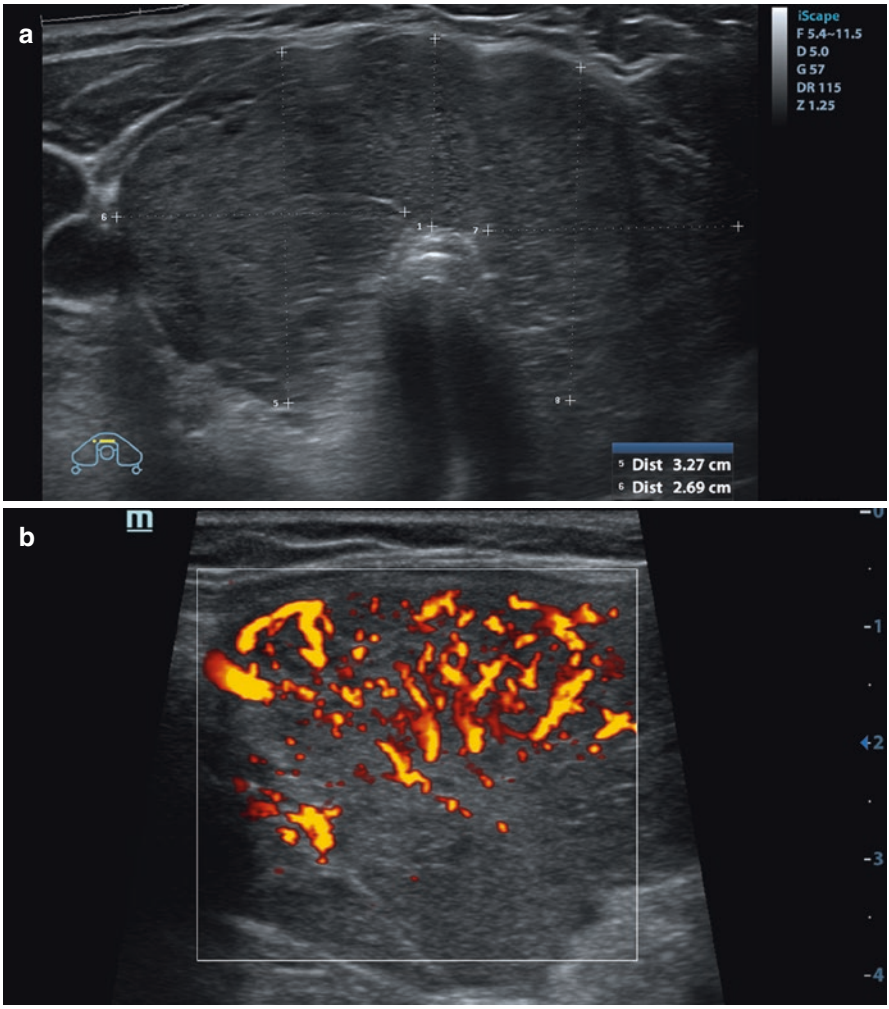

Fig. 10.3 Hyperthyroidism in a 31-week pregnant woman with Graves' disease. (**a**) Grayscale US. Panoramic transverse scan. (**b**) PDI

pregnancy. Multiparametric echography of thyroid lesions with implementation of TIRADS permits the malignancy risk stratification and a more reasonable approach to the indication of FNAB.

Thyroid US in pregnant women is done with the same technique and technologies as in all other people. The only exception is that ultrasound contrast media are not permitted for use during the entire gestation and the subsequent lactation period.

Benign colloid nodes do not require treatment. Adequate iodine supplement and follow-up inclusive of ultrasound imaging are advised (Fig. 10.5). The incidence of benign thyroid nodules during pregnancy is variable and depends mainly on the population, region of residence, genetic, and other individual factors.

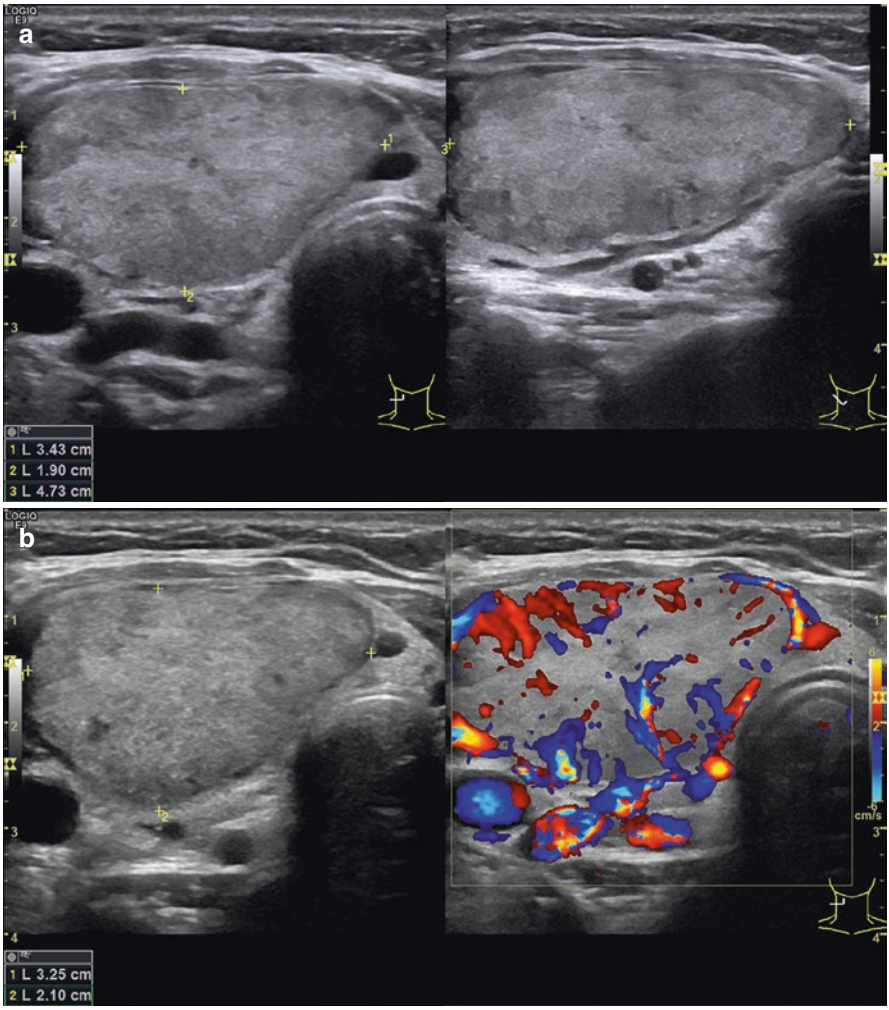

Fig. 10.4 Toxic thyroid adenoma. Hyperthyroidism. Pregnancy 37 weeks. Echograms of the thyroid gland. (**a**) Grayscale US. (**b**) CDI. Hypervascular lesion with typical vascular pattern

Malignant thyroid nodules diagnosed with FNAB and cytology in pregnant women demand a different management. Smith et al. [32] in a population-based retrospective analysis revealed the incidence of thyroid cancer during pregnancy of 14.4 per 100,000. The management of highly differentiated thyroid cancer in pregnancy depends on the term of gestation. When diagnosed in the first trimester of pregnancy, follow-up is recommended. In the case of a significant growth of the nodule, a change in its structure or vascularization, surgical treatment is proposed in the second trimester. If thyroid cancer is detected in 2nd–3rd trimesters, surgical treatment is usually delayed for the postpartum period. This is due to the fact that highly differentiated thyroid cancer does not progress rapidly during pregnancy [1] (Fig. 10.6). Other less differentiated types of thyroid cancer require a more aggressive medical approach.

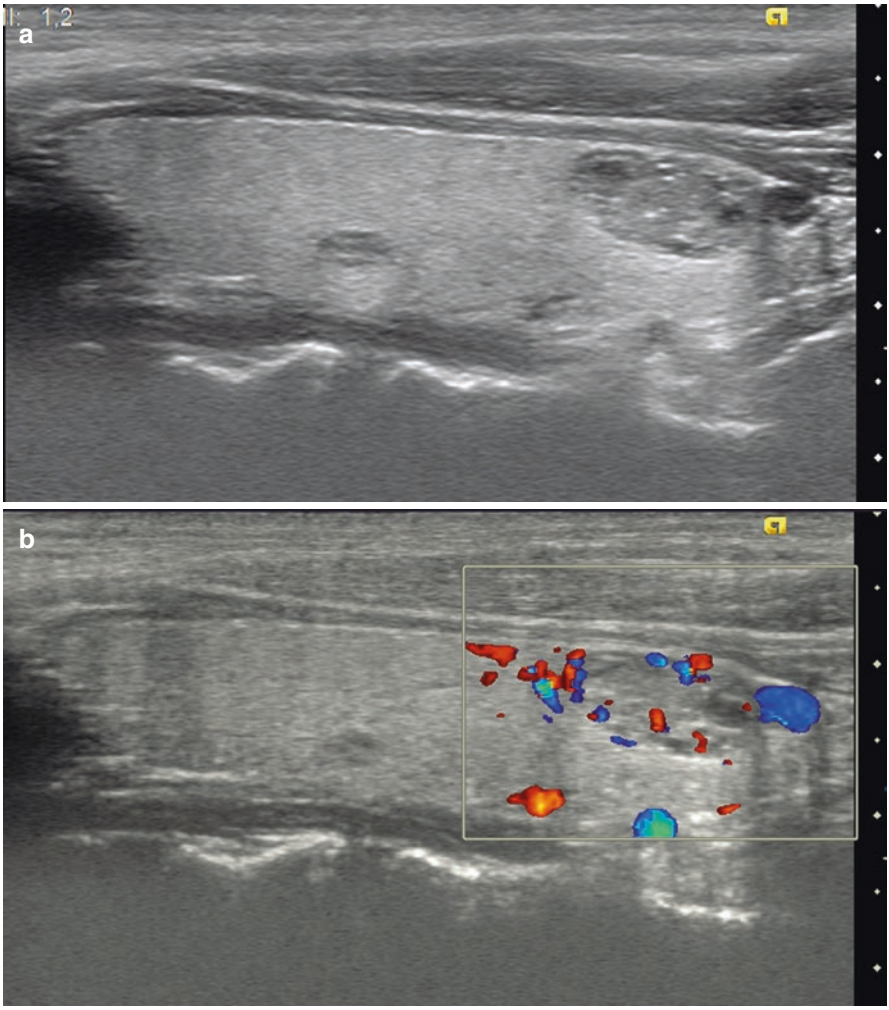

Fig. 10.5 Colloid nodule. Pregnancy 34 weeks. (**a**) Grayscale US. (**b**) CDI. The nodule exhibited no change during 3 years of follow-up

It is important to plan pregnancy only after ultrasound and biochemical tests confirm full remission of cancer. Pregnancy is considered not to increase the risk of thyroid cancer recurrence in women with the history of cured cancer. These women do not require any special monitoring during pregnancy, except for correction of postoperative hypothyroidism [1].

Understanding the mutual influence of the thyroid gland and the female reproductive system, as well as the timely diagnosis and therapeutic correction of the functional status of the thyroid gland, is an important factor necessary for the successful realization of female reproductive function.

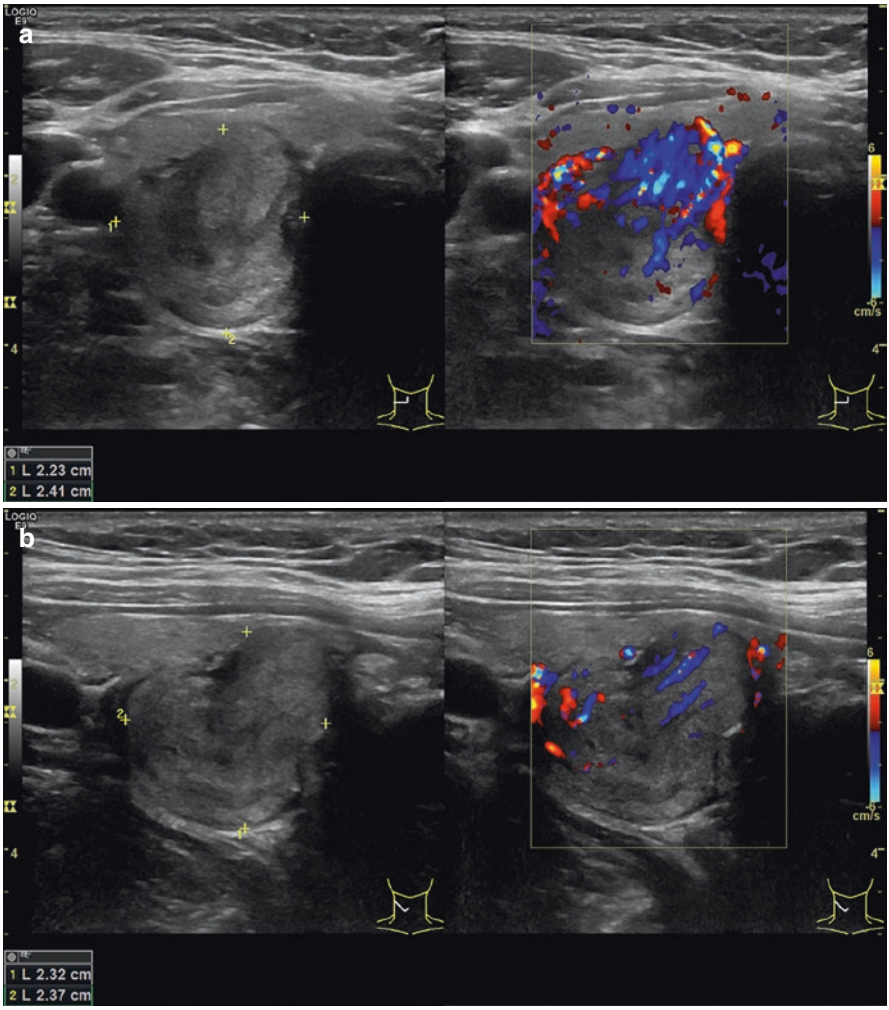

Fig. 10.6 Papillary thyroid cancer in a 38-week pregnant woman. Grayscale US and CDI. (**a**) Transverse scan. (**b**) Longitudinal scan. The tumor was verified with FNAB and cytology at 34 weeks of gestation. The woman had a successful surgery 45 days after delivery

References

1. Haugen BR, Alexander EK, Bible KC, et al. 2015 American Thyroid Association management guidelines for adult patients with thyroid nodules and differentiated thyroid cancer: the American Thyroid Association guidelines task force on thyroid nodules and differentiate d thyroid cancer. Thyroid. 2016;26(1):1–133.
2. Alexander EK, Pearce EN, Brent GA, et al. Guidelines of the American Thyroid Association for the diagnosis and management of thyroid disease during pregnancy and the postpartum. Thyroid. 2017;27(3):315–89.

3. Perminova SG. Pathology of the thyroid gland in women with infertility. Clin Exp Thyroidol. 2011;7(4):44–50.
4. Quintino-Moro A, Zantut-Wittmann DE, Tambascia M, et al. High prevalence of infertility among women with Graves' disease and Hashimoto's thyroiditis. Int J Endocrinol. 2014:982705. https://doi.org/10.1155/2014/982705.
5. Kachuei M, Jafari F, Kachuei A, Keshteli AH. Prevalence of autoimmune thyroiditis in patients with polycystic ovary syndrome. Arch Gynecol Obstet. 2012;285(3):853–6.
6. Monteleone P, Parrini D, Faviana P, et al. Female infertility related to thyroid autoimmunity: the ovarian follicle hypothesis. Am J Reprod Immunol. 2011;66(2):108–14.
7. Chai J, Yeung WY, Lee CY, et al. Live birth rates following in vitro fertilization in women with thyroid autoimmunity and/or subclinical hypothyroidism. Clin Endocrinol. 2014;80(1):122–7.
8. Karacan M, Alwaeely F, Cebi Z, et al. Effect of antithyroid antibodies on ICSI outcome in antiphospholipid antibody-negative euthyroid women. Reprod Biomed Online. 2013;27(4):376–80.
9. Łukaszuk K, Kunicki M, Kulwikowska P. The impact of the presence of antithyroid antibodies on pregnancy outcome following intracytoplasmatic sperm injection-ICSI and embryo transfer in women with normal thyreotropine levels. J Endocrinol Investig. 2015;38(12):1335–43.
10. Tan S, Dieterle S, Pechlavanis S, et al. Thyroid autoantibodies per se do not impair intracytoplasmic sperm injection outcome in euthyroid healthy women. Eur J Endocrinol. 2014;170(4):495–500.
11. Toulis KA, Goulis DG, Venetis CA, et al. Risk of spontaneous miscarriage in euthyroid women with thyroid autoimmunity undergoing IVF: a meta-analysis. Eur J Endocrinol. 2010;162(4):643–52.
12. Zhong YP, Ying Y, Wu HT, et al. Relationship between antithyroid antibody and pregnancy outcome following in vitro fertilization and embryo transfer. Int J Med Sci. 2012;9(2):121–5.
13. Chen L, Hu R. Thyroid autoimmunity and miscarriage: a meta-analysis. Clin Endocrinol. 2011;74(4):513–9.
14. Thangaratinam S, Tan A, Knox E, et al. Association between thyroid autoantibodies and miscarriage and preterm birth: meta-analysis of evidence. BMJ. 2011;342:d2616.
15. Negro R. Thyroid autoimmunity and pre-term delivery: brief review and meta-analysis. J Endocrinol Investig. 2011;34(2):155–8.
16. Männistö T, Vääräsmäki M, Pouta A, et al. Perinatal outcome of children born to mothers with thyroid dysfunction or antibodies: a prospective population-based cohort study. J Clin Endocrinol Metab. 2009;94(3):772–9.
17. Abbassi-Ghanavati M, Casey BM, Spong CY, et al. Pregnancy outcomes in women with thyroid peroxidase antibodies. Obstet Gynecol. 2010;116(2 Pt 1):381–6.
18. Negro R, Schwartz A, Gismondi R. Thyroid antibody positivity in the first trimester of pregnancy is associated with negative pregnancy outcomes. J Clin Endocrinol Metab. 2011;96(6):E920–4.
19. Haddow JE, Cleary-Goldman J, McClain MR, First- and Second-Trimester Risk of Aneuploidy (FaSTER) Research Consortium, et al. Thyroperoxidase and thyroglobulin antibodies in early pregnancy and preterm delivery. Obstet Gynecol. 2010;116(1):58–62.
20. Groer MW, Vaughan JH. Positive thyroid peroxidase antibody titer is associated with dysphoric moods during pregnancy and postpartum. J Obstet Gynecol Neonatal Nurs. 2013;42(1):E26–32.
21. Yoshioka W, Amino N, Ide A, et al. Thyroxine treatment may be useful for subclinical hypothyroidism in patients with female infertility. Endocr J. 2015;62:87–92.
22. Van den Boogaard E, Vissenberg R, Land JA, et al. Significance of (sub)clinical thyroid dysfunction and thyroid autoimmunity before conception and in early pregnancy: a systematic review. Hum Reprod Update. 2011;17(5):605–19.
23. Lazarus J, Brown RS, Daumerie C, et al. European thyroid association guidelines for the management of subclinical hypothyroidism in pregnancy and in children. Eur Thyroid J. 2014;3(2):76/94.

24. Stagnaro-Green A, Abalovich M, Alexander E, et al. Guidelines of the American thyroid association the diagnosis and management of thyroid disease during pregnancy and postpartum. Thyroid. 2011;21:1081–125.
25. Liu H, Shan Z, Li C, et al. Maternal subclinical hypothyroidism, thyroid autoimmunity, and the risk of miscarriage: a prospective cohort study. Thyroid. 2014;24(11):1642–9.
26. Chan S, Boelaert K. Optimal management of hypothyroidism, hypothyroxinaemia and euthyroid TPO antibody positivity preconception and in pregnancy. Clin Endocrinol. 2015;82(3):313–26.
27. Maraka S, Ospina NMS, Mastorakos G, O'Keeffe DT. Subclinical hypothyroidism in women planning conception and during pregnancy: who should be treated and how? J Endocr Soc. 2018;2(6):533–46.
28. Bernardi LA, Cohen RN, Stephenson MD. Impact of subclinical hypothyroidism in women with recurrent early pregnancy loss. Fertil Steril. 2013;100(5):1326–31.
29. Shan Z, Teng W, Yu X, et al. Abnormalities of maternal thyroid function during pregnancy affect neuropsychological development of their children at 25–30 months. Clin Endocrinol. 2010;72(6):825–9.
30. Krassas GE, Pontikides N, Kaltsas T. Menstrual disturbances in thyrotoxicosis. Clin Endocrinol. 1994;40(5):641–4.
31. Cooper DS, Laurberg P. Hyperthyroidism in pregnancy. Lancet Diabetes Endocrinol. 2013;1(3):238–49.
32. Smith LH, Danielsen B, Allen ME, Cress R. Cancer associated with obstetric delivery: results of linkage with the California cancer registry. Am J Obstet Gynecol. 2003;189:1128–35.

Ultrasound of Neck Lymph Nodes

11

Yury N. Patrunov, Alexander N. Sencha,
Munir G. Tukhbatullin, and Ekaterina A. Sencha

Lymph nodes (LN) are peripheral organs of the lymphatic system that function as a biological filter for the lymph that flows up from organs and parts of the body.

Regional LN form a barrier to the spread of both infection and cancer cells from nearby organs. LN are located along the lymphatic vessels and form groups (clusters) in the places of their confluence. Normally, up to 300 LN may be found in the neck. The number of LN in each zone may vary depending on individual features.

Several classifications of neck LN are utilized. Lymph nodes in the neck have been historically divided into seven levels based upon surgical anatomy (Fig. 11.1). Neck LN conditionally may be divided into the following levels [1]:

- Superior (located in the upper third of the neck, above the CCA bifurcation)
- Middle (at level of the CCA bifurcation and 3 cm below it)
- Lower (inferior one-third of the neck)

Y. N. Patrunov (✉)
Department of Ultrasound Diagnostics, Center for Radiological Diagnostics of Non-State Healthcare Institution Yaroslavl Railway Clinic of JSC "Russian Railways", Yaroslavl, Russia

A. N. Sencha
Department of Visual and Functional Diagnostics, National Research Center for Obstetrics, Gynecology and Perinatology, Ministry of Healthcare of the Russian Federation, Moscow, Russia

M. G. Tukhbatullin
Department of Ultrasound Diagnostics, Kazan State Medical Academy – Branch Campus of the Federal State Budget Educational Institution of Further Professional Education, Russian Medical Academy of Continuing Professional Education of the Ministry of Healthcare of the Russian Federation, Kazan, Russia

E. A. Sencha
Ultrasound Diagnostics Department, Medical Diagnostic Center, Moscow, Russia

A. N. Sencha, Y. N. Patrunov (eds.), *Thyroid Ultrasound*,
https://doi.org/10.1007/978-3-030-14451-7_11

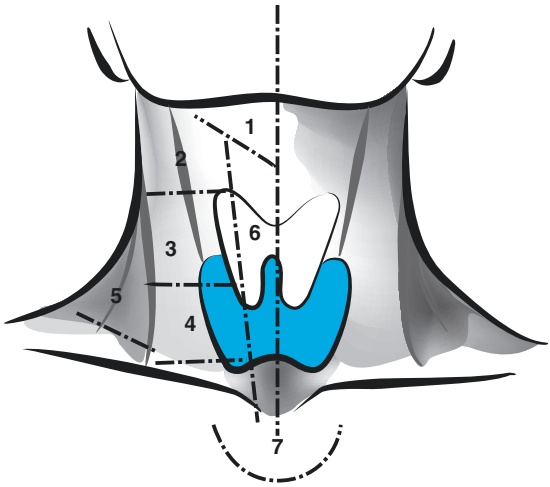

Fig. 11.1 Classification of cervical lymph nodes. (1) Submental and submandibular groups; (2) upper internal jugular (deep cervical) chain; (3) middle internal jugular (deep cervical) chain; (4) lower internal jugular (deep cervical) chain; (5) posterior triangle (spinal accessory) group; (6) anterior compartment, prelaryngeal, pre- and paratracheal groups; (7) (anterior) superior mediastinal group

An examination of the lymph nodes of the neck is an essential part of thyroid US. In some cases, the appearance of metastatic lymph nodes is the first clinical sign of thyroid cancer. The main problem with the US assessment of regional metastases of thyroid malignancies is the large number of diseases that are accompanied by lymph node enlargement and thus the difficulties involved in the differential diagnosis of the origin of the enlargement. Lymphadenopathies show benign character in 80% of patients younger than 30 years, although only 40% of enlarged lymph nodes appear to be benign in patients over 50 years old [2].

Sonography of the lymph nodes of the neck is performed in the standard position of the patient for thyroid US: supine with a bolster under the shoulders and the head thrown back (Fig. 11.2). To facilitate the examination of the right half of the neck, the patient may be asked to turn their head to the left and vice versa. A linear US probe with a frequency of 7.5–15 MHz is utilized.

US characterization of the lymph nodes of the neck involves evaluating the following aspects:

- Site, according to anatomical area
- Number
- Dimensions (in three planes)
- Short/long axis in transverse view
- Similarity of changes
- Shape (flat, oval, spherical, or irregular)
- Echodensity of the lymph node in general (increased, medium, or decreased)
- Differentiation of lymph node parts (present/absent)
- Differentiation of the hilum (present/absent)
- Core echodensity (high, low, or isoechoic)
- Status of the cortex of the lymph node (narrow/wide)
- Vascularity

Fig. 11.2 (**a**, **b**) Position of the patient while examining the lymph nodes of the neck

- Mobility upon compression with the probe
- Elasticity with compression US elastography

The principle ultrasound signs of LN differentiation are the size, shape, structure, and vascularization.

Normal lymph nodes of the neck demonstrate the following sonographic features (Fig. 11.3):

- Oval (or bean-like, tape-like) shape, close proximity to neck vessels, often near large veins
- Length smaller than 10 mm

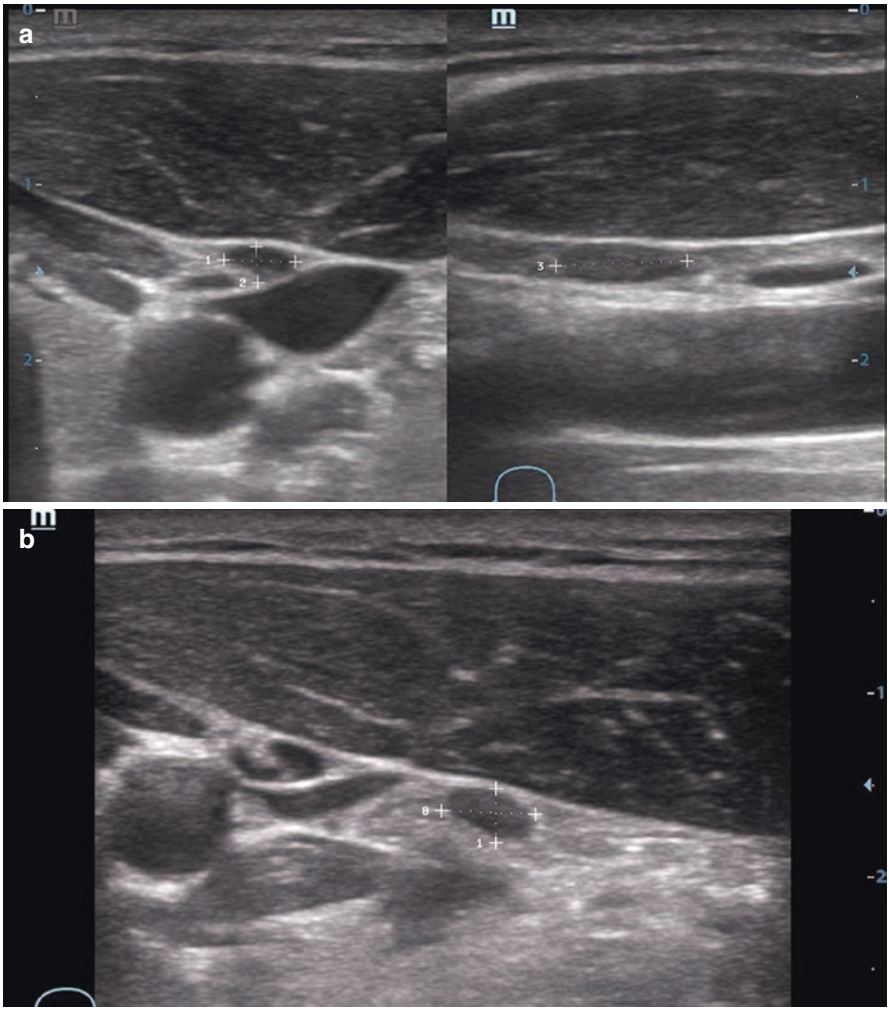

Fig. 11.3 (**a**, **b**) Normal neck lymph nodes. Grayscale US

- Short/long size ratio less than 0.5
- Regular, well-defined contours
- Hypo- or isoechoic peripheral part and hyperechoic central part
- Common visualization of the hilum
- Painless, moderately mobile upon compression with the US probe
- Avascular or hypovascular in CDI and PDI with predominant vascularity of the hilum
- No specific pattern with compression US elastography

According to Zabolotskaya [2], a normal lymph node has a width of up to 10 mm on transverse scan, although, according to a number of authors, the dimensions of

normal lymph nodes vary significantly. However, normal jugulodigastric lymph nodes can exceed this limit. Two main components of the LN—the cortex and medulla—are usually well differentiated. Their ratio and echogenicity depend on many factors, such as age, node localization, etc. The Solbiati index, which is the ratio of the largest to the smallest diameter of a lymph node, is normally 2.9 ± 0.13 in adults and 2.4 ± 0.05 or above in children [3].

The assessment of vascularity with CDI and PDI supplies additional data for the differential diagnosis of the origin of an enlarged lymph node (Fig. 11.4). Vessels, if any are detected, are usually located within the hilum in normal or reactive lymph nodes. Even in large benign hyperplastic lymph nodes, the vascular pattern remains regular. Vessels are normally observed along the capsule and radially from the hilum to the periphery [4].

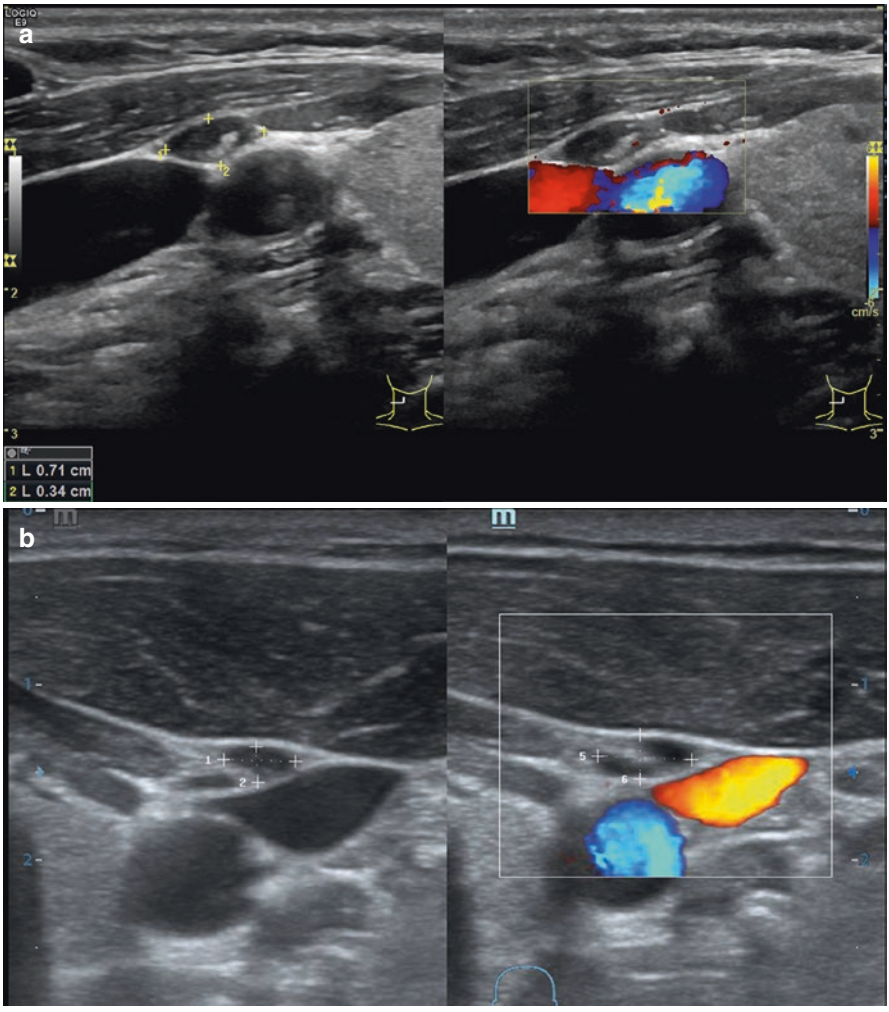

Fig. 11.4 (**a**, **b**) Normal neck lymph nodes. Grayscale US and CDI

Abbasova et al. [5] classify the vascular pattern of the lymph node into the following four categories:

1. Hilar: individual arterial and/or venous flow signals without diffusion to the parenchyma of the lymph node and without branching
2. Activated hilar (central) type: venous and arterial flow signals branching radially within the hilum and medulla
3. Peripheral: flow signals along the periphery of the lymph nodes without subcapsular branches arising from the hilar vessels
4. Mixed: presence of hilar and peripheral flow signals
   a. One large artery in the hilum with individual dot-shaped color signals in the periphery
   b. Fragments of afferent artery and chaotic flow signals within the solid component of the lymph node

Pulsed-wave Doppler data, according to Abbasova et al. [5], do not affect the differential diagnosis of enlarged lymph nodes.

Enlargement of a lymph node of the neck may appear as a manifestation of a variety of diseases, such as specific or nonspecific inflammation of head and neck organs, metastases, and hemoblastoses (e.g., Hodgkin's disease).

Nonspecific types of lymphadenitis are divided into the following groups [4]:

1. According to disease severity
   - Acute
   - Subacute
   - Chronic
2. According to dispersion
   - Isolated
   - Regional (in groups)
   - Extended
   - Generalized

Individual and multiple lymph nodes as well as lymph node conglomerations can be also described.

Reactive hyperplasia of lymph nodes may result from different pathological processes (an inflammatory process, vaccination, injections, etc.). Lymph nodes that are close to a tumor can also present a nonspecific reaction of inflammatory character [4]. Abbasova et al. [5] differentiate the following types of US image for inflammatory processes in lymph nodes (Fig. 11.5):

- Reactive hyperplasia (minimal sonographic changes, accurate regular margins, distinct differentiation of the hilum, and activated hilar type of blood flow)
- Subacute lymphadenitis (multiple enlarged lymph nodes of decreased echodensity, indistinct differentiation of echostructure, morbidity upon compression with the probe, and activated hilar type of blood flow, often with branching)

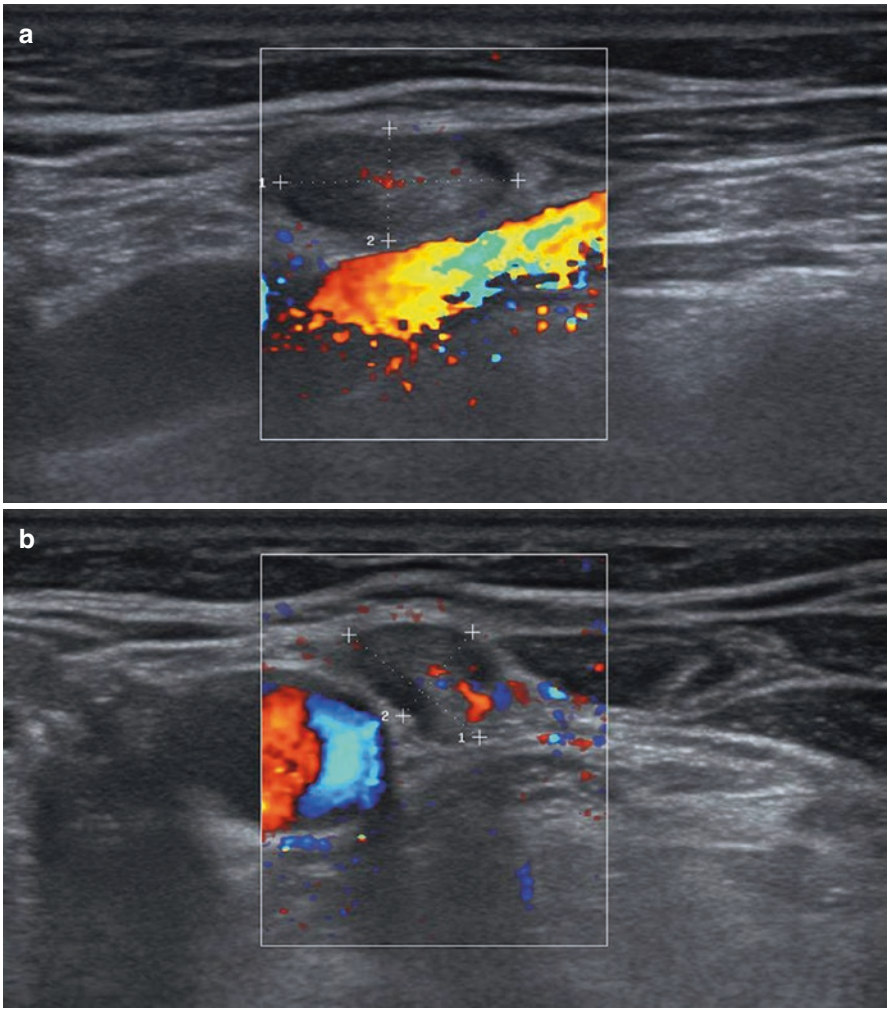

Fig. 11.5 (**a**, **b**) Reactive neck lymph nodes. CDI

- Acute lymphadenitis (enlargement of lymph nodes with roundish shape, significant decrease in echodensity, sharp morbidity upon compression, disturbance of corticomedullary differentiation, and activated hilar blood flow pattern)
- Chronic lymphadenitis (enlargement of lymph nodes with roundish shape, decrease in echodensity, thickening of echogenic medulla and hilum, and hilar blood flow pattern)

CEUS of neck LN with SonoVue® requires an intravenous injection of 2.4–4.8 mL of contrast. The larger amount for the study of deeply located LN is necessary. Various types of lymphadenopathy are often characterized with different types

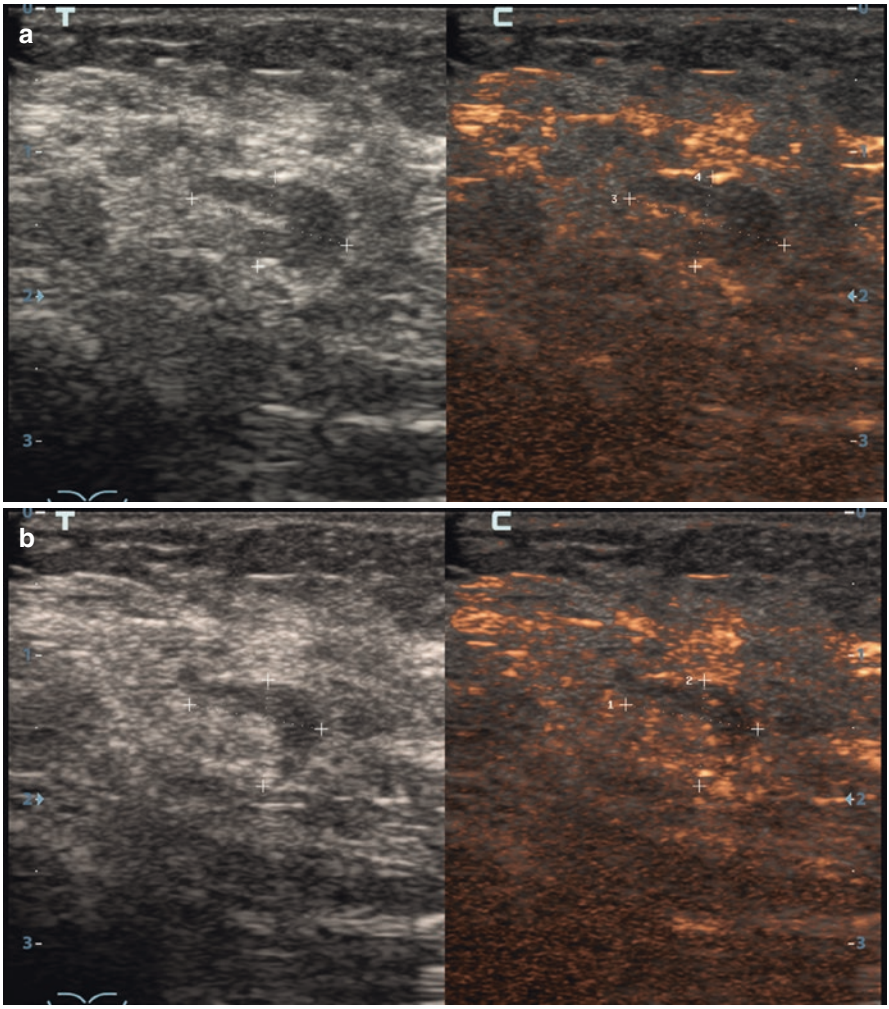

Fig. 11.6 (**a**, **b**) Reactive neck lymph nodes. Contrast-enhanced ultrasound with SonoVue®, 2.4 mL. Echograms

of contrast enhancement. It is important to differentiate the hilum and assess the homogeneity, caliber, and regularity of vascular structures within the node. Contrast enhancement of the hilum of normal or reactive LN is commonly observed at 10–15 s after contrast medium injection followed by uniform enhancement of the cortex. Washout normally starts at 40–45 s and completes after 60–90 s. Confident visualization of the blood flow in the hilum of the LN usually excludes malignant or other specific changes (Fig. 11.6). Alternatively, deformation of the hilar enhancement is often characteristic of metastatic lesions.

Complex US is effective for monitoring how changes in lymph node develop. Inflammatory lymph nodes show fast dynamics. Even without therapy, they often sonographically disappear after 5–7 days [2]. Treatment speeds up their involution,

resulting in the restoration of the oval shape of the node and sharpness of margins, an increase in the general echodensity with more accurate corticomedullary differentiation, and a decrease in blood flow intensity and morbidity upon compression.

Patients with metastases in lymph nodes of the neck with an unknown primary tumor are observed in 3–8% of cases [6].

The incidence of metastases of thyroid cancer in regional lymph nodes is 9–90% [7]. Unilateral lymph node affection is registered in 85% and bilateral metastases in 15% of cases. Regional metastases are most often observed in anaplastic cancer (32%). Papillary and medullary cancer have local metastasis rates of 18–36%, and the metastasis rate for follicular carcinoma is 7–17% of cases.

Some US features that are suspicious for a malignant process in a neck lymph node are listed below (Fig. 11.7):

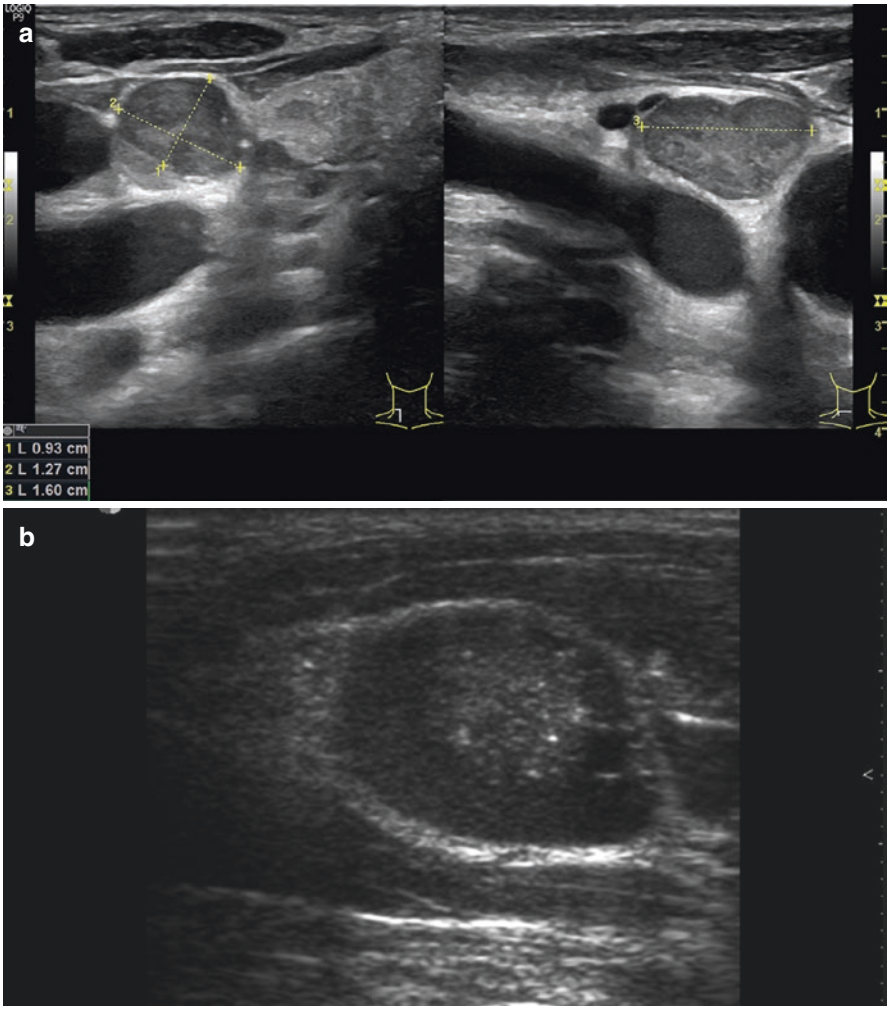

Fig. 11.7 (**a**–**d**) Neck lymph nodes metastases. Grayscale US

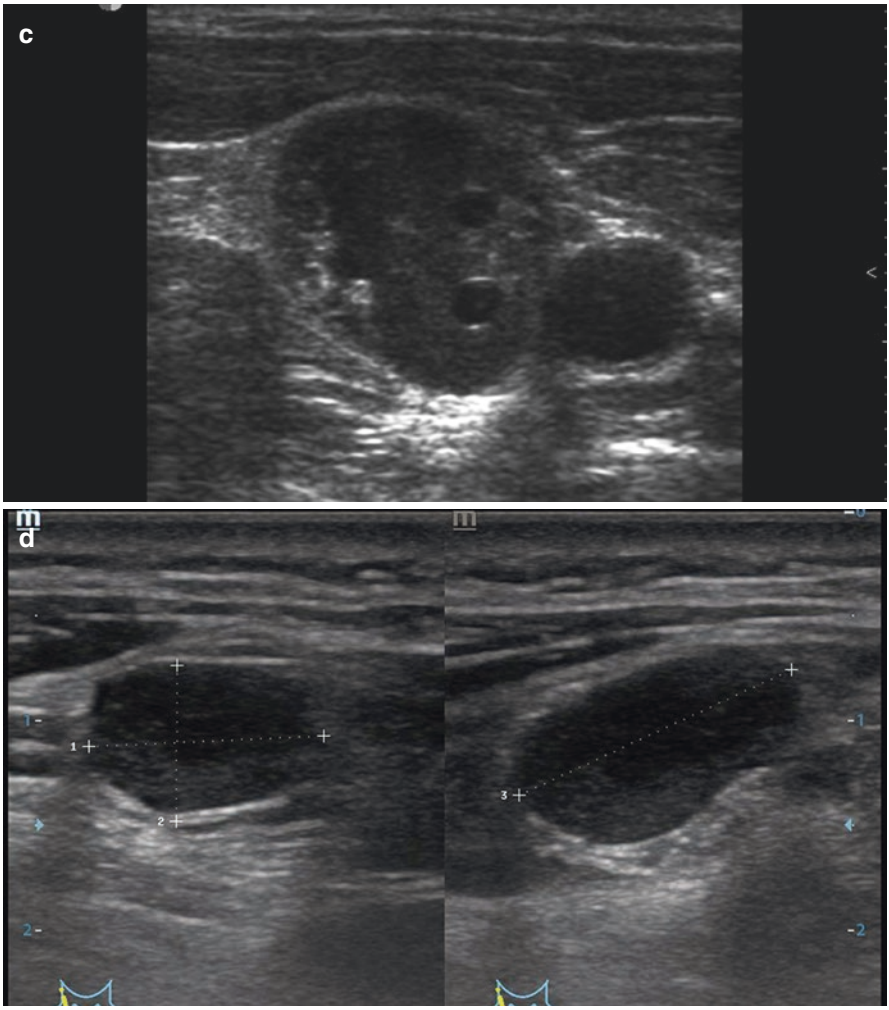

Fig. 11.7 (continued)

- Size of >10 mm
- Short/long size ratio higher than 0.5
- Roundish shape
- Irregular blurred contours
- Decreased general echodensity
- Heterogeneous echostructure
- Pathological echogenic inclusions
- Anechoic component
- Dislocation or deformation of the hilum, indistinct image of the hilum of the lymph node up to its full disappearance

- Local thickening of the cortex of the lymph node in combination with dislocation of the hilar vessels
- Conglomerations of lymph nodes
- Immobility or limited mobility against the surrounding tissues
- Pathological vascular patterns in CDI and PDI (Fig. 11.8)

The probability of malignancy increases if two or more of the features specified above are present. According to Kotlyarov et al. [8], enlarged regional lymph nodes in the case of verified thyroid cancer are indicative of a metastatic origin with an accuracy of 95–100%.

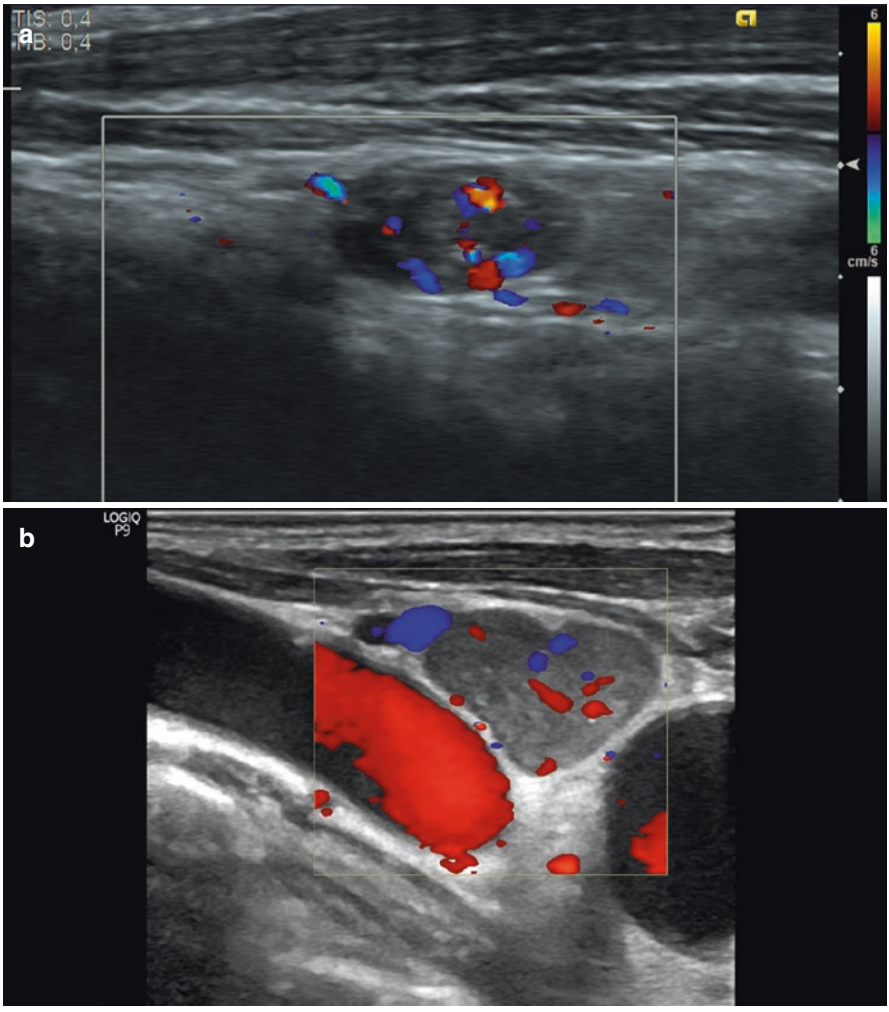

Fig. 11.8 (**a**–**d**) Neck lymph nodes metastases. CDI

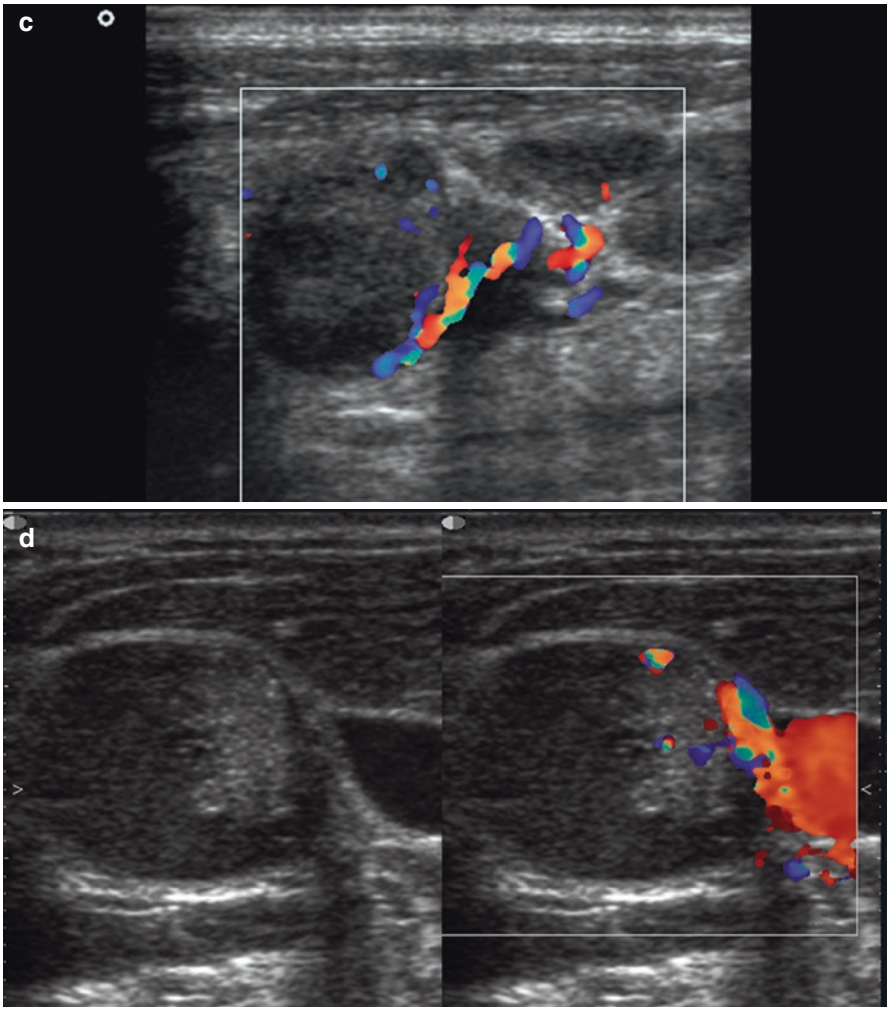

Fig. 11.8 (continued)

The site of the metastasis does not directly correspond to the location of the primary tumor. Metastases are more often observed on the same side of the neck as the primary tumor. Bilateral affection is seen less often. According to Sencha [9], in 76% of cases of verified thyroid cancer, metastases affect only the jugular group and are combined with other groups of lymph nodes in 24%. A combination of metastases in jugular lymph nodes and submandibular or submental lymph nodes was detected in 12%, with posterior neck lymph nodes in 8% and with supraclavicular or anterior mediastinum lymph nodes in 4% of cases.

Allahverdieva et al. [10] report that metastatic lymph nodes in cases of papillary thyroid carcinoma are characterized by a diffuse distribution of vessels (a "glowing"

lymph nodule). According to Ahuja [11], CDI and PDI do not supply any significant information for the differential diagnosis of enlarged lymph nodes of the neck.

Compression US elastography and elastometry, as a rule, rarely reveal the change in LN elasticity against the background of the surrounding neck tissue, but high strain tends to prove the malignancy (Fig. 11.9).

Extracapsular expansion of the metastases in lymph nodes often leads to the integration of several affected lymph nodes into amorphous conglomerations that merge into surrounding structures. The basic US feature of invasion is indistinct contour of the lymph node [4].

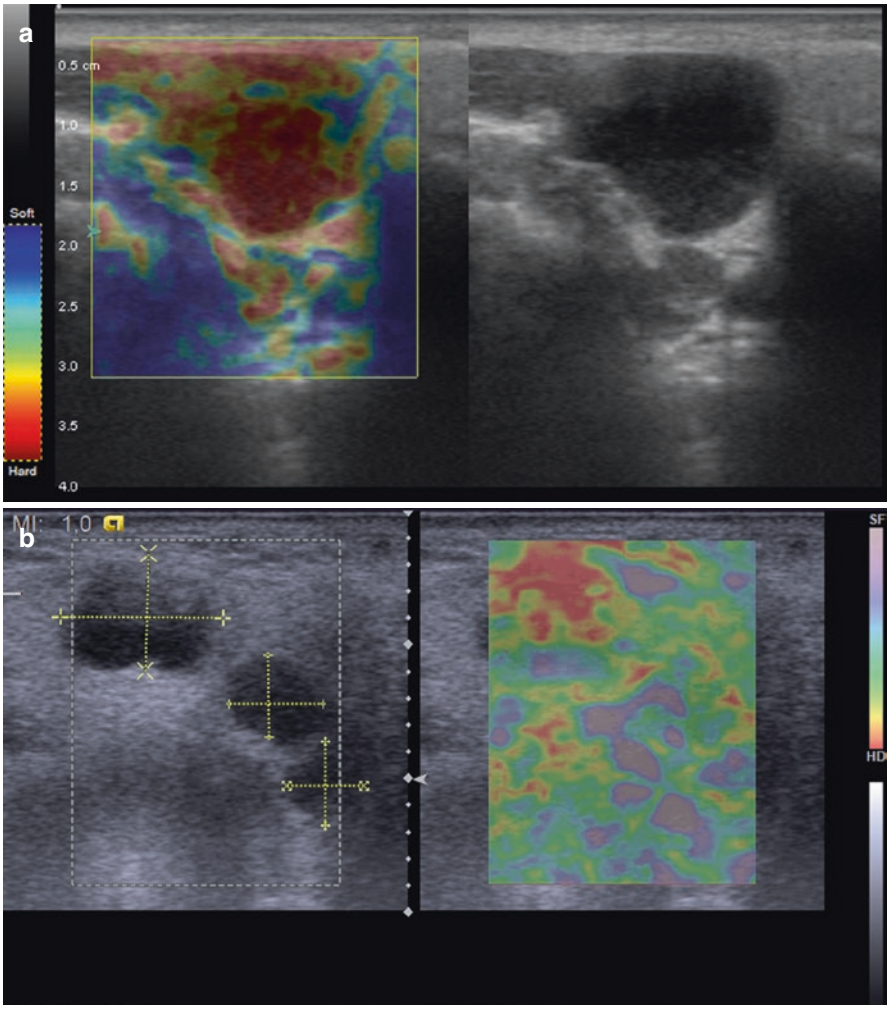

Fig. 11.9 Neck lymph nodes metastases. (**a**–**c**) Compression US elastography. Hard pattern. (**d**) Elastometry with ARFI. High shear-wave velocity

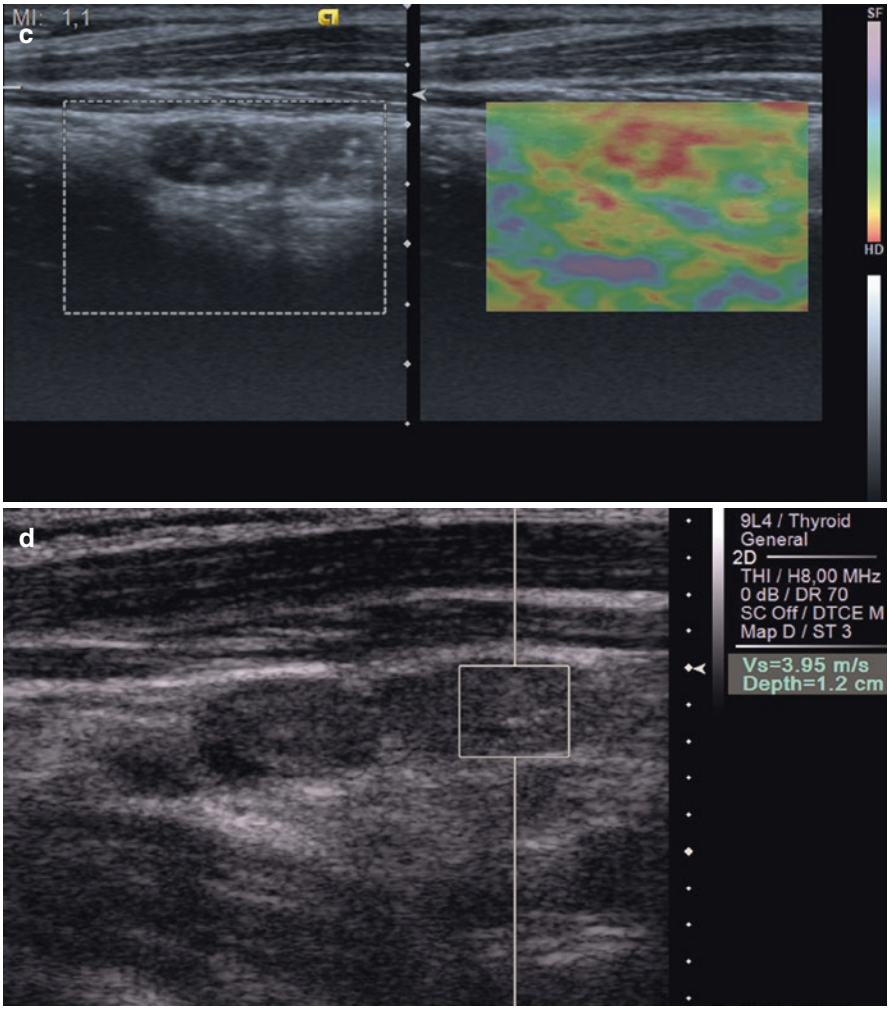

Fig. 11.9 (continued)

CEUS has been used relatively recently for the study of LN. It allows to improve the differential diagnosis of malignant and reactive LN and provides a more accurate selection of lymph nodes for FNAB if regional metastases are suspected. In metastatic LN, tumor deposits distort the vascular structures including the blood vessels of the hilum. In addition, tumor infiltration of the cortex combines with neoangiogenesis and increases in the number of subcapsular vessels. It leads to peripheral hypervascularization with tortuous and aberrant vessels feeding the periphery and sinusoids (Fig. 11.10).

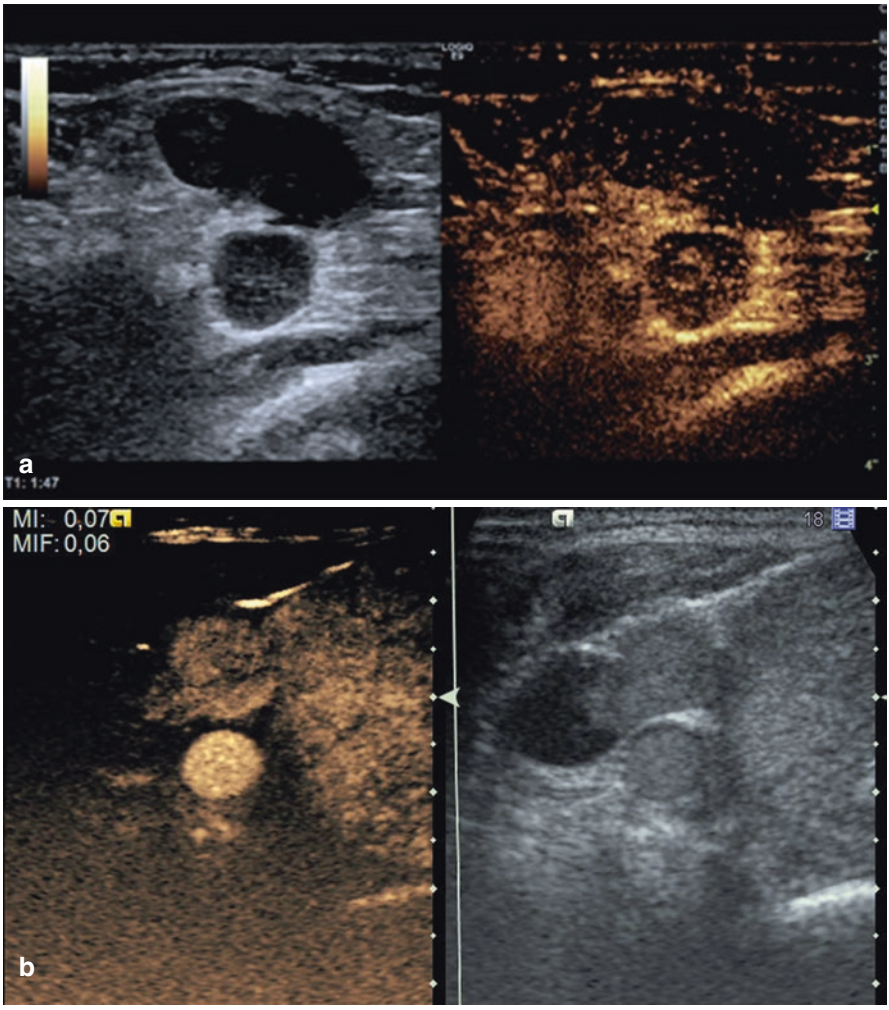

Fig. 11.10 (**a**, **b**) Neck lymph nodes metastases. Contrast-enhanced ultrasound with SonoVue®, 2.4 mL. Echograms

Remote metastases are observed in 6–55.5% of patients with thyroid cancer [12]. They are most often detected in lungs (62.5%), bones (20%), and mediastinal lymph nodes (7.5%). US often fails to visualize metastases within the thorax, so other radiological methods are preferable.

The sensitivity of US for the detection and differential diagnosis of lymph nodes in thyroid cancer is 30–87%, with a specificity of 57–84% and a diagnostic accuracy of 56–81%. These figures appear to be highly dependent on the quality of the

equipment as well as the skill and experience of the operator, especially in cases with small local metastases within lymph nodes.

Most authors agree that, in many cases, sonography does not allow the ultimate definition of the nature of the lymph nodes of the neck, although it does detect indirect features that facilitate further diagnostics. US-guided FNAB with definition of the thyroglobulin level and cytological examination is feasible.

References

1. Gritzmann N, Czembirek H, Hajek P, et al. Sonographic anatomy of the neck and its importance in lymph node staging of head and neck cancer. Rofo. 1987;146(1):1–7.
2. Zabolotskaya NV. The use of ultrasound to assess the condition of surface groups of lymph nodes. Sonoace Int. 1999;5:42–5.
3. Solbiati L. Ultrasound of superficial structures. London: Churchill Livingstone; 1995.
4. Trofimova EY. Ultrasound examination of lymph nodes. SonoAce-Ultrasound. 2008;18:59–64.
5. Abbasova EV, Parhomenko RA, Shcherbenko OI. (2005) Echography in differential diagnosis of benign and malignant lymphadenopathies in children. Materials of the scientific forum "Radiology-2005", Moscow, pp. 3–4 (Article in Russian).
6. Karmazanovsky GG, Nikitaev NS (2005) Computed tomography of the neck: differential diagnosis of extraorgan lesions. Vidar, Moscow (Book in Russian).
7. Pinsky SV, Dvornichenko VV, Beloborodov VA (1999) Thyroid tumors. Irkutsk (Book in Russian).
8. Kotlyarov PM, Yanushpolskaya TO, Aleksandrov YK, et al. Ultrasound in the diagnosis of thyroid cancer and its recurrence. Dent Echo. 2001;2(4):349–54.
9. Sencha AN. Ultrasonic visualization of malignant tumors of the thyroid gland. Ultrazvukovaya i Funkcionalnaya Diagnostika. 2008;2:20–9.
10. Allahverdieva GF, Sinyukova GT, Sholokhov VN, Romanov IS. Possibilities of complex ultrasound examination in diagnosis of metastatic lymph nodes of the neck. Ultrazvukovaya i Funkcionalnaya Diagnostica. 2005;1:18–22.
11. Ahuja A. The thyroid and parathyroid. In: Ahuja A, Evans R, editors. Practical head and neck ultrasound. London: Greenwich Medical Media; 2000.
12. Altunina VS. (1996) Ultrasound diagnosis of recurrence of thyroid cancer. PhD thesis, Obninsk (Book in Russian).

Ultrasound-Guided Fine Needle Aspiration Biopsy

12

Yuriy K. Aleksandrov, Yury N. Patrunov, and Alexander N. Sencha

A biopsy with cytology is currently the only preoperative method of assessment of morphology of thyroid lesions. It is a mandatory method in many diagnostic algorithms. Morphological analysis of the tissue allows to identify and differentiate thyroid diseases at early stages.

The use of ultrasound for choosing a puncture site greatly facilitates the procedure and significantly increases its value [1–4]. Fine needles with inner diameters of up to 1 mm or core needles can be used for the biopsy. Fine needle aspiration biopsy (FNAB) is now the most popular procedure. It commonly utilizes 21G disposable needles and can be performed on an outpatient basis without any anesthesia. The method is efficient, inexpensive, and safe.

Ultrasound guidance in real time permits identification and precise puncture of small deeply located nonpalpable lesions of 3–5 mm in size and larger. Ultrasound Doppler options, such as CDI and PDI, permit assessment of vascularity of the target lesions and differentiate fluid collections from vessels to avoid hemorrhagic complications.

A number of authors regard FNAB as the main screening method for diagnosing thyroid diseases and the only preoperative method of morphological verification [1, 5, 6].

Y. K. Aleksandrov (✉)
Department of Surgery, Federal State Budget Educational Institution of Higher Education Yaroslavl State Medical University of the Ministry of Healthcare of the Russian Federation, Yaroslavl, Russia

Y. N. Patrunov
Department of Ultrasound Diagnostics, Center for Radiological Diagnostics of Non-State Healthcare Institution Yaroslavl Railway Clinic of JSC "Russian Railways", Yaroslavl, Russia

A. N. Sencha
Department of Visual and Functional Diagnostics, National Research Center for Obstetrics, Gynecology and Perinatology, Ministry of Healthcare of the Russian Federation, Moscow, Russia

A. N. Sencha, Y. N. Patrunov (eds.), *Thyroid Ultrasound*,
https://doi.org/10.1007/978-3-030-14451-7_12

The indications for US-guided FNAB are as follows:

- Nodules of various sizes and echostructures (TIRADS 3–5), in order to specify morphological structure in suspicion for malignancy
  - First time detected nodules
  - Nodules with fast growth
  - Malignant features with US (inclusive of significant change in echostructure, vascularization or other US or clinical features within a year of follow-up)
- Multichamber and complex cysts (especially with a hypervascular solid component)
- Nodules of ectopic or aberrant thyroid
- Substernal goiter
- Recurrent goiter in suspicion for malignancy
- Contradictory data from US or other diagnostic methods with clinical implications
- Metastatic neck lymph nodes of unknown origin
- Cytological verification prior to minimally invasive modalities or surgery

Many authors consider that all thyroid nodules should be necessarily biopsied. Palpable nodules are biopsied more often. Nonpalpable nodules that are smaller than 1 cm tend to be followed up. They should be biopsied if malignant US features are present or there is a family history of medullary carcinoma. In cases with multiple identical lesions, the question of whether to biopsy each nodule or only a dominant one is controversial.

Contraindications for FNAB are as follows [7]:

- Severe coagulation system disorders
- Diseases associated with abnormalities of the vascular wall when the risk of the procedure exceeds its diagnostic value
- Flat refusal of the patient to undergo the procedure
- Acute psychiatric disorders

Thyroid puncture may be carried out using the following methods:

1. “Blind” puncture. This is performed without instrumental guidance. The nodule is detected with palpation.
2. With preliminary US marking. This implies that the nodule site has been previously specified by US and that its projection onto the skin of the neck has been indicated.
3. US-guided biopsy. The real-time guidance ensures precise placement of the needle tip within the lesion.

The technology of thyroid FNAB with ultrasound guidance is recommended. It is predictable and comfortable for the patient ensuring reliable and precise data for the doctor. “Blind” and pre-marked punctures are used extremely rarely; they are

substantially less valuable from the point of view of evidence-based medicine. Takashima et al. [4] report that FNAB without guidance shows a higher incidence of diagnostic mistakes than cases with US guidance (19.5% vs. 0.04%, respectively). According to Alexandrov [1], the sensitivity of US-guided FNAB is 80%, that of FNAB with US marking is 72%, and that of "blind" FNAB is 69%.

The productivity of FNAB is significantly influenced by the skills of the personnel, the accuracy of needle introduction, the amount of material obtained, the smear technique, and the skill of the cytologist. The rate of nondiagnostic biopsies (BSRTC 1 with cytology) in specialized centers is less than 5%. Alexandrov [1] reported nondiagnostic samples in 0.2%.

US guidance for FNAB of thyroid lesions confers the following advantages:

- Fast real-time management.
- Precise targeting when obtaining the specimen.
- It is harmless to the patient and the staff; there is no ionizing radiation involved.
- High resolution (although this depends significantly on the quality of the scanner).

The disadvantages of US guidance for thyroid biopsy are as follows:

- Dependence on the class of equipment used
- High dependence on the experience and skill of the operator
- Dependence of the quality of visualization on the individual patient's features (density of tissues, site of the nodule, position and somatic status of the patient, etc.)

US-guided biopsies can be performed by the following techniques:

1. Freehand biopsy is often utilized by specialists with confident puncture skills, especially for large lesions or in the absence of a puncture adapter to mount on the US probe. The advantages of this technique are a high degree of freedom to manipulate the needle and good needle visualization. This is a common way to perform FNAB.
2. Utilizing a puncture probe allows the needle course to be determined prior to the puncture. However, the needle is often poorly visualized during the procedure, course correction is limited, and special (commonly core) needles are required.
3. Mounting a puncture adapter on the US probe allows precise needle course determination and good visualization of the needle but limits the needle's mobility due to its rigid construction. The number of biopsies is limited by the package of sterile instruments. That biopsy is usually a core-needle biopsy.
4. Specialized hardware options for needle tracking that are available in some manufacturers of US diagnostic equipment (such as SonixGPS by Ultrasonix). They need special expensive equipment and disposable core needles. This technology is good for deeply located abdominal lesions. This is not a fine needle biopsy and is not used for typical thyroid lesions.

Fig. 12.1 Fine needle aspiration biopsy with freehand technique performed with two specialists. Photo

US guidance of FNAB of thyroid nodules is performed with linear 7.5–15 MHz probes. A team of two specialists (the sonographer and surgeon/endocrinologist) is preferable (Fig. 12.1). Special preparation of the patient for the procedure is not required. The patient is positioned supine with a cushion under the shoulders and the head hyperextended. Local anesthesia is usually not necessary, since the pain of injection is comparable to that of biopsy. Additionally, the administration of anesthetic can lead to deterioration in the US visualization of the target region and change the quality of the smear. The US probe is positioned on the neck in the most convenient way. The path of the needle to the target lesion is determined. The probe is covered and prepped with an antiseptic. The skin of the neck is carefully cleaned with an antiseptic; a sterile coupling gel is utilized. The biopsy is carried out under aseptic conditions with a disposable 5–10 mL syringe and a 21 G needle and generally takes only a few minutes to perform. The motion of the needle in the lesion is registered on the screen of the US scanner. The needle may be introduced from the lateral side of the US probe or directly over the nodule (midway along the probe's length). This corresponds to an echogenic point in a transverse scan or an echogenic line in a longitudinal scan, which changes position in accordance with the motion of the needle (Fig. 12.1).

The needle is introduced into the target lesion. Samples for cytological examination are aspirated from at least three areas within the lesion. When the nodule has heterogeneous echostructure, the samples should be obtained from the most suspicious areas in the center and periphery of the lesion. The solid component of the cyst must also be biopsied. The sample obtained is spread across a glass slide, smeared, and delivered to a cytological laboratory for analysis. The site of puncture is compressed with a sterile dressing for 10–15 min to prevent hemorrhage (Fig. 12.2).

The incidence of complications depends on how experienced the experts who carry out the biopsy are, the concurrence of their actions, how closely the correct technique is followed during the procedure, the equipment utilized, and other aspects. According to different authors, complications can develop in 1–12% of patients [1, 8].

Side-effects and complications may be divided into local (pain, local inflammation, damage of the recurrent nerve, etc.) and general (discomfort, fever, hormonal disorders, etc.).

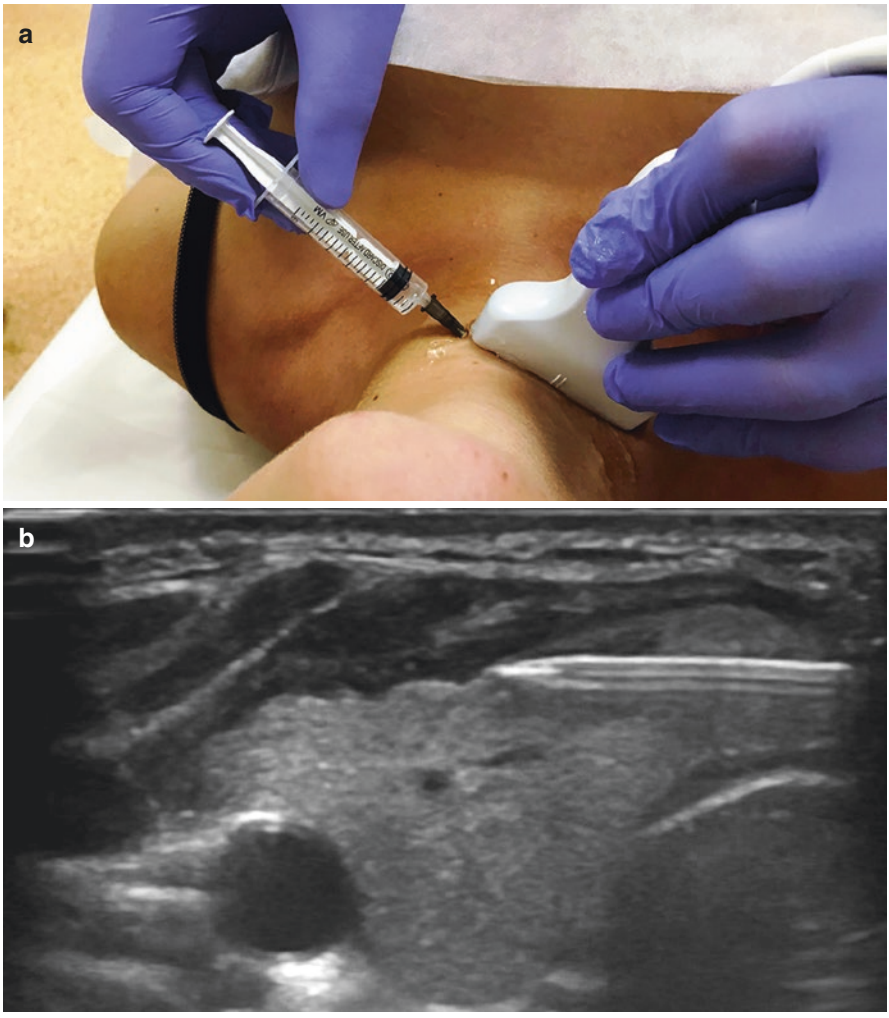

Fig. 12.2 Fine needle aspiration biopsy. (**a**) Position of an US probe and the needle introduced from its lateral edge, photo. (**b**) US image of the needle as a hyperehoic line as introduced on Fig. 12.1a. (**c**) Position of an US probe and the needle introduced midway along the probe's length, photo. (**d**) US image of the needle in the nodule as a hyperehoic dot as introduced on Fig. 12.1c

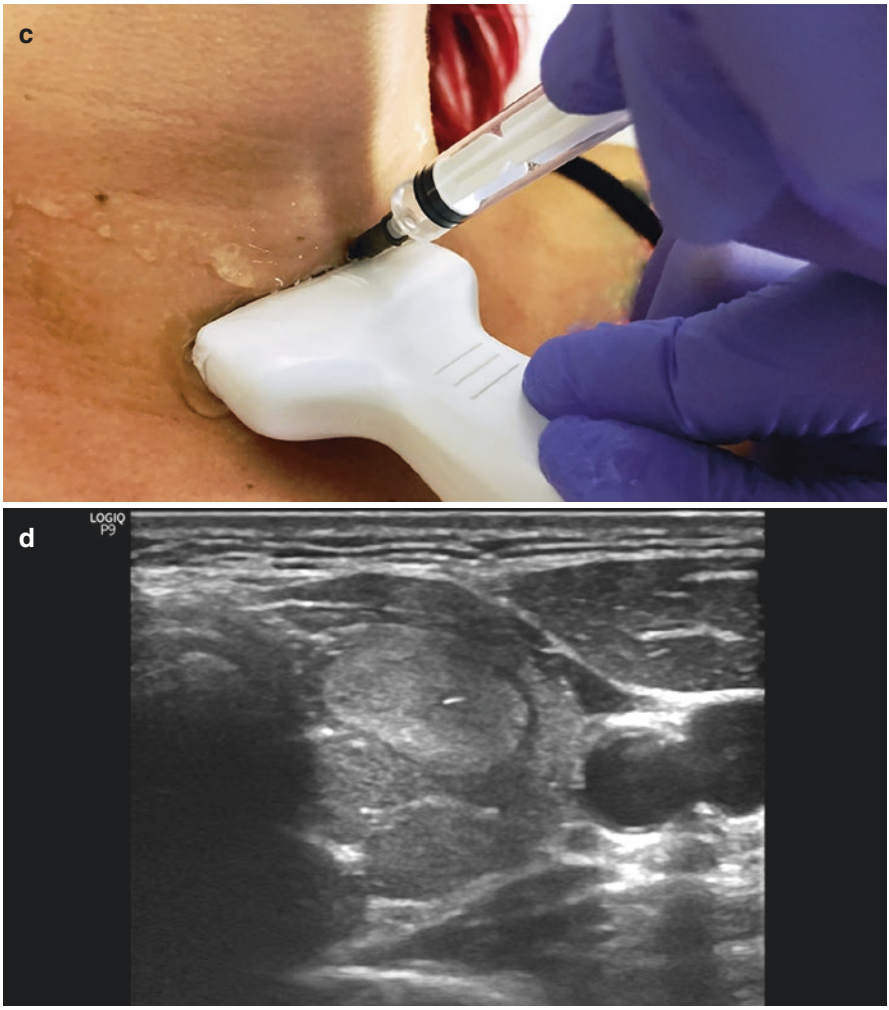

Fig. 12.2 (continued)

The most frequently registered complications [3, 7, 9] are listed below:

- Cervicalgia
- Impaired phonation
- Hemorrhage in the nodule or cystic lumen
- Hemorrhage, subcutaneous hematomas
- Damage to the large vessels, trachea, esophagus, or nerves

The early occurrence of pain at the site of puncture may be a consequence of local tissue damage or hematoma. Its intensity depends on the severity of the damage. Local hemorrhagic complications, such as subcapsular, interfascial, intermuscular,

or subcutaneous hematomas, result from injury to blood vessels at different locations, including subcutaneous veins. They may also arise with hypervascular lesion puncture and with some diffuse thyroid diseases associated with thyroid parenchyma hypervascularity (AIT or Graves' disease).

Subcapsular hematoma is accompanied by the following US signs (Fig. 12.3a):

- Hypoechoic avascular area with irregular margins under the thyroid capsule.
- Enlargement of the thyroid lobe.
- It does not change shape with compression.
- Significantly painful with compression.

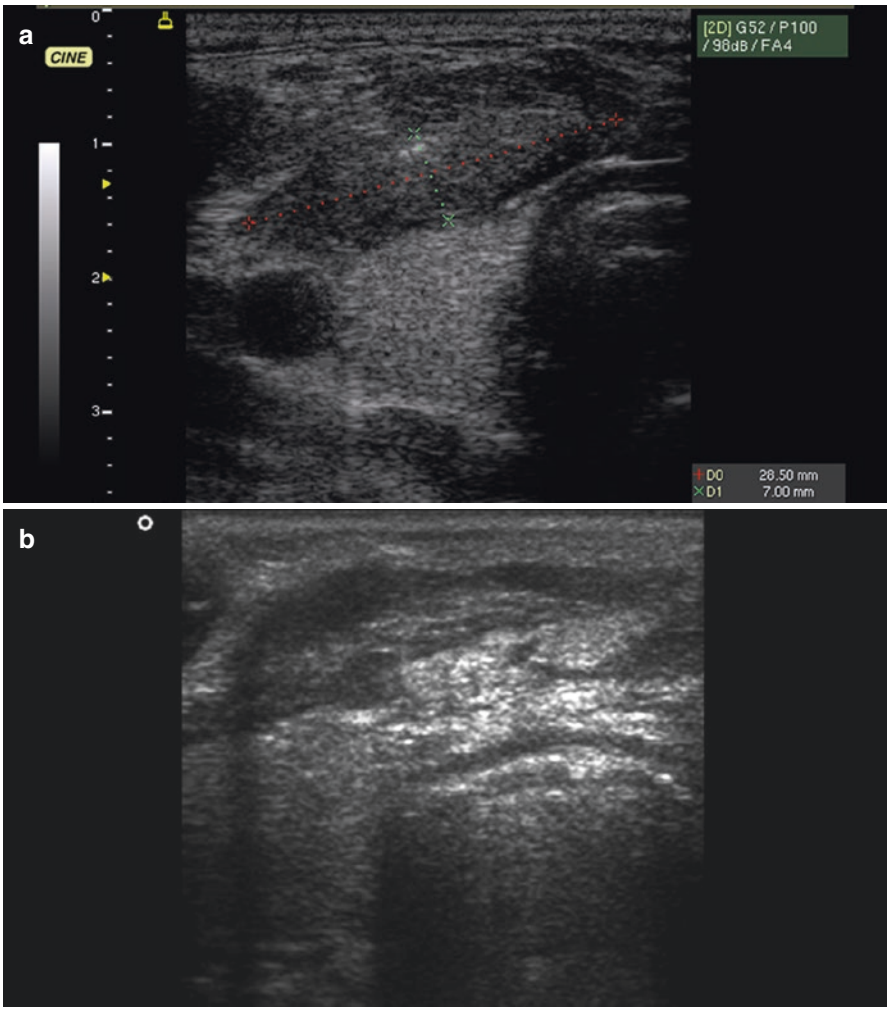

Fig. 12.3 FNAB complication. (**a**) Subcapsular hematoma of the thyroid gland. Grayscale US image. (**b**) Interfascial hematoma of the thyroid gland. Grayscale US image

The patient sustains increasing pain in the region of puncture. The hematoma, as a rule, disappears within a period of 2–5 days.

Interfascial and intermuscular hematomas commonly exhibit the following US signs (Fig. 12.3b):

- Homogeneous avascular hypoechoic structures that cover the anterior and lateral thyroid surfaces, spreading along interfascial spaces outside the thyroid gland
- The shape of such a hematoma changes with compression
- Moderately painful with compression

The enlargement of the hematoma can be seen as an increase in its thickness between the surface of the thyroid and the neck muscles. These hematomas are normally a relatively small size, expand downward, and do not enlarge after the puncture is ceased. Nevertheless, the occurrence of a hematoma demands an US follow-up and certain measures to prevent its enlargement. Interfascial hematomas are sometimes accompanied by a bruise in the suprasternal fossa or on the anterior surface of the neck within 2–3 days of the procedure. This quickly resolves and is sonographically unidentifiable after a few more (5–7) days.

In some cases, usually in nodules with prevalent fluid components and cysts, the hemorrhage can affect not the surrounding tissues but the cystic lumen. After aspirating the contents, the cystic lumen is filled to primary volume with blood, and in some cases enlargement is possible. US reveals heterogeneous masses with hypoechoic and echogenic inclusions within the nodule. The heterogeneity increases for a few days, and the echostructure shows a cellular pattern with echogenic structures of various shapes along the inner surface. CDI and PDI demonstrate the avascularity of the lesion. Such a hemorrhage may develop full or partial lysis with sonographic features of a cyst or organization resulting in a heterogeneous hypoechoic nodule with echogenic inclusions and calcifications. These nodules can later be penetrated by blood vessels, so the nodule vascularity may correspond to a true thyroid nodule.

The puncture of large venous or arterial vessels may occur if the path of the needle passes close to these structures. A blood vessel is evidently punctured if the syringe is filled with blood at aspiration. US images the needle as an echogenic point or a line within the vessel lumen. Injuries to large arteries, including the carotids, can lead to a hematoma in the vascular wall with stenosis. This is sonographically observed as a hypoechoic crescent-shaped lesion with eccentric wall thickening and protrusion of endothelium into the lumen (Fig. 12.4a). Hematomas outside of arteries are rare. Injuries to large veins are also seldom accompanied by hematomas, although they increase the risk of thrombosis.

Ultrasound image of venous thrombosis is typical and characterized with the following US features (Fig. 12.4b):

- Hypo- or isoechoic homogeneous avascular structures a lumen of the vein up to complete occlusion. The longer the thrombus exists, the more heterogeneous and echogenic it becomes.

- Narrowed vein lumen with CDI and PDI up to complete absence of flow.
- Ineffective compression of the vein with US probe.
- Tendency to grow and spread caudally in the direction of superior vena cava.

A rare complication of FNAB is the puncture of large nerves, including the branches of the cervical plexus. Such a nerve injury is followed by severe pain in the corresponding half of the neck, shoulder joint, or the upper extremity. Damage to the superior or inferior (recurrent) laryngeal nerves results into corresponding neurologic symptoms, such as hoarse voice (recurrent nerve), fast

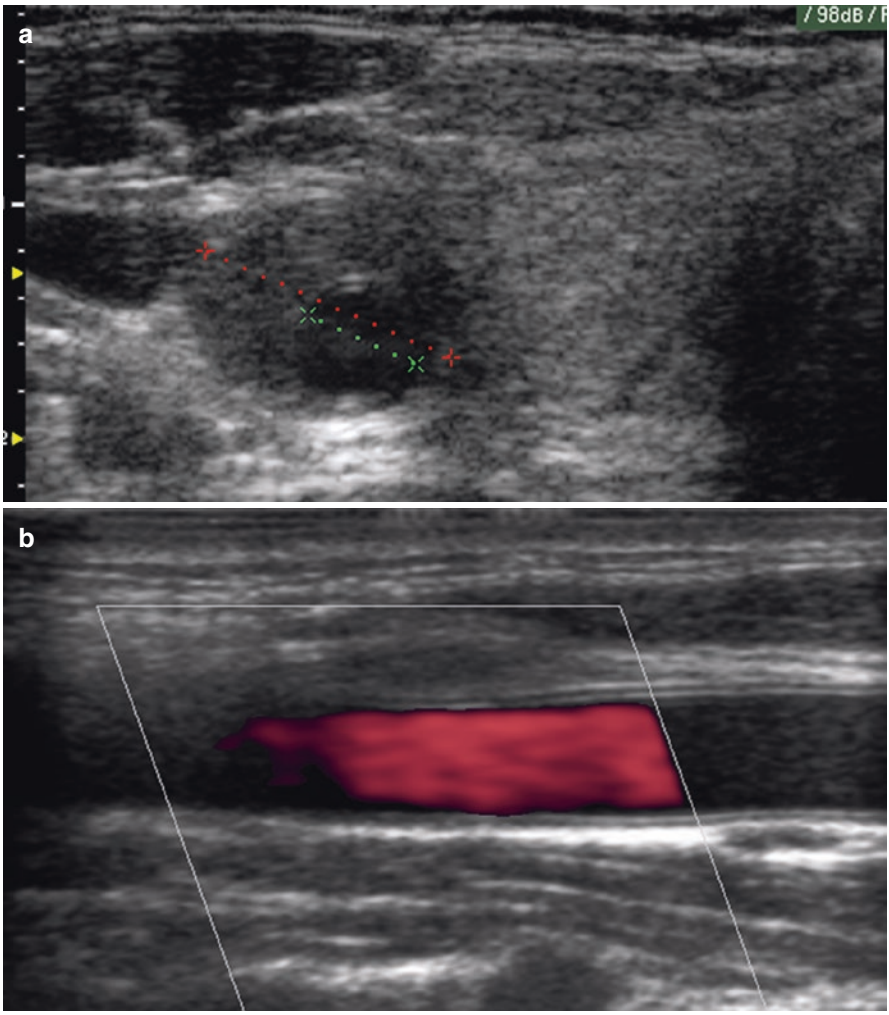

Fig. 12.4 FNAB complication. (**a**) Hematoma within CCA wall. Transverse grayscale US image. (**b**) Hematoma within CCA wall. Longitudinal PDI scan. (**c**, **d**) Left IJV thrombosis. Transverse grayscale US image

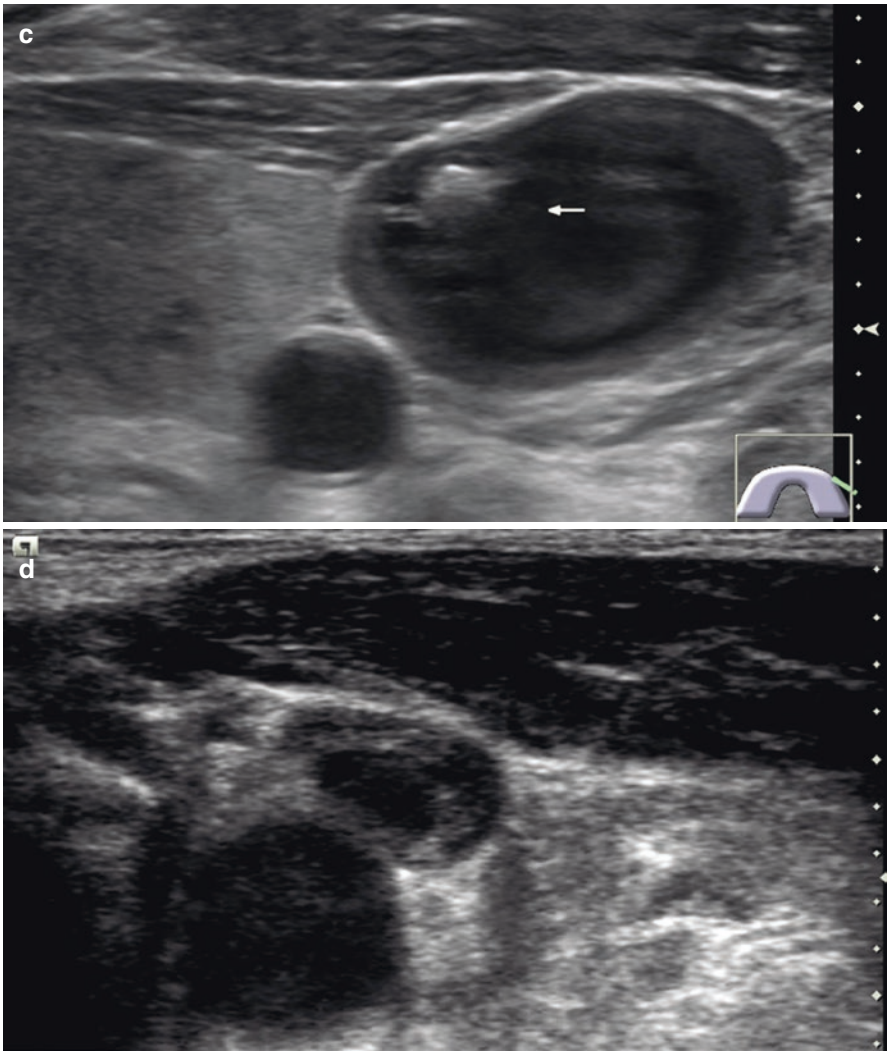

Fig. 12.4 (continued)

fatigue during loud speech, and choking, especially with liquids (superior laryngeal nerve).

Paratracheal nodule puncture may be complicated by the puncture of the trachea in cases with inaccurate US visualization of the needle tip. This causes an instant dry, hoarse cough for 1–5 min. Insignificant subcutaneous emphysema is sometimes possible. This does not require any special therapy.

The probability of puncture of the esophagus largely depends on the experience of the US specialist. A roundish (oval) lesion seen in the dorsal aspect of the left thyroid lobe with a transverse scan can be misinterpreted as a nodule.

Therefore, such a lesion should be considered with special care; assessment in several planes is necessary.

After FNAB, the patient does not normally require US follow-up. The efficacy of cytological diagnosis is defined by the skills of four experts: the surgeon performing the FNAB; the US specialist, who provides accurate visualization; the laboratorian staining the smears; and the pathologist.

Many researchers report the sensitivity of FNAB in detection of thyroid cancer of 70–98%, the specificity of 70–100%, the accuracy of 87–92%, the rate of false-positive results up to 20%, and the false negative results up to 2–15%. According to Semikov [10], the sensitivity of FNAB in the diagnosis of goiter, adenoma, and thyroid cancer was 87, 93, and 70%, respectively. FNAB is of particular importance in the diagnosis of nodules combined with diffuse thyroid diseases (AIT, Graves's disease).

At present, thyroid nodule FNAB cytology should be reported using diagnostic groups outlined in the Bethesda System for Reporting Thyroid Cytopathology (BSRTC) adopted at a conference of the National Cancer Institute (USA) in 2007 in Betesda. According to the requirements of the Bethesda system, patients with the results of FNAB interpreted as nondiagnostic or unsatisfactory, atypia of undetermined significance, or follicular lesion of undetermined significance should repeat FNAB [11]. The ATA guidelines state that there is no need to wait several months before repeating the FNAB [12].

Errors in the cytological examination are reported in 10–60% of cases, suspicious or undetermined changes occur in 10–30% of patients, false-negative results of cytology in 5.7%, and false-positive in 6.7%. Special difficulties arise in the cytological differentiation of highly differentiated follicular cancer and follicular adenoma. All follicular thyroid tumors confer a group of follicular neoplasia, which implies further verification and surgical intervention. According to Severskaya [13], the probability of thyroid cancer in the case of cytological report of a follicular tumor is 23%.

FNAB must precede minimally invasive manipulations on the thyroid gland [1, 14, 15]. The following minimally invasive modalities are more commonly applied for thyroid abnormalities in daily practice:

- Percutaneous ethanol injections
- Percutaneous laser ablation
- Radiofrequency thermoablation of thyroid nodules
- Intraglandular injections of glucocorticoids in subacute thyroiditis

These technologies are highly efficient in selected groups of patients. Their feature is selective destruction of thyroid lesions with insignificant damage to the surrounding tissue. The advantages also confer no need for general (and commonly local) anesthesia, significantly lower rate and severity of possible complications and side effects, cost-effectiveness, fast rehabilitation, and possibility of utilization in severe patients. Ultrasound guidance is an essential component of all minimally invasive techniques on the thyroid gland.

References

1. Alexandrov YK. Puncture methods in the diagnosis and treatment of thyroid diseases. Yaroslavl: MP Diabet; 1996. (Book in Russian).
2. Gismant M, Tittoto P, Riccardi L, et al. Role of contrast enhanced ultrasound with SonoVue® in characterization of thyroid nodules in comparison with color-power Doppler and fine needle aspiration biopsy. Ultrasound Med Biol. 2006;32(5):284.
3. Kotlyarov PM, Kharchenko VP, Alexandrov YK, et al. Ultrasound diagnosis of the diseases of the thyroid gland. Moscow: Vidar-M; 2009. (Book in Russian).
4. Takashima S, Fukuda H, Nomura N, et al. Thyroid nodules: reevaluation with ultrasound. J Clin Ultrasound. 1995;23(3):179–84.
5. Burch HB. Fine needle aspiration of thyroid nodules. Determinants of insufficiency rate and malignancy yield at thyroidectomy. Acta Cytol. 1996;40:1176–83.
6. Paches AI, Propp RM. Thyroid cancer. Moscow; 1995 (Book in Russian).
7. Trofimova EY, Frank GA, et al. Puncture of tumors of superficial organs and soft tissues under the control of ultrasound. Russ Oncol J. 1999;4:39–43. (Article in Russian).
8. Brom-Ferral R, Reyes-Devesa S, Ferral H, et al. Image-guided fine-needle aspiration biopsy. One-year experience. Rev Investig Clin. 1993;45(1):49–55.
9. Pashchevsky SA. Possibilities of ultrasonography in complex radiodiagnosis and treatment of thyroid diseases. PhD thesis, Sankt-Peterburg; 2004 (Book in Russian).
10. Semikov VI. Therapeutic and diagnostic strategy in thyroid nodules. PhD thesis, Moscow; 2004 (Book in Russian).
11. Cibas ES, Ali SZ. The 2017 Bethesda system for reporting thyroid cytopathology. Thyroid. 2017;27(11):1341–6.
12. Haugen BR, Alexander EK, Bible KC, et al. 2015 American Thyroid Association management guidelines for adult patients with thyroid nodules and differentiated thyroid cancer: the American Thyroid Association guidelines task force on thyroid nodules and differentiate d thyroid cancer. Thyroid. 2016;26(1):1–133.
13. Severskaya NV. Evaluation of the importance of radiation and non-radiation methods in the diagnosis of thyroid cancer. PhD thesis, Obninsk; 2002 (Book in Russian).
14. Mogutov MS. Ultrasound assisted surgery for diseases of the thyroid gland. PhD thesis, Moscow; 2009. (Book in Russian).
15. Sencha AN. Ultrasound diagnostics. Surface-located organs. Moscow: Vidar M Publishing House; 2015. (Book in Russian).

Main Challenges and Pitfalls in Thyroid Ultrasound

13

Ella I. Peniaeva, Alexander N. Sencha, Yury N. Patrunov, Liubov A. Timofeyeva, and Munir G. Tukhbatullin

Despite recent advances in thyroid imaging, approximately 30–50% of patients with thyroid cancer are misdiagnosed [1]. Sixty percent of patients with cancer are diagnosed at stage III and IV. The number of diagnostic errors at initial stages of the disease is 50–100%. The difficulties arise basically in identification of early or minor cancer in subcentimeter lesions.

Factors that result in inaccurate US assessment of the status of the thyroid gland can be divided into the following groups:

1. Objective
   - Anatomical, physiological, and constitutional features of the patient leading to a decrease in visualization
   - Limitations of the equipment (the quality of the scanner, the characteristics of the probes, etc.)

E. I. Peniaeva (✉) · Y. N. Patrunov
Department of Ultrasound Diagnostics, Center for Radiological Diagnostics of Non-State Healthcare Institution Yaroslavl Railway Clinic of JSC "Russian Railways", Yaroslavl, Russia

A. N. Sencha
Department of Visual and Functional Diagnostics, National Research Center for Obstetrics, Gynecology and Perinatology, Ministry of Healthcare of the Russian Federation, Moscow, Russia

L. A. Timofeyeva
Department for Internal Diseases Propaedeutic, Course of Diagnostic Radiology of Medical Faculty of Federal State Budget Educational Institution of Higher Education "I. N. Ulianov Chuvash State University", Cheboksary, Russia

M. G. Tukhbatullin
Department of Ultrasound Diagnostics, Kazan State Medical Academy – Branch Campus of the Federal State Budget Educational Institution of Further Professional Education, Russian Medical Academy of Continuing Professional Education of the Ministry of Healthcare of the Russian Federation, Kazan, Russia

A. N. Sencha, Y. N. Patrunov (eds.), *Thyroid Ultrasound*,
https://doi.org/10.1007/978-3-030-14451-7_13

2. Subjective
   - Insufficient US specialist experience
   - Faulty thyroid US technique

Convenient ultrasound access, "sufficient" neck size, some constitutional features, and other individual patients' factors influence the quality of thyroid ultrasound imaging. Various techniques have been developed to improve poor thyroid visualization. It is possible to change the position of the patients' head and arms; use swallowing movements; utilize US probes of lower frequencies, curved or microconvex probes; and use alternative acoustic access (such as upper intercostal spaces in retrosternal goiter).

High intra- and interobserver variations in thyroid sonography are largely due to the quality of the equipment and the skill level of the operator. According to Bataeva et al. [2], an expert fails to reproduce ones' own results of the 2D thyroid volume calculation in 8.7% of cases; assessments performed by different experts differ by 12.8%. Measurements taken in 3D methods of surface reconstruction and segmentation show differences of 4 and 4.8%, respectively. One disadvantage of using US in some cases is a low detection efficacy for thyroid dystopia and ectopia. Retrosternal location of the thyroid below the tracheal bifurcation significantly limits the possibility of ultrasonography.

High-resolution US equipment allows several thyroid pathologies to be detected, which used to be considered the norm. For example, medium- and large-sized cellular patterns (multiple fine hypo- and anechoic lesions 2–4 mm in size) that were interpreted as the norm years ago are now considered abnormal. This kind of sonogram is widely seen for people living in iodine-deficient regions and precedes a diffuse endemic goiter. It corresponds to colloid cystic change with dilation of the follicles due to extra colloid accumulation. The hyperechoic points within such follicles are a consequence of the dense consistency of the colloid. Another type of small change is inflammatory foci during the initial stages of AITD. These relate to a tendency for a decrease in echodensity and a slight heterogeneity of thyroid tissue resulting from small foci of lymphoplasmacytic infiltration and edema. The common difficulty is differential diagnosis of small nodes and foci of AIT (Fig. 13.1).

In this case, special attention is to be paid to the clarity of lesions margins, its shape, vascular pattern, and a number of other signs inclusive of US elastography and CEUS. Correct conclusion sometimes is a result of follow-up or the use of other diagnostic methods.

Alternatively, there are hyperdiagnostic cases when normal thyroid structures are interpreted as nodules. This especially concerns structures behind the left lobe or along the posterior margin of the inferior compartment of the right lobe. This type of error can be caused by the proximity of the esophagus, which may be reported as a nodule if imaged only with a transverse scan. The normal vascular pattern of the inferior thyroid artery can result in hyperdiagnostics of thyroid nodules. In some cases, the ITA trunk does not split into fine branches when entering the inferior pole of the thyroid lobe. It may be traced within the lobe, where it borders a roundish region of healthy tissue that imitates a nodule.

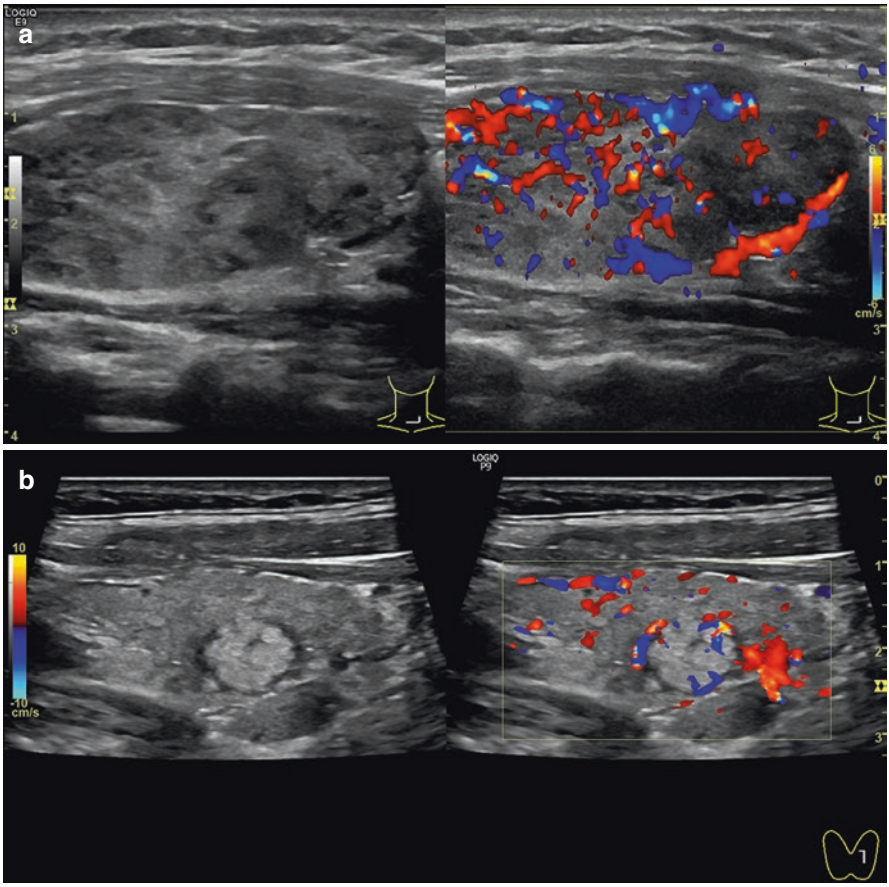

Fig. 13.1 (**a**, **b**) Difficulties in differentiation of thyroid nodules and local changes in AIT. Grayscale US and CDI

Lymph nodes adjacent to the isthmus frequently complicate the diagnosis. The enlarged lymph nodes present in AITD are often located close to the upper or inferior part of the isthmus and can be interpreted as thyroid nodules. Differential diagnosis may benefit from the use of the highest probe frequency, as it permits a more detailed image. It is necessary to pay attention to specific features of lymph nodes, such as form, echostructure with differentiation of the cortical and central parts, and type of blood flow. The opposite types of error, where nodules of the thyroid isthmus are interpreted as neck lymph nodes, are quite rare.

Rare neck pathologies may be misdiagnosed due to insufficient experience of the US operator. In many cases, adenomas and hyperplasia of the parathyroid glands are interpreted as thyroid nodules. This pathology is relatively rare, so general practitioners or US specialists who do not practice at a specialized endocrinology center are not aware of it and have little experience in its diagnosis (Fig. 13.2).

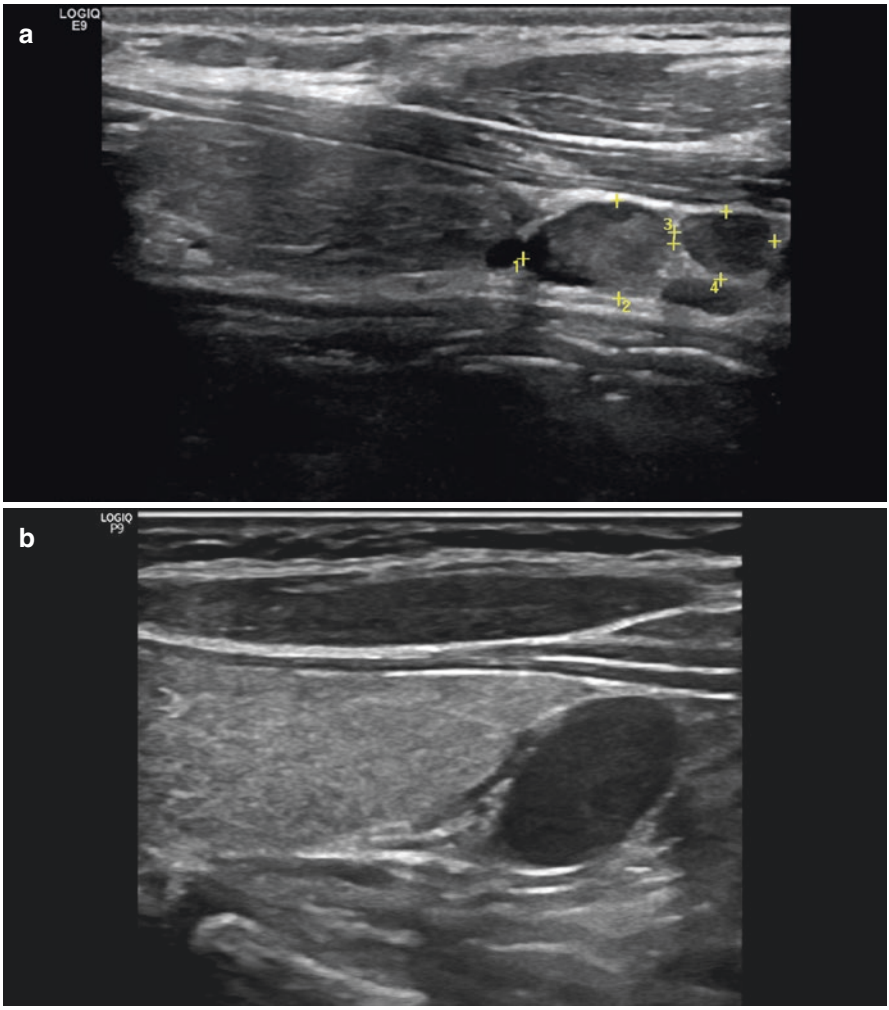

Fig. 13.2 Difficulties in differential diagnosis of neck lymph nodes and parathyroid lesions. Grayscale US. (**a**) Reactive lymph nodes adjacent to the inferior pole of the thyroid lobe. (**b**) Adenoma of the left inferior parathyroid gland adjacent to the inferior pole of the thyroid lobe

The same can be said about esophageal diverticulum. In most cases, sonographers have a mental image of "typical" thyroid nodules based on their own experience, so any lesion differing from this typical image should be interpreted with extra caution.

Congenital anomalies of the thyroid gland and surrounding organs may also cause difficulties. The beginning sonographer may experience certain doubts, for example, with aplasia/agenesis, severe thyroid hypoplasia, right-sided location of the esophagus, etc.

Special opportunities for differential diagnosis are provided by auxiliary methods, such as turning the patient's head, compression of the neck tissues with fingers, swallowing, and others. Modern equipment permits accurate US visualization of solid thyroid nodules larger than 2–3 mm in size. The presence of smaller lesions is preferably reported without the term "nodule." Drawing a conclusion about the lesion is expedient only when it can be clearly visualized in at least two mutually perpendicular scans.

It is important to adhere to the correct examination technique. Thyroid structure including small parts can be estimated only with linear probes at frequencies of 7.5 MHz and higher. Convex abdominal probes may be used to measure the lengths of thyroid lobes or for large thyroids. The use of a convex probe alone for thyroid examination results in multiple severe errors and discredits the field of sonography.

Imaging of the thyroid diseases may be accompanied with US artifacts that are common not only of the thyroid gland. The main ones are listed below:

- Acoustic shadowing is typical for calcifications (e.g., in thyroid cancer, coarse, and egg-shell calcification in benign nodules).
- Reverberation "comet's tail" artifact appears in colloid lesions, inclusive of macrofollicles.
- Marginal artifact of lateral acoustic shadows is characteristic of some types of solid nodules and can be combined with "hallo" sign, for example, in thyroid adenoma.
- Posterior echo enhancement is typical of fluid collections.

Similarly, some artifacts arise in color-coded modes. It is important to set optimal parameters in CDI, PDI, and PW Doppler to ensure the quality of obtained data. Visualization of blood flow with incorrect settings, particularly low velocity threshold, is accompanied with an aliasing artifact in both color and spectral Doppler (Fig. 13.3). Here, the velocity exceeds the Nyquist Limit, and the image displayed would suggest flow is heading in the opposite direction.

When utilizing ultrasound elastography technologies, it is extremely important to adhere the technique. Differences in technology, measurements, and ways of interpretation of tissue strain on scanners of different manufacturers lead to high number of uncertain conclusions. Quantitative data of tissue rigidity/elasticity supply some objective data, but different units of measurement (kPa, m/s, etc.) make the studies hard to compare. Compression ultrasound elastography can also be accompanied with some artifacts [3, 4], such as listed below:

- "Maltese cross"—the emergence of shadows around a hard formation, which entrains soft tissues adjacent to its boundaries in the process of compression. The latter are shown more rigid than they are in fact.
- Edge enhancement of hard lesion due to the involvement and displacement of the surrounding tissues during compression.

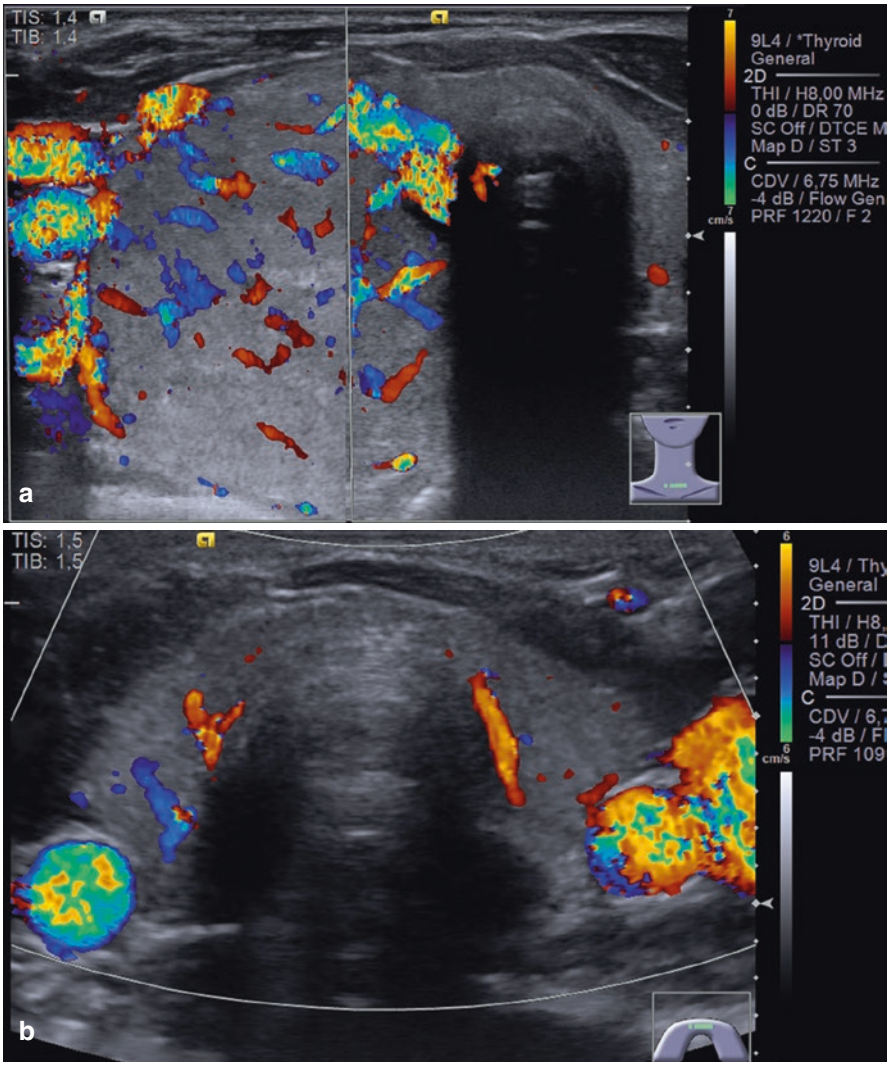

Fig. 13.3 Aliasing artifact in under-sampling in CDI assessment of blood flow

- Artifacts of incorrect compression (excessively strong or weak). Too much pressure applied to the tissues can reduce the clarity of the boundaries of the lesion and sometimes causes lateral displacement of the tissues.
- Artifacts of large liquid collections. When tissue is compressed, random character of fluid movement can also generate artifacts that mimic the solid structure of the lesion.

Differential diagnosis of thyroid tumors does not always depend on radiologist or clinician. Despite all the advances in ultrasound imaging, innovation, and

progress, more than 4% of malignant thyroid tumors have atypical ultrasound features [1] (Fig. 13.4).

The result of an ultrasound study should be presented as a clear conclusion. It influences the choice of further diagnostic and treatment. It helps a surgeon to determine the volume and type of operation, an endocrinologist to assign therapy, and a radiologist to plan follow-up.

The conclusion is a clear summary of the descriptive part and regarding the thyroid gland, in our opinion, should necessarily contain the following four aspects:

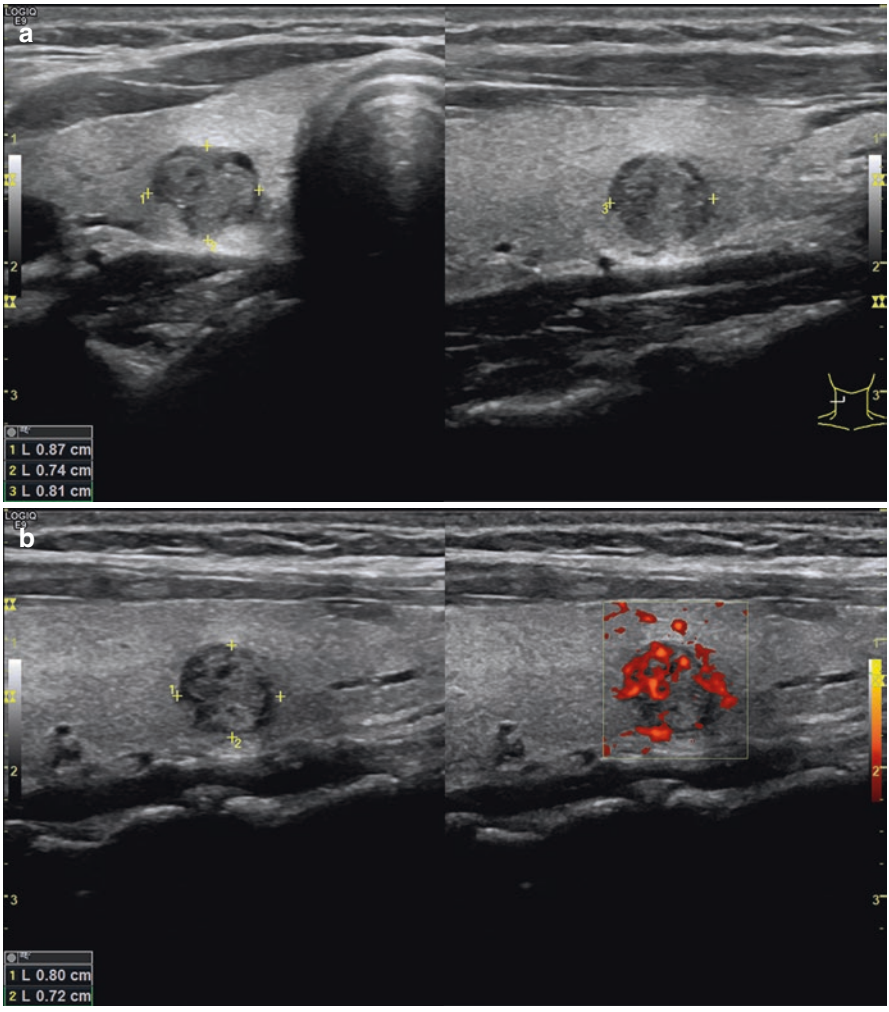

Fig. 13.4 Thyroid cancer. Sonograms. Benign ultrasound signs with (**a**) grayscale US and (**b**) PDI. Malignant hard pattern with (**c**) compression USE and (**d**) shear wave elastography

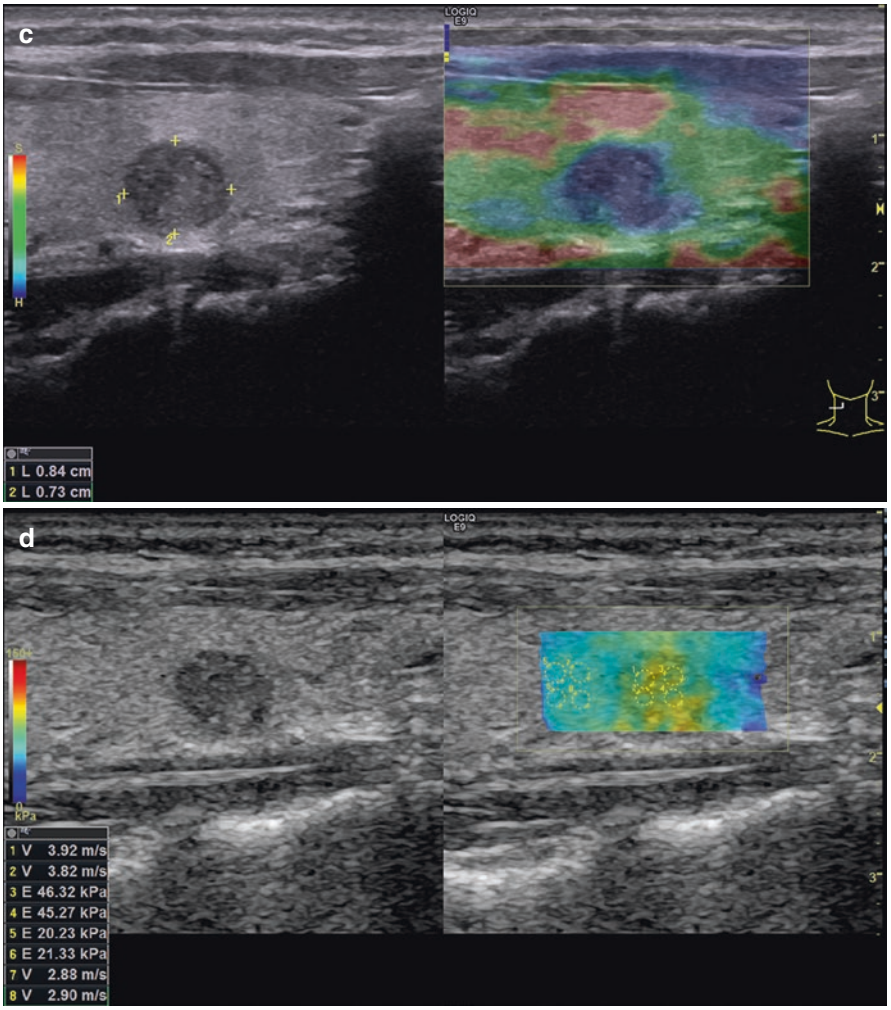

Fig. 13.4 (continued)

1. Data of echovolumetry (thyroid enlargement)
2. The condition of the thyroid parenchyma (e.g., diffuse changes of the parenchyma characteristic of AIT)
3. Summary on the detected lesions (e.g., nodule of the right thyroid lobe)
4. Specification of thyroid lesions according to the TIRADS (e.g., TIRADS 2)

An important component of echography is digital archive of the obtained data. Almost all ultrasound devices can store and transmit digital information in universal DICOM format. It facilitates follow-up and further diagnosis and provides easy, convenient, and efficient communication between various medical equipment, clinics, and networks. Some advantages, like fusion technology, are already utilized in everyday practice; the prospects are obvious.

References

1. Sencha AN. Ultrasound diagnostics. Surface-located organs. Moscow: Vidar M Publishing House; 2015. (Book in Russian).
2. Bataeva RS, Mitkov VV, Mitkova MD. Evaluation of the reproducibility of the results of ultrasound volumetry of the thyroid gland. Ultrazvukovaya i Funkcionalnaya Diagnostica. 2006;1:37–43. (Article in Russian).
3. Bamber J, Cosgrove D, Dietrich CF, et al. EFSUMB guidelines and recommendations on the clinical use of ultrasound elastography. Part 1: basic principles and technology. Ultraschall Med. 2013;34(2):169–84.
4. Osipov LV. Ultrasound diagnostic devices. Modes, methods and techniques. Moscow: Izomed; 2011 (Book in Russian).